Aus der Medizinischen Klinik und Poliklinik III
der Ludwig-Maximilians-Universität München
Direktor: Prof. Dr. Dr. Michael von Bergwelt

Dissertation
zum Erwerb des Doctor of Philosophy (Ph.D.)
an der Medizinischen Fakultät der
Ludwig-Maximilians-Universität München

FLT3-Directed Antibody-Drug Conjugates to Target Leukemic Stem Cells in Acute Myeloid Leukemia

vorgelegt von

Marina Sandra Able

aus

Straubing, Germany

Jahr: 2025

Mit Genehmigung der Medizinischen Fakultät der
Ludwig-Maximilians-Universität München

First evaluator (1. TAC member): Prof. Dr. med. Karsten Spiekermann
Second evaluator (2. TAC member): Prof. Dr. Heinrich Leonhardt
Third evaluator: Prof. Dr. Dr. Fabian Hauck
Fourth evaluator: Prof. Dr. Sebastian Theurich

Dean: **Prof. Dr. med. Thomas Gudermann**

date of the defense:

26.02.2025

Table of Content

Abstract

A large part of acute myeloid leukemia (AML) patients is either refractory to induction therapy or relapses after treatment stop leading to poor prognosis especially in patients that are ineligible for hematopoietic stem cell transplantation. While fast-proliferating blasts are eradicated by chemotherapy, quiescent and drug resistant leukemic stem cells (LSCs) persist and fuel disease re-occurrence. Fms-like receptor tyrosine kinase 3 (FLT3) is overexpressed on LSCs and antibody-drug conjugates (ADCs) provide one elegant way to target this receptor and specifically deliver a toxin that is capable to eliminate those cells.

In this project, two FLT3-targeting ADCs were developed either incorporating a microtubule-toxin or a DNA-damaging drug. Primary goal was to investigate if those ADCs can eradicate LSCs and which payload to choose for this purpose. To this end, the previously generated chimeric FLT3 monoclonal antibody (mAb) 20D9 was humanized and out of several candidates 20D9h3-mAb was selected due to high and specific binding to wildtype and mutant FLT3, fast internalization and good producibility. I show here that while microtubule-toxins have a largely reduced toxicity on cell lines in proliferation arrest, the activity of the DNA-damaging drug DUBA is sustained in this setting which may indicate its better suitability for LSC targeting. Drugs from both classes were conjugated to 20D9h3-mAb resulting in 20D9h3-DUBA and 20D9h3-MMAF. Both ADCs effectively eliminated FLT3-positive cell lines via inhibition of proliferation and apoptosis induction. While 20D9h3-MMAF arrests cells in G2/M, 20D9h3-DUBA halts the cell cycle in G1/S and triggers DNA damage repair via ATR-CHK1 pathway.

The efficacy of either ADC towards leukemic stem and progenitor cells was analyzed in-depth *in vitro*/*ex vivo* using AML patient-derived xenograft (PDX) and primary cells. 20D9h3-DUBA was highly effective in preventing colony growth in colony-forming unit (CFU) and long-term culture initiating cell (LTC-IC) assays as well as leukemic outgrowth in NSG mice even at concentrations as low as 0.025 µg/ml. It could be shown that its anti-LSC activity is mediated via both FLT3 and FcγRI, which is targeted by the IgG1 antibodies' constant part. Despite the common notion that microtubule-toxins are not suitable to eliminate LSCs, also 20D9h3-MMAF treatment of AML-393 or -388 PDX cells prevented engraftment in 4/5 and 5/5 mice, respectively. However, in colony assays 20D9h3-MMAF had a reduced activity compared to 20D9h3-DUBA. Either ADC only marginally affected healthy CD34-positive bone marrow cells at the relevant doses which highlights the suitability of FLT3 as an LSC target.

In contrast to the stable P5-conjugated 20D9h3-MMAF, 20D9h3-DUBA employs a maleimide-linker and a hydrophobic linker payload which comes with several limitations. Those include ADC aggregate formation and instability *in vivo* due to thiol-exchange reaction and rodent-specific carboxylesterase 1c (CES1c) cleavage. Despite those short-comings, 2x3 mg/kg intravenous dosage of either ADC led to strong and durable leukemia reductions in AML-388 PDX mouse

models. Lastly, combinations of 20D9h3-DUBA with inhibitors of ATR and BCL-2 were tested, which both synergistically enhanced the ADC's activity and could be especially promising for certain patient subsets e.g., p53 mutated patients.

Overall, it was shown that FLT3-ADCs can be used for the targeted elimination of LSCs and that both DUBA and MMAF are possible payloads for this purpose. Further improvements of the linker of the DUBA-ADC and the drug loading of the MMAF-ADC will eventually allow the selection of a candidate to enter pre-clinical evaluations.

List of Figures

List of Tables

List of Abbreviations

%	Percent
°C	Degree Celsius
µ	Micro
A	Ampere
AAR	Anti-antibody response
ABCB1	ATP-binding cassette sub-family B member 1
ADC	Antibody-drug conjugate
ADCC	Antibody-dependent cell-mediated cytotoxicity
ADCP	Antibody-dependent cellular phagocytosis
ADME	Absorption, distribution, metabolism and excretion
AFDN	Afadin, Adherens Junction Formation Factor
AML	Acute myeloid leukemia
ATM	Ataxia telangiectasia mutated
ATR	Ataxia telangiectasia and rad3-related
ATRi	ATR inhibitor
B7H3	B7 homolog 3
BCL-2	B cell lymphoma 2
BCL-2i	BCL-2 inhibitor
BiTE	Bispecific T cell engager
BLI	Bioluminescence imaging
BM	Bone marrow
bp	Base pairs
BSA	Bovine serum albumin
CAR	Chimeric antigen receptor
CDC	Complement-dependent cytotoxicity
CDR	Complementarity-determining regions
CES1c	Carboxylesterase 1c
CFC	Colony-forming cell
CFU	Colony-forming unit
cGy	Centrigray
C_H	Constant domain of the heavy chain
CHIP	Clonal hematopoiesis of indeterminate potential
CHK1	Checkpoint kinase 1
C_L	Constant domain of the light chain
CLL1	C-type lection domain family 12 member A
CLP	Common lymphoid progenitor
CML	Chronic myeloid leukemia
CMP	Common myeloid progenitor
CR	Complete remission
CRS	Cytokine release syndrome
CSF1R	Colony stimulating factor 1 receptor
CV	Column volumes
d	Day
Da	Dalton
DAPI	4’,6-Diamidino-2-phenylindole
DAR	Drug-to-antibody ratio
DCMs	Duocarmycins
DM1	Maytansine derivatives 1

DM4	Maytansine derivatives 4
DMEM	Dulbecco's Modified Eagle Medium
DMSO	Dimethyl sulfoxide
DNA	Deoxyribonucleic acid
DNTM3A	DNA methyltransferase 3 alpha
DSMZ	German Collection of Microorganisms and cell culture
DUBA	Duocarmycin
e.g.	For example
EC_{50}	Half-maximal effective concentration
ECL	Enhanced chemiluminescence
EGFR	Epidermal growth factor receptor
eIF4B	Eukaryotic translation initiation factor 4B
ELISA	Enzyme-linked immunosorbent assay
ELN	European LeukemiaNet
Em	Emission
EPO	Erythropoietin
ER	Endoplasmic reticulum
ev	Empty vector
Ex	Excitation
f	female
Fab	Fragment antigen binding
FAB	French-American-British
FACS	Fluorescence activated cell sorter
FBS	Fetal bovine serum
Fc	Fragment crystallizable
FcγR	Fc gamma receptor
FDA	Food and Drug Administration
FLT3	Fms-like tyrosine kinase 3
FLT3L	FLT3 ligand
g	Gravitational constant, gram
gDNA	Genomic DNA
GI	Germinality index
GMP	Granulocyte-macrophage progenitors
GO	Gemtuzumab ozogamicin
h	Hour
HBS	HEPES-buffered saline
HER2	Human epidermal growth factor receptor 2
HIC	Hydrophobicity interaction chromatography
HMA	Hypomethylating agent
HOX	Homeobox
HRP	Horseradish peroxidase
HS	Human serum
HSC	Hematopoietic stem cell
HSCT	Hematopoietic stem-cell transplantation
HSPC	Hematopoietic stem and progenitor cell
i.v.	Intravenous
IC_{50}	Half-maximal inhibitory concentration
ICC	International consensus classification
IDH1/2	Isocitrate dehydrogenase 1/2
IgG	Immunoglobulin G

IGNs	Indolinobenziodiazepine dimers
IL-3	Interleukin-3
IL-6	Interleukin-6
IRES	Internal ribosome entry site
ITD	Internal tandem duplication
JMD	Juxtamembrane domain
KD	Knockdown
kDa	Kilodalton
kg	Kilo
KMT2A	Lysine methyltransferase 2A
KO	Knockout
l	Liter
LALA	Leu234Ala + Leu235Ala mutation
LDAC	Low-dose cytarabine
LIC	Leukemia-initiating cell
LL4	Four-parameter logistic regression
LMPP	Lymphoid-primed multipotent progenitors
LSC	Leukemic stem cell
LTC-IC	Long-term culture initiating cell
m	Male, meter, milli
M	Molar
mAb	Monoclonal antibody
MELK	Maternal embryonic leucine zipper kinase
MEP	Megakaryocyte-erythroid progenitor
MFI	Mean fluorescence intensity
min	Minute
MLL	Mixed Lineage Leukemia
m-LSC	Monocytic LSC
MM-6	Mono-Mac 6
MMAE	Monomethyl auristatin E
MMAF	Monomethyl auristatin F
MPP	Multipotent progenitor
MRD	Minimal residual disease
MS	Mass spectrometry
n	Nano
n.s.	Not significant
na	Not assessed
NGS	Next-generation sequencing
NK	Natural killer (cell)
NPM1	Nucleophosmin-1
NSG	NOD scid gamma
OS	Overall survival
OXPHOS	Oxidative phosphorylation
p	Pico, p value for statistical analysis
P5-(OEt)	Phosphonamidate linker
PAGE	Polyacrylamide gel electrophoresis
PBD	Pyrrolobenzodiazepine
PBS	Phosphate buffered saline
PCR	Polymerase chain reaction
PDGFR	Platelet-derived growth factor receptor

PDX	Patient-derived xenograft
PEG	Polyethylenglycol
pH	Potentia hydrogenii
PI	Propidium iodide
PK	Pharmacokinetic
P/S	Penicillin/streptomycin
PTK7	Protein tyrosine kinase 7
PVDF	Polyvinylidene difluoride
qPCR	Quantitative PCR
RNA	Ribonucleic acid
rpm	Rounds per minute
RPMI	Roswell Park Memorial Institute
RT	Room temperature
RTK	Receptor tyrosine kinase
s	Second
s.d.	Standard deviation
SCF	Stem cell factor
SDS-PAGE	Sodium dodecyl sulfate polyacrylamide gel electrophoresis
SEC	Size-exclusion chromatography
shRNA	Short hairpin RNA
SOC	Super Optimal Brooth
ssDNA	Single-stranded DNA
STR	Short tandem repeats
T-DM1	Trastuzumab emtansine
TKD	Tyrosine kinase domain
TKI	Tyrosine kinase inhibitor
TP53	Tumor protein p53
TPO	Thrombopoietin
US	United states
UV	Ultraviolet
V	Volt
VC	Valine-citrulline
VC-PAB	Valine-citrulline-p-aminobenzoyloxycarbonyl
VEGFR	Vascular endothelial growth factor receptor
V_H	Variable domain of the heavy chain
V_L	Variable domain of the light chain
WHO	World health organization
wt	Wildtype
YFP	Yellow fluorescent protein
ZIP	Zero interaction potency

1 Introduction

Globally, leukemia is currently the 13th most common type of cancer with 487 294 new cases worldwide in 2022. Despite being not among the most prevalent malignancies, leukemia has been responsible for 305 405 deaths worldwide in 2022 and with this is ranked 10th leading cause of cancer-related death. (1)

1.1 Acute myeloid leukemia

1.1.1 Epidemiology, survival, risk factors and diagnosis

Leukemia is classified into acute or chronic and myeloid or lymphoid forms depending on the disease course and the blood lineage it originated from (2). Of the different leukemia types, acute myeloid leukemia (AML) makes up 33.1% of all cases in the USA (3) and 24.5% in Germany (4). It is thus the most common acute leukemia type in the USA and the second most common after chronic lymphocytic leukemia (CLL) in Germany (3, 4). The onset of AML is typically in the second half of life with a median age of 69 at the time of diagnosis and only 9.5% of patients being < 35 years (SEER 22 2017-2021). Despite major improvements in therapy in the last decade, the overall 5-year survival rate of AML is only 31.9% in the USA (SEER 2014-2020) and 23% in Germany. (4, 5) Outcomes are particularly poor for patients ≥ 60 with 5-year survival rates of around 17% (MD Anderson data 1970-2017) and only slight improvements from the 1970s until today (6). Several risk factors have been mentioned predisposing to AML; most notably advanced age, genetic predisposition, previous cytotoxic chemotherapy e.g. with alkylating agents, and age-related clonal hematopoiesis of indeterminate potential (CHIP). The latter describes mutations particularly of genes encoding epigenetic modifiers that occur in approximately 10% of individuals > 65 years before the onset of AML. Further aspects include environmental factors (e.g. smoking, exposure to benzenes and pesticides), preceding hematological disorders, genetic syndromes (e.g. Down syndrome), and also increasingly appreciated, familial germ line predisposition (e.g. *CEBPA* or *GATA2* mutations). (7, 8) In all types of leukemia, the uncontrolled proliferation of blasts – immature precursors of the myeloid (AML) or lymphoid (ALL) lineage – interferes with normal hematopoiesis leading to clinical symptoms. The interference of blast cells with healthy hematopoiesis results in symptoms related to leukocytosis, immuno- and myelosuppression such as anemia, fatigue, fever, bleeding or impaired wound healing (2, 7). Further, a fraction of patients has extramedullary manifestations including in the central nervous system (9). AML is diagnosed if the patient either has defining genetic abnormalities (e.g. *RUNX1*:*RUNX1T1* fusion) or if blast in morphological evaluations of bone marrow or peripheral blood are ≥ 20% of all blood cells in all other cases (10). Alongside morphological assessments, diagnostics usually includes immunophenotyping with flow cytometry to aid with AML subtype classification, molecular testing for gene mutations and cytogenetic analyses (8).

1.1.2 AML gene mutations, classification and risk stratification

AML patients can have a variety of cytogenetic abnormalities e.g. chromosomal translocations or inversions leading to fusion genes such as *RUNX1::RUNX1T1*, *CBFB::MYH11* or various different lysine methyltransferase 2A (*KMT2A*) fusions (11, 12). Yet there is still a proportion of almost 50% of AML cases that do not have any chromosomal abnormalities at diagnosis (13). Although genome mutations in AML are relatively infrequent compared to many solid tumors – with on average ~5 recurrent mutations / genome (14) – 96% of patients harbor at least one and 86% two or more mutations at the time of diagnosis (15). Frequently mutated genes are involved in receptor signaling, DNA-methylation, chromatin-modification, splicing, transcription, tumor suppression and cohesin-complex formation (Figure 1) (11, 16). The top 5 mutated genes are *FLT3* (39%), *NPM1* (33%), *DNMT3A* (31%), *NRAS* (22%) and *RUNX1* (15%) (16). Tumor protein p53 (*TP53*) gene mutations are relatively infrequent in AML (9% of patients) compared to other malignancies but have a high prognostic relevance as they are associated with worse outcomes (12, 16).

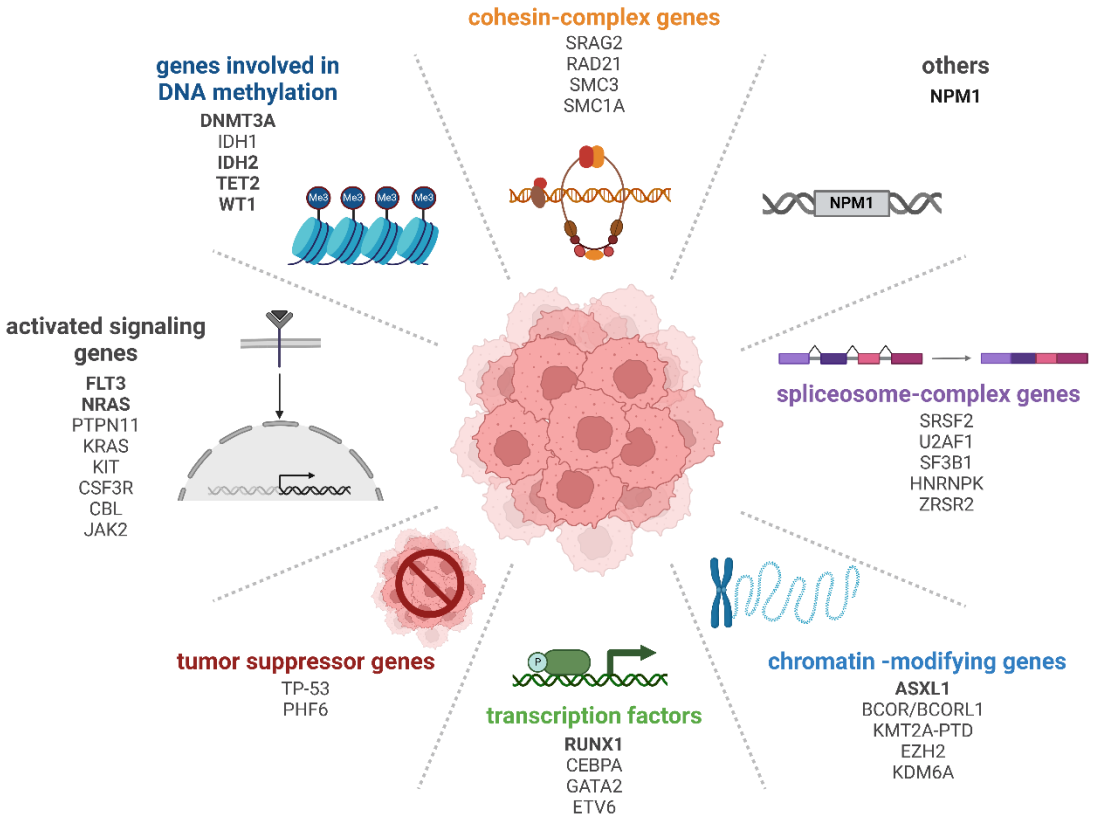

Figure 1: Frequently mutated genes in AML. Genes in bold: Frequency of mutation in patients > 10%. Data was obtained from Metzeler et al. (16). Figure was created with Biorender.com.

The classification of AML was originally based mainly on cytomorphological features e.g. in the French-American-British (FAB) system which is step-wise replaced by newer classifications, e.g.

the International Consensus Classification (ICC) (17) and the system of the World Health Organization (WHO) (10), that both also integrate molecular and genetic features. The ICC classification also served as a basis for the European LeukemiaNet recommendations (ELN) which are used for risk stratification into favorable, intermediate and adverse (12, 18). The ELN risk stratification is summarized in Table 1.

Table 1: AML risk stratification according to ELN 2022. Table was adapted from Döhner et al. (12) and Short et al. (7).

	Cytogenetic features	**Molecular features**
Favorable	• t(8;21)(q22;q22.1)/*RUNX1*::*RUNX1T1* • inv(16)(p13.1q22) or t(16;16)(p13.1;q22)/*CBFB*::*MYH11*	• mutated *NPM1*, without *FLT3*-ITD • bZIP in-frame mutated *CEBPA*
Intermediate	• t(9;11)(p21.3;q23.3)/*MLLT3*::*KMT2A* • cytogenetic and/or molecular abnormalities not classified as favorable or adverse	• mutated *NPM1* with *FLT3*-ITD • wild-type *NPM1* with *FLT3*-ITD (no adverse-risk genetic lesions)
Adverse	• t(6;9)(p23.3;q34.1)/*DEK*::*NUP214* • t(v;11q23.3)/*KMT2A*-rearranged • t(9;22)(q34.1;q11.2)/*BCR*::*ABL1* • t(8;16)(p11.2;p13.3)/*KAT6A*::*CREBBP* • inv(3)(q21.3q26.2) or t(3;3)(q21.3;q26.2)/*GATA2*, *MECOM(EVI1)* • t(3q26.2;v)/*MECOM(EVI1)*-rearranged • -5 or del(5q); -7; -17/abn(17p) • complex karyotype, monosomal karyotype	• mutated *ASXL1*, *BCOR*, *EZH2*, *RUNX1*, *SF3B1*, *SRSF2*, *STAG2*, *U2AF1*, and/or *ZRSR2* • mutated *TP53*

1.1.3 AML therapy: Current standard-of-care

In the last decade the Food and Drug Administration (FDA) has approved various agents for AML therapy rapidly shaping the current treatment paradigm. Despite those advances, the 7+3 intensive chemotherapy regimen developed in 1973 and consisting of a combination of 7 days cytarabine and 3 days of anthracyclines still forms the backbone of AML induction therapy for the majority of patients. In a subset of patients, chemotherapy is complemented by Fms-like tyrosine kinase 3 (FLT3) inhibitors (midostaurin, gilteritinib or quizartinib), CD33-directed antibody-drug conjugate (ADC) gemtuzumab ozogamicin (GO)/Mylotarg, BCL-2 or IDH1/2 inhibitors (BCL-2: venetoclax, IDH1: ivosidenib, IDH2: enasidenib) depending on their molecular features. (12) CPX-351, a 5:1 formulation of cytarabine and daunorubicin encapsulated in liposomes, has been approved as therapeutic option for patients with secondary AML (19). Until recently, patients that do not tolerate intensive chemotherapy, e.g. because of age or co-morbidities, had only limited therapeutic options. They usually received either a low-dose cytarabine (LDAC) regimen or a hypomethylating agent (HMA) such as azacytidine both with dismal outcomes of only 5-10 months median survival (20, 21). With the FDA approval of venetoclax in 2018, a new standard-

of-care has evolved for those patients consisting of LDAC or HMA in combination with venetoclax (12). The latter leading to a considerable improvement of overall survival (OS) from 9.6 to 14.7 months (22). For chemotherapy ineligible patients with *FLT3* or *IDH1/2* mutation, HMA in combination with FLT3 or IDH inhibitors offers another option (12). After induction therapy, the further treatment scheme depends on the risk stratification. Patients classified in the favorable risk group typically receive high-dose cytarabine while patients within the adverse risk group usually proceed to hematopoietic stem cell transplantation (HSCT) due to their high risk of relapse (11). For patients within the intermediate risk group, the decision for or against HSCT is made on a case-by-case basis dependent on the risk of relapse and the persistence of measurable residual disease (MRD) as assessed by flow cytometry, next-generation sequencing (NGS) or quantitative polymerase chain reaction (qPCR) (8). When complete remission (CR) is reached after induction and consolidation – meaning that the patient has a hematological recovery and < 5% of blasts in the bone marrow (7) – there is the possibility to continue with a repetitive low-dose maintenance therapy e.g. with midostaurin or oral azacytidine (12). The ultimate goal of this is to increase the duration of remission and to reduce the chances of relapse, however the overall benefit of maintenance therapy for patients of the different risk groups is not yet clearly established (23). Despite these advances, refractory disease and relapse still present a major challenge in AML therapy.

1.2 Challenges to AML therapy: Refractory disease and relapse

1.2.1 AML relapse and leukemic stem cells

Around 50-70% of older and 30-40% of younger AML patients fail to reach CR after two courses of induction chemotherapy commonly defined as refractory disease (24). Additionally, most patients who achieve CR will eventually relapse, the majority (~70%) already in the first year after CR with the chances of relapse declining after 4-5 years to < 10%. The relapse probability is amongst other factors influenced by cytogenetic and molecular risk classification and age. (25) MRD positivity has further been found to be associated with relapse risk (55.4% versus 31.9% for patients with no MRD) and OS (41.9% versus 66.1% for patients with no MRD) (26). Relapsed leukemia patients usually present with multiple new mutations and subclones which increases molecular complexity and complicates further therapy (27-29). The best chance for relapsed patients is continuing treatment with a different regimen to eventually reach remission followed by HSCT; in patients that are ineligible for HSCT further therapy is mostly palliative (7). Altogether the prognosis for relapsed patients is poor with a median survival after first relapse of only around 6 months with 90% of patients not surviving > 5 years (30, 31). Leukemic stem cells (LSCs) that reside within MRD have been identified as the source of disease re-occurrence (32) and LSC gene expression signatures such as the LSC-17 score have been shown to correlate with treatment outcomes (33, 34). As illustrated in Figure 2, LSCs are thought to mainly originate from healthy

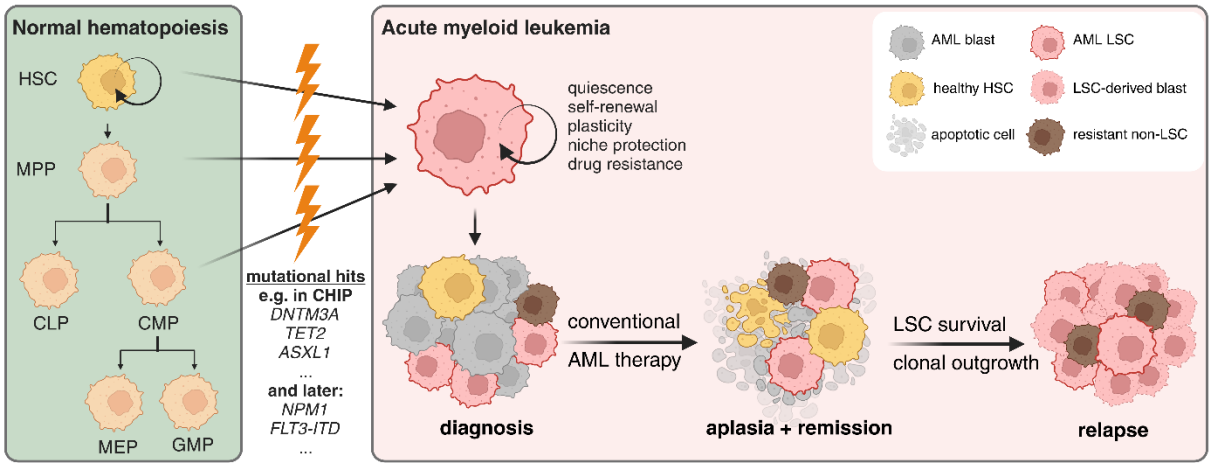

Figure 2: AML development and relapse. Quiescent hematopoietic stem cells (HSCs) are at the apex of normal hematopoiesis. They differentiate to multipotent progenitors (MPP), which in turn give rise to common myeloid (CMP) and common lymphoid (CLP) progenitors. CMPs then differentiate to megakaryocyte erythroid progenitors (MEP) and granulocyte-macrophage progenitors (GMP). CLP, MEP and GMP produce then more differentiated cells that form the lymphoid, erythroid and myeloid lineages, respectively. Acute myeloid leukemia (AML) stem cells (LSCs) are thought to originate from HSCs or more committed progenitors that reacquire stem-cell features through mutational hits. Those LSCs than again give rise to more differentiated leukemic blasts. AML therapy is able to remove those fast-proliferating blasts, but not their source of origin the LSCs, which eventually drives relapse. Figure was created with Biorender.com and adapted from van Gils et al (35) and Stelmach et al (36).

progenitor cells like granulocyte-macrophage progenitors (GMP) or lymphoid-primed multipotent progenitors (LMPPs) that reacquire stem cell features rather than from actual hematopoietic stem cells (HSCs) (35, 37, 38). Nevertheless, LSCs resemble HSCs concerning their quiescence, their capability to self-renew and their position at the apex of a hierarchy with AML blasts rather than healthy blood cells as their progeny (39, 40). The quiescent state of LSCs as well as their localization in the bone marrow niche also contributes to their resistance to drugs (41, 42). LSCs have further been described to have increased DNA damage repair (43), elevated levels of drug-efflux transporters such as ATP-binding cassette sub-family B member 1 (ABCB1) (44) and resistance to apoptosis induction e.g. due to *TP53* inactivation (45). Due to these characteristics, LSCs are capable to survive AML chemotherapy and eventually fuel AML relapse. Despite the similarities of LSCs to HSCs, differences between both subsets have been identified and are exploited for therapeutic targeting as detailed in the following paragraph.

1.2.2 LSC-specific therapy

Several pathways and targets have been identified that present unique vulnerabilities of LSCs and that could potentially be exploited to eradicate them and to prevent AML relapse (summarized in Figure 3): **1)** Pathways that govern LSC quiescence **2)** Metabolic pathways **3)** Epigenetic regulators **4)** Pathways of stress response **5)** Signaling pathways **6)** Bone marrow microenvironment and finally **7)** LSC-specific surface markers.

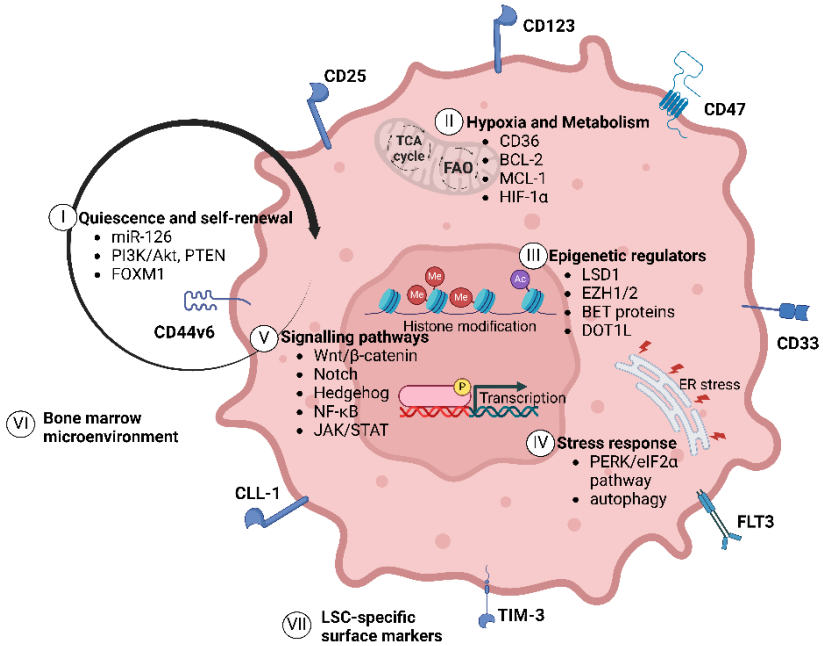

Figure 3: LSC-specific vulnerabilities and options for therapeutic targeting. Leukemic stem cells (LSCs) have many similarities with healthy stem and progenitor cells; however, a variety of unique features have been described that can be exploited for their targeted elimination. Those include factors/proteins related to: I) Quiescence and self-renewal II) Hypoxia and metabolism III) Epigenetics IV) Stress response V) Signaling VI) Bone marrow microenvironment and VII) LSC surface markers. Figure was created with Biorender.com. Information was used from van Gils 2021 (35).

The idea of LSC elimination via surface targets that are unique to those cells is particularly intriguing and has fueled the development of several therapies directed against those markers including monoclonal antibodies (mAbs), ADCs, chimeric antigen receptor T cells (CAR-T) and bispecific T cell engagers (BiTEs) (46). Frequently mentioned LSC markers include CD25, CD123, CD47, CD33, TIM-3, CLL1 and CD44 (36, 46, 47). Most agents targeting LSC surface antigens or intrinsic pathways are in early phases of clinical trials, however some are already approved or advanced in later phases. The FDA-approved BCL-2 inhibitor venetoclax for example has been demonstrated to inhibit oxidative phosphorylation (OXPHOS) in LSCs (48). In contrast to HSCs and other cancer cells, LSCs are uniquely dependent on OXPHOS, which could explain the superiority of venetoclax-based regimens concerning the duration of remission compared to conventional treatment in older patients (49).

Of the AML surface markers, CD33 is best characterized as a therapeutic target with one already FDA-approved ADC – GO / Mylotarg – and another one –SGN-CD33A – that reached late-stage clinical trials, but was discontinued (46). For patients of the favorable and intermediate risk groups, it has been described that a combination of chemotherapy and GO reduces the chances of relapse and increases OS in clinical trials (50). Pre-clinically it has been demonstrated that GO effectively eradicates leukemia-initiating cells (LICs) in patient-derived xenograft (PDX) models (51). The success of GO therapy is however limited by on-target, off-leukemia effects caused by the expression pattern of CD33 which is also present in substantial amounts on healthy stem and progenitor cells and on differentiated myeloid cells (47, 52). Similar problems could occur with CD123, which is also expressed on normal blood cells such as monocytes and additionally in several other healthy tissues (47, 53). CLL1 on the contrary has a better therapeutic window, but is only present on a subset of LSCs with interindividual variability (47). This highlights the need for more specific LSC markers. A particularly promising option is the receptor tyrosine kinase (RTK) FLT3.

1.3 FLT3 as AML LSC target

1.3.1 Structure and function of FLT3 and its role in AML development

The *FLT3* gene is located on chromosome 13q12 and encodes for a type III RTK, a family that also includes c-KIT, colony stimulating factor 1 receptor (CSF1R) and platelet-derived growth factor receptor (PDGFR). The protein was discovered independently by two groups in the early 90s in murine fetal liver cells and later also described in human cells. (54-56) The FLT3 receptor is built of five extracellular immunoglobulin-like domains, a transmembrane domain, a juxtamembrane domain (JMD) and two tyrosine kinase domains (TKD) interrupted by a kinase insert domain (57). While FLT3 ligand (FLT3L) is broadly expressed in various tissues (58), FLT3 receptor expression in normal hematopoiesis is limited to a subset of hematopoietic progenitors including common myeloid and lymphoid progenitors (CMPs, CLPs) and GMPs but excluding megakaryocyte-erythroid progenitors (MEPs) (59-63). The expression on HSCs is low to absent (63). Low expression was reported on dendritic cells, but FLT3 is not present on granulocytes, macrophages, mast cells, megakaryocytes and thrombocytes, erythrocytes, B and T cells (59, 60, 64, 65). In non-hematopoietic tissues FLT3 appears extracellularly solely on rare cells in the tonsil and otherwise occurs only intracellularly, e.g. in pancreas and cerebellum (63). In AML, FLT3 is expressed on the majority of patient blasts and more importantly, it was reported, that it is also present on 79% of patient LSCs independent of disease stage, risk class, or FLT3 mutational status (63). FLT3 is thus increasingly appreciated as LSC target, which might offer a wider therapeutic window compared to other LSC surface markers as its expression on HSCs and healthy progenitors is low and limited to a subset of cells (46, 63, 66).

Two differentially glycosylated structures of FLT3 have been described, a 150 kDa form that is anchored in the plasma membrane and a 130 kDa weaker glycosylated form that is primarily present in *FLT3*-mutated cells and that is retained in the endoplasmic reticulum (ER) (67). Concerning the role of FLT3, it has been reported that its knockout (KO) in mouse models is not lethal, it does however affect healthy hematopoiesis, in particular the development of B cells and T cells, and myeloid differentiation (68). Besides cell differentiation, FLT3 is important for cell proliferation and apoptosis (69). Wildtype (wt) FLT3 receptor signaling is triggered by the binding of FLT3L, which works via paracrine and possibly also autocrine mechanisms (69, 70). Binding of FLT3L leads to receptor dimerization and transphosphorylation of intracellular tyrosine residues. This triggers a rapid internalization of the receptor and activates diverse signaling pathways, most notably RAS-MAPK and PI3K-AKT. (69, 71) Due to its key-role in hematopoiesis, it is not surprising that mutations in *FLT3* are pathogenic. In AML, *FLT3* mutations are found in 39% of patients thus representing the number 1 gene mutation in AML (16), and they are probably associated with higher age and normal cytogenetics (72). There are two types of *FLT3* mutations: internal tandem duplications (ITD) and TKD point mutations found in 15-35%

and 5-10% of adult patients, respectively (73-75). ITDs, which were first identified in 1996, occur in the JMD and can be 3 to > 400 bp long (76). Several groups showed that their occurrence is negatively correlated with survival in AML patients (77). The impact of *FLT3*-TKD mutations on long-term prognosis is controversial, however a 2005 meta-analysis also suggested its negative impact (77). Currently only *FLT3*-ITD but not *FLT3*-TKD status is included in the ELN risk stratification (12). The role of *FLT3*-ITD for AML development was investigated in mouse models. Here, it has been shown that mice that receive HSCs expressing FLT3-ITD develop myeloproliferative disorder (78), but in order to develop AML, additional mutations affecting differentiation and/or proliferation (e.g. in *DNMT3A*) are required (79). Mechanistically, both *FLT3*-ITD and -TKD mutations lead to constitutive receptor phosphorylation and autonomous ligand-independent cell proliferation, which was shown in cytokine-dependent cell lines such as Ba/F3 and 32D cells (80, 81). FLT3-ITD further activates STAT5 in addition to the already mentioned downstream signaling pathways (81, 82), which might be a result of the mislocalization of the underglycosylated FLT3-ITD in the ER (83).

1.3.2 FLT3-directed therapies

Due to its important role in AML pathogenesis and prognosis and the frequent occurrence of genetic mutations, FLT3 has a longstanding history as a drug target. Tyrosine kinase inhibitors (TKIs) are the best characterized and most advanced therapeutics targeting FLT3. The first generation of TKIs faced many problems such as dismal pharmacokinetics (PK) and side-effects due to limited FLT3 specificity which led to disappointing results as single-agents. (72) In combination with chemotherapy, however, the TKI midostaurin led to significant improvements in OS in the phase III RATIFY study leading to its approval in 2017 (84). Subsequently, more FLT3-specific second-generation TKIs were developed including gilteritinib, quizartinib and crenolanib (72). After a phase 3 trial in *FLT3*-mutated patients with relapsed/refractory AML (ADMIRAL study), which showed a significant benefit in OS for patients treated with gilteritinib (OS: 9.3 months) in comparison to conventional chemotherapy (OS: 5.6 months), gilteritinib was approved in 2018 as first FLT3 inhibitor to be used as a single agent (85, 86). Based on the results of the QuANTUM-First study, where quizartinib in combination with chemotherapy (OS: 32 months) significantly improved survival over chemotherapy only (OS: 15 months) in newly diagnosed *FLT3*-ITD-mutated AML patients, quizartinib plus chemotherapy was similarly approved by the FDA in 2023 (87). Currently, most FLT3-targetd therapies that are or have been in clinical development comprise kinase inhibitors (Figure 4, clinicaltrials.gov).

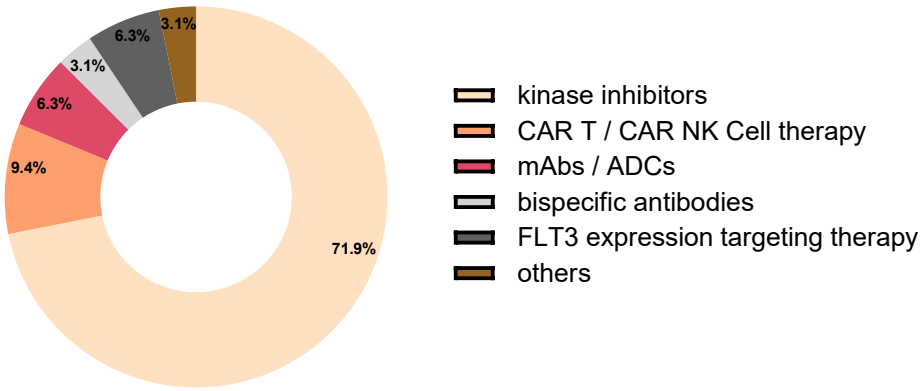

Figure 4: FLT3-targeting therapeutics in clinical trials. Clincaltrials.gov was searched (on 29.05.2024) for all clinical trials (phase I-IV) that investigate FLT3-directed therapies and that are either not yet recruiting, recruiting, active or completed, excluding terminated trials. Figure was created with Biorender.com.

However, TKI therapy still faces some issues especially concerning resistance development, e.g. due to acquired additional mutations in the *FLT3* gene (88), mutations in either RAS/MAPK pathway (89), transcription factors or epigenetic regulators (90), activation of parallel pathways (91) or inactivation of TKIs by CYP3A4 (92). Therefore, there is need to investigate alternative, non-kinase inhibiting FLT3-targeting strategies. Options include T- and NK- cell therapy, agents that target FLT3 expression or degradation, and native or crystallizable fragment (Fc)-optimized mAbs, bispecifics, and ADCs (93). CAR-T and CAR-NK cell therapy has been very promising for other targets and disease entities e.g. in ALL, B cell malignancies and multiple myeloma (94). Phase I clinical trials are currently on the way for CAR-T and CAR-NK cell therapy in FLT3-positive AML and results are being eagerly awaited (95) (NCT05432401, NCT06325748, and NCT05023707). Further, there are also approaches that target FLT3 expression or degradation e.g. maternal embryonic leucine zipper kinase (MELK) inhibitor OTS167, which blocks FLT3 translation by inhibiting phosphorylation of eukaryotic translation initiation factor 4B (eIF4B) (96). A phase I/II study of this molecule has, however, been terminated due to slow patient accrual (NCT02795520). The most promising agent of this class of therapeutics is pevonedistat, an inhibitor of NEDD8-dependent ubiquitin ligase, which is currently in numerous clinical trials for AML – the most advanced ones in phase III (NCT04090736, NCT03268954). This agent acts by downregulation of *miR-155*, which has been shown to cooperate with *FLT3*-ITD to enhance expansion of myeloid cells (97). Lastly, an advancing class of agents targeting FLT3 are antibody-based therapeutics. At first, mostly native mAbs have been developed and tested pre-clinically (98, 99) and in early clinical trials (NCT00887926), albeit with limited success. Engineering of the antibodies constant Fc part presents a strategy to enhance the activity of native mAbs by increasing antibody effector functions such as antibody-dependent cellular cytotoxicity (ADCC), antibody-dependent cellular phagocytosis (ADCP) or complement-dependent cytotoxicity (CDC)

(100). FLYSYN/4G8-SDIEM is such an Fc-optimized antibody that is currently in phase I/II clinical trials with promising first results (64, 101) (NCT02789254). Lastly, a lot of progress has recently been made with ADCs, especially in breast cancer; the only FLT3-targeting ADC that has advanced to clinical trials, however, was discontinued due to lack of efficacy (102) (NCT02864290). As described, FLT3 as a target is well-established, leading to the assumption that targeting it with an ADC is feasible provided that the molecule has been carefully designed and adjusted to the low expression of FLT3. Considerations for the design of a FLT3-targeting anti-LSC ADC are detailed in the next section.

1.4 ADCs as LSC targeting therapeutics

1.4.1 Function of ADCs

More than 100 years ago, Paul Ehrlich had the appealing idea to design a drug that – similar to a "Trojan horse" – carries its toxic content to a desired target as an approach to fight cancer (103). ADCs are therapeutics that consist of a target-specific antibody linked to a highly potent toxin or drug (payload) thus combining specificity and effectivity making Paul Ehrlich's vision come true (Figure 5).

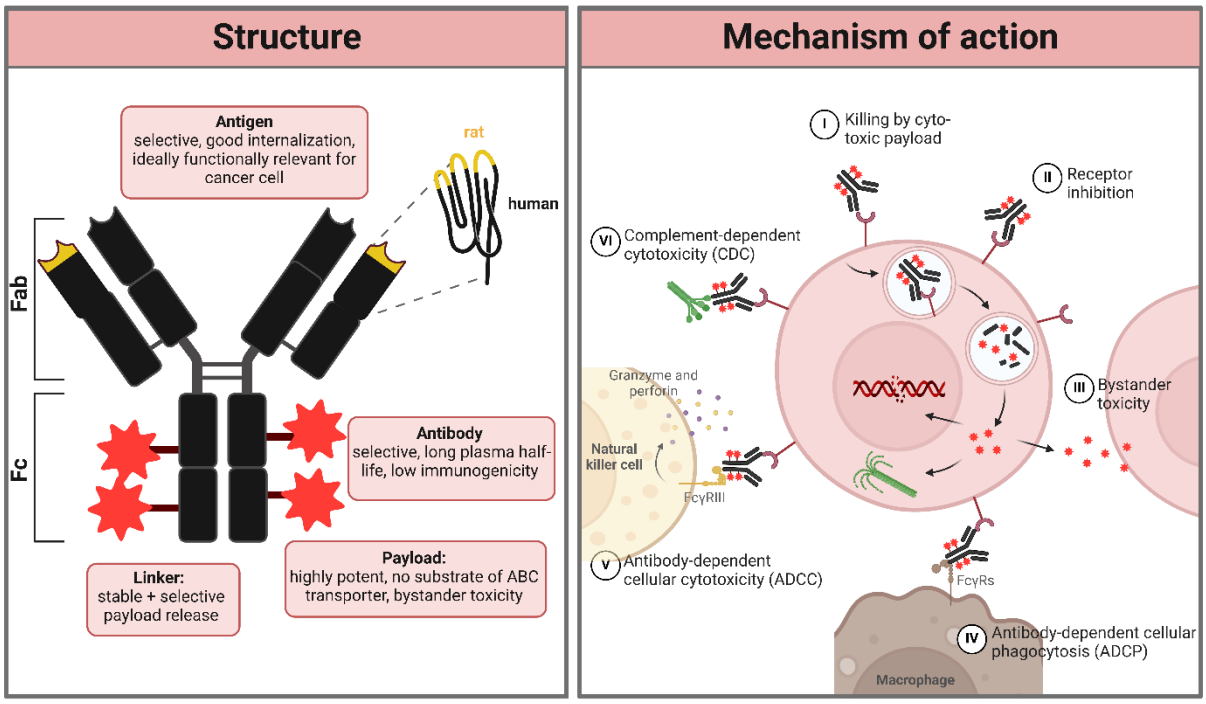

Figure 5: Antibody-drug-conjugates - structure and mechanism of action. Left image: Structure of antibody-drug-conjugates (ADCs). Boxes detail important considerations for each part of the ADC. Right image: Summary of the different mechanisms of action of an ADC. Figure was created with Biorender.com and adapted from Fu et al (104).

Upon binding of the target – most commonly receptor molecules – ADCs are taken up by endocytosis, the payload is freed from the linker and kills the cell. (I). (105) Dependent on their design ADCs can also have additional functions that may contribute substantially to their efficacy. For example, if a receptor is selected as target, the binding of the antibody part can – dependent on its binding site – inhibit the receptor and block downstream signaling (II). Further, lipophilic payloads that are able to cross the cell membrane of the targeted cell can induce bystander toxicity in neighboring cells (III). And finally, the antibody can bind to macrophages, natural killer cells or complement proteins via an interaction of its crystallizable fragment (Fc) region with Fcγ receptors (FcγRs). This interaction mediates antibody-dependent cellular phagocytosis (ADCP, IV), antibody-dependent cellular cytotoxicity (ADCC, V) or complement-dependent cytotoxicity

(CDC, VI), respectively. (106) At present, there are 15 ADCs approved worldwide and over 150 candidates are in clinical development, 12% thereof in late-stage trials (phase III/IV). 44% of the ADCs in clinical trials target hematological disease, 55% solid tumors and only 1% diseases other than cancer.

1.4.2 Design of ADCs and special considerations for the targeting of LSCs

1.4.2.1 ADC target

ADC targets should ideally be highly and uniformly expressed on the malignant cell with limited to no expression on healthy cells to avoid side-effects. A fast internalization of the target is also crucial. Most ADCs are directed towards oncogenic targets e.g. receptors that are involved in cell growth or survival. (105, 107) The advantages of that are exemplified by human epidermal growth factor receptor 2 (HER2)-directed trastuzumab-conjugates where the antibody alone already exerts an anti-proliferative effect (108). Concerning the target expression levels, quantitative studies with an HER2-directed ADC suggested that the target antigen density should be at least 10 000 copies/cell (109). However, many factors determine the effectivity of ADC therapy such as antibody affinity, efficiency of internalization, potency of the payload, payload molecules per antibody (drug-to-antibody ratio = DAR), therapeutic window and other factors. For instance, it was recently shown that trastuzumab-deruxtecan/Enhertu is also highly effective in $HER2^{low}$ patients (110) illustrating that careful ADC design makes it possible to address lowly expressed targets. As FLT3 expression is rather low, this also has to be considered for an FLT3-targeting ADC. Therefore, an FLT3-ADC will probably require a highly potent payload and ideally a high DAR. The selection of an appropriate target for the extinction of AML LSCs has been described in chapter 1.2.2.

1.4.2.2 The antibody molecule

The antibody part of an ADC is crucial to direct the cytotoxic cargo to the right cell. Antibodies should have a high target affinity, low cross-reactivity with receptor paralogues/no off-target binding, long serum half-life and low immunogenicity. (105) Most ADCs use immunoglobulin G1 (IgG1) antibodies due to their ability to trigger immune effector functions and their long half-life (104). IgG1 antibodies have a size of approximately 150 kDa and consist of two heterodimers of a heavy and a light chain, respectively, which are in turn connected through disulphide bonds (111, 112). The fragment antigen binding (Fab) region consist of light chain, heavy chain variable region and a part of the heavy chain constant region (the C_H1 domain). This is followed by the hinge region and C_H2 + C_H3 domains of the heavy chain which together form the Fc region. The Fc region is important for the mediation of effector functions such as ADCC, ADCP and CDC. (113) This is achieved by interaction with Fc gamma receptors (FcγRs) on target cells which bind to the Fc

region of antibodies, whereof 5 act activating (FcγRI, FcγRIIa, FcγRIIc, FcγRIIIa, and FcγRIIIb) and one inhibitory (FcγRIIb) on the binding cell (114). Most ADCs use humanized antibodies to avoid immunogenicity. Recent advances in antibody design are revolutionizing the ADC field. Examples are biparatropic antibodies (targeting two different epitopes on the same antigen which can improve internalization), bispecific antibodies (targeting two different antigens), Fc-engineered antibodies (increasing or ablating effector functions, improving serum half-life), use of antibody fragments (advantages in production, conjugation and solubility), and finally antibodies with a masked binding domain (selective activation in the tumor microenvironment). (105)

1.4.2.3 Linking antibody and payload

ADC payload and antibody are connected by linkers, which are another key-component determining the success of ADC therapy and which have to fulfil certain requirements. Firstly, the two connection points on antibody and drug should be selected in a way so that neither the antibody nor the drug functionality or stability is altered. Also, the linker should be stable in blood circulation and have no tendency to aggregate as both would impair the ADC's effectivity. For production it is further relevant that the conjugation technique is simple, rapid and with high yield; the sites of conjugation should also be predictable and selective to avoid heterogeneous product mixtures. All currently approved ADCs use lysine or cysteine residues on the native antibody as attachment points for the linker. There are approximately 40 lysine residues in IgG1 antibodies that can be conjugated to a drug. It is possible to control the number of attached drug molecules when conjugating to lysine residues, however, the position of the drug molecules on the antibody is difficult to control resulting in a mixture of different ADC species, which is a disadvantage of lysine conjugation. Cysteine conjugation mostly uses the 4 interchain S-S bonds that hold the antibody together. (105, 115) Maleimides are frequently used for their functionalization, however, maleimide conjugation is prone to thiol-exchange reaction leading to the loss of linker-payload to blood proteins (116) being a drawback of this method. It is also possible to modify the native antibody and create a handle for linker connection. Several methods have been suggested. For instance, one possibility is the incorporation of additional free cysteines (e.g. THIOMAB technology) (117) as naturally occurring cysteines in IgG are normally in S-S bonds and cannot be used directly for conjugation. Other possibilities to create attachment points are the incorporation of amino acids that are not naturally occurring in antibodies (non-canonical amino acids) (118) or enzymatic methods using transglutaminases (119), sortases (120) or glycotransferases (121).

Linker molecules on all currently approved ADCs can be divided into cleavable or non-cleavable. ADCs with non-cleavable linkers are degraded by proteolysis in lysosomes after internalization (e.g. T-DM1/Kadcyla) freeing the payload. Cleavable linkers are either acid-sensitive (e.g. GO/Mylotarg), cleaved by reduction or by enzymes overexpressed in tumor cells, such as

cathepsin B (e.g. Brentuximab vedotin/Adcetris), which cleaves between the amino acids valine and citrulline. The latter group of linkers is currently more popular in ADC development, as non-cleavable linkers have the disadvantage that the drug is still connected to a peptide-fragment which decreases membrane permeability and prevents bystander effects on neighboring cells, which is commonly regarded as favorable for ADC effectivity. (105)

1.4.2.4 Choice of payload

The ADC's main function is mediated by the cytotoxic payload. As most payloads are lipophilic, only few molecules can be conjugated per antibody without increasing the chances of aggregation. Therefore, the chosen drug must be highly toxic – usually 100 to 1000-fold more potent than conventional chemotherapeutics. This is especially relevant for lowly expressed targets like FLT3. Further, the drug should be stable when stored or administered, and ideally no substrate of ABC transporters, which are a key-factor for ADC resistance development well-known from GO/Mylotarg in AML treatment. (105, 122) Of the 15 currently approved ADCs, more than half incorporate microtubule inhibitors (8 ADCs), three use DNA-damaging agents, two topoisomerase I inhibitors and the remaining two are conjugated to the peptide toxin pseudomonas exotoxin A (moxetumomab pasudotox/Lumoxiti), and the photosensitizer IRDye700DX (cetuximab saratalocan/Akalux), respectively. (104, 105) Microtubule-targeting agents include auristatins like the structural homologues monomethyl auristatin E and F (MMAE, MMAF), and maytansinoids. DNA-damaging agents comprise pyrrolobenzodiazepines (PBDs), indolino-benziodiazepine dimers (IGNs), calicheamicin γ, and duocarmycins (DCMs) including *seco*-DUBA and CC-1065. PBD and IGN crosslink DNA through binding to the N2-position in guanine. Calicheamicin γ binds DNA and after Bergmann cyclization forms diradicals which lead to DNA double strand breaks. DCMs alkylate the N3-position of adenine residues in the DNA minor groove ultimately also resulting in DNA strand breaks. A third class of ADC payloads are topoisomerase I inhibitors like camptothecin and its derivatives irinotecan, topotecan, SN-38, exatecan, and deruxtecan. Apart from that, inhibitors of the spliceosome, RNA polymerase inhibitors, protein toxins, immunomodulating agents or antibiotics are conjugated to ADCs, however so far not as frequently as the other payload classes. (105, 123)

To target LSCs, the ADC payload should have a mechanism of action that is independent of cell proliferation and division as LSCs are quiescent. Therefore, microtubule-targeting agents are commonly not regarded as ideal choice for stem-cell eradication and other payloads such as DNA-damaging or topoisomerase I-targeting ones are preferred (123-125). Of the DNA-damaging agents DUBA is a promising payload candidate as it is highly potent with picomolar to nanomolar half-maximal inhibitory concentration (IC_{50}) values (123). So far DUBA-ADCs have been studied mostly pre-clinically except for the HER2-directed DUBA-ADC SYD985 (by Byondis), which

advanced to phase III clinical trials (126). The FDA however recently issued a complete response letter suspending the decision on the ADC's approvability (127).

Lastly, after the payload has been chosen, the number of drug molecules conjugated per antibody molecule, the DAR, has to be refined. Depending on the linker system used, this might not always be possible but is an important factor for successful ADC design. Currently approved ADCs have DARs of 1.8-8, most frequently around 4. Depending on the properties of the payload such as hydrophobicity a very high DAR might result in aggregation, might increase toxicity, and increase clearance in the blood, which reduces efficacy. A very low DAR in turn might be a disadvantage if the target expression is low and the payload not so potent. (105) Finally, it should be noted that especially the linkage of the payload and the antibody is chemically quite challenging and not every linker system can be applied to every payload. Therefore, although knowledge about ideal ADC design is rapidly increasing, the realization of ideal ADCs can be difficult.

1.5 Aims of this work

Despite recent advances, relapse and refractory disease pose major challenges to AML therapy and LSCs have been identified as a major driving factor in this. The RTK FLT3 is a well-known therapeutic target in AML and has been described as an LSC-specific surface marker. ADCs represent an elegant option to selectively target those LSC surface markers like FLT3 as they combine the specificity of antibodies with highly potent toxins. In a previous project, our group developed the FLT3-targeting ADC 20D9-MMAF, but its potency towards LSCs has not yet been evaluated. Aim of this project was to further develop this ADC and to optimize it for LSC targeting. This also included the question if LSC-targeting via FLT3 with an ADC is generally possible, which payload to choose for this purpose and if DNA-damaging agents are superior to microtubule-toxins, which is a common notion in the ADC community.

To this end, 20D9 antibody was humanized and the binding, cross-reactivity and internalization were extensively evaluated for these humanized clones, resulting in the selection of 20D9h3-mAb as lead candidate for further development. Different payloads were then tested on cell lines regarding their potency and their ability to eliminate proliferation-inhibited cells. DUBA and MMAF were chosen as representatives of DNA-damaging and microtubule-targeting agents, respectively, and conjugated to humanized 20D9h3-mAb. The resulting FLT3-ADCs were evaluated for their efficacy using cytotoxicity assays in AML cell lines and in FLT3-expressing transgenic Ba/F3 cells, and mechanistically assessed in cell cycle and apoptosis assays. The linker stability of both ADCs was evaluated in pharmacokinetic studies and the ADCs were tested *in vivo* in NSG mice. The following and main part of this work focused on the activity analysis of both ADCs towards leukemic stem and progenitor cells *in vitro*/*ex vivo* using gold-standard assays: colony-forming unit (CFU) assay, long-term culture initiating cell (LTC-IC) assay, and leukemia-initiating cell (LIC) assay. Similar assays were carried out with hematopoietic stem and progenitor cells from healthy donors to evaluate toxicities. Finally, for the DUBA-ADC, combinations with either ATR or BCL-2 inhibitors were tested which both could be promising approaches to potentiate the ADC's efficacy regarding LSC-elimination.

2 Material and Methods

2.1 Material

2.1.1 Chemical reagents

Table 2: List of chemical reagents.

reagent	supplier
2-propanol	AppliChem (Darmstadt, Germany)
20D9h3-ADCs	Own production
20D9h3-LALA-ADC	Own production
Agarose	Carl Roth (Karlsruhe, Germany)
Ampicillin sodium salt	Sigma-Aldrich (St. Louis, MO, USA)
Annexin V Binding Buffer, 10X concentrate	BD Biosciences (Franklin Lakes, USA)
APC Annexin V	BD Biosciences (Franklin Lakes, USA)
Aphidicolin	Sigma-Aldrich (St. Louis, MO, USA)
AttoPhos AP fluorescent substrate system	Promega (Madison, WI, USA)
Beta-Mercaptoethanol	Sigma-Aldrich (St. Louis, MO, USA)
Biocoll solution	Sigma-Aldrich (St. Louis, MO, USA)
Bovine serum albumin (BSA), fraction V, IgG-free, NZ-origin	Carl Roth (Karlsruhe, Germany)
Bradford Protein Assay Dye	Biorad (Hercules, CA, USA)
Calcium chloride 2-hydrate ($CaCl_2 \cdot 2H_2O$)	AppliChem (Darmstadt, Germany)
Ceralasertib (AZD6738)	Sellekchem (Houston, TX, USA)
Carboxylesterase 1c protein, mouse	MedChemExpress (Monmouth Junction, NJ, USA)
Collagen Solution	STEMCELL Technologies (Vancouver, Canada)
Coulter Clenz Cleaning Agent	Beckman Coulter (Krefeld, Germany)
Coulter Isoton II Diluent	Beckman Coulter (Krefeld, Germany)
DAPI (4′,6-Diamidin-2-phenylindol)	Sigma-Aldrich (St. Louis, MO,USA)
DEPC-treated water	Thermo Fisher Scientific (Waltham, MA, USA)
DH5α competent bacteria	Thermo Fisher Scientific (Waltham, MA, USA)
Dimethyl sulfoxide (DMSO)	Sigma-Aldrich (St. Louis, MO,USA)
Disodium hydrogen phosphate (Na_2HPO_4)	Carl Roth (Karlsruhe, Germany)
Duocarmycin	MedChemExpress (Monmouth Junction, NJ, USA)
EcoRI	New England Biolabs (Frankfurt, Germany)
Ethanol	Merck Millipore (Darmstadt, Germany)
Ethanol, absolute	Sigma-Aldrich (St. Louis, MO, USA)
Ethylene glycol-bis(β-aminoethyl ether)-N,N,N′,N′-tetraacetic acid (EGTA)	Carl Roth (Karlsruhe, Germany)
Exatecan	MedChemExpress (Monmouth Junction, NJ, USA)
Glycerol	AppliChem (Darmstadt, Germany)
Glycine	Sigma-Aldrich (St. Louis, MO,USA)
HBS 2x	Sigma-Aldrich (St. Louis, MO,USA)
Human serum	PAN-Biotech (Aidenbach, Germany)
Hydrochloric acid (HCl)	Carl Roth (Karlsruhe, Germany)
4-(2-hydroxyethyl)-1-piperazineethanesulfonic acid (HEPES)	AppliChem (Darmstadt, Germany)
Laemmli sample buffer 2x	Biorad (Hercules, CA, USA)
LB-agar (Lennox)	Carl Roth (Karlsruhe, Germany)
LB-medium	Carl Roth (Karlsruhe, Germany)

Magnesium chloride 6-hydrate	AppliChem (Darmstadt, Germany)
Methanol	Carl Roth (Karlsruhe, Germany)
Milk powder (for blotting)	Carl Roth (Karlsruhe, Germany)
Monomethyl auristatin E	MedChemExpress (Monmouth Junction, NJ, USA)
Monomethyl auristatin F	MedChemExpress (Monmouth Junction, NJ, USA)
Novex Wedgewell 4-20%, Tris-Glycin,1,0 mm, Mini-Protein-Gel,10 or 12 Wells	Thermo Fisher Scientific (Waltham, MA, USA)
O'GeneRuler 1 kb Plus DNA ladder	Thermo Fisher Scientific (Waltham, MA, USA)
Orange DNA loading dye (6x)	Thermo Fisher Scientific (Waltham, MA, USA)
PBS Dulbecco w/o Mg^{2+}, Ca^{2+}	PAN-Biotech (Aidenbach, Germany)
Pierce ECL Plus Western Blotting Substrate	Thermo Fisher Scientific (Waltham, MA, USA)
PNGase F solution	Promega (Madison, WI, USA)
Polybrene	Sigma-Aldrich (St. Louis, MO, USA)
Potassium chloride (KCL)	AppliChem (Darmstadt, Germany)
Pre-diluted BGG Protein Assay Standard	Thermo Fisher Scientific (Waltham, MA, USA)
Propidium iodide solution	Sigma-Aldrich (St. Louis, MO, USA)
Protease inhibitor cocktail (100x)	Cell Signaling Technology (Danvers, MA, USA)
Resazurin sodium salt	Sigma-Aldrich (St. Louis, MO, USA)
Restore™ PLUS Western Blot Stripping buffer	Thermo Fisher Scientific (Waltham, MA, USA)
RNase A	Thermo Fisher Scientific (Waltham, MA, USA)
RNase AWAY	Thermo Fisher Scientific (Waltham, MA, USA)
S.O.C. Medium	Thermo Fisher Scientific (Waltham, MA, USA)
Sodium azide (NaN_3)	Carl Roth (Karlsruhe, Germany)
Sodium chloride (NaCl)	Carl Roth (Karlsruhe, Germany)
Sodium citrate ($C_6H_5Na_3O_7$)	Sigma-Aldrich (St. Louis, MO, USA)
Sodium dihydrogen phosphate (NaH_2PO_4)	Carl Roth (Karlsruhe, Germany)
Sodium dodecyl sulfate (SDS)	Sigma-Aldrich (St. Louis, MO, USA)
Sodium fluoride (NaF)	Sigma-Aldrich (St. Louis, MO, USA)
Sodium orthovanadate (Na_3VO_4)	Sigma-Aldrich (St. Louis, MO, USA)
Sodium pyrophosphate decahydrate ($Na_4P_2O_7x10H_2O$)	Sigma-Aldrich (St. Louis, MO, USA)
Spectra™ Multicolor Broad Range Protein Ladder	Thermo Fisher Scientific (Waltham, MA, USA)
Stellar™ competent cells	Takara (Kyoto, Japan)
Sulphuric acid (H_2SO_4)	Sigma-Aldrich (St. Louis, MO, USA)
SYBR Safe DNA gel stain	Thermo Fisher Scientific (Waltham, MA, USA)
TAE Buffer 10x	Apotheke LMU Klinikum (Munich, Germany)
TBS Buffer 10x	Apotheke LMU Klinikum (Munich, Germany)
Tris(2-Carboxyethyl)phosphine (TCEP)	Merck Millipore (Darmstadt, Germany)
Tris-(hydroxymethyl)-aminomethan (TRIS)	Carl Roth (Karlsruhe, Germany)
Triton X-100	Sigma-Aldrich (St. Louis, MO, USA)
Trypan Blue	Sigma-Aldrich (St. Louis, MO, USA)
Tween 20	Sigma-Aldrich (St. Louis, MO, USA)
Ultra TMB-ELISA substrate solution	Thermo Fisher Scientific (Waltham, MA, USA)
Vc-*seco*-DUBA	MedChemExpress (Monmouth Junction, NJ, USA)
Venetoclax (ABT-199)	MedChemExpress (Monmouth Junction, NJ, USA)
XhoI	New England Biolabs (Frankfurt, Germany)

2.1.2 Media and cytokines

Table 3: List of used media, supplements and antibiotics for cell culture.

name	supplier	catalogue number
Advanced RPMI 1640	Thermo Fisher Scientific (Waltham, MA, USA)	12633020
Alpha MEM with Nucleosides	STEMCELL Technologies (Vancouver, Canada)	36450
BIT 9500 Serum Substitute	STEMCELL Technologies (Vancouver, Canada)	09500
BM cyclin	Merck (Darmstadt, Germany)	10799050001
DMEM, high glucose	Thermo Fisher Scientific (Waltham, MA, USA)	11965092
DNAse I	Merck (Darmstadt, Germany)	04536282001
DPBS, w/o: Ca and Mg	PAN-Biotech (Aidenbach, Germany)	P04-36500
Fetal bovine serum (FBS)	PAN-Biotech (Aidenbach, Germany)	P30-3306
Geneticin™	Thermo Fisher Scientific (Waltham, MA, USA)	10131035
GlutaMAX™ Supplement	Thermo Fisher Scientific (Waltham, MA, USA)	35050061
HBSS, Modified (Without Ca++ and Mg++)	STEMCELL Technologies (Vancouver, Canada)	37250
Hydrocortisone	STEMCELL Technologies (Vancouver, Canada)	74142
Iscove's MDM with 2% FBS	STEMCELL Technologies (Vancouver, Canada)	07700
Iscove's Modified Dulbecco's Medium	STEMCELL Technologies (Vancouver, Canada)	36150
L-Glutamine	STEMCELL Technologies (Vancouver, Canada)	
MethoCult™ H4034 Optimum	STEMCELL Technologies (Vancouver, Canada)	04034
MethoCult™ H4330	STEMCELL Technologies (Vancouver, Canada)	04330
MyeloCult™ H5100	STEMCELL Technologies (Vancouver, Canada)	05150
Penicillin-Streptomycin (10.000 U/ml Penicillin, 10 mg/ml Streptomycin)	PAN-Biotech (Aidenbach, Germany)	P06-07050
RPMI 1640, GlutaMAX™ supplement	Thermo Fisher Scientific (Waltham, MA, USA)	61870044
StemMACS™ HSC-CFU Media complete with EPO, human	Miltenyi Biotec (Bergisch Gladbach, Germany)	130-091-280
StemPro™-34 SFM	Thermo Fisher Scientific (Waltham, MA, USA)	10639011
Sterile water, for cell culture	PAN-Biotech (Aidenbach, Germany)	P04-991000
Trypsin-EDTA (0.25%)	Thermo Fisher Scientific (Waltham, MA, USA)	25200056

Table 4: Used cytokines and recombinant proteins.

name	species	application	supplier	catalogue number
EPO	human	Colony assays, healthy BM cell cultivation	ImmunoTools	11344795
FLT3	human	ELISA	Sino biologics	10445-H08H
FLT3L	human	PDX cell cultivation	R&D Systems	308-FKN-100
G-CSF	human	Colony assays, healthy BM cell cultivation	ImmunoTools	11343123
GM-CSF	human	Colony assays, healthy BM cell cultivation	ImmunoTools	11343133
IL-3	human	Colony assays, PDX and healthy BM cell cultivation	ImmunoTools	11340033
IL-3	mouse	Ba/F3 cell culture	ImmunoTools	12340035
IL-6	human	Colony assays, healthy BM cell cultivation	ImmunoTools	11340064
SCF	human	Colony assays, PDX and healthy BM cell cultivation	ImmunoTools	11343325
TPO	human	PDX cell cultivation	Peprotech	300-18-100

2.1.3 Kits and buffers

Table 5: List of used kits.

kit	application	supplier
Bovine Gamma Globulin Standard Pre-Diluted Set	Determination of protein/ADC concentration	Thermo Fisher Scientific (Waltham, MA, USA)
CD34 MicroBead kit, human	Enrichment of CD34-positive HSPCs from bone marrow	Miltenyi Biotec (Bergisch Gladbach, Germany)
CellTiter-Glo 3D Cell Viability Assay	Cytotoxicity assays	Promega (Madison, WI, USA)
CloneAmp™ HiFi PCR Premix	High-fidelity fast PCR, used with In-fusion cloning	Takara (Kyoto, Japan)
Dead cell removal kit	Remove dead PDX cells after thawing	Miltenyi Biotec (Bergisch Gladbach, Germany)
Endofree Plasmid Maxi Kit	Purification of plasmid-DNA (up to 10 mg)	Qiagen (Hilden, Germany)
ExpiCHO™ Expression System Kit	mAb production	Thermo Fisher Scientific (Waltham, MA, USA)
In-Fusion Snap Assembly Master Mix with Competent Cells	Cloning of PCR fragments into linearized vectors	Takara (Kyoto, Japan)

LIVE/DEAD™ Fixable Aqua Dead Cell Stain Kit, 405 nm	Live-dead stain for flow cytometry	Thermo Fisher Scientific (Waltham, MA, USA)
Mouse Cell Depletion Kit	Removal of mouse cells from PDX samples after isolation from spleen/BM of NSG mice	Miltenyi Biotec (Bergisch Gladbach, Germany)
pHrodo Deep Red antibody labelling kit	Labelling of anti-human IgG1 with pHrodo dye	Thermo Fisher Scientific (Waltham, MA, USA)
QIAamp DNA Blood Mini Kit	gDNA isolation from cell lines for cell line authentication	Qiagen (Hilden, Germany)
QIAprep Spin Miniprep Kit	Purification of plasmid-DNA (up to 20 µg)	Qiagen (Hilden, Germany)
QIAquick Gel Extraction Kit	Agarose gel extraction (up to 10 µg DNA)	Qiagen (Hilden, Germany)
QIAquick PCR Purification Kit	Purification of PCR products (up to 10 µg)	
QuikChange II XL Site-Directed Mutagenesis Kit	Introduction of site-specific mutations into double-stranded plasmid DNA	Agilent (Santa Clara, CA, USA)
Rapid Gold BCA Protein Assay	Determination of protein/ADC concentration	Thermo Fisher Scientific (Waltham, MA, USA)

Table 6: List of used buffers and their composition.

buffer	**components**
Agarose gels (0.8 % - 1.5 %)	0.8-1.5 % agarose in 1x TAE buffer with SYBR Safe (1:10,000)
Annexin binding buffer 1x	10x Annexin binding buffer 1:10 diluted in d_2H_2O
A-SEC phosphate buffer, pH 7 (A-SEC, Dr. Marc-André Kasper, Tubulis)	20 mM Na_2HPO_4/NaH_2PO_4, 300 mM NaCl, 5% v/v isopropyl alcohol
Blocking buffer (ELISA)	PBS-T, 0.5% BSA IgG-free
Blocking solution (Western Blot)	TBS-T, 5% milk powder or TBS-T, 5% BSA IgG-free (for phospho-proteins)
Calciumchlorid	2 M $CaCl_2$, sterile filtered
Electrophoresis buffer 10x (Western Blot)	151.4 g Tris, 720.7 g glycin, 50 g sodium dodecyl sulfate → Add up to 5 l with d_2H_20
FACS buffer	PBS, 2% FBS
Freezing buffer	FBS, 10% DMSO
KCM 5x	500 mM KCL, 150 mM $CaCl_2$ 250 mM $MgCl_2$
LB agar plates	35 g LB-agar, add up to 1 l d_2H_20, autoclave → 20 ml were added per 10 cm Petri dish → after solidification: mix 40 µl 100 µg/ml ampicillin and 60 µl SOC medium and distribute on each plate
LB medium	20 g LB-medium, add up to 1 l d_2H_20, autoclave
Lysis buffer (Western Blot)	25 ml 1 M HEPES (pH 7.5), 15 ml 5 M NaCl, 2.5 ml 200 mM EGTA, 100 ml 50% glycerol, 5 ml Triton X-100, 2.1 g NaF, 2.2 g $Na_4P_2O_7x10H_2O$ → Add up to 0.5 l with d_2H_20
mAb binding buffer pH 7.5 (antibody purification, Jonathan Schwach, LMU)	20 mM NaH_2PO_4, 50 mM NaCl, 1 mM EDTA, sterile filtered
mAb elution buffer pH 3.0 (antibody purification, Jonathan Schwach, LMU)	100 mM sodium citrate, sterile filtered

mAb neutralization buffer pH 9.0 (antibody purification, Jonathan Schwach, LMU)	1 M Tris-HCl, sterile filtered
mAb storage buffer pH 7.3	100 mM L-arginine in PBS, sterile filtered
P5-conjugation buffer pH 8.3 (MMAF-conjugation, Dr. Marc-André Kasper, Tubulis GmbH)	50 mM Tris, 1 mM EDTA, 100 mM NaCl
PBS-T (Washing buffer for ELISA)	PBS, 0.05% Tween 20
Phosphate buffer pH 7.0 (analytical SEC, Dr. Marc-André Kasper, Tubulis GmbH)	20 mM Na_2HPO_4/NaH_2PO_4, 300 mM NaCl, 5% v/v isopropyl alcohol as a mobile phase
Propidium iodide buffer pH 8.0 (cell cycle analysis)	10 ml PI solution (1 mg/ml), 500 mg sodium citrate, 500 µl Triton X-100, 500 ml d_2H_2O
TAE, 10x	242.3 g Tris, 18.61 g Na_2H_2EDTA, 59.85 g HCl → add up to 5 l with d_2H_2O
TBS 10x, pH 8.0	60.57 g Tris, 483.3 g sodium chloride → add up to 5 l with d_2H_2O
TBS-T (Western Blot)	100 ml TBS (10x), 900 ml d_2H_2O, 1% Tween 20
Transfer buffer (Western Blot)	15 g Tris, 71 g glycine, 790 g methanol → add up to 5 l with d_2H_2O

2.1.4 Consumables, laboratory equipment and software

Table 7: List of consumables.

name	supplier
µ-slide 8 Well high Glass Bottom	Ibidi (Gräfelfing, Germany)
3cc syringes	STEMCELL Technologies (Vancouver, Canada)
Acquity UPLC Protein BEH C4 Column, 300 Å, 1.7 µm, 2.1 mm x 50 mm	Waters Corporation (Milford, MA, USA)
Amicon® Ultra 0.5/2 ml Centrifugal Filters	Merck (Darmstadt, Germany)
Blunt-end needles, 16 gauge	STEMCELL Technologies (Vancouver, Canada)
Cell scraper, 25 cm	Greiner Bio One (Frickenhausen, Germany)
Combitips advanced (1 ml, 5 ml, 10 ml)	Eppendorf (Hamburg, Germany)
Cryo Tube Vial	Sarstedt (Numbrecht, Germany)
Cuvettes, macro and halfmicro, PMMA	Brand (Wertheim, Germany)
Deepwell Plate 96/1000 µl	Eppendorf (Hamburg, Germany)
Diamond Tower Pack (D10, D200, D1000)	Gilson (Middleton, WI, USA)
Disposable bags	Brand (Wertheim, Germany)
EASYstrainer 40 µm, 70 µm	Carl Roth (Karlsruhe, Germany)
epT.I.P.S Reloads 2-200 µl, 50-1000 µl	Eppendorf (Hamburg, Germany)
Gel-loading pipet tips	Thermo Fisher Scientific (Waltham, MA, USA)
HiTrap MabSelect SuRe	Cytiva (Marlborough, MA, USA)
MabPac HIC Butyl 4.6 x 100 mm column	Thermo Fisher Scientific (Waltham, MA, USA)
MAbPac SEC-1 300 Å, 4 x 300 mm column	Thermo Fisher Scientific (Waltham, MA, USA)
Microplate 96-well, F-bottom black, MaxiSorp	Thermo Fisher Scientific (Waltham, MA, USA)
Mr. Frosty™ Freezing Container	Thermo Fisher Scientific (Waltham, MA, USA)
Neubauer Counting Chamber	Paul Marienfeld GmbH & Co. KG (Lauda Königshofen, Germany)
Novex Empty Gel Cassette, 1.0 mm	Thermo Fisher Scientific (Waltham, MA,USA)

Nunc™ multidish 48wp	Thermo Fisher Scientific (Waltham, MA,USA)
OPS™ essential drapes	Medline (Northfield, IL, USA)
Parafilm	Sigma-Aldrich (St. Louis, MO, USA)
Purple Nitril Gloves	Halyard Health (Alpharetta, GA, USA)
Reagent reservoirs, 50 ml	Heathrow Scientific (Vernon Hills, IL, USA)
Safe-Lock Tubes (1.5 ml, 1.5 ml brown, 2 ml)	Eppendorf (Hamburg, Germany)
Serological pipettes (2 ml, 5 ml, 10 ml , 25 ml)	Sarstedt (Numbrecht, Germany)
SmartDish™ 6-well plates	STEMCELL Technologies (Vancouver, Canada)
Square 245 mm Bio-Assay trays	Corning (Corning, NY, USA)
STEMgrid™-6 counting grid	STEMCELL Technologies (Vancouver, Canada)
Superdex™ 200 Increase 10/300GL	Cytiva (Marlborough, MA, USA)
TC Flask T25, T75, T175, suspension	Sarstedt (Numbrecht, Germany)
TC Plate 6-well - 96-well, suspension	Sarstedt (Numbrecht, Germany)
TC-treated culture dish 35 mm	Corning (Corning, NY, USA)
Transfer membrane PVDF 0.45, 375×30 cm	Carl Roth (Karlsruhe, Germany)
Tube 5 ml, 75x12 mm (for FACS)	Sarstedt (Numbrecht, Germany)
Tube 15 ml, 120x17 mm	Sarstedt (Numbrecht, Germany)
Tube 50 ml, 114x28 mm	Sarstedt (Numbrecht, Germany)
U-bottom plate, 96-well	Sarstedt (Numbrecht, Germany)
Ultrafree-MC, GV 0,22 µm, steril, centrifugal filters	Merck (Darmstadt, Germany)
Vanquish™ Flex UHPLC-System	Thermo Fisher Scientific (Waltham, MA,USA)
Vasco Nitrile Blue Gloves	B. Braun (Melsungen, Germany)
V-bottom plate, 96-well	Sarstedt (Numbrecht, Germany)
Zeba Spin Desalting Columns	Thermo Fisher Scientific (Waltham, MA,USA)

Table 8: List of laboratory equipment.

device	supplier
Acquity UPLC H-Class PLUS System	Waters Corporation (Milford, MA, USA)
Äkta pure FPLC system	GE Healthcare (Chicago, IL, USA)
Äkta pure™ chromatography system	Cytiva (Marlborough, MA, USA)
Analytical balance ABJ 220-4NM	Kern & Sohn (Balingen-Frommern, Germany)
BioPhotometer	Eppendorf (Hamburg, Germany)
Biorad Mini Protean Tetra system	Biorad (Hercules, CA, USA)
Centrifuge 5424R, 5430	Eppendorf (Hamburg, Germany)
CO_2 incubator CB210	BINDER (Tuttlingen, Germany)
DeNovix DS-11+ spectrophotometer	DeNovix (Wilmington, DE, USA)
E-BOX VX2	Vilber Lourmat (Eberhardzell, Germany)
Flow Cytometer Canto II	BD Biosciences (Franklin Lakes, USA)
Fluorescent microscope DMi8	Leica Microsystems (Wetzlar, Germany)
Freezer -20 °C	Liebherr (Bulle FR, Switzerland)
Freezer -80 °C, TLE	Thermo Fisher Scientific (Waltham, MA, USA)
Fusion SL4 imaging system	Vilber Lourmat (Eberhardzell, Germany)
Heating block Thermomixer compact	Eppendorf (Hamburg, Germany)
Heraeus Megafuge 40R, X10R	Thermo Fisher Scientific (Waltham, MA, USA)
High precision scale PCB 2500-2	Kern & Sohn (Balingen-Frommern, Germany)
Ice machine FM-170AKE	Hoshizaki (Amsterdam, NL)
Inverted microscope AE2000	Motic (Hong Kong, China)
Liquid nitrogen tank	Cryoson (Schollkrippen, Germany)
Magnetic stirrer MR3001	Heidolph (Schwabach, Germany)

Microplate reader GloMax® Discover	Promega (Madison, WI, USA)
Microscope Keyence BZ-X810	Keyence (Osaka, Japan)
Microscope ZEISS Primovert	Carl Zeiss (Oberkochen, Germany)
Multichannel pipettes Research Pro	Eppendorf (Hamburg, Germany)
Multipette E3X	Eppendorf (Hamburg, Germany)
Multitron incubation shaker	Infors HAT (Basel, Switzerland)
NanoDrop spectrophotometer 1000	Thermo Fisher Scientific (Waltham, MA, USA)
PCR cycler PeqSTAR 2x Gradient	Peqlab (Wilmington, DE, USA)
Pipetus accu-jet pro	Brand (Wertheim, Germany)
PowerPac 300 electrophoresis power supply	Biorad (Hercules, CA, USA)
Research Plus Pipettes (0.1-2.5 µl, 2-20 µl, 20-200 µl, 100-1000 µl)	Eppendorf (Hamburg, Germany)
Roll mixer Start SRT6	Merck (Darmstadt, Germany)
Tecan Infinite 200 PRO microplate reader	Tecan Group (Männedorf, Switzerland)
Thermomixer compact	Eppendorf (Hamburg, Germany)
Ultrapure water system Milli-Q System	Merck Millipore (Darmstadt, Germany)
Vertical Autoclave VX-150, VX-95	Systec (Linden, Germany)
Vi-CELL™ XR Cell Viability Analyzer	Beckman Coulter (Krefeld, Germany)
Vortexer Genie II	Scientific Industries (Bohemia, NY, USA)
Water Bath Type 1003	GFL (Burgwedel, Germany)
Water Bath Hydro H16	Lauda (Lauda-Königshofen, Germany)
Waters XEVO G2-XS QTof	Waters Corporation (Milford, MA, USA)
Xcell SureLock Mini Cell for SDS gel electrophoresis	Invitrogen (Darmstadt, Germany)

Table 9: List of used software applications.

software	application	supplier
Benchling	Sequence alignment	Benchling (San Francisco, CA, USA)
Biorender	Design of biological schemes and illustrations	Biorender AG (Munchwilen TG, CH)
BZ-X810 Analyzer software	Analysis and processing of microscopy images	Keyence (Osaka, Japan)
CLASTR 1.4.4 online tool	Cell line authentication	Swiss Institute of Bioinformatics (Lausanne, Switzerland)
E-Capt 15.06	Agarose gel imaging	Vilber Lourmat (Eberhardzell, Germany)
Ensembl Release 109	Genome browser	EMBL-EBI (Cambridge, UK)
FlowJo™ v10.8.1	Analysis of flow cytometry data	BD Biosciences (Franklin Lakes, USA)
FusionCapt Advance 16.11	Western Blot imaging	Vilber Lourmat (Eberhardzell, Germany)
GraphPad Prism 10.1.2	Data analysis, statistics and blotting	GraphPad Software (La Jolla, CA, USA)
MaxEnt 1	Analysis of MS data	Waters Corporation (Milford, MA, USA)
Microsoft Office 2016	Data analysis, figure design, writing	Microsoft (Redmond, WA, USA)
SnapGene 6.0.6	Primer design, vector maps	GSL Biotech LLC (Boston, MA, USA)

SynergyFinder web application (version 3.0)	Interactive analysis of drug combination data, calculation of synergy scores	Institute for Molecular Medicine Finland (FIMM), HiLIFE, University of Helsinki, Finland
Vast+ NCBI online tool	Identification of similar protein 3D structures	NCBI (Bethesda, MD, USA)

2.1.5 Antibodies

Table 10: List of used commercial antibodies: Western Blot

target	species of origin	clonality and isotype	protein size	supplier	catalogue number
Primary antibodies					
β-Actin	mouse	monoclonal IgG1	42 kDa	Merck	A5441
ATR (C-1)	mouse	monoclonal IgG1 κ	250 kDa	Santa Cruz Biotechnology	sc-515173
Chk1 (2G1D5)	mouse	monoclonal IgG1	56 kDa	Cell Signaling	2360S
FLT3	rabbit	polyclonal IgG	160/130 kDa.	Santa Cruz Biotechnology	sc-340
p53	mouse	monoclonal IgG2b	53 kDa	Cell Signaling	48818
Phospho-ATR(Thr1989)	rabbit	polyclonal IgG	250 kDa	Genetex	GTX128145-25
Phospho-Chk1(Ser345)	rabbit	monoclonal IgG	56 kDa	Cell Signaling	2348T
Secondary antibodies					
Mouse anti-rabbit IgG-HRP	mouse	monoclonal IgG1	-	Santa Cruz Biotechnology	sc-2357
m-IgGκ BP-HRP	-	-	-	Santa Cruz Biotechnology	sc-516102

Table 11: List of used commercial antibodies: Flow cytometry and ELISA

antibody name	fluorophore / Conjugate	supplier	catalogue number (clone)
Anti-duocarmycin (human IgG1 backbone)	Unconjugated	In-house production	patent WO2016046173A1 (B6-2-10)
Goat F(ab')2 anti-human IgG	Alexa Fluor 647	Southern Biotech	2042-31

Mouse anti-human CD64 (FcγRI)	PE	BD Biosciences	558592 (10.1)
Mouse anti-human CD117 (c-kit)	Alexa Fluor 647	Biolegend	313235 (104D2)
Mouse anti-human CD135 (FLT3)	Alexa Fluor 647	BD Biosciences	563494 (4G8)
Mouse anti-human CD140a (PDGFRα)	Alexa Fluor 647	BD Biosciences	562798 (αR1)
Mouse anti-human CD309 (VEGFR-2)	Alexa Fluor 647	BD Biosciences	560871 (89106)
Mouse anti-human IgG Fc specific antibody	Unconjugated	Sigma-Aldrich	I6260 (GG-7)
Mouse IgG1 κ isotype control	Alexa Fluor 647	BD Biosciences	565571 (MOPC-21)
Mouse IgG1 κ isotype control	PE	BD Biosciences	555749 (MOPC-21)
Mouse IgG2a κ isotype control	Alexa Fluor 647	BD Biosciences	557715 (G155-178)
Rabbit Anti-MMAF pAb	Unconjugated	Levena	LEV-PAF1-100
Rat anti-human CD115 (CSF1-R)	Alexa Fluor 647	BD Biosciences	564945 (9-4D2-14)
Rat IgG1 κ isotype control	Alexa Fluor 647	BD Biosciences	557731 (R3-34)
Secondary anti-human IgG	Alexa Fluor 647	Southern Biotech	2015-31
Secondary goat anti-human kappa light chain	HRP	Thermo Fisher Scientific	A18853
Secondary goat anti-human IgG	In-house conjugation	Jackson ImmunoResearch	109-005-008
Secondary	Alkaline phosphatase	Jackson ImmunoResearch	309-055-008

Table 12: List of used experimental antibodies.

name	type of antibody	supplier
20D9	Chimerized IgG1 anti-human FLT3	In-house production
20D9h1	Humanized IgG1 anti-human FLT3	In-house production
20D9h2	Humanized IgG1 anti-human FLT3	In-house production
20D9h3	Humanized IgG1 anti-human FLT3	In-house production
20D9h3-LALA	Humanized IgG1 anti-human FLT3 with engineered Fc (Leu234Ala, Leu235Ala)	In-house production

20D9h4	Humanized IgG1 anti-human FLT3	In-house production
20D9h5	Humanized IgG1 anti-human FLT3	In-house production
20D9h6	Humanized IgG1 anti-human FLT3	In-house production
20D9h7	Humanized IgG1 anti-human FLT3	In-house production
20D9h8	Humanized IgG1 anti-human FLT3	In-house production
20D9h9	Humanized IgG1 anti-human FLT3	In-house production
20D9h10	Humanized IgG1 anti-human FLT3	In-house production
20D9h11	Humanized IgG1 anti-human FLT3	In-house production
20D9h12	Humanized IgG1 anti-human FLT3	In-house production
20D9h13	Humanized IgG1 anti-human FLT3	In-house production
20D9h14	Humanized IgG1 anti-human FLT3	In-house production
20D9h15	Humanized IgG1 anti-human FLT3	In-house production
20D9h16	Humanized IgG1 anti-human FLT3	In-house production
IgG1	Synagis, Palivizumab IgG1 anti-RSV	AbbVie (404770)
IgG1-LALA	Synagis, Palivizumab IgG1 anti-RSV	In-house production

2.1.6 Plasmids and primers

Table 13: List of used plasmids.

plasmid name	application	supplier
pCDH-EF1a-eFFly-mCherry	Lentiviral expression vector	Addgene (104833, Watertown, MA, USA)
pMIY-FLT3 NPOS F691I	Retroviral expression vector	This work
pMIY-FLT3 NPOS F691L	Retroviral expression vector	This work
pMIY-rat FLT3	Retroviral expression vector	This work
pRP[Exp]-CAG>rFlt3	Cloning of rat FLT3	VectorBuilder (Chicago, IL, USA)

Table 14: List of used primers. All primers were ordered at metabion (Planegg, Germany).

primer name	5' → 3' sequence	application
hFLT3-F691I for	CAC CAT AGC AAC AGT ATT CAA TAA TCA AGT AAA TTG GTC CTG AC	Mutagenesis
hFLT3-F691I rev	GTC AGG ACC AAT TTA CTT GAT TAT TGA ATA CTG TTG CTA TGG TG	Mutagenesis
hFLT3-F691L for	CCA TAG CAA CAG TAT TCT AAA ATC AAG TAA ATT GGT CCT GAC AGT GT	Mutagenesis
hFLT3-F691L rev	ACA CTG TCA GGA CCA ATT TAC TTG ATT TTA GAA TAC TGT TGC TAT GG	Mutagenesis
pMIY-hFLT3 For1	CATCAGTGGGGAAGTCATC	Sequencing
pMIY-hFLT3 Rev1	TGTCATTTTCAAAATGACCATGGAAACAACT	Sequencing

pMIY-hFLT3 For2	GAGAGCGTTCCAGAGCCGATC	Sequencing
pMIY-hFLT3 For3	GCCTACCCACAAATCAGATG	Sequencing
pMIY-hFLT3 For4	CTCATTCTATGCAACAATTGG	Sequencing
pMIY-hFLT3 For5	CCTGGTTCAAGAGAAGTTCAG	Sequencing
pMIY-hFLT3 For6	GGATTGGCTCGAGATATCATG	Sequencing
pMIY-hFLT3 For7	GCAATCCTGCTGGGCTTTTGAC	Sequencing
pMIY-rFLT3 For1	CTA ACA TCG TGA CCT GGG AAG	Sequencing
pMIY-rFLT3 For2	CAG CTG TAC GTG CTA AGA AGA CC	Sequencing
pMIY-rFLT3 For3	CGT ACC CAC AAA TCC GAT G	Sequencing
pMIY-rFLT3 For4	CCC TGG ATA ACG AGT ACT TCT AC	Sequencing
pMIY-rFLT3 For5	TTC CTG GAG TTC AAG TCG TG	Sequencing
rFLT3 for	CTA GGC GCC GGA ATT CAT GCG GGC GTT GGC GCG	Cloning
rFLT3 rev	TCG AGT TTT TCT CGA GCT AAC TTC TTT CTC TGT GAG TCT TCT CCT	Cloning

2.1.7 Biological material

Table 15: List of used cell lines. ExpiCHO-S cells were purchased from Thermo Fisher Scientific (Waltham, MA, USA), M2-10B4 cells, MV4-11 cells and Phoenix-Eco cells from ATCC (Manassas, VA, USA) and SLSL-J-IL3-neo from Terry Fox laboratory (Vancouver, Canada). All other cell lines were purchased from DSMZ (Braunschweig, Germany). AML = acute myeloid leukemia; CML = chronic myeloid leukemia; FBS = fetal bovine serum; f = female; m = male; P/S = Penicillin-Streptomycin

name	cell type	gender	human FLT3 expression	culture medium
Ba/F3	Murine pro B cells	-	no	RPMI, 1% P/S, 10% FBS, 10 ng/ml IL-3
ExpiCHO-S	Protein expression system	-	-	ExpiCHO expression medium (Thermo Fisher Scientific, A29133)
HL-60	Human AML	f	no	RPMI, 1% P/S, 10% FBS
K-562	Human CML in blast crisis	f	no	RPMI, 1% P/S, 10% FBS
M2-10B4	Murine fibroblast cell line	-	-	RPMI, 10% FBS, 0.4 mg/ml Geneticin
MM-6	Human acute monocytic leukemia	m	yes	Advanced RPMI, 1% P/S, 5% FBS, 2 mM GlutaMAX
MOLM-13	Human AML	m	yes	RPMI, 1% P/S, 20% FBS
MV4-11	Human acute monocytic leukemia	m	yes	RPMI, 1% P/S, 10% FBS

OCI-AML3	Human AML	m	yes	RPMI, 1% P/S, 10% FBS
Phoenix-Eco	Embryonic kidney	f	-	DMEM, 1% P/S, 10% FBS
SLSL-J-IL3-neo	Murine fibroblast cell line	-	-	DMEM, 15% FBS, 0.8 mg/ml Geneticin

Table 16: Characteristics of bone marrow cell donors for CFU and LTC-IC assays. Bone marrow cells for CFU assays were isolated by Dr. Marit Leilich (MRI). Bone marrow cells for LTC-IC assays were purchased from Stem cell technologies. f = female; m = male

	age (years)	sex	ethnicity	weight (kg)	donor number*
			CFU assay		
donor 1	63	f			
donor 2	61	f			
donor 3	76	m			
donor 4	63	m			
donor 5	81	m			
			LTC-IC assay		
donor 1	25	f	african american	90	CE0009389
donor 2	55	m	asian	66	CE0006429
donor 3	23	f	african american	66	CE0009455

**StemCell Technologies catalogue number: 70002.1*

Table 17: Characteristics of *KMT2A*-rearranged AML PDX samples used for stem cell assays. ID = initial diagnosis; R1 = first relapse; R2 = second relapse; f = female; m = male.

sample	disease stage	age (years)	sex	cytogenetics	mutations panel seq[128]	references
AML-388	ID	57	m	*KMT2A*::*AFDN*	*KRAS*^{Q61H}	(129-131)
AML-393	R1	47	f	ins(10;11)(p12;q23q23) *KMT2A*::*MLLT10*	*KRAS*^{G12A}, *BCOR*^{1012del}	(129-135)
AML-579	R	51	m	normal	*DNMT3A*^{R882C}, *DNMT3A*^{F868L}, *NPM1*^{L287fs}, *FLT3-ITD*, *IDH1*^{R132H}	(130, 134-137)
AML-669	R2	49	f	*KMT2A*::*MLLT3*	*KRAS*^{G13D}	(129)

2.2 Methods

2.2.1 Cell biological methods

2.2.1.1 Cell collection and cultivation

Suspension cells

MV4-11 cells were purchased from ATCC (Manassas, VA, USA), all other suspension cell lines were purchased from DSMZ (Braunschweig, Germany). All human leukemia cell lines were cultivated in RPMI + 10% FBS + 1% P/S except MOLM-13 (RPMI + 20% FBS + 1% P/S). IL-3 dependent Ba/F3 cells were cultivated in RPMI + 10% FBS + 1% P/S + 10 ng/ml IL-3, except those that express *FLT3*-ITD constructs as these mutations allow the cells to grow independent of IL-3. Cells were cultivated in T25 flasks unless larger amounts were needed, then cells were cultivated in T75 flasks. Cells were continually kept at 37 °C, 5% CO_2 in a cell culture incubator. Viability and cell density was assessed every 2-3 days using Vi-CELL XR Cell Viability Analyzer and cells were then subcultured according to the DSMZ recommendations.

Adherent cells

ExpiCHO-S cells were purchased from Thermo Fisher Scientific (Waltham, MA, USA), M2-10B4 cells and Phoenix-ECO cells from ATCC (Manassas, VA, USA) and SLSL-J-IL3-neo from Terry Fox laboratory (Vancouver, Canada). ExpiCHO-S cells were cultivated according to the manufacturer's instructions using the ExpiCHO expression system kit. SLSL-J-IL3-neo and M2-10B4 murine fibroblasts were cultivated in DMEM + 15% FBS + 0.8 mg/ml geneticin and RPMI-1640 + 10% FBS, respectively. Phoenix-ECO cells were cultivated in DMEM + 10% FBS + 1% P/S. For sub-culturing, cells were washed with PBS, and incubated with trypsin-EDTA for 2-3 min at 37 °C to detach the cells. Trypsin reaction was stopped by adding culture medium. Generally, all cells were kept at 37 °C, 5% CO_2 (except CHO cells: 37 °C, 8% CO_2). Cell viability and density was assessed every 2-4 days by trypan blue exclusion count using a Neubauer chamber and cells were subcultured as recommended by the manufacturer when they reached a confluency of about 80-90%.

AML PDX and primary cells

Primary AML cells were collected from patient BM aspirates or peripheral blood at the time of initial diagnosis or follow-up after obtaining written informed consent by the Department of Internal Medicine III of the LMU hospital Munich, Germany. All studies were carried out in compliance with the Helsinki Declaration of 1975, revised in 2013, and written approval was obtained by the responsible committee on human experimentation (Ethikkommission des Klinikums der LMU München, ethikkommission@med.uni-muenchen.de, number 068-08 and 222-10). AML PDX cells were serially transplanted and amplified in 10-26 week-old female or male NOD.Cg-*Prkdc*^{scid} *Il2rg*^{tm1Wjl}/SzJ (NSG, The Jackson Laboratory, Bar Harbour, Maine, USA)

mice and reisolated from spleen or BM, as previously described (132). Animal trials were carried out in accordance with the current ethical standards of the official committee on animal experimentation (written approval by Regierung von Oberbayern, tierversuche@reg-ob.bayern.de, ROB-55.2Vet-2532.Vet 03-21-9). AML PDX and primary cells were cultivated in StemPro-34 medium with nutrient supplement, additionally including 2% FBS, 1% P/S, 1% L-glutamine, 10 ng/ml recombinant human FLT3L, SCF, TPO and IL-3 (DD medium). Nutrient supplement was thawed on ice. Medium was used for a maximum of one month. Cells were kept in T25 flasks or 6-well plates at a density of 1-2x10^6 cells per ml until experiment start and cultured at 37 °C, 5% CO_2. For PDX cells isolated freshly from BM or spleen of donor mice, experiments were started on the same day or the day after isolation. Thawed cells were recovered for 2-7 days until they had a viability of > 70% before the experiments were started.

Healthy CD34-positive bone marrow cells

CD34-positive cells for LTC-IC assays were purchased from STEMCELL Technologies (see Table 16). CD34-positive cells for CFU assays were isolated from femoral heads by Dr. Marit Leilich (TUM): After written informed consent, femoral heads were collected from patients without hematologic disease that underwent hip replacement surgery. This was performed as described previously (138, 139), in accordance with ethical standards for human experimentation of the responsible ethics committee (Ethikkomission an der Technischen Universität München, ethikkommission@mri.tum.de, number 339/21S) and the Helsinki Declaration of 1975, revised in 2013. Briefly, the collected femoral heads were minced and the fragments transferred to PBS-containing tubes. The mixture was shaken and filtered with a 70 µm cell strainer. Biocoll solution was used to isolate mononuclear cells from the mixture and those cells were frozen as described below until use. Before the start of experiments cells were enriched for CD34-expression by magnetic bead separation using the CD34 MicroBead kit according to the manufacturer's instructions. The cultivation of healthy CD34-positive BM cells was performed in IMDM with GlutaMAX including 10% BIT9500, 3 U/ml EPO, 20 ng/ml G-CSF, GM-CSF, IL-3 and IL-6 and also 100 ng/ml SCF and FLT3L at 37 °C, 5% CO_2.

2.2.1.2 Cell freezing and thawing

Cell lines

Cell lines were only frozen at a viability of > 95%. Cells were collected in falcon tubes and washed once with PBS (300xg, 5 min, RT). Subsequently, cells were resuspended at a concentration of 5-10x10^6 cells/ml in FBS + 10% DMSO and transferred to cryovials (1 ml per tube). The vials were frozen using Mr. Frosty filled with 100% isopropanol to ensure a freezing speed of -1 °C/min. On the next day, the vials were transferred to the liquid nitrogen tank.

For thawing cells, the frozen cryovial was transferred to a 37 °C water bath for 1-2 min until only a small amount of ice was left over. Cells were immediately transferred into a falcon tube filled with 2 ml pre-warmed cell culture medium and centrifuged for 5 min at 300xg, at RT. The supernatant was carefully removed to avoid contamination and the cell pellet was resuspended in warm cell culture medium and transferred to a T25 flask. The flask was incubated in an upright position overnight at 37 °C, 5% CO2 before adding another 5 ml of culture medium.

AML PDX and primary cells

Thawing of AML PDX and primary cells was performed according to a protocol by Dominique Bonnet (140). Briefly, cells were rapidly thawed in the water bath at 37 °C. 100 µl DNAse (1 mg/ml) were added dropwise into the cryovial, gently mixed with the cells and incubated for 1 min at RT. Subsequently the cells were transferred to a 50 ml tube, 1 ml pure FBS was carefully added, gently mixed with the cells and incubated for 1 min at RT. Then, 10 ml PBS + 2% FBS was added and the mixture was incubated again for 1 min at RT before slowly adding up to 30 ml with PBS + 2% FBS. Cells were then centrifuged for 5 min at 200xg, at RT, the supernatant was removed, the cells were resuspended in PBS + 2% FBS and filtered through a 30 µm cell strainer to remove cell clumps. Viable cells were counted with the Neubauer chamber using trypan blue exclusion count. Cells were then centrifuged again for 5 min at 200xg, RT, resuspended in culture medium and cultivated until experiment start as described.

For AML PDX cell freezing, the required volume of cell suspension was centrifuged at 300xg for 5 min at RT. The supernatant was removed and the cells resuspended in 0.5 ml cold FBS. 0.5 ml of AML PDX freezing medium (80% FBS + 20% DMSO) was added dropwise over a period of 2 min and the cells were transferred in labelled cryotubes. The cryotubes were placed in the Mr. Frosty filled with 100% isopropanol to ensure a freezing speed of -1 °C/min. On the next day, the vials were transferred to the liquid nitrogen tank.

Healthy CD34-positive BM cells

Cells were thawed in the water bath at 37 °C and immediately transferred to 50 ml falcon tubes. 9 ml BM cell thawing medium (IMDM + 10% FBS + DNAse) were slowly added to the vial. Cells were left alone for 5 min at RT. Subsequently, cells were centrifuged at 350xg for 5 min and resuspended in culture medium. This procedure was carried out by Dr. Marit Leilich (TUM, for CFU assay) or Dr. Xiang Gao (Ulm University, for LTC-IC assay).

2.2.1.3 Quality control in cell culture

Cell line authentication

Cell line authentication was routinely performed for all AML cell lines using the following procedure: $4x10^6$ cells were collected in 15 ml tubes and washed once with PBS (300xg, 5 min,

RT). gDNA was isolated following the instructions of the QIAamp DNA Blood Mini Kit. In the last step, gDNA was eluted in 2 ml tubes using 150 µl of elution buffer (provided in the kit). gDNA concentration was measured with DeNovix DS-11+ spectrophotometer. If the quality was appropriate (260/280 ratio of ~1.8; 260/230 ratio of 2.0-2.2) and the desired concentration was reached (> 10 ng/µl), gDNA was sent to Eurofins Genomics (Ebersberg, Germany) for external analysis by short tandem repeat (STR) profiling. STR profiles were then examined using the online similarity search tool CLASTR 1.4.4 (141) and cell lines were only used further if they were correct (similarity > 95%).

Mycoplasma testing

Before mycoplasma testing, suspension cell cultures were kept in the same medium for 3 d. On the day of sample analysis, culture flasks were incubated vertically for 30 min allowing the cells to accumulate on the flask bottom. 500 µl of supernatant were carefully collected from the cell culture flaks and transferred to a 1.5 ml tube. The supernatant was boiled for 10 min at 95 °C. Subsequently, the tubes were centrifuged for 5 s at ~13,000 rpm to pellet debris and 100-200 µl were transferred in a new 1.5 ml tube. Tubes were labelled and sent to Eurofins Genomics (Ebersberg, Germany) for external analysis by qPCR. Samples were tested for all common mycoplasma species (M. arginini, M. fermentans, M. gallisepticum, M. genitalium, M. hyorhinis, M. hominis, M. orale, M. pirum, M. pneumoniae, M. salivarium, M. synoviae, M. yeatsii, Acholeplasma laidlawii and Spiroplasma citri).

2.2.1.4 Overexpression of surface receptors in Ba/F3 cells

Transient transfection of Phoenix-ECO cells

Transient transfection of the adherent retrovirus producer cell line Phoenix-ECO was performed to control for successful protein expression and to produce virus-containing medium for stable Ba/F3 cell transduction. To this end, $7x10^6$ cells were seeded in 10 cm dishes in DMEM + 10% FBS + 1% P/S and incubated overnight at 37 °C, 5% CO_2. On the next day, cells typically reached a confluency of 80-90%. First, medium was carefully changed (now medium without P/S) and cells were put back in the incubator for 1 h for recovery. Meanwhile, 10 µg plasmid DNA was diluted in 450 µl sterile dH_2O and 50 µl sterile 2 M $CaCl_2$ solution was added drop-by-drop and mixed. HBS buffer was slowly added to the $CaCl_2$-DNA solution, carefully mixed and incubated at RT for 3-4 min to form $Ca_3(PO_4)_2$-DNA precipitates. The mixture was subsequently slowly added onto the cell layer and the cells were incubated overnight at 37 °C. Then medium was changed to remove calcium crystals and the cells were further incubated for 24-48 h to allow sufficient endocytosis of the DNA. Transfection efficiency was controlled by fluorescence microscopy. Finally, either

protein lysates were generated to analyze protein expression or virus-conditioned medium was collected for stable Ba/F3 cell transduction, which is described in the following.

Stable retroviral transduction of Ba/F3 cells

$1.5x10^6$ native Ba/F3 cells were resuspended in 3.5 ml of sterile filtered virus-conditioned medium that had been produced after transient transfection of the retrovirus producer cell line Phoenix-ECO; polybrene solution was added at a final concentration of 8 µg/ml and mixed with the cells. After careful mixing, cells were seeded in two wells of a 6-well plate and the plate was centrifuged at 2500 rpm for 90 min at 32 °C to have greater virus stability. The used retroviral expression vector pMSCV-IRES-EYFP (pMIY) contains the internal ribosome entry site (IRES) sequence connecting the "gene of interest" to the reporter gene yellow fluorescent protein (YFP) so that both genes will be expressed simultaneously in the cell and "gene of interest" expressing cells can be sorted based on YFP fluorescence. Therefore, cells were expanded in T25 flasks for 24-72 h and then sorted for YFP positivity using a sorter (FACS). After sorting, cells were once more expanded for approximately one week before sorting again for YFP positivity (this was repeated a third time to get high expressing cells e.g., Ba/F3 pMIY hFLT3high). The following Ba/F3 cell lines with receptor surface expression were generated as part of this work: Ba/F3-pMIY hFLT3/NPOS F691I, Ba/F3-pMIY hFLT3/NPOS F691L, Ba/F3-pMIY rFLT3 (rat FLT3). All other used Ba/F3 cell lines were generated by Dr. Harald Polzer or Dr. Maike Roas (both LMU, AG Spiekermann) as part of their doctoral thesis (142, 143).

2.2.1.5 P53 knockdown AML cell lines

MOLM-13, MV4-11 and OCI-AML3 cell lines with P53 knockdown (KD) were generated by the group of Dr. Andreeff (MD Anderson Cancer Center) as described using lentiviral shRNA (144) and kindly made available for experiments. Successful knockdown was confirmed again in this work by Western Blot.

2.2.2 Cytotoxicity assays

2.2.2.1 Vi-CELL trypan blue exclusion assay: Ba/F3 cells

A 2-fold dilution row of ADCs was prepared freshly in 1.5-5 ml tubes in Ba/F3 cell culture medium. The last tube of the dilution row contained just medium without ADC (untreated control). ADCs were visually inspected for the presence of aggregates before use and only clear solutions were used. All ADC tubes were vortexed before pipetting to make sure that the solution is homogenous. 100 µl/well of each ADC dilution was pipetted in 48-well plates. Afterwards, Ba/F3 cells were prepared in culture medium at a concentration of $1.66x10^4$ cells per ml. 900 µl of the cell

suspension were added per well of the 48-well plate to have a final concentration of $1.5x10^4$ Ba/F3 cells/well (1:10 dilution). Cells were incubated with ADCs for 72 h at 37 °C, 5% CO_2. After 72 h, viable cells were counted by trypan blue exclusion using the Vi-CELL XR Cell Viability Analyzer. Viable cells/ml for each concentration were normalized to untreated control and plotted in GraphPad Prism 10.1.2 using non-linear fit variable slope analysis, which was also used to calculate 50% inhibitory concentrations (IC_{50}) values.

2.2.2.2 CellTiter-Blue and -Glo cell viability assays: AML cell lines and PDX cells

Assays with ADCs and ADC payloads

A 2- or 3-fold dilution row of ADCs (20D9h3-DUBA, 20D9h3-MMAF, IgG1-DUBA, IgG1-MMAF) or ADC payloads (duocarmycin, MMAE, MMAF, exatecan) was freshly prepared in RPMI + 10% FBS + 1% P/S (AML cell lines) or DD medium (AML PDX cells) in 96-well (normal or deep-well) plates. The last well contained medium only (ADCs) or medium with DMSO (payloads). ADCs were only used if no aggregates were present in the tube and the tubes were vortexed before pipetting. 10 µl/well of each ADC/payload dilution was transferred in 96-well suspension plates (AML cell lines: standard transparent plates; Ba/F3 cells: white plates; AML PDX cells: transparent U-bottom plates) using a multichannel pipette. Outer wells of the plate were not used for the experiment, but filled with sterile PBS to prevent evaporation. Further a background control (only medium, not for flow cytometry readout) was included on each plate. After drug preparation, AML cell lines and Ba/F3 cells or AML PDX cells were suspended in their respective culture medium at concentrations of $1.11x10^5$ cells/ml (final concentration in the well: $1x10^4$ cells/well) or $5.55x10^5$ cells/ml (final concentration in the well: $5x10^4$ cells/well), respectively. 90 µl of cell suspension were transferred to each well of the 96-well plates that already contained ADC using a multichannel pipette. Plates were briefly centrifuged (100xg, 5-10 s) to make sure that all liquid is in the bottom. The plates were then incubated for 24 h (payloads) or 96 h (ADCs) at 37 °C, 5% CO_2. After 24-96 h, AML cell lines were analyzed by resazurin readout, Ba/F3 cells by CellTiter Glo assay and AML PDX cells by flow cytometry. The resazurin method determines the ability of cells to convert resazurin to fluorescent resorufin, which is an indicator for their metabolic activity and thus viability. For this assay, 10 µl of resazurin solution (final concentration: 50 µM) were added in each well of the 96-well plate using a multichannel pipette. The plate was briefly centrifuged (100xg, 5-10 s) and placed in the incubator for 4 h before measuring the plate at the GloMax® Discover microplate reader using the 520 nm excitation filter and the 580-640 nm emission filter (Promega CellTiter-Blue protocol). CellTiter-Glo Assay determines the amount of ATP present in cells as an indicator for their viability. This assay was carried out for Ba/F3-pMIY cells as they express YFP, which might interfere with resazurin readout, but not with CellTiter-Glo Assay as the latter is based on luminescence and not fluorescence. The assay was carried out as described by

the manufacturer. Briefly, CellTiter-Glo substrate was added 1:1 to the cells and the mixture was shaken for 2 min on an orbital shaker to lyse the cells. The plate was then incubated at RT for 10 min to stabilize the luminescent signal and subsequently recorded with the GloMax® Discover microplate reader using 0.3 s integration time (Promega CellTiter-Glo protocol). Viable AML PDX cells were analyzed by flow cytometry. To this end, 96-well U-bottom plates were centrifuged at 300xg for 3 min, RT. The supernatant was removed and cells were washed once with 200 µl FACS buffer. Cells were resuspended in 200 µl FACS buffer. Shortly before analysis 2 µl of 10 ng/µl DAPI solution were added per well (final concentration: 0.1 ng/µl) and the plate was measured at the FACS Canto II connected to a high-throughput sampler.

All cytotoxicity assays were evaluated in the following way: For all values a background control (medium only) was subtracted (except for flow cytometry readout). Then, all values were normalized to untreated control and plotted in GraphPad Prism 10.1.2 using non-linear fit variable slope analysis, which was also used to calculate 50% inhibitory concentrations (IC_{50}) values.

Aphidicolin experiment

A dilution row of aphidicolin was prepared in 1.5 ml tubes. Further a vehicle-control was prepared, which contained DMSO at the highest concentration used in the aphidicolin dilution row. 10 µl/well of the dilution row were added in 96-well suspension plates. Subsequently, AML cells were prepared at a concentration of $3.33x10^5$ cells/ml in culture medium. 90 µl of cell suspension was added per well (final concentration: $3x10^4$ cells/well). The plates were then incubated for 24 h with aphidicolin at 37 °C, 5% CO_2. On the next day, dilution rows of different ADC payloads (duocarmycin, MMAE and exatecan) were prepared again including a vehicle-control with DMSO. 10 µl/well of the toxin dilution row were subsequently added on the aphidicolin pre-incubated cells without changing the medium or removing the aphidicolin. All concentrations of aphidicolin-toxin combinations were tested in duplicates. The plate was incubated for another 24 h at 37 °C, 5% CO_2 before measuring viable cells with resazurin readout as described in detail above.

CES1c experiment

100 µl human serum was mixed with ADCs (final ADC concentration: 100 µg/ml) and recombinant murine carboxylesterase 1 c (CES1c; final CES1c concentration: 80 µg/ml). The mixtures were incubated for 1 d, 4 d or 7 d at 37 °C and immediately frozen at the end of the incubation period. Furthermore, two controls were used one containing only ADC but no CES1c or human serum and one containing ADC and human serum but no CES1c. A 3-fold dilution row was then prepared of the ADCs from all conditions and incubated with FLT3-negative HL-60 cells. The readout was by resazurin assay on day 4, as described before.

Combination assays and synergy calculation

For drug combination experiments, 3-fold dilution rows of each of the drugs (20D9h3-DUBA, venetoclax, ceralasertib) were prepared in 96-well plates or tubes using the culture medium of the respective cell line. Further a vehicle-control was prepared containing the highest DMSO concentration used in the drug dilution row. 10 µl of each drug dose or vehicle-control were added per well of a 96-well plate, respectively, using a multichannel pipette. Experiments were designed in a way that all possible drug combinations were tested. All conditions were set up in triplicates. Next, a cell solution was prepared in culture medium with a concentration of $1.25x10^5$ cells/ml. 80 µl of cell solution were added to the 20 µl drugs/vehicle-controls in each well to have a final concentration of $1x10^4$ cells/well. Plates were briefly centrifuged (100xg, 5-10 s) to make sure that all liquid is in the bottom and incubated for 96 h. On the day of analysis plates were measured by resazurin readout as explained in detail above. The results were collected in a combination dose-response matrix table and uploaded to the SynergyFinder Online Tool (145) choosing "viability" as readout and using four-parameter logistic regression (LL4) curve fitting. Synergy scores were calculated with the zero interaction potency (ZIP) method (146) without baseline correction. Generally, the different synergy reference models all compare observed versus expected drug combination responses. According to the tool's user guide, a drug-combination is likely synergistic if the calculated synergy score δ is above +10, antagonistic if below -10 and additive if in between.

2.2.3 Flow cytometry methods

2.2.3.1 Expression and binding analyses

Expression analyses

For the analysis of surface receptor expression, $0.5x10^6$ cells per antibody staining were collected in Falcon tubes, washed once with 1 ml PBS and centrifuged for 3 min at 300xg. Cells were resuspended in FACS buffer at a concentration of $5x10^6$ cells/ml in 100 µl. Cells were stained with fluorophore-labelled primary antibodies directed against the target of interest and the respective isotype controls using the suggested antibody concentrations of the manufacturer. Staining was carried out for 30 min on ice in the dark either in 96-well plates or in FACS tubes. Afterwards, the cells were washed 3x with 200 µl (plate) or 500 µl (FACS tube) FACS buffer (3 min, 300xg). After the last wash the cells were resuspended in 400 µl FACS buffer, respectively, transferred from the plate to FACS tubes and immediately measured at BD FACSCanto™ II (BD Biosciences).

Binding analyses

For the binding analyses of the in-house produced mAbs, $0.5x10^6$ cells per antibody were washed and resuspended in 100 µl of FACS buffer as described for the expression analyses. Cells were

stained in 96-well plates with 10 µg/ml (1 µg in 100 µl) of the in-house produced mAbs 20D9h1-12, 20D9h3-LALA, IgG1 (Palivizumab), IgG1-LALA (Palivizumab-LALA) or no-antibody (only secondary antibody control) for 30 min on ice under light protection. Afterwards, the plate was washed 3x with 200 µl FACS buffer (3 min, 300xg). After the third wash, cells were resuspended in FACS buffer containing anti-human IgG1 secondary fluorophore-coupled antibodies at the concentration recommended by the manufacturer to detect the binding of the in-house antibodies. Cells were incubated for another 30 min on ice in the dark and the plate was again washed 3x with 200 µl FACS buffer. Finally, cells were resuspended in 400 µl FACS buffer, transferred to FACS tubes and immediately measured at BD FACSCanto™ II. Data was evaluated with FlowJo software version 10.8.1.

2.2.3.2 Apoptosis assay

MOLM-13 or MV4-11 cells were seeded in T25 flasks at a concentration of $0.35x10^6$ cells/ml in 12 ml. They were treated with 100 ng/ml of 20D9h3-DUBA, 20D9h3-MMAF or PBS. After 24 h, 48h, 72h and 96h, $0.3x10^6$ cells were taken from each flask, respectively, and transferred to FACS tubes. 0.5 ml ice-cold PBS were added and the cells were centrifuged at 300xg, 5 min. Cells were subsequently washed once with 1 ml PBS and once with 1 ml 1x Annexin binding buffer. After the two washes, each sample was resuspended in 100 µl Annexin binding buffer containing APC Annexin V in a 1:25 dilution (4 µl per 100 µl) and stained for 10 min at RT in the dark. Then, 300 µl of Annexin binding buffer were added to each tube. Right before measurement at the BD FACSCanto™ II, 0.05 ng/µl (final concentration) DAPI were added. Data was evaluated with FlowJo software version 10.8.1.

2.2.3.3 Cell cycle analysis

MV4-11 cells were cultivated in T25 flasks at a concentration of $0.35x10^6$ cells/ml in the presence of 100 ng/ml 20D9h3-DUBA, 20D9h3-MMAF or PBS. After 48 h, $0.5x10^6$ cells were transferred to FACS tubes and centrifuged at 2000 rpm for 5 min at 4 °C. Cells were then washed once with 1 ml of ice-cold PBS and centrifuged again as before. Subsequently, each sample was resuspended in 1 ml of ice-cold 70% (v/v) ethanol and incubated on ice for 30 min. Afterwards, samples were frozen at -20 °C overnight or it was directly proceeded to the next step. The ethanol-fixed cells were centrifuged at 2000 rpm for 10 min at RT. The supernatant was carefully removed and cells were washed once with 1 ml PBS (2000 rpm, 5 min, RT). Once again, the supernatant was removed and 50 µl of RNAse (100 µg/ml) were added, followed by 200 µl of propidium iodide buffer. Samples were then measured directly at the BD FACSCanto™ using a low flow-rate for

better accuracy. FlowJo software version 10.8.1 was used to evaluate cell cycle phases with Watson pragmatic algorithm.

2.2.3.4 Internalization assay

Conjugation of secondary antibody with pHrodo Deep Red

pHrodo Deep Red antibody labelling was performed by Dr. Saskia Schmitt (Tubulis GmbH) following the manufacturer's instructions. First, 1 ml of d_2H_2O were added to the provided vial of sodium bicarbonate to obtain a 1 M solution. 10 µl sodium bicarbonate solution was subsequently added to a vial containing 90 µl of unlabeled goat anti-human IgG1 secondary antibody at a concentration of 1.1 mg/ml in PBS. The 100 µl antibody solution was then transferred into the vial containing pHrodo Deep Red tetrafluorophenyl ester reactive dye and thoroughly mixed to dissolve the dye. The solution was incubated for 2 h, RT. For antibody purification a spin column was prepared 10 min before the end of the incubation time. To this end, the spin column was placed in a wash vial and the assembly centrifuged at 1000xg for 2 min to remove the storage buffer. The flow-through was discarded and the column placed back in the wash vial. 400 µl supplied PBS exchange buffer was loaded on the column for equilibration and the column was centrifuged again as before. The flow-through and wash vial were discarded and the column placed in a collection vial. The whole reaction-mixture was slowly added onto the column and the assembly again centrifuged as before. Afterwards the column was discarded. The antibody pHrodo deep red conjugate was transferred from the collection tube into a common 1.5 ml tube.

Flow cytometry analysis of antibody internalization

Ba/F3-pMIY ev / hFLT3high / hFLT3low cells were seeded in 96-well plates at a density of $6.25x10^5$ cells/ml in 80 µl (final concentration: $5x10^4$ cells/well). 3 µg/ml 20D9h3-mAb and pHrodo-labelled anti-human secondary antibody, respectively, were mixed in a total volume of 20 µl/sample in cell culture medium (RPMI + 20% FBS + 1% P/S) and incubated for 15 min to get a complex of primary and secondary antibody. 20 µl/well of the mix were added to the cells to have a final volume of 100 µl/well and cells were incubated with the antibody complex for 1 h, 5 h or 24 h at 37 °C. The unstained control only received 20 µl cell culture medium without antibodies. After the respective time span, the 100 µl of cells/well were transferred into FACS tubes, respectively, washed 2x with FACS buffer and resuspended in 150 µl FACS buffer. Subsequently, samples were measured at BD FACSCanto™ II. Data was evaluated with FlowJo software version 10.8.1.

2.2.4 *In vivo* therapy

The establishment of AML PDX models and animal handling have been described in detail by Vick et al. (132) and Zeller et al. (147). For *in vivo* therapy, luciferase-expressing PDX cells were transplanted into the bone marrow of NSG mice and engraftment was monitored with bioluminescence imaging (BLI). After successful engraftment (BLI values > $1x10^8$ photons/s), ADC treatment was started. Mice were therefore injected intravenously (i.v.) once per week 2x (AML-388, 5 mice per group) or 3x (AML-579, 5 mice per group for 20D9h3-DUBA, 3 mice per group for 20D9h3-MMAF and PBS control) with 3 mg/kg of either 20D9h3-DUBA, or 20D9h3-MMAF or PBS. Treatment response was monitored by regular BLI measurements for around 115 d or until the mice showed advanced leukemic disease (indicated by BLI signal and clinical signs such as rough fur, reduced motility, paralysis, weight loss and hunchback). Then mice were sacrificed by cervical dislocation. Those experiments were planned and analyzed in collaboration with Dr. Binje Vick and carried out by Annette Frank and Sandro Aidone (all AG Jeremias, Helmholtz Zentrum München). Animal trials were carried out in accordance with the current ethical standards of the official committee on animal experimentation (written approval by Regierung von Oberbayern, tierversuche@reg-ob.bayern.de, ROB-55.2Vet-2532.Vet 03-21-9).

2.2.5 Stem cell assays

2.2.5.1 Drug pre-incubation for stem cell assays

$5x10^4$ and $1.7x10^4$ CD34-positive healthy BM cells and $3x10^5$ and $5x10^6$ AML PDX cells were treated per condition for CFU and LTC-IC assays, respectively. For LIC assays, $1x10^5$ AML-388 PDX cells or $5x10^4$ AML-393 AML PDX cells were plated per mouse and condition corresponding to 100x of their LIC frequency (130). Cell concentrations in the pre-incubation were adjusted to $1x10^6$ cells/ml. Cells were treated with 0.3-1 µg/ml of the isotype control ADCs IgG1-DUBA/IgG1-MMAF or 0.005-1 µg/ml of the FLT3-ADCs 20D9h3-DUBA/20D9h3-LALA-DUBA/20D9h3-MMAF (as individually stated) for a period of 48 h (LTC-IC assays) or 96 h (CFU assays) in the respective culture medium (see 2.2.1.1).

2.2.5.2 Colony-forming unit (CFU) assay

AML samples

After 96 h of treatment as described above, cells were collected in 1.5 ml tubes and washed 3x with PBS to remove remaining ADC and toxin (400xg, 5 min, RT). After the third wash, cells were resuspended in 300 µl DD medium ($1x10^6$ cells/ml) and added to one of the 3 ml methylcellulose H4034 Optimum aliquots, respectively, that had been prepared before in 15 ml falcon tubes. The tube containing methylcellulose and cells was vortexed for 5 s and left standing for 5 min to allow

air bubbles to raise to the top. Syringes with blunt-end needles were prepared and the needle was rinsed once with methylcellulose to remove air. Subsequently, 2.6 ml of the solution was drawn up and 2x 1.1 ml of the solution were transferred in two wells of a SmartDish 6-well plate (technical duplicates) to have a final concentration of $1x10^5$ cells/well. The remaining 0.4 ml of the solution was discarded together with the syringe and the needle. Sterile H_2O was added to the middle part of the SmartDish plate and the plate was put in a 245 mm x 245 mm square culture dish with several open 35 mm dishes that were also filled with sterile H_2O to prevent drying of the methylcellulose. The dish was placed in an incubator and incubated for 12-14 d at 37 °C, 5% CO_2. It was made sure that the water pan in the incubator is filled and the door of the incubator was not opened for the whole period to ensure optimal conditions for colony growth. On the day of evaluation, colonies were counted using ZEISS Primovert microscope with Primo Plan-ACHROMAT 4x/0.10 Ph0 objective. SmartGrid was used to facilitate the counting procedure. Clusters (20-50 cells) and colonies (> 50 cells) were counted. For the primary sample reddish colonies were observed, which were probably remaining healthy CFU-E. They were not counted and excluded from further analyses.

Healthy samples

After pre-treatment, all remaining healthy CD34-positive BM cells were plated in Methylcellulose (StemMACS™ HSC-CFU complete with EPO, human) in 35 mm petri dishes for 14 d at 37 °C, 5% CO_2. These assays were carried out by Dr. Marit Leilich (TUM), as described in detail before (138, 139).

2.2.5.3 Long-term culture initiating cell (LTC-IC) assay

Preparation of collagen-coated dishes with feeder cells

A few days before the start of the LTC-IC assays, 6-well tissue culture plates were coated with collagen solution in the following way: The bottom of every well was uniformly covered with collagen solution (approximately 0.5-1 ml per well). Excess solution was removed and the dishes were dried with open lids at RT for at least 1 h within a biosafety cabinet. The dried dishes were used immediately or stored tightly wrapped at 4 °C for a maximum of two weeks. Prior to use the wells were carefully rinsed once with Myelocult™ H5100 to neutralize acidity. M2-10B4 (for CD34-positive BM cells) or SLSL-J-IL3-neo (for AML PDX cells) feeder cells were detached from T175 flasks using Trypsin-EDTA incubation for around 2 min. Trypsin reaction was stopped by adding the respective feeder cells culture medium without geneticin (see 2.2.1.1). Feeder cells were collected in a 50 ml tube and centrifuged at 1400 rpm for 5 min, RT. Cells were resuspended in 5 ml Myelocult™ H5100 and counted by trypan blue exclusion. Feeder cells were then plated on the collagen-coated dishes at the density recommended by STEMCELL Technologies ($3x10^5$ cells/well) in 1 ml Myelocult™ H5100. On the following day, it was visually inspected whether the

feeder cells are attached, alive and form an around 80% confluent layer. Then, the feeder cells were irradiated at 8000 cGy and medium was exchanged to 2 ml fresh, warm Myelocult™ H5100 including 1 µM hydrocortisone.

Feeder cell co-incubation

After 48 h drug treatment as described above, all remaining AML PDX / CD34-positive BM cells were harvested in 15 ml tubes and centrifuged for 10 min at 200xg, RT. They were then re-suspended in 500 µl of MyeloCult™ H5100 including 1 µM hydrocortisone and transferred on the prepared feeder cell layer (total volume 2.5 ml per well). For the AML PDX cells, SCF was additionally added into the medium at a final concentration of 50 ng/ml. During the 5-week co-incubation of the cells on the feeder layer, the medium was changed half-weekly: Therefore, the plate was carefully shaken horizontally to homogenize the cell suspension, as the cells tend to accumulate in the middle part of the well. The plate was tilted and all medium carefully sucked up with a serological pipette. Half of the medium was slowly put back in each well, respectively, the other half of the medium was discarded. 1.25 ml of new medium was added drop-wise containing 50 ng/ml of fresh SCF (only for AML PDX) and 1 µM of fresh hydrocortisone. Additionally, 50 ng/ml of fresh SCF (only for AML PDX) were added a second time each week, as SCF gets rapidly degraded.

Harvest from feeder cell layer and plating in methylcellulose cultures

After 5 weeks of co-incubation AML PDX / CD34-positive BM cells were harvested from the feeder layers. To this end, all medium – containing non-adherent cells – was collected in a 15 ml tube for each well, respectively. The adherent layer in each well was subsequently washed 2x with 1 ml HBSS, also collecting the solution in the 15 ml tube after each wash step. Afterwards Trypsin-EDTA (0.25%) was added and the plate incubated for 10 min at 37 °C, 5% CO_2 to detach the adherent layer. 0.2 ml FBS was added to stop the reaction and the wells were rinsed 2x with IMDM + 2% FBS, adding all solution after each step to the 15 ml tube. The 15 ml tube was filled up to 10 ml with IMDM + 2% FBS and centrifuged at 300xg for 10 min at RT. The supernatant was discarded and the cell pellet was resuspended in 300 µl IMDM + 2% FBS. The whole volume was added to 3 ml Methocult H4230 containing 3 U/ml EPO, 50 ng/ml SCF and 20 ng/ml IL-3, IL-6, GM-CSF and G-CSF for healthy CD34-positive BM cells or to Methocult H4034 Optimum for AML PDX cells. Methylcellulose cultures were then prepared and evaluated after 14 d as described for CFU assay. LTC-IC assays were performed by me together with Dr. Xiang Gao under the supervision of Prof. Michaela Feuring (both from university hospital Ulm). Further details are also described in publications by Feuring-Buske et al. (148) and Ailles et al. (149)

2.2.5.4 Leukemia-initiating cell (LIC) assay

After 96 h drug treatment, all remaining AML PDX cells were collected from the plate, centrifuged at 400xg for 5 min at RT and resuspended in PBS. They were then retransplanted into five NSG mice per treatment group using tail vein injection. Subsequently AML PDX engraftment was monitored in regular intervals by BLI. A positive and negative engraftment were pre-specified as total flux > $1x10^8$ photons/s in at least two BLI images and total flux < $4x10^6$ photons/s for at least 100 d since transplantation, respectively. After the pre-specified time or at advanced leukemic disease (indicated by BLI signals above $1x10^{10}$ photons/s and/or clinical signs such as rough fur, reduced motility, paralysis, weight loss and hunchback), mice were sacrificed using cervical dislocation. One AML-388 transplanted mouse of the 1 µg/ml 20D9h3-DUBA group had to be sacrificed on day 34 due to clinical signs of illness that were most likely unrelated to leukemia development, as the BLI imaging signal two days before was negative. This mouse was therefore excluded from the analyses. Further details on animal handling, randomization and blinding have been described in a recent publication by Zeller et al (147). The LIC assays were planned and analyzed in collaboration with Dr. Binje Vick and performed by Dr. Binje Vick together with Annette Frank and Sandro Aidone (all AG Jeremias, Helmholtz Zentrum München). Animal trials were carried out in accordance with the current ethical standards of the official committee on animal experimentation (written approval by Regierung von Oberbayern, tierversuche@reg-ob.bayern.de, ROB-55.2Vet-2532.Vet 03-21-9).

2.2.6 Microscopy

2.2.6.1 Internalization assay

400 µl Ba/F3-pMIY ev or hFLT3high cells were seeded in 48-well plates at a density of $1x10^6$ cells/ml in their culture medium. 1 µg 20D9h3-mAb and pHrodo-labelled anti-human secondary antibody, respectively, were mixed in a 1.5 ml tube and incubated for 30 min, at RT. The mixture was then added to the cells (final antibody concentration: 2.5 µg/ml). As a control, Ba/F3-pMIY hFLT3 high cells were incubated with pHrodo-labelled secondary antibody only. After 5 h and 24 h, cell samples were taken from each well and pipetted on an 8-well glass bottom slide. Microscopic images were acquired with a Nikon TiE microscope using Yokogawa CSU-W1 spinning disk confocal unit with 50 µm pinhole size, Andor Borealis illumination unit, Andor ALC600 laser beam combiner, Andor IXON 888 Ultra EMCCD camera using Nikon CFI Apochromat TIRF 60x NA 1.49 objective with oil immersion (pixel size: 217 nm) and Nikon Software NIS Elements version 5.02.00. YFP and pHrodo deep red signals were captured with 525/50 nm and 700/75 nm emission filters, respectively.

2.2.6.2 Colony imaging

AML PDX CFU assay plates were imaged on the final day of the experiment using Keyence BZ-X810 microscope with a PlanApo 2x 0.10/8.50 mm objective and no digital zoom. 60-80 images were acquired per well of the 6-well plate and were stitched together using Keyence BZ-810 Analyzer Software. Furthermore, single colonies were imaged using ZEISS Primovert microscope with Axiocam 208 color microscope camera and Primo Plan-ACHROMAT 4x/0.10 Ph0 objective.

2.2.7 Generation of antibodies and antibody-drug-conjugates (ADCs)

2.2.7.1 Antibody expression and purification

Antibody expression

For the expression of chimeric 20D9, humanized 20D9h1-h16 and Fc-mutated 20D9h3-LALA, ExpiCHO expression system was used according to the manufacturer's instructions (standard protocol). Briefly, a day before transfection ExpiCHO-S cells were subcultured at a density of $3x10^6$ cells/ml and incubated at 37 °C, 8% CO_2. A day after, transfection was carried out only if the cell viability was > 95%. For transfection, cells were collected and diluted in 25 ml fresh pre-warmed ExpiCHO™ expression medium at a density of $6x10^6$ cells/ml. 10 µg of light and heavy chain plasmid (1:1 ratio), respectively, were pipetted into cold 1 ml OptiPRO™ SFM (tube 1); 80 µl cold ExpiCHO transfection reagent (ExpiFectamine™ CHO reagent) and 920 µl cold OptiPRO™ SFM were pipetted into tube 2. The content of both tubes was then mixed, left standing for a period of 3 min at RT and subsequently added to the cells. Cells were incubated over night at 37 °C, 8% CO_2 on an orbital shaker before adding 6 ml of ExpiCHO™ feed medium including 150 µl enhancer reagent. The total duration of expression before harvest was typically between 7 and 10 d.

Antibody purification

ExpiCHO-S cells were harvested by centrifugation at 1000xg for 10 min at RT. Supernatant was collected, centrifuged at 4000-5000xg for 30 min at 4 °C and subsequently filtered with a 0.22 µm filter for clarification. mAbs were purified from the supernatant with Äkta pure™ FPLC chromatography system using MabSelect SuRe Protein A column. 5 CV mAb binding buffer were used for system and column equilibration prior to loading of the cleared supernatant onto the column (used flow rate: 0.5 ml/min). This was followed by a washing step where the column was loaded with 10 CV mAb binding buffer at a flow rate of 1 ml/min. For antibody elution 10 CV mAb elution buffer were loaded on the column and the antibodies were eluted into prepared tubes with mAb neutralization buffer (final pH 7-7.5). Fractions were pooled and loaded on Amicon® ultra 0.5 ml centrifugal filters for concentration followed by buffer exchange to mAb storage buffer using Zeba spin desalting columns. Both antibody expression and purification were carried out by Jonathan Schwach (AG Leonhardt, LMU).

2.2.7.2 mAb stability test

Humanized mAbs were tested for their long-term stability at different temperatures. Aliquots of each mAb were split into three tubes at concentration of 1 mg/ml, respectively, in storage buffer including 0.1% sodium azide to prevent bacterial contamination. The three tubes were incubated at 4 °C, 25 °C and 37 °C, respectively. After one, two and four weeks, aliquots of each tube were centrifuged for 10 min at 10 000xg and subsequently analyzed for their stability using HPLC-hydrophobicity interaction chromatography (HIC), HPLC-size-exclusion chromatography and Nanodrop measurements. This experiment was done by Jonathan Schwach (AG Leonhardt, LMU).

2.2.7.3 ADC generation

Generation of 20D9h3-DUBA

2.67 µl of a 10 mM TCEP solution (in PBS) were added to 200 µl of 20D9h3-mAb at a concentration of 5 mg/ml in PBS, mixed and incubated at RT. After 1 h, 3.33 µl of vc-*seco*-DUBA linker-payload (10 mM in DMSO) were added and the mixture was incubated for another hour at RT. Afterwards, the mixture underwent purification by preparative SEC at a flow rate of 0.8 ml/min using a 25 ml Superdex™ 200 Increase 10/300GL column and ÄKTA Pure FPLC system with F9-C-fraction collector. Elution was done with PBS. The fractions with antibodies were pooled and loaded on Amicon Ultra-2 ml centrifugal filters for protein concentration. A schematic illustration of 20D9h3-DUBA is depicted in supplemental Figure 2A.

Generation of 20D9h3-MMAF

3.33 µl of a 10 mM TCEP solution (in P5-conjugation buffer) were added to 50 µl of 20D9h3-mAb at a concentration of 10 mg/ml in P5-conjugation buffer and mixed. Immediately after, 1.67 µl of P5(OEt)-VC-PAB-MMAF (40 mM in DMSO) – which was generated as described recently (150) – were added and the mixture was incubated for 16 h at 25 °C on a shaker (350 rpm). Afterwards, the mixture underwent purification by preparative SEC followed by concentration with spin-filtration as described for 20D9h3-DUBA. A schematic illustration of 20D9h3-MMAF is depicted in supplemental Figure 3A.

Both conjugations were carried out by Dr. Marc-André Kasper and Dr. Philipp Ochtrop (both Tubulis GmbH).

2.2.7.4 Quality control of antibodies and ADCs

Determination of ADC/antibody concentration

The concentration of all mAbs was determined using NanoDrop spectrophotometer measurement. For ADCs, the concentration was determined using Bradford reagent and Pierce™ rapid gold BCA protein assay kit according to the manufacturer's instructions. The standard

curves were generated using pre-diluted bovine gamma globulin standards. BCA and Bradford assay were measured at 480 nm and 595 nm, respectively, using Tecan Infinite 200 PRO microplate reader. For analysis, respective blank controls were subtracted and the mean of both readouts was calculated.

Sample preparation for mass spectrometry

50 µl of ADC/mAb at a concentration of 0.2 mg/ml in PBS were mixed with 0.5 µl of the N-glycosidase PNGase F and 5 µl of DTT (100 mM in H_2O). the mixture was incubated at 37 °C for a minimum duration of 2 h before subjecting the samples to liquid chromatography / mass spectrometry (LC/MS).

Analytical size-exclusion chromatography

For analytical SEC, 8 µg mAbs/ADCs were loaded on MAbPac SEC-1 300 Å, 4 x 300 mm columns and analyzed at a flow rate of 0.15 ml/min using Vanquish Flex UHPLC System, DAD detector, split sampler FT (4 °C), column compartment H (25 °C) and binary pump F. A-SEC phosphate buffer at pH 7 was used as a mobile phase to separate ADC/mAb populations during a 30 min isocratic gradient. UV chromatograms were recorded at 220 and 280 nm.

Analytical hydrophobic interaction chromatography

For analytical HIC, 15 µg mAbs/ADCs were loaded on MabPac HIC Butyl 4.6 x 100 mm columns and analyzed at a flow rate of 700 µl/min using Vanquish Flex UHPLC System (2.9). mAbs/ADCs were separated using this gradient: A: 1 M $(NH_4)_2SO_4$, 500 mM NaCl, 100 mM NaH_2PO_4 pH 7.4 B: 20 mM NaH_2PO_4, 20% (v/v) Isopropyl alcohol, pH 7.4. 0% B: 0-1 min, 0-95% B: 1-15 min, 95% B: 15-20 min, 95-0% B: 20-23 min, 0% B: 23-25 min. UV chromatograms were recorded at 220 and 280 nm.

Quality control and concentration determination of all antibodies and ADCs were carried out by Dr. Marc-André Kasper / Dr. Philipp Ochtrop (both Tubulis GmbH) and Jonathan Schwach (AG Leonhardt, LMU), respectively.

2.2.8 Other protein biochemistry methods

2.2.8.1 Lysates

To show the expression of cellular proteins $1x10^7$ Ba/F3- or MOLM-13, MV4-11 or OCI-AML3 cells (with p53 KD or ctrl.) were used to generate protein lysates. In the experiment where the DNA damage repair was analyzed, the treatment with 50 ng/ml ADCs was started with a total of $1x10^7$ MOLM-13 cells in 6-well plates ($2.2x10^6$ cells/ml) and after 24 h all remaining cells of each well were used to generate lysates. In all cases, cells were collected in 15 ml falcons and centrifuged at 300xg for 3 min, RT. The supernatant was removed, the cells resuspended in 1 ml cold PBS and

transferred to a 1.5 ml tube. All further steps were carried out on ice. Cells were now washed twice with cold PBS (3550 rpm, 5 min, 4 °C). After the last wash, all supernatant was carefully removed and lysis buffer was added (a 1:100 dilution of a 100 mM Na_3VO_4 solution and a 1:100 dilution of 100x protease inhibitor cocktail were added to the lysis buffer shortly before use; 100 µl lysis buffer were used per $1x10^7$ cells). Samples were incubated for at least 30 min on a rotary mixer at 4 °C. Afterwards, samples were centrifuged at full speed for 10 min. The supernatant was carefully transferred in a new tube and mixed 1:2 with 2x Laemmli buffer (bought from Biorad, β-mercaptoethanol was added to the buffer shortly before use according to the supplier's instructions). Subsequently, the sample was incubated for 5 min at 95 °C on a heating block and transferred on ice immediately after. The lysates were either directly used for Western Blot or stored at -20 °C until usage.

2.2.8.2 Determination of protein concentration

The concentration of protein lysates for Western blotting was determined by Bradford assay. 1 µl of lysate was therefore added to 799 µl water in a 1.5 ml tube. After mixing, 200 µl Bradford protein dye reagent concentrate was added, the tube was vortexed and the whole volume was transferred to a cuvette. Further, BSA standards were prepared with concentrations between 1 and 25 mg/ml. Both standards and samples were measured at 595 nm using a UV-VIS-photometer.

2.2.8.3 Western blotting

Gel electrophoresis

For the molecular weight-based separation of proteins ready-to use 4-20% tris-glycine precast gels with 10 or 12 wells were used. Combs were carefully removed from the gels and the gels were inserted into the electrophoresis chamber of Xcell SureLock Mini Cell. The chamber was filled with 1x electrophoresis buffer. 50 µg of protein lysate per condition and 10 µl of Spectra Multicolor Broad Range Protein Ladder (10-260 kDa) were loaded into the gel pockets using gel loading tips. Gels were run at 50 V for around 1.5 h (stacking gel), then the voltage was increased to 100 V until the dye front reached the bottom of the gel.

Protein transfer to PVDF membranes

For the protein transfer, PVDF membranes (0.45 µm) were pre-wetted in methanol for 30 s, then transferred to d_2H_2O for 5 min and finally incubated in 1x transfer buffer for 10 min. Further, two sponges and two filter papers per gel were also pre-wetted with transfer buffer. Sponges, filter papers, gel and PVDF membrane were subsequently assembled in a cassette, air bubbles were removed and the closed cassette was inserted into a wet-blotting chamber that was filled with ice-

cold 1x transfer buffer. The protein transfer was done overnight using Biorad Mini Protean Tetra system at 100 mA and 4 °C under continuous stirring using a magnet stirring rod.

Antibody staining

On the next day, the PVDF membrane was blocked for 1-2 h (RT) with 5% (w/v) milk powder or BSA (for phospho-proteins) in TBS-T on an orbital shaker. Then, the membrane was washed once with TBS-T for 5 min and subsequently stained with primary antibody (Table 10) at the dilution recommended by the manufacturer in 5 ml of the respective blocking buffer for 1 h at RT or overnight at 4 °C on a roller mixer. Afterwards, the PVDF membrane was washed 3x for 5 min with TBS-T on a roller mixer to remove unbound primary antibody. Subsequently, the membrane was stained with HRP-coupled secondary antibody diluted in blocking buffer 1:10 000 for β-actin and 1:5 000 for all other proteins for 1-2 h on a roller mixer (RT). Afterwards, the membrane was washed again 3x for 5 min with TBS-T on a roller mixer to remove unbound secondary antibody. Pierce ECL plus solution was warmed to RT 15 min before use. 1 ml solution A and 25 µl solution B were mixed according to the supplier's instructions and the mixture was distributed over the antibody-stained PVDF membrane. The membrane was incubated with ECL solution for 2 min in the dark and then immediately imaged on Fusion SL imaging system.

Membrane stripping

In some cases, membranes were stained a second time with different antibodies after the first imaging. Therefore, PVDF membranes were washed 1x with TBS-T for 5 min at RT on an orbital shaker to remove ECL solution. Subsequently, membranes were incubated for 10 min with Restore™ PLUS Western Blot Stripping buffer at RT on an orbital shaker to remove the bound antibodies. Membranes were again washed 2x with TBS-T for 5 min before proceeding to membrane blocking and antibody staining as described above.

2.2.8.4 Enzyme-linked immunosorbent assay (ELISA)

Analysis of humanized mAbs

Recombinant human FLT3 protein was coated on 96-well black MaxiSorp plates by incubating the plate overnight at 4 °C with a solution of 100 µl PBS/well containing 1 µg/ml FLT3 protein on a shaker. On the next day, the plate was washed 3x with 250 µl/well PBS containing 0.05% Tween 20 (PBS-T, washing buffer). After each wash, the solution was removed by inverting the plate. Subsequently, 250 µl/well of 2% BSA (w/v) in PBS-T (blocking solution) was added and the plate was incubated for 1 h at RT on an orbital shaker (250-300 rpm). Then, the plate was washed again 3x with washing buffer as before. A concentration row of the FLT3-mAbs 20D9 and 20D9h1-20D9h12 was prepared in blocking solution starting from 10 µg/ml with 1:4 dilutions. After the last wash, 100 µl of each dilution was added per well, and the plate was incubated with antibodies

for 2 h at RT on an orbital shaker (250-300 rpm). The plate was washed again 3x with washing buffer as before. Subsequently, 100 µl of blocking solution containing alkaline phosphatase coupled anti-human secondary antibody at a dilution of 1:5000 was added to each well for 1 h at RT on an orbital shaker (250-300 rpm). The plate was washed again 3x with washing buffer as before. 100 µl of AttoPhos fluorescent alkaline phosphatase substrate solution was added per well for detection. After a 20 min incubation at RT on an orbital shaker (250-300 rpm), the plate was read on GloMax® Discover microplate reader at an excitation of 405 nm and an emission of 500-550 nm. The half maximal effective concentration (EC_{50}) was calculated using GraphPad Prism 10.1.2 non-linear fit "one site – total and nonspecific binding".

Pharmacokinetic analysis of ADCs in mouse serum

3 mg/kg 20D9h3-DUBA or 20D9h3-MMAF were injected i.v. into 20-weeks-old male NSG mice (n = 1). After 24 h, 48 h and 72 h blood samples were collected for analysis with ELISA according to the following protocol: 1 µg/ml mouse anti-human IgG Fc specific antibody in PBS, anti-MMAF antibody or anti-duocarmycin antibody were coated on 96-well black MaxiSorp plates, respectively, to determine total antibody and intact ADC content within the mouse serum. Plates were then incubated with blocking solution as described above before serum samples were loaded onto the plate. Furthermore, dilution rows of 20D9h93-DUBA or 20D9h3-MMAF with concentrations ranging from 15.6-100 000 ng/ml were loaded on the plate to generate standard curves. All other steps were carried out as described above using an HRP-labelled goat anti-human kappa light chain secondary antibody (1 h incubation) and Ultra-TMB substrate (reaction was stopped with 1 M sulphuric acid after 15 min) for detection. The plate was measured at 450 nm on Tecan Infinite 200 PRO microplate reader.

2.2.9 Molecular biological work

2.2.9.1 Site directed mutagenesis

Generation of FLT3 mutations

QuickChange Site-Directed Mutagenesis Kit was used according to the supplier's recommendations to introduce point mutations in the FLT3 sequence (F691I, F691L mutations into pMIY hFLT3/NPOS*). Individual mutagenic primers were designed using Agilent QuikChange Primer Design Program. The following reaction mixture and PCR protocol were used:

Reaction buffer 10x	5 µl
dNTP mix	1 µl
QuikSolution	3 µl
PfuUltra HF DNA polymerase	1 µl

Primer, forward (10 µM)	Volume corresponding to 125 ng
Primer, reverse (10 µM)	Volume corresponding to 125 ng
dsDNA template	Volume corresponding to 10 ng
d_2H_2O	Fill up to 50 µl

PCR program

	95 °C	1 min
18x	95 °C	50 s
	60 °C	50 s
	68 °C	1 min/kb plasmid length
	68 °C	7 min

Afterwards 1 µl Dpn I restriction enzyme was added and the mixture incubated for 1 h at 37 °C to digest the methylated parental DNA. XL10-Gold Ultracompetent Cells were thawed on ice. 45 µl cells were mixed with 2 µl β-mercaptoethanol and incubated for 10 min on ice, swirling the tube every 2 min. 2 µl of the mutated DNA were now added to the tube and the mixture incubated on ice for 30 min before heat-pulsing the tube at 42 °C for 30 s. The tube was afterwards again incubated on ice for 2 min. 0.5 ml prewarmed SOC medium (42 °C) were now added per tube and the sample incubated for 1 h at 37 °C under continuous shaking (210 rpm). 250 µL of the transformation reaction was then plated on an LB-ampicillin agar plate. After an overnight incubation at 37 °C, single colonies were picked and plasmid DNA isolated with QIAprep Spin Miniprep Kit according to the manufacturer's instructions.

**pMIY hFLT3/NPOS vector was generated by AG Spiekermann/KKG Leukämie.*

Generation of Leu234Ala/Leu235Ala (LALA) point mutations in 20D9h3/IgG1

Leu234Ala/Leu235Ala (LALA) point mutations were generated by Jonathan Schwach (AG Leonhardt, LMU) as described in his thesis (soon to be published).

2.2.9.2 In-Fusion cloning

In-fusion seamless ligase-independent cloning was used according to the supplier's instructions. It was applied to clone target sequences (e.g. rFLT3) into the pMIY vector. Briefly, the target vector was linearized using suitable restriction enzymes (e.g. EcoRI and XhoI). The insert was PCR amplified using special primers (designed by SnapGene software) to achieve 15 bp overhanging ends complementary to the vector. The following protocol was used:

CloneAmp Hifi PCR Premix 2x	12.5 µl
Primer, forward (10 µM)	0.75 µl
Primer, reverse (10 µM)	0.75 µl
Template (vector)	Volume corresponding to 10 ng
d_2H_2O	Fill up to 25 µl

PCR program

33x	Denaturation	98 °C	10 s
	Annealing	55 °C	15 s
	Elongation	72 °C	5 s / kb

After the PCR, the reaction mix was loaded on an agarose gel to verify that the amplicon has been amplified successfully and appears at the desired size. The amplicon was then cleaned up from the gel using QIAQuick PCR Purification kit and ligated with the linearized target vector for 15 min at 50 °C using the following mixture:

Purified PCR fragment	Volume corresponding to 10-200 ng*
Linearized vector	Volume corresponding to 50-200 ng**
5x In-Fusion HD enzyme premix	2 µl
d_2H_2O	Fill up to 10 µl

**<0.5 kb: 10-50 ng, 0.5-10 kb: 50-100 ng, >10 kb: 50-200 ng*

***<10 kb: 50-100 ng, >10 kb: 50-200 ng*

Meanwhile, Stellar™ Competent Cells were thawed on ice. 10 ng of the In-Fusion reaction mixture were added to 30 µl cells and incubated on ice for 30 min, heat-shocked 45 s at 42 °C and transferred back to ice for 1-2 min. 500 µl warm SOC medium were added to the cells and the mixture was incubated for 1 h at 37 °C under continuous shaking (210 rpm). 100 µl were spread on LB agar plates containing 100 µg/ml ampicillin for selection. After an overnight incubation at 37 °C, single colonies were picked and plasmid DNA was isolated with QIAprep Spin Miniprep Kit according to the manufacturer's instructions and sequenced as described.

2.2.9.3 Bacterial retransformation and plasmid DNA isolation

To expand plasmid DNA, Stellar™ Competent Cells were used as described above. After the overnight incubation on LB agar plates, a single colony was transferred to 2 ml ampicillin-containing LB medium (100 µg/ml) and incubated for 8 h at 37 °C, 300 rpm. 150 µl of the pre-culture was transferred into 100 ml LB medium with 100 µg/ml ampicillin in an Erlenmeyer flask and again incubated overnight under the same conditions as before. Only then, plasmid DNA was

isolated, now using EndoFree Plasmid Maxi Kit as described by the manufacturer. Plasmid DNA concentration and quality was determined using DeNovix DS-11+ spectrophotometer, afterwards aliquots of the isolates were stored at -20 °C until further use.

2.2.9.4 Restriction digest

Restriction digest was used to linearize vectors for In-fusion cloning and to check for correct products afterwards. Enzymes were applied as recommended by the manufacturer mostly using adaptions of the following protocol:

Restriction buffer 10x	2 µl
Fast digest restriction enzyme(s)	1 µl of each
Template (vector)	Volume corresponding to 1 µg
d_2H_2O	Fill up to 20 µl

Incubation for 5-15 min at 37 °C.

2.2.9.5 Agarose gel electrophoresis of nucleic acids

Agarose gel electrophoresis was used after PCR amplification and to assess correct cloning (after restriction digestion). 0.8-1.5% agarose gels were prepared by solving agarose in 1x TAE buffer and adding 0.1 µg/ml SYBR-Safe fluorescent dye, and subsequently carefully heating the mixture in the microwave until the agarose dissolved. Afterwards the soluble agarose mix was cooled down to 50 °C and gels were prepared in gel trays. A running chamber was set up, in which the solidified gel was placed in 1x TAE buffer. DNA samples were mixed with Orange DNA loading dye (6x) and pipetted into the gel pockets together with a molecular weight marker. Samples were run for around 2 h at 80-100 V before visualizing the DNA fragments under the UV light.

2.2.9.6 Sanger sequencing

Correct sequences after cloning or mutagenesis were confirmed by Sanger sequencing using the primers listed in Table 14. Sequencing was performed externally by Sequiserve (Vaterstetten, Germany).

2.2.10 Statistical analyses

All statistical analysis was done with GraphPad Prism version 10.1.2. IC_{50} and EC_{50} values for cytotoxicity assays and ELISA were calculated using non-linear fit variable slope analysis or one

site - total and nonspecific binding analysis, respectively. For statistical analyses, data was first tested for normal distribution and the appropriate statistical test was chosen as specified in each figure legend together with the p values (which were adjusted for multiple comparisons). Data is depicted as mean ± standard deviation (SD) from three biological replicates, unless explicitly described otherwise.

3 Results

LSCs represent the source of AML blasts and are a main cause of treatment failure. Finding ways to specifically eliminate LSCs is crucial for therapeutic success. Targeted agents such as ADCs have become increasingly important in all cancer entities including AML and represent a promising anti-LSC approach. Goal of this work was thus the development of an LSC-targeting ADC. To this end, the previously generated chimeric FLT3-mAb 20D9 was humanized and the clone with the best characteristics was identified out of 16 candidates. Two payloads with different mechanisms of action were selected and conjugated to the antibody to yield ADCs. This was followed by extensive *in vitro* activity studies, mechanistic analyses and most importantly evaluation of the ADCs activity towards leukemic stem and progenitor cells in comparison to their healthy equivalents. Finally, for the ADC with a higher anti-LSC activity a combination with two other agents that could potentiate its effectivity towards LSCs was tested.

3.1 FLT3 antibody humanization and selection of the lead candidate 20D9h3

In a previous project, the chimeric FLT3-mAb 20D9 had been generated serving as basis for my work (139, 143). 20D9-mAb was raised in rat but has been chimerized by cloning the variable domain into human IgG1 expression vectors. Chimeric antibodies possess human constant domains (C_H1-C_H3 and C_L); however, the variable domain is still from the animal of origin. To reduce immunogenicity, antibodies that are used in humans are usually fully humanized (151), which was the first aim of my project.

3.1.1 20D9 humanization and basic characterization of the humanized mAbs

The process of antibody humanization and identification of a lead candidate for ADC development is schematically illustrated in Figure 6.

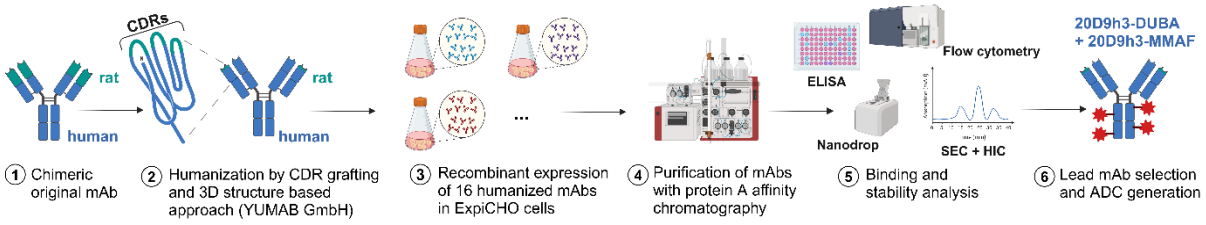

Figure 6: Humanization workflow for FLT3-mAb 20D9. 20D9 monoclonal antibody (mAb) has been originally generated in rats and was chimerized as part of a previous project (139, 143). In this project, 20D9-mAb was now humanized using complementarity-determining region (CDR) grafting and a 3D structure-based approach. 16 humanized sequences were cloned in immunoglobulin G1 (IgG1) expression vectors and transfected in Chinese hamster ovary (CHO) cells for expression. The mAbs were harvested after 7-10 d and purified by FPLC protein A affinity chromatography. 12 mAbs could be successfully produced and were analyzed extensively for stability and binding properties to find an ideal clone for later ADC generation. Humanization and cloning of the mAb sequences in expression vectors was carried out externally by YUMAB GmbH. Antibody production, purification and stability analyses were done by Jonathan Schwach (AG Leonhardt, LMU). Schematic was generated with Biorender.com.

Humanization was carried out by the company YUMAB GmbH (Braunschweig, Germany). Using complementarity-determining region (CDR) grafting technology, rat amino acids in the V_H and V_L framework regions were stepwise replaced by their human analogues. This process yielded three different variable heavy (V_H) and variable light (V_L) chain sequences, respectively, with an increasing proportion of human amino acids. Additionally, a fourth sequence variant of V_H and V_L was generated by *in silico* 3D structure-based humanization. By combining the sequences of V_H and V_L in a 4x4 matrix, 16 different mAbs with degrees of humanization varying between 90.2% and 100% (versus 84.7% for the 20D9 original chimeric clone) have been generated. Humanized antibodies were produced by Jonathan Schwach (AG Leonhardt, LMU) via transient expression in ExpiCHO-S cells (high-expressing Chinese hamster ovary (CHO) cell line) followed by purification with protein A affinity chromatography on an FPLC system. Four antibodies (20D9h13-20D9h16) were excluded from further analysis as they could not be successfully expressed. The remaining mAbs showed variable yields between 18-166 mg/l cell culture with 20D9h7 and 20D9h3 as best candidates in this category (Table 18).

Table 18: Characterization of the 12 humanized mAbs in different assays. Dark grey indicates above average performance, light grey average performance and white below average performance in the respective category; the selected lead candidate is marked in orange. Production efficiency was measured by Jonathan Schwach (AG Leonhardt, LMU).

		Humanized 20D9-											
	20D9	**h1**	**h2**	**h3**	**h4**	**h5**	**h6**	**h7**	**h8**	**h9**	**h10**	**h11**	**h12**
production efficiency (mg/l cell culture)	30	58	92	**144**	126	103	140	166	85	47	49	48	18
affinity (EC_{50} in ng/ml)	10.9	11.4	11.4	**11.3**	11.0	29.3	33.5	37.1	29.3	83.4	77.8	111.6	55.3
binding to human FLT3 (MFI ratio to IgG1 control)	84.7	96.0	96.0	**95.3**	98.2	42.4	41.3	45.7	43.7	21.3	20.2	20.5	24.8
mean degree of humanization/GI (in %)*	84.7	90.2	91.2	**94.7**	94.1	93.1	94.4	97.6	97.1	95.5	96.8	100	99.5
humanized V_H and V_L chain combination	chimeric	V_H1	V_H2	V_H3	V_H4	V_H1	V_H2	V_H3	V_H4	V_H1	V_H2	V_H3	V_H4
		V_L1				V_L2				V_L3			

*mean GI (V_H+V_L); EC_{50} = half-maximal effective concentration; GI = germinality index; MFI = mean fluorescence intensity; V_H = variable domain of immunoglobulin heavy chain; V_L = variable domain of immunoglobulin light chain

Next, 20D9h1-20D9h12 were tested in different assays to evaluate their stability and affinity. To test the former, all mAbs were incubated at 37 °C in storage buffer (PBS with 50 mM L-arginine and 0.1% sodium azide) for up to 28 d. At regular intervals, samples were taken and analyzed by HPLC-size exclusion chromatography (SEC) and HPLC-hydrophobic interaction chromatography (HIC). All mAbs appeared to be stable over the course of the study since no significant aggregation could be detected in any of the above-mentioned assays (further details: Thesis Jonathan Schwach). The binding affinity of the antibodies was subsequently evaluated in ELISA. For this

purpose, recombinant human FLT3 was coated on plates and incubated with the different antibody clones. Binding affinities ranged from half-maximal effective concentration (EC_{50}) values of 11.0 ng/ml to 111.6 ng/ml. The antibodies 20D9h1-20D9h4 performed best with similar EC_{50} values compared to the original chimeric 20D9 (Table 18). To further evaluate binding in a cellular context, the antibodies were incubated with murine Ba/F3 cells stably expressing human wildtype FLT3 (hFLT3high), cynomolgus monkey FLT3 (cynoFLT3) or no surface receptor (ev). Those Ba/F3 cells were generated previously by Maike Roas and successful expression of surface receptors was demonstrated (139, 143). Binding of the humanized anti-FLT3 mAbs to those cells was now assessed by flow cytometry. Similar as in the ELISA, 20D9h1-20D9h4 mAbs showed the highest binding to hFLT3 (Table 18) of all humanized antibody clones, slightly increased compared to 20D9 chimeric mAb. All humanized clones also maintained the ability to bind to cynoFLT3 (supplemental Figure 1A). None of the clones bound to empty vector control cells (supplemental Figure 1B) confirming specificity of binding. Considering the results of the binding studies together with production efficiency, stability and degree of humanization, 20D9h3 and 20D9h4 clones were the best candidates. Due to the higher degree of humanization of 94.7 %, we finally selected 20D9h3 as single lead candidate for ADC generation and went on to characterize it further.

3.1.2 In-depth characterization of 20D9h3-mAb

Next, 20D9h3-mAb was examined in more detail. I was particularly interested in antibody internalization and in the cross-reactivity towards mutants, orthologues and paralogues of FLT3 receptor.

3.1.2.1 Analysis of antibody internalization

For an ADC, a fast and target-dependent internalization is crucial as it delivers the effective agent inside the cell (152). Two different methods were used to evaluate if the high internalization efficiency that had been previously observed for the chimeric 20D9-mAb (139, 143) is preserved in 20D9h3-mAb upon humanization. First, Ba/F3-pMIY ev cells or Ba/F3 cells expressing FLT3 at a high (hFLT3high) or low (hFLT3low, expression in Figure 9B) level were incubated with a mixture of 20D9h3-mAb complexed with pHrodo-labelled secondary antibody – kindly provided by Dr. Saskia Schmitt (Tubulis GmbH) – for 1 h, 5 h and 24 h. The pHrodo fluorophore is only fluorescent at low pH in the late endosome or lysosome. Thus, successful internalization can be monitored by flow cytometry or confocal microscopy (Figure 7A). The former demonstrated fast and FLT3-level dependent mAb internalization with intracellular 20D9h3 present after 1 h (Figure 7B). This finding was also supported by microscopy data (Figure 7C, microscopy was carried out in collaboration with Jonathan Schwach, AG Leonhardt, LMU).

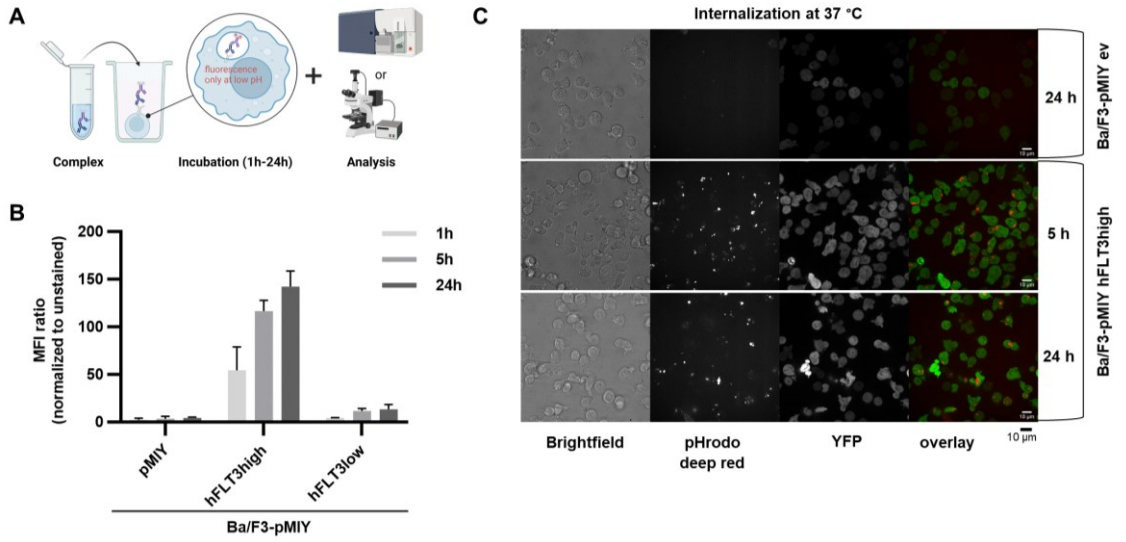

Figure 7: Analysis of 20D9h3-mAb internalization by flow cytometry and confocal microscopy. (A) Scheme of the internalization assay. 20D9h3 was incubated for 15 min with goat anti-human pHrodo-labelled secondary antibody. The mixture was then added to Ba/F3-pMIY cells expressing hFLT3 or ev for 1-24 h at 37 °C. The cells were subsequently analyzed with flow cytometry or microscopy. (B) Flow cytometry analysis of cells incubated 1 h, 5 h or 24 h with complexed 20D9h3. mean ± s.d.; n = 3 biological replicates. (C) Confocal microscopy after 5 h and 24 h incubation. Green = YFP expression, red = 20D9h3-mAb complexed with pHrodo-labelled secondary antibody. scale bar = 10 µm. pHrodo-labelled secondary antibody was conjugated by Dr. Saskia Schmitt (Tubulis GmbH). Microscopy was performed together with Jonathan Schwach (AG Leonhardt, LMU). Image A was generated with Biorender.com.

To further confirm successful internalization and verify that 20D9h3-mAb is suitable for ADC generation, it was conjugated with the microtubule-targeting payload MMAF that had already been shown to be functional together with chimeric 20D9 in the context of previous work (139, 143), as demonstrated *in vitro* and *in vivo*. The efficacy of 20D9h3-MMAF ADC was evaluated in comparison to 20D9-MMAF in Ba/F3 cells expressing hFLT3high or empty control construct and in the FLT3-positive and FLT3-negative cell lines MOLM-13 and K-562, respectively (Figure 8).

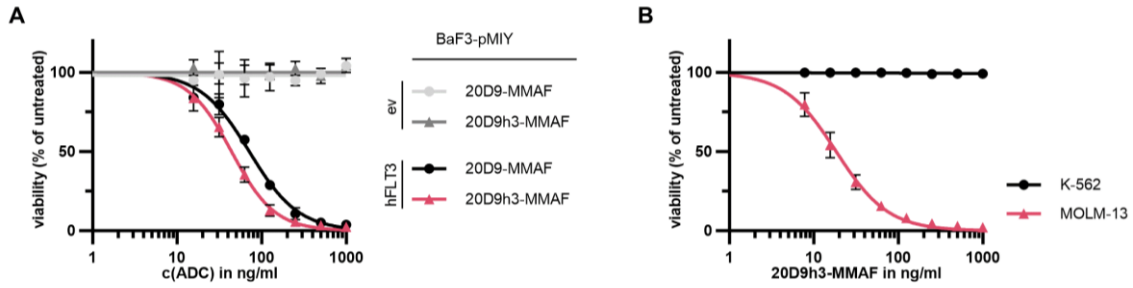

Figure 8: Analysis of 20D9h3-MMAF internalization by cytotoxicity assay. (A) Ba/F3-pMIY ev or hFLT3 cells were incubated with 20D9-MMAF or 20D9h3-MMAF for 72 h. Viable cells were assessed by trypan blue exclusion count and are depicted normalized to untreated control. Non-linear fit analysis was done with GraphPad Prism 10.1.2. mean ± s.d.; n = 3 biological replicates. (B) FLT3-positive MOLM-13 cells and FLT3-negative K-562 cells were incubated with 20D9h3-MMAF for 96 h. Viable cells were assessed by resazurin assay and are depicted normalized to untreated control. Non-linear fit analysis was done with GraphPad Prism 10.1.2. mean ± s.d.; n = 3 biological replicates.

20D9h3-MMAF ADC showed similar or even slightly superior efficacy compared to chimeric 20D9-MMAF ADC in the Ba/F3 model (Figure 8A). Further it was cytotoxic to FLT3-positive MOLM-13 cells, but not to FLT3-negative K-562 cells (Figure 8B). Taken together, these results indicate that the 20D9h3 antibody fulfils important criteria for ADC development.

3.1.2.2 Cross-reactivity with orthologues and paralogues of FLT3

Next, it was tested if 20D9h3-mAb binds to orthologues of FLT3 from cynomolgus monkey, mouse or rat as this might be relevant for further pre-clinical tests. Chimeric 20D9-mAb was generated in rats which made cross-reactivity with rodent FLT3 unlikely also for the humanized version 20D9h3. Indeed, flow cytometry with Ba/F3-pMIY cells expressing human, cynomolgus monkey (cynoFLT3), rat (rFLT3) or murine FLT3 (mFLT3) confirms that 20D9h3-mAb only binds to human and cynomolgus monkey FLT3, but not rat or murine FLT3 (Figure 9A, surface expression confirmed in Figure 9B-C and in Roas et al. (139) for cynoFLT3 and mFLT3).

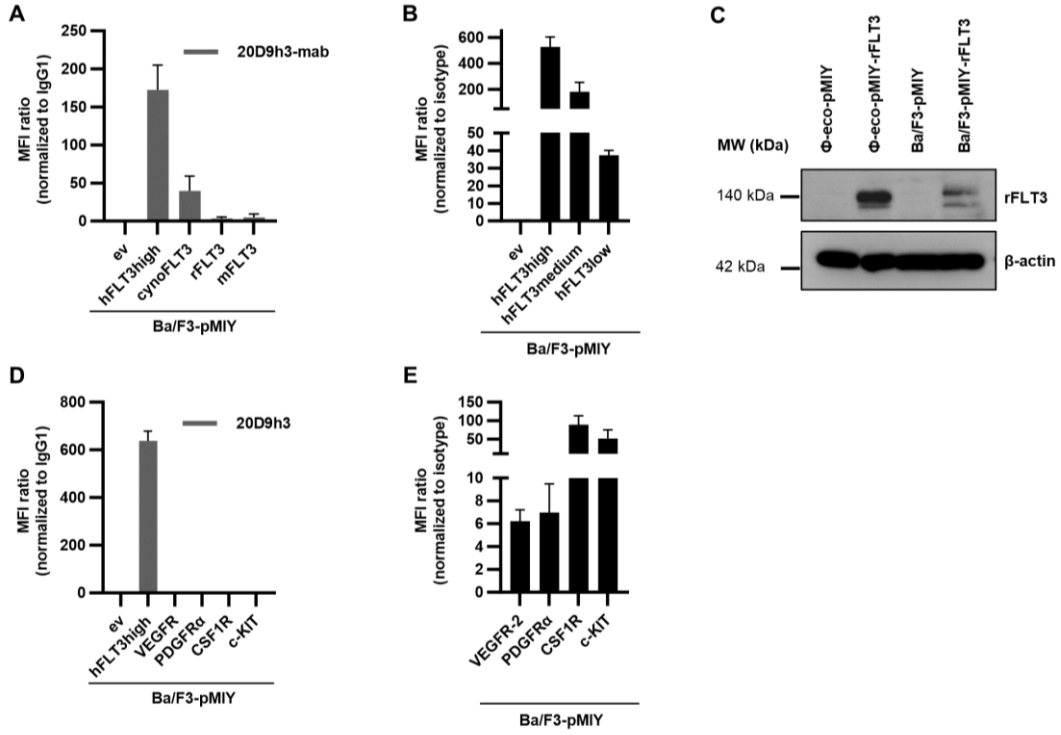

Figure 9: Cross-reactivity of FLT3 antibodies with paralogues and orthologues of FLT3. Experiments were carried out with murine Ba/F3 cells as model system stably expressing YFP and different human receptors or empty vector (ev) control. (A) Binding of 20D9h3-mAb to FLT3 orthologues from human (hFLT3high), cynomolgus monkey (cynoFLT3), rat (rFLT3) and mouse (mFLT3) measured by flow cytometry and depicted as mean fluorescence intensity (MFI) ratio to IgG1 control. (B) Cell surface expression of hFLT3 was measured in Ba/F3 cells by flow cytometry. MFI was normalized to isotype control. Note the break in the y-axis. mean ± s.d.; n = 3 biological replicates. (C) Expression of rFLT3 in stably transfected Ba/F3 cells and transiently transfected Φ-eco cells was verified by Western Blot. β-actin was used as loading control. MW = molecular weight. (D) Binding of 20D9h3-mAb to FLT3 paralogues depicted as MFI ratio normalized to IgG1 control. mean ± s.d.; n = 3 biological replicates. (E) Cell surface expression of FLT3 paralogues VEGFR-2, PDGFRα, CSF1R and c-KIT was measured in Ba/F3 cells by flow cytometry. MFI was normalized to isotype control. Note the break in the y-axis. mean ± s.d.; n = 3 biological replicates.

Second, it was evaluated if 20D9h3-mAb is specific for FLT3 or if it also binds to structurally related RTKs, which would increase side effects. Ensembl.org (Ensembl Release 109, (153)) and the NCBI Tool Vast+ (154) were used to screen for paralogues of FLT3 with similar sequence or high 3D structural similarity, respectively. To select the most relevant RTKs out of these, the sequences were aligned to FLT3 using Benchling software (www.benchling.com) to compare homologies of the epitope region of 20D9-mAb on the FLT3 receptor with the corresponding regions on the other receptors. Of all RTKs, vascular endothelial growth factor receptor 2 (VEGFR-2), platelet-derived growth factor receptor alpha (PDGFRα), macrophage colony-stimulating factor 1 receptor (CSF1R) and stem cell growth factor receptor kit (c-KIT) show the highest degree of homology with FLT3. Ba/F3 cells were used that stably express those human RTKs to test 20D9h3-mAb binding via flow cytometry. It is evident that despite the structural resemblance of the receptors, 20D9h3-mAb is highly specific for FLT3 and does not show binding to any of the other RTKs (Figure 9D, receptor surface expression in Figure 9E, Ba/F3 cells expressing FLT3 paralogues were generated by Dr. Harald Polzer, AG Spiekermann, as part of his thesis (142)).

3.1.2.3 Cross-reactivity with mutants of FLT3

FLT3 mutations are quite common in AML and negatively correlate with outcome (77). Around one third of the patients are affected by either ITD mutations in the JMD or point mutations in the TKD and very rarely JMD (73-75). TKIs are the most advanced FLT3-directed therapy and are frequently used in *FLT3*-ITD mutated patients. However, they have the disadvantage that their effectivity is negatively influenced by TKD mutations that are either initially present or arise as secondary mutations in *FLT3*-ITD cells in response to therapy. (90, 155) For successful FLT3-directed therapy, it is thus of high relevance, that the drug is also active in *FLT3*-mutated cells. As both ITD and TKD mutations are located in the intracellular part of FLT3, it is unlikely that they affect the activity of an ADC. To confirm this, I analyzed the binding of the FLT3-mAb to different FLT3 mutants. As these experiments were already performed as part of a previous project (139), they were carried out with the chimeric 20D9 antibody rather than its humanized version 20D9h3. As repeatedly seen, both mAbs have very similar binding properties as the binding epitope was not changed during the humanization procedure. Therefore, the results generated with 20D9-mAb should be transferrable to 20D9h3-mAb. It was observed that 20D9-mAb binds to all mutant FLT3 versions (Figure 10A). Compared to the binding of 20D9-mab to wildtype FLT3 (hFLT3high), the binding to FLT3-mutated cells was reduced in all cases except for hFLT3/NPOS N676K. It is known that the ITD-mutated FLT3 receptor is retained in intracellular compartments (67). Therefore, less binding is most likely due to reduced surface expression of the FLT3-mutants compared to wildtype FLT3 and not due to impaired antibody binding. This lower cell surface expression compared to wildtype FLT3 was confirmed by flow cytometry (Figure 10B).

Collectively, the results from the cross-reactivity studies show that 20D9h3-mAb affinity is most likely not affected by FLT3 mutations. 20D9h3-mAb does bind to FLT3 orthologues from cynomolgus monkey but not from rat or mouse. This is not unusual for therapeutic mAbs and ADCs but hampers toxicological investigations in those species and limits them to nonhuman primates (156). Lastly, 20D9h3-mAb does not bind to FLT3 paralogues which is favorable concerning the side effect profile of the planned ADC.

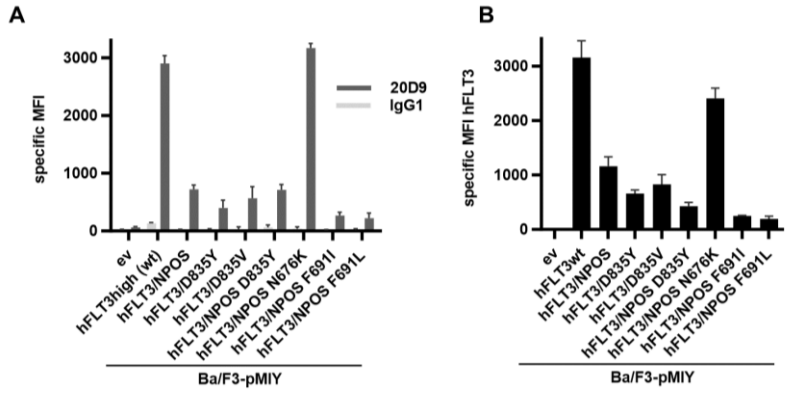

Figure 10: Cross-reactivity of FLT3 antibodies with mutants of FLT3. Experiments were carried out with murine Ba/F3 cells as model system stably expressing YFP and different human surface receptors or empty vector (ev) control. (A) Binding of 20D9- and IgG1-mAbs to wildtype (wt) FLT3 (hFLT3high) or FLT3 versions with primary or secondary resistance mutations. Binding was measured by flow cytometry. MFI = mean fluorescence intensity. mean ± s.d.; n = 3 biological replicates. (B) Cell surface expression of wildtype FLT3 and different FLT3 mutants. mean ± s.d.; n = 3. Figure was adapted from Roas et al (139) with permission from *Blood*.

3.1.3 Generation and analysis of Leu234Ala/Leu235Ala mutated mAbs

The constant Fc region of an antibody is not involved in antigen binding, however it interacts with FcγRs and can lead to effector functions carried out by macrophages (ADCP) or NK cells (ADCC) or complement-dependent effects (CDC) (106). For unconjugated therapeutic antibodies those effector functions are crucial to mediate their effect. For ADCs, however, it remains unclear whether the positive aspects outweigh the increased off-target toxicity caused by internalization of the ADC via FcγRs. Further, it is not known whether and to what extent FcγR-mediated uptake enhances the killing of LSCs and leukemic progenitors. To investigate these questions, the Fc part of 20D9h3-mAb was modified to inhibit the binding to FcγRs. As reviewed by Kevin O. Saunders 2019, different modifications are possible in the Fc region – some enhancing and some ablating effector functions. One very elegant way to ablate effector functions is a combination of the two amino acid exchanges Leu234Ala and Leu235Ala (the so-called “LALA” mutation). This mutation has been reported to eliminate binding of IgG1 antibodies to FcγRI, FcγRII and FcγRIII. (100, 157) As a control for FcγR binding the antibody palivizumab (referred to as IgG1-mAb) was used, which has an identical IgG1 backbone compared to 20D9h3 but a variable domain directed towards

respiratory syncytial virus glycoprotein F (158), which is irrelevant in AML cells. The LALA-mutation was introduced in the Fc part of 20D9h3-mAb and the palivizumab IgG1 control by Jonathan Schwach (AG Leonhardt, LMU) to generate 20D9h3-LALA and IgG1-LALA antibodies (Figure 11A). In flow cytometry it was evaluated if the ablation of FcγR binding has been successful without affecting FLT3 binding. This was carried out using Ba/F3 cells that express FcγRI, FcγRII, FcγRIII or hFLT3high (Figure 11B, expression was confirmed in (139)). The binding to FcγRIII and FcγRII was low to absent in the non-mutated mAbs and completely abolished by LALA mutation.

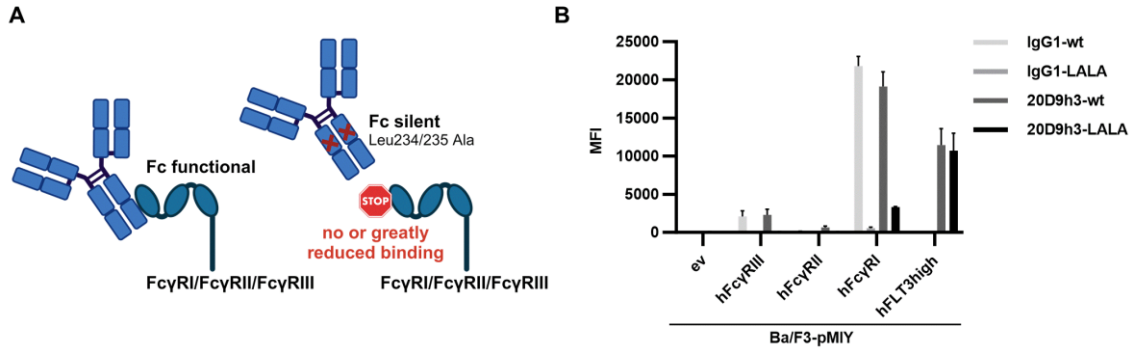

Figure 11: Generation and analysis of 20D9h3 antibodies with Leu234Ala/Leu235Ala (LALA) mutated Fc part. (A) Scheme of antibody modification by Leu234Ala/Leu235Ala (LALA) mutation. This mutation is introduced in the antibody's Fc part to ablate binding to Fc gamma receptors (FcγRs). (B) Binding of 20D9h3 and IgG1 control antibody with either wildtype (wt) or LALA-mutated Fc region, respectively, to Ba/F3-pMIY cells expressing ev, FcγRI, FcγRII or FcγRIII. Values are depicted as mean fluorescence intensity (MFI). mean ± s.d.; n = 4. LALA-mutated antibodies were generated by Jonathan Schwach (AG Leonhardt, LMU). Figure 11A was generated with Biorender.com.

In contrast, mAbs with unmodified Fc region (20D9h3-wt, IgG1-wt) showed a high binding affinity to FcγRI, which was greatly reduced but not completely abolished by the introduction of the LALA mutation. As expected, hFLT3 binding – which is mediated by the Fab region – was unaffected by Fc engineering (Figure 11B).

3.2 Payload selection

In the first part of this project, the FLT3 antibody 20D9h3 has been identified as suitable candidate for ADC development. The second important component of an ADC is the payload. In this part the goal was to find a suitable agent fulfilling the following criteria: 1) A FLT3-targeting ADC should ideally be equipped with a highly potent payload. The reason being that the expression of FLT3 – compared to other AML targets such as CD33 – is relatively low (47, 63). 2) Successful killing of LSCs requires a payload with a mechanism of action that that is efficient in quiescent cells. At the moment mainly two classes of toxins are very common in the ADC field: microtubule disrupting agents such as auristatins, e.g. MMAE or MMAF, and DNA-damaging agents of the class of calicheamicins, PBDs, IGNs, DCMs e.g. DUBA or exatecans (104). Of those two classes the DNA-damaging agents are commonly regarded as the better choice to address stem cells due to their cell-cycle independent mechanism of action (123-125).

3.2.1 Potency of different ADC payloads in leukemia cell lines and Ba/F3 cells

To identify a potent payload for the FLT3-ADC, the cytotoxicity of toxins of different classes was first analyzed in four human leukemia cell lines – MOLM-13, MV4-11, K-562 and HL-60 – and in the murine pro-B cell line Ba/F3. Overall, the DNA-damaging payload DUBA was most effective in all cell lines with IC_{50} values of 0.58 – 21.25 nM after 24 h compared to 1.56-2834 nM for MMAE and 2.42 – 790.9 nM for exatecan (Figure 12). MMAF – a structural analogue of MMAE – is an efficient ADC payload but difficult to directly compare with other payloads as a toxin alone as it has a low membrane-permeability on its own (159). Therefore, the IC_{50} values are quite high (> 1000 nM for all cell lines). Remarkably, DUBA was also very effective in the K-562 cell line, which shows a generally higher resistance towards all other payloads (Figure 12D).

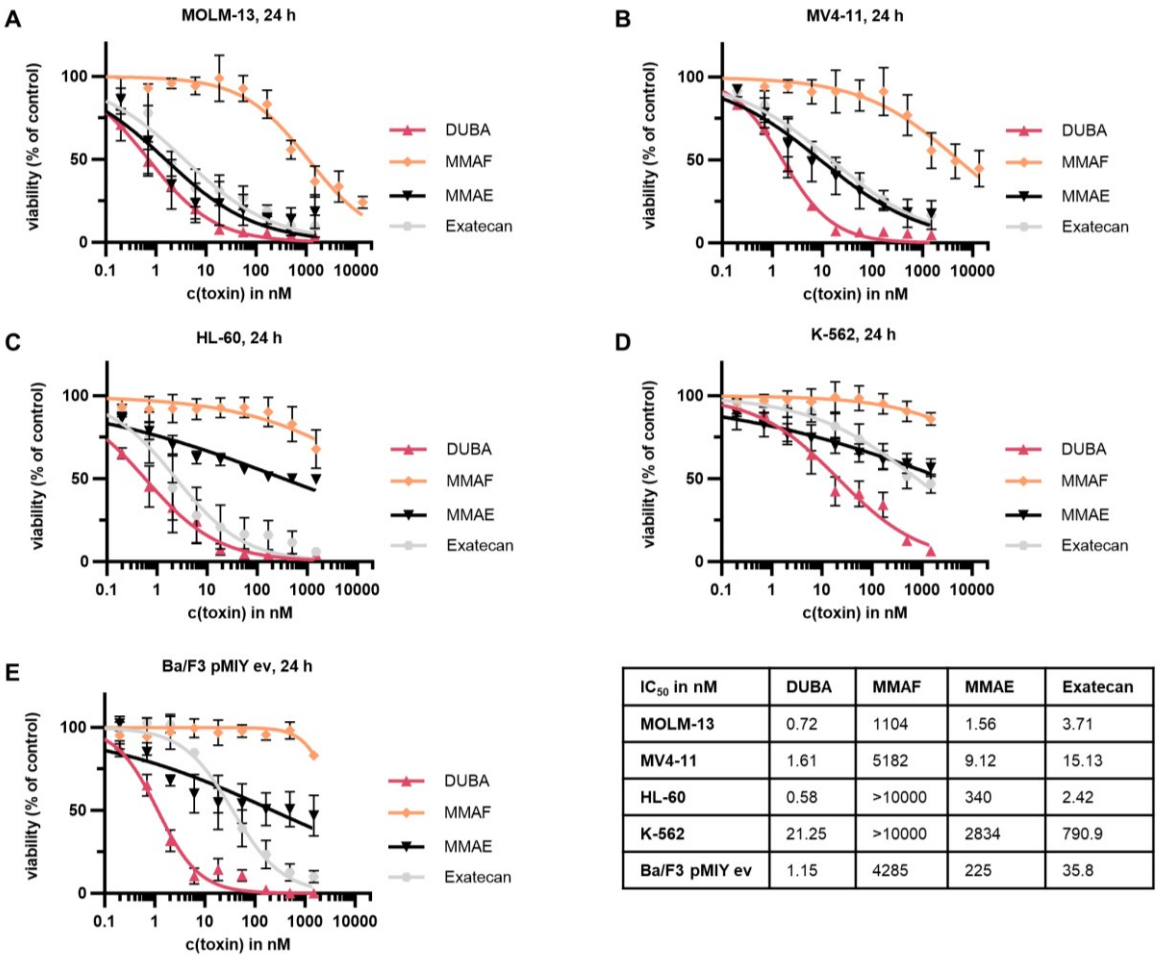

IC_{50} in nM	DUBA	MMAF	MMAE	Exatecan
MOLM-13	0.72	1104	1.56	3.71
MV4-11	1.61	5182	9.12	15.13
HL-60	0.58	>10000	340	2.42
K-562	21.25	>10000	2834	790.9
Ba/F3 pMIY ev	1.15	4285	225	35.8

Figure 12: Analysis of different ADC payloads in leukemia cell lines and the Ba/F3 model. MOLM-13 (A), MV4-11 (B), HL-60 (C), K-562 (D) and Ba/F3-pMIY ev cells (no surface receptor expression) were incubated with different concentrations of DUBA, MMAF, MMAE or exatecan. After 24 h, viable cells were assessed by resazurin assay (AML cell lines) or CellTiter-Glo luminescence assay (Ba/F3 cells). Values were normalized to vehicle-treated control (treatment with dimethyl sulfoxide (DMSO)). Calculation of inhibitory concentration (IC_{50}) values was performed with GraphPad Prism 10.1.2 using nonlinear fit variable slope. mean ± s.d.; n = 3 biological replicates.

3.2.2 Evaluation of DNA-damaging and microtubule-targeting payloads in proliferation-inhibited cells

I further wanted to address the question whether either payload class had the capability to kill cells that do not proliferate. In order to mimic such a resting state with cell lines, they were treated with aphidicolin. Aphidicolin is a drug that inhibits the DNA polymerases α and δ and is often used as a tool to synchronize cells in their cell cycle progression (160, 161). In a preliminary experiment, it was confirmed that aphidicolin completely arrests cell proliferation of MOLM-13 and MV4-11 cells at doses ≥ 0.37 µM with only minor effects on viability (Figure 13A). In cell cycle analysis, it was evident that aphidicolin treatment accumulates cells in G1 (Figure 13B), which is in line with its mechanism of action.

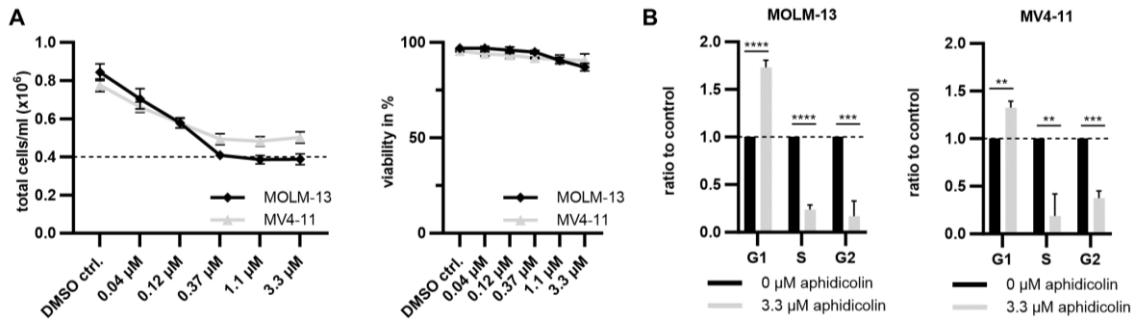

Figure 13: Effect of aphidicolin treatment on proliferation, viability and cell cycle progression. (A) After treatment of MOLM-13 and MV4-11 cells with 0.04-3.3 µM of aphidicolin for 24 h, cell proliferation (total cells/ml) and viability (%) were assessed by trypan blue exclusion count. Dashed line represents seeded cell number. mean ± s.d.; n = 3 biological replicates. (B) MOLM-13 and MV4-11 cells were incubated with aphidicolin for 48 h. Subsequently, cell cycle was measured by flow cytometry and normalized to DMSO-treated control. mean ± s.d.; n = 3 biological replicates. **P<.01; ***P<0.001; ****P<0.0001 by Unpaired Student's t test.

Next, MOLM-13 and MV4-11 cells were pre-treated with aphidicolin for 24 h and then incubated for 24 h with either DUBA (Figure 14A), MMAE (Figure 14B) or exatecan (Figure 14C). MMAF was not included due to its low membrane-permeability. In MOLM-13 cells, the IC_{50} values in G1-arrested cells (treated with 3.3 µM of aphidicolin) in comparison to non-arrested cells (treated with DMSO as vehicle-control) were reduced by a factor of 127.7 for MMAE, 55.4 for exatecan and 9.8 for DUBA, respectively. Similarly, in MV4-11 cells the biggest reduction of the IC_{50} value in presence of 3.3 µM aphidicolin was observed for MMAE (4.4x), followed by exatecan (3x) and DUBA (2.4x). These differences are illustrated by the green arrows (see also supplemental Table 1). Generally, the inhibitory effect of aphidicolin on the cytotoxicity of the ADC payloads was dose-dependent and fully apparent at aphidicolin doses ≥ 0.37 µM, a dose at which a full arrest in cell proliferation was observed. Taken together, those results indicate that indeed DNA-damaging agents outperform microtubule-targeting agents in resting cells. Proliferation-inhibited cell lines are, however, no adequate model for AML LSCs. Instead, these experiments only gave a first hint at which agents could be promising and should be further evaluated in the context of ADCs. DUBA was selected for ADC generation because of its potency and promising activity in resting cells. Furthermore, MMAF was chosen, as I was interested in the question whether microtubule-targeting agents are inferior to DNA-damaging agents in the elimination of LSCs. Additionally, MMAF was already well-known to function in the context of a FLT3-targeting ADC due to the previous projects of our group thus being a good control. Both selected payloads were conjugated to 20D9h3-mAb and analyzed for their efficacy in cytotoxicity assays and for their potential to eliminate LSCs in colony and LIC assays.

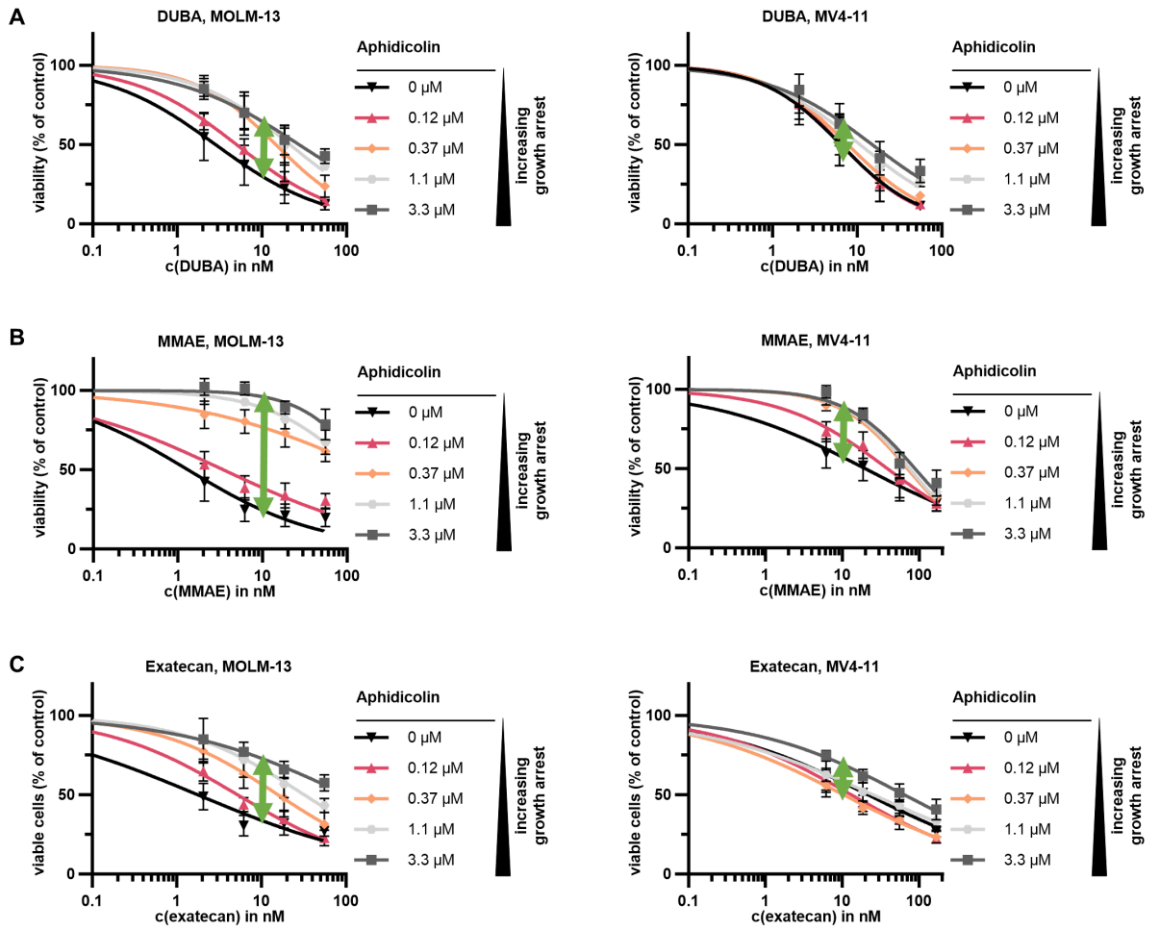

Figure 14: Payload toxicity in cell lines arrested with aphidicolin. After 24 h pre-treatment of MOLM-13 and MV4-11 cells with 0.12-3.3 µM aphidicolin, cells were incubated with a dilution row of DUBA (A), MMAE (B) or exatecan (C) for another 24 h. Viable cells were assessed with resazurin assay. Values are depicted normalized to the respective aphidicolin-only control. Green arrows should illustrate the difference in the IC_{50} values between proliferating (treated with DMSO vehicle-control only) and arrested cells (pre-treated with 3.3 µM aphidicolin). mean ± s.d.; n = 4 biological replicates.

3.3 ADC generation and *in vitro* evaluation

Anti-FLT3 mAb 20D9h3 was identified as lead candidate for ADC generation, DUBA and MMAF were selected as payloads, and 20D9h3-ADCs were generated with each drug, respectively. These ADCs were first evaluated in the Ba/F3 model. Here, I also investigated how FLT3-mediated and FcγRI-mediated effects contribute to overall ADC efficacy using 20D9h3-DUBA. Further, both ADCs were tested side-by-side on different leukemia cell lines and their mechanism of action was evaluated in more detail.

3.3.1 ADC conjugation, analysis of DAR and quality control

To generate 20D9h3-DUBA, the commercially available vc-*seco*-DUBA linker-payload and maleimide-cysteine conjugation (162) was used. 20D9h3-MMAF was conjugated with Tubulis' proprietary P5-technology (150, 163, 164). This technology makes use of ethynyl-phosphonamidates, which react with cysteines. It further allows the conjugation of additional hydrophilic compounds e.g. polyethylenglycol (PEG) chains to the linker which can be advantageous if the used drug is highly hydrophobic. The conjugations were carried out by Dr. Marc-André Kasper and Dr. Philipp Ochtrop (Tubulis GmbH). 20D9h3-DUBA and 20D9h3-MMAF both possess a Val-Cit cleavable linker. After conjugation, the ADCs were analyzed using HIC, SEC and mass spectrometry (MS). Even though the DAR was determined to be higher for 20D9h3-MMAF (DAR = 8.0) than for 20D9h3-DUBA (DAR = 4.8), 20D9h3-DUBA was prone to aggregation (supplemental Figure 2), while 20D9h3-MMAF conjugation resulted in a homogenous product (supplemental Figure 3) as evident from the HIC and SEC chromatograms.

3.3.2 Basic evaluation of FLT3-ADCs in the Ba/F3 model

For a first evaluation of the ADC's functionality, I once again used the murine Ba/F3 model stably expressing different human surface receptors. First, it was evaluated whether the two ADCs mediate the desired cytotoxic effect via FLT3 and if the effect is FLT3-specific or also present in cells expressing the structurally similar receptors VEGFR-2, PDGFRα, CSF1R and c-KIT. (Figure 15A-B, receptor expression in Figure 9B and E). In general, both 20D9h3-ADCs were able to reduce viable cells in FLT3-expressing Ba/F3 cells in a dose-dependent manner. As expected from the binding studies (see chapter 3.1.2.2), cytotoxicity of both 20D9h3-ADCs was restricted to hFLT3 expressing cells once again highlighting the antibodies' specificity for FLT3. Next, the effect of FLT3 surface expression levels on efficacy was analyzed using 20D9h3-DUBA (Figure 15C). After 72 h of incubation with 20D9h3-DUBA, viable cells were counted by trypan blue exclusion. The ADC was exclusively cytotoxic to Ba/F3-pMIY cells expressing hFLT3 but not to those without surface receptor expression (empty vector control). Further, the cytotoxic effect correlated with the level of surface FLT3. The IC_{50} values were 105.4 ng/ml, 177.4 ng/ml and 2814 ng/ml for Ba/F3-pMIY cells with high, medium and low hFLT3 expression, respectively. Collectively, these

data demonstrate that 20D9h3-ADCs with both MMAF and DUBA as payloads are functional, specific for FLT3 but not FLT3 paralogues and that their cytotoxic effect is dependent on FLT3 surface levels.

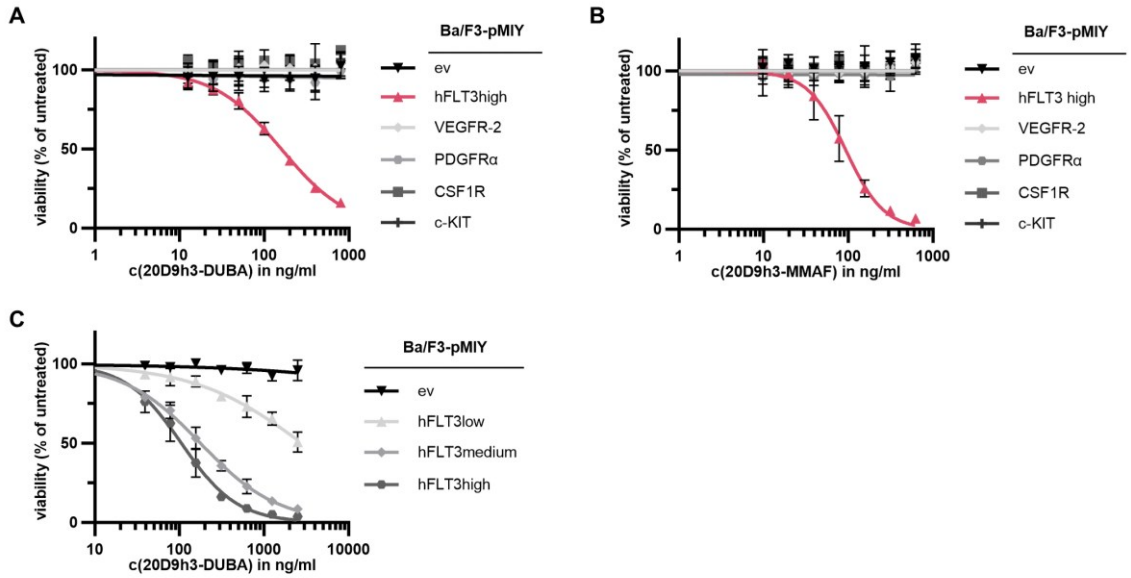

Figure 15: Basic evaluation of 20D9h3-DUBA in the Ba/F3 model. Ba/F3-pMIY cells expressing FLT3 receptor paralogues VEGFR-2, PDGFRα, CSF1R and c-KIT (A, B) or hFLT3 at high, medium or low surface levels (C) were incubated with 20D9h3-DUBA (A, C) or 20D9h3-MMAF (B) for 72 h. Viable cells were subsequently assessed by trypan blue exclusion and are depicted normalized to untreated control. mean ± s.d.; n = 3 biological replicates.

3.3.3 Evaluation of FLT3-ADCs in the FLT3 mutant setting

As described in 3.1.2.3, FLT3 mutations are quite frequent in AML and either occur initially (primary) or in response to therapy (secondary) (155). I already confirmed above that 20D9h3-mAb also binds mutant FLT3. I now followed up on this and tested FLT3-ADC activity in Ba/F3-pMIY cells expressing hFLT3 wildtype or hFLT3 with primary (Figure 16A) or secondary (Figure 16B) FLT3 resistance mutations. As these experiments were carried out as part of a previous project (139), chimeric 20D9-MMAF was used as an ADC. Chimeric 20D9-mAb and humanized 20D9h3-mAb show almost identical behavior in all binding studies (see chapter 3.1.1). The results gained in the following are therefore most probably also applicable to 20D9h3-ADCs. In general, all Ba/F3-pMIY cells expressing mutant human FLT3 were sensitive towards 20D9-MMAF. Ba/F3-pMIY cells expressing hFLT3 with the secondary resistance mutations NPOS F691L, NPOS F691I and NPOS D835Y seemed to be less sensitive towards the ADC with IC_{50} values of 8762 ng/ml, 4368 ng/ml and 1993 ng/ml, respectively, versus 209 ng/ml for Ba/F3-pMIY cells expressing wildtype FLT3. However, since expression levels of these FLT3 mutants are lower than wildtype FLT3 in the Ba/F3 model this could explain the lower sensitivity of these cells (see Figure 10B). This is also in line with the results from the binding studies (see chapter 3.1.2.3 and Figure 10A).

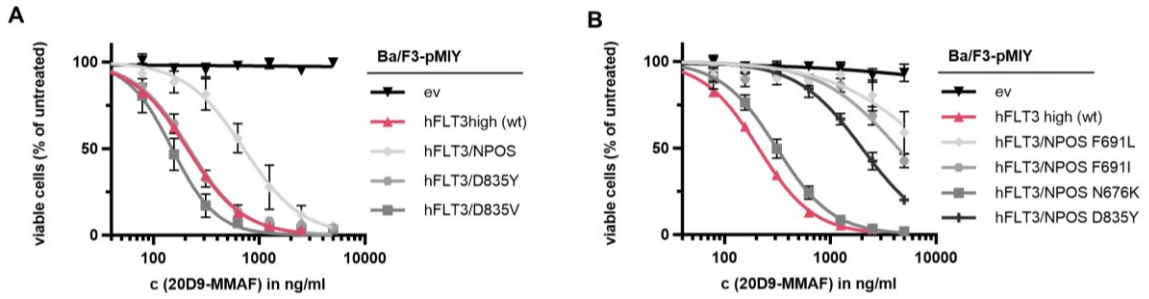

Figure 16: Evaluation of FLT3-ADCs in the FLT3 mutant setting. Ba/F3-pMIY cells expressing empty vector (ev), hFLT3 wildtype (wt) or different primary (A) or secondary (B) mutant versions of FLT3 were treated with a dilution row of 20D9-MMAF ADC for 72 h. Viable cells were assessed using trypan blue exclusion and normalized to untreated control. mean ± s.d.; n = 3 biological replicates. Figure was adapted from Roas et al (139) with permission from *Blood*.

3.3.4 Evaluation of the role of FLT3 and FcγRI for the cytotoxicity of FLT3-ADCs using the transgenic Ba/F3 model

As mentioned in the section about antibody binding studies (chapter 3.1.3), I was interested how ablation of FcγR binding by introduction of LALA mutations in the Fc region changes the activity of ADCs in general and also towards LSCs. The Ba/F3 model system was used to study the individual cytotoxic effects mediated via FLT3 and FcγRs. As the binding to FcγRII and FcγRIII was low to absent even for the non-mutated IgG1 antibodies (see chapter 3.1.3) and it has been shown by Roas et al. that they do not play a role in ADC-mediated cytotoxicity (139, 143), I focused on FcγRI. Using murine Ba/F3-pMIY cells that express either human FLT3, FcγRI, both receptors or no surface receptors, the activity of 20D9h3-DUBA, 20D9h3-LALA-DUBA and the respective wildtype and LALA-mutated isotype control constructs was evaluated (Figure 17, supplemental Table 2). Ba/F3-pMIY cells expressing no surface receptor (ev) were not affected by any of the ADCs (Figure 17A). The FLT3-directed ADCs 20D9h3-DUBA and 20D9h3-LALA-DUBA had a similar cytotoxic effect on Ba/F3-pMIY hFLT3high cells with IC_{50} values of 69.3 ng/ml and 142.9 ng/ml, respectively (Figure 17B). IgG1 isotype control ADCs, however, remained ineffective in those cells. Ba/F3-pMIY hFcγRI cells were eliminated only by those ADCs with an intact Fc region, namely 20D9h3-DUBA and its non-mutated isotype control (Figure 17C). The IC_{50} values were 86.5 ng/ml and 125.3 ng/ml for 20D9h3-DUBA and IgG1-DUBA, respectively. In cells expressing both – FLT3 and FcγRI – 20D9h3-DUBA was most effective with an IC_{50} value of 30.1 ng/ml. This was followed by 20D9h3-LALA-DUBA, IgG1-DUBA and IgG1-LALA-DUBA with IC_{50} values of 107.6 ng/ml, 552.2 ng/ml and 1433 ng/ml, respectively (Figure 17D). In summary, in the Ba/F3 model co-targeting FcγRI and hFLT3 was superior to targeting either of the receptors alone. This is in line with previous findings were deglycosylation instead of LALA mutation was used in 20D9-MMAF to ablate Fc effector functions (139).

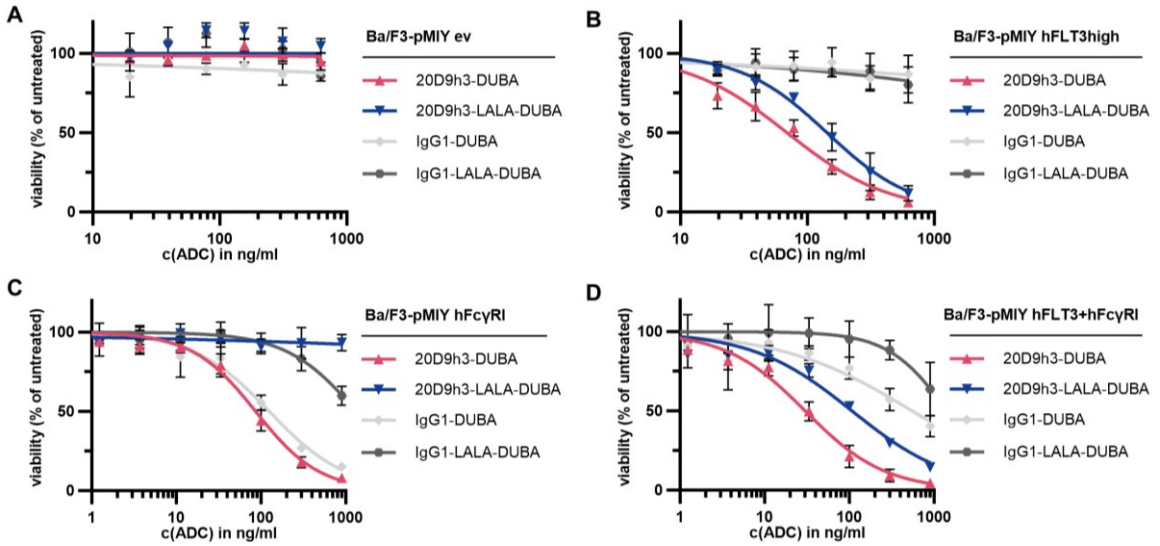

Figure 17: Evaluation of the effect of LALA-mutation on the activity of 20D9h3-ADC in the Ba/F3 model. Ba/F3-pMIY cells with empty vector (ev, A), hFLT3high (B), hFcγRI (C) or hFLT3+FcγRI (D) were incubated with a dilution row of 20D9h3-DUBA, 20D9h3-LALA-DUBA, IgG1-DUBA or IgG1-LALA-DUBA. After 72 h, viable cells were assessed by flow cytometry. Dead cells were excluded using LIVE/DEAD fixable far red dead cell stain. Values are shown normalized to untreated control. mean ± s.d.; n = 3 biological replicates. Cytotoxicity assays were carried out together with Belay Tizazu (AG Spiekermann, LMU Klinikum).

3.3.5 *In vitro* cytotoxicity of FLT3-ADCs on leukemia cell lines

In the following, the efficacy of 20D9h3-DUBA was tested in relation to 20D9h3-MMAF *in vitro* on different leukemia cell lines. As controls, IgG1 isotype control ADCs and unconjugated 20D9h3-mAb were included. The FLT3 and FcγRI expression of different leukemia cell lines has already been extensively analyzed as part of the previous project (139, 143). For ADC analysis, I selected three cell lines with FLT3 expression – MOLM-13, MV4-11 and OCI-AML3 – and two FLT3-negative ones – HL-60 and K-562 – as control. FcγRI is expressed in low levels on HL-60, K-562 and MOLM-13 cells. MV4-11 and OCI-AML3 have the highest FcγRI expression of the tested cell lines. (139, 143) All FLT3-positive cell lines were highly sensitive towards 20D9h3-DUBA with IC_{50} values of 15.9 ng/ml, 8.7 ng/ml and 8.2 ng/ml for MOLM13, MV4-11 and OCI-AML3 respectively (Figure 18A-C, supplemental Table 3). Remarkably, 20D9h3-DUBA was more effective than 20D9h3-MMAF on MV4-11 cells (IC_{50} = 8.7 ng/ml versus 25.7 ng/ml for 20D9h3-MMAF) and OCI-AML3 cells (IC_{50} = 8.2 ng/ml versus 35.5 ng/ml for 20D9h3-MMAF) despite having a lower DAR. The FLT3-negative cell lines HL-60 and K-562 were not affected by the FLT3-directed 20D9h3-ADCs with both payloads (Figure 18D-E). MOLM-13, MV4-11 and OCI-AML3 were also sensitive to control IgG1-DUBA with IC_{50} values of 360.5 ng/ml, 143.6 ng/ml and 159.3 ng/ml, respectively, and to control IgG1-MMAF with IC_{50} values of 153.8 ng/ml, 247.4 ng/ml and 43.4 ng/ml, respectively (Figure 18A-C). K-562 and HL-60 were not sensitive towards the IgG1-ADCs (Figure 18D-E), correlating with FcγRI surface expression levels of these cell lines (139, 143). Further,

incubation of all cell lines with 20D9h3-mAb did not show any effect, indicating that the efficacy of 20D9h3-ADC is solely attributed to the payload and not to any inhibitory effects of the antibody on proliferation. Collectively, these results demonstrate that the efficacy of 20D9h3-DUBA on leukemia cell lines *in vitro* is comparable or increased compared to 20D9h3-MMAF despite a lower DAR.

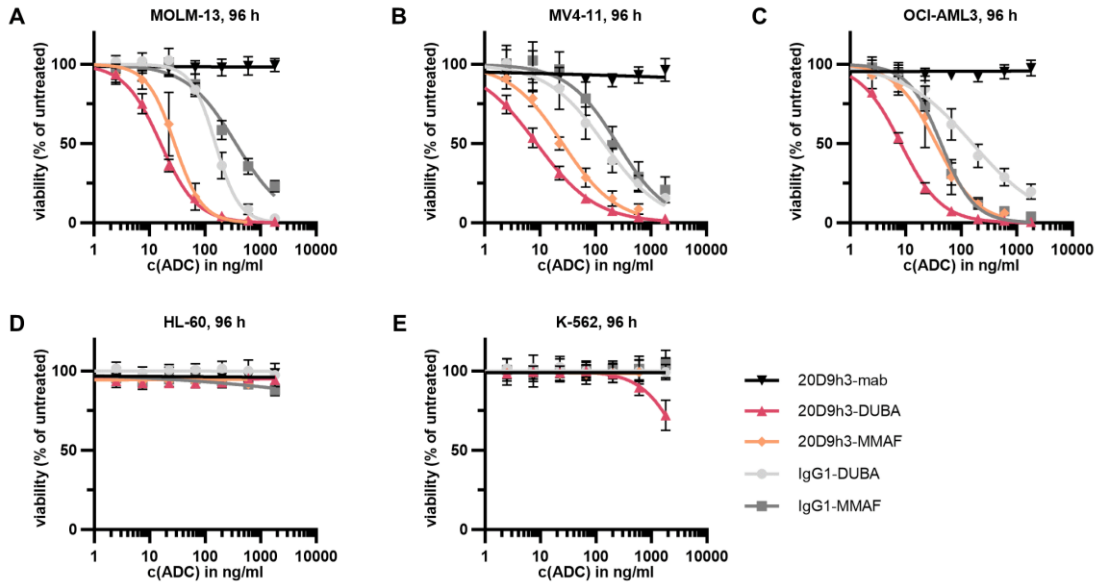

Figure 18: Cytotoxicity evaluation of FLT3-ADCs *in vitro* in leukemia cell lines. FLT3-positive MOLM-13 (A), MV4-11 (B) and OCI-AML3 (C) cells, and FLT3-negative HL-60 (D) and K-562 (E) cells were incubated with different concentrations of 20D9h3-mAb, 20D9h3-DUBA, 20D9h3-MMAF, IgG1-DUBA and IgG1-MMAF. After 96 h, viable cells were measured with resazurin readout. Values are depicted normalized to untreated control. mean ± s.d.; n = 3 biological replicates.

3.3.6 Mechanistic analysis of FLT3-ADCs

As a next step, I wanted to investigate in more detail how 20D9h3-DUBA exerts its effect on leukemia cell lines in comparison to 20D9h3-MMAF. The payload DUBA belongs to the DNA-damaging drugs (123). As DNA integrity is daily challenged with many threats, cells have a sophisticated system to prevent the carry-over of DNA damage to daughter cells during replication. Different cell cycle checkpoints exist, that when triggered stop cell cycle progression in order to enable repair. If repair is not possible, cells undergo mitotic catastrophe and are driven into apoptosis. (165) In this chapter, it was first evaluated if 20D9h3-DUBA triggers DNA repair pathways, then if this leads to a cell cycle stop and apoptosis induction. 20D9h3-MMAF was used for comparison as it employs a payload that does not induce DNA damage.

3.3.6.1 Evaluation of DNA damage response after treatment with FLT3-ADCs

The mechanism of action of DUBA has been described as follows: During replication, the progression of DNA polymerase is hindered by the DNA alkylation caused by DUBA on the DNA strand. This leads to uncoupling of DNA polymerase and formation of single-stranded DNA (ssDNA). ssDNA in turn activates ataxia telangiectasia and rad3-related (ATR) pathway. ATR is a master regulator of DNA damage response. Among other things it is important for cell cycle regulation via phosphorylation of checkpoint kinase 1 (CHK1) and prevents replication fork collapse and eventually replication catastrophe and cell death. (165, 166) For MMAF, a different mechanism of action has been reported. It acts by perturbation of microtubule growth thus interfering with cell division (167). I wanted to verify if the ATR-CHK1 damage repair pathway is activated upon 20D9h3-DUBA treatment using 20D9h3-MMAF as a comparison (Figure 19). Indeed, I could show that both ATR and CHK1 are phosphorylated in MOLM-13 cells that have been treated for 24 h with 20D9h3-DUBA, but not in cells treated with 20D9h3-MMAF. This confirms that DUBA causes DNA damage and cells subsequently initiate a repair response.

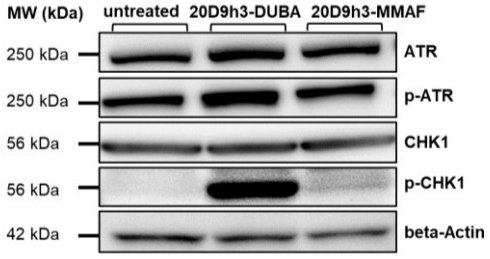

Figure 19: Analysis of ATR-CHK1 DNA-damage repair pathway after FLT3-ADC treatment. After treatment of MOLM-13 cells with 50 ng/ml of either DUBA- or MMAF-ADC for 24 h, expression of ATR, p-ATR, CHK1 and p-CHK1 was analyzed by Western blotting. Beta-Actin was used as loading control. Blots are representative of three biological replicates. MW = molecular weight.

3.3.6.2 Evaluation of cell cycle after treatment with FLT3-ADCs

Next, it was evaluated how 20D9h3-DUBA and -MMAF with their differential mechanisms of action affect cell cycle progression. Therefore, MV4-11 cells were treated with 100 ng/ml of both ADCs or left untreated for 48 h (Figure 20).

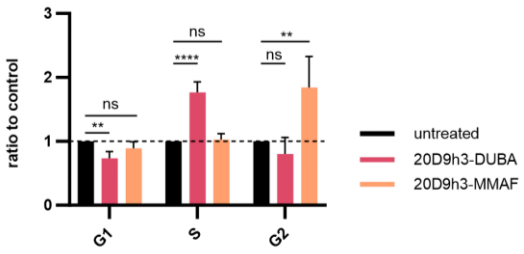

Figure 20: Evaluation of cell cycle progression after FLT3-ADC treatment. MV4-11 cells were treated with either 20D9h3-DUBA or 20D9h3-MMAF or left untreated for 48 h. Cells were subsequently fixed with 80% ethanol (v/v), stained with propidium iodide (PI), and analyzed at BD FACSCanto II. Values are given as ratio to control. Dashed line marks untreated condition. mean ± s.d.; n = 4 biological replicates. **P<.01; ****P<.0001; ns, not significant by One-way ANOVA;

On the day of analysis, cells were fixed and stained with propidium iodide (PI) to evaluate the percentage of cells in G1, S and G2/M cell cycle phases using flow cytometry. 20D9h3-DUBA treatment significantly increased the percentage of cells in S phase while decreasing the

percentage of cells in G1. In contrast, 20D9h3-MMAF significantly increased the proportion of cells in G2/M. This is in line with DUBA causing DNA damage which delays replication and MMAF hampering cell division by microtubule-targeting.

3.3.6.3 Evaluation of the apoptosis induction potential of FLT3-ADCs

Cells that cannot repair DNA damage or that are in mitotic arrest eventually enter apoptosis (165). Apoptosis induction cannot be distinguished from proliferation-inhibition by cytotoxicity assays. Thus, to investigate the latter, 20D9h3-DUBA- and 20D9h3-MMAF-treated MOLM-13 and MV4-11 cells were analyzed every 24 h by APC Annexin V and DAPI staining in flow cytometry (Figure 21A-B).

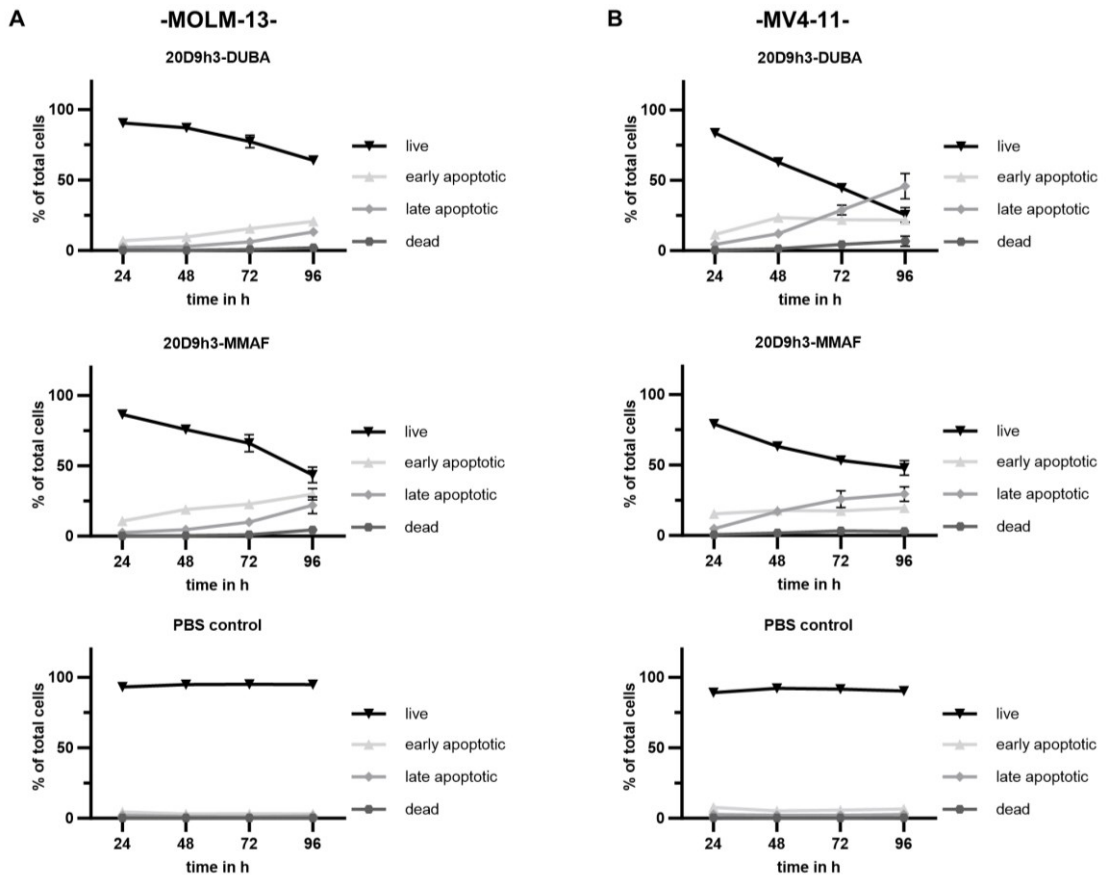

Figure 21: Evaluation of apoptosis induction by FLT3-ADCs in MOLM-13 and MV4-11 cells. MOLM-13 cells (A) and MV4-11 cells (B) were treated with 100 ng/ml of either 20D9h3-DUBA, 20D9h3-MMAF or PBS control. Every 24 h, cell samples were stained with APC Annexin V and DAPI for flow cytometric evaluation of live (double negative), dead (double positive), early (Annexin V-positive) and late (DAPI-positive) apoptotic cells. mean ± s.d.; n = 4 biological replicates.

In this assay early apoptotic cells are Annexin V-positive and late apoptotic cells that lost membrane integrity are Annexin V and DAPI double-positive. Upon treatment with 20D9h3-DUBA ADC, apoptotic cells were present after 24 h and clearly evident after 48 h. After 96 h, 35.9% of all

MOLM-13 cells and 74.5% of all MV4-11 cells were in apoptosis or dead, respectively, versus < 10% of apoptotic and dead cells in the respective PBS controls. Upon 20D9h3-MMAF ADC treatment, apoptosis was more pronounced after 24 h in both cell lines, suggesting that the effect was faster compared to 20D9h3-DUBA. The strength of the effect over the four days was, however, quite comparable for both ADCs. After 96 h, 56.4% MOLM-13 cells and 52.1% MV4-11 cells were apoptotic or dead. These results demonstrate that both ADCs act in part via apoptosis induction.

3.4 Pharmacokinetic analysis of FLT3-ADCs in mouse serum

In order for an ADC to be safe and efficacious *in vivo*, the linker has to be stable in the blood circulation. One of the most frequently used technologies to connect antibody and drug – also applied for 20D9h3-DUBA – is maleimide linkage. Those linkers are, however, prone to retro-Michael addition leading to a transfer of payload to cysteine-rich blood proteins. This could potentially diminish ADC activity and increase toxicities. (116) Additionally, it has been recently reported that ADCs which employ vc-*seco*-DUBA are challenging to evaluate in mice as the linker-drug is susceptible to cleavage by and covalent bond formation with murine carboxylesterase 1c (CES1c). This instability is rodent-specific and has not been observed in monkeys and humans. (168) Still, it poses challenges to adequate preclinical evaluation of such ADCs, which is typically done in rodents. 20D9h3-MMAF is conjugated by P5-technology which has been invented to tackle exactly those instability issues (150, 163, 164). Being aware of those potential challenges for *in vivo* application of 20D9h3-DUBA, the stability and PK of this ADC was analyzed in comparison to 20D9h3-MMAF in the following section.

3.4.1 MS analysis of FLT3-ADCs after incubation in mouse serum

During conjugation (performed by Dr. Marc-André Kasper and Dr. Philipp Ochtrop, Tubulis GmbH), a strong aggregation tendency was observed for 20D9h3-DUBA ADC in contrast to 20D9h3-MMAF ADC (supplemental Figure 2-3). To follow up on this, both FLT3-ADCs were incubated with fresh mouse serum for 6 d at 37 °C and subsequently analyzed by MS (supplemental Figure 4). In accordance with previous reports by Dr. Marc-André Kasper et al. and others (116, 150), loss of linker-payload via retro-Michael addition and maleimide hydrolysis could be confirmed for 20D9h3-DUBA. However, fragments that would indicate CES1c-cleavage were not observed in MS analysis. 20D9h3-MMAF, in contrast, did not show any loss of payload.

3.4.2 *In vitro* cytotoxicity of FLT3-ADCs after incubation with recombinant murine CES1c

To further analyze the reported instability of the vc-*seco*-DUBA linker-drug caused by murine CES1c, both FLT3-ADCs were pre-incubated with recombinant murine CES1c and then added to FLT3-negative cell lines. It was shown in chapter 3.3.5, that the FLT3-negative leukemia cell line HL-60 is not affected by 20D9h3-ADCs with either payload. However, HL-60 cells are sensitive to free DUBA toxin (see chapter 3.2.1). HL-60 cells would thus only be killed by 20D9h3-DUBA if CES1c cleaves the toxin from the ADC. Indeed, it was observed that 20D9h3-DUBA killed HL-60 cells when the ADC was pre-treated with CES1c 1 d, 3 d or 7 d, while the cells were unaffected by 20D9h3-DUBA ADC that has not been pre-incubated with CES1c (Figure 22A). Unexpectedly, there was an inverse correlation between duration of CES1c pre-incubation and HL-60 killing. This might be explained by the dual activity of CES1c which on one hand liberates unconjugated toxin

but on the other hand also undergoes covalent bond formation with vc-*seco*-DUBA withdrawing unconjugated toxin (168), which could have different kinetics. CES1c pre-treated 20D9h3-MMAF, on the contrary, did not kill HL-60 cells (Figure 22B). It has to be noted that MMAF, however, has a low membrane permeability (159) and is therefore not very toxic to HL-60 cells on itself (see chapter 3.2.1). Thus, to evaluate both ADCs in a less artificial setting, their stability was next analyzed after *in vivo* administration.

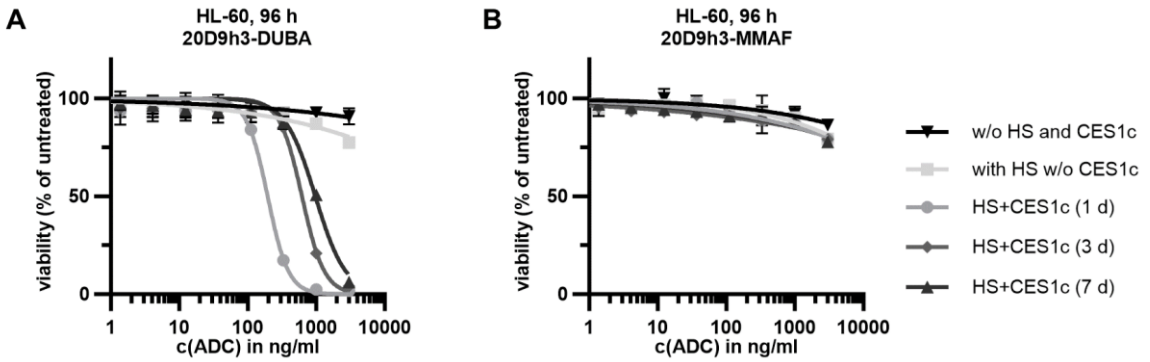

Figure 22: Evaluation of CES1c pre-treated ADCs *in vitro* in FLT3-negative HL-60 cells. Recombinant murine carboxylesterase 1c (CES1c) was spiked in human serum (HS) together with 20D9h3-DUBA (A) or 20D9h3-MMAF (B), and the mixture was incubated for 1-7 d. As a negative control, ADCs were incubated with HS only (with HS w/o CES1c control) or with neither HS nor CES1c (w/o HS and CES1c control). Afterwards, FLT3 negative HL-60 cells were treated with those ADCs for 4 d. Viability was subsequently assessed by resazurin assay. mean ± s.d.; n = 3 technical replicates. CES1c pre-incubation was carried out by Dr. Saskia Schmitt (Tubulis GmbH), cytotoxicity assays were done by me.

3.4.3 *In vivo* pharmacokinetics of FLT3-ADCs in NSG mice

To investigate how much of the ADCs remains stable over time in the blood circulation, NOD.Cg-*Prkdc*^{scid} *Il2rg*^{tm1Wjl}/SzJ (NSG) mice were administered i.v. with a single dose of 3 mg/kg 20D9h3-DUBA or 20D9h3-MMAF. These mice are the main *in vivo* model to evaluate AML therapies as their immunodeficiency – caused by a lack of T cells, B cells and NK cell as well as different cytokine signaling pathways – allows stable engraftment of primary human AML cells (132). Treatment dose was selected based on previous results (139, 143). 24 h, 48 h and 72 h after treatment, serum samples were taken and analyzed by ELISA (Figure 23A-B). In this assay, two antibodies were used. One directed against human IgG Fc to measure total antibody content and the other one directed against the payload – DUBA or MMAF – to measure intact ADC. As expected from the *in vitro* results, the levels of intact conjugated 20D9h3-DUBA ADC rapidly decreased in NSG blood circulation (Figure 23A). This was not observed for 20D9h3-MMAF ADC (Figure 23B) confirming the improved stability of the P5-linkage leading to this superior PK profile. Collectively, these results suggest that 20D9h3-DUBA using vc-*seco*-DUBA linker-drug is unstable in the blood circulation of NSG mice.

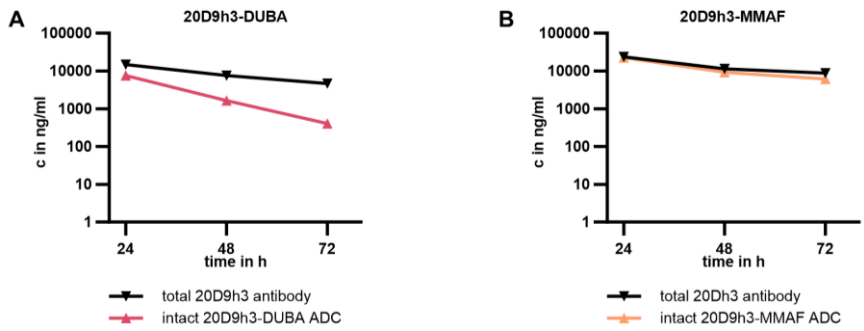

Figure 23: *In vivo* pharmacokinetic analysis of FLT3-ADCs. NSG mice were administered i.v. with a single dose of either 20D9h3-ADC. At 24 h, 48 h and 72 h, serum samples were taken and analyzed by ELISA. Total antibody was measured with mouse anti-human IgG Fc specific antibody and intact ADC with anti-DUBA or anti-MMAF antibodies. Concentrations were calculated using a standard curve generated with a dilution row of either 20D9h3-ADC. mean ± s.d.; n = 1 mouse per treatment group with 2 technical replicates. Experiments were planned with Dr. Binje Vick (AG Jeremias, Helmholtz Zentrum München) and Dr. Saskia Schmitt (Tubulis GmbH). Mouse work was performed by Annette Frank and Sandro Aidone (both AG Jeremias, Helmholtz Zentrum München) and ELISA by Isabelle Mai (Tubulis GmbH).

3.5 *In vivo* therapy of patient-derived xenograft (PDX) mouse models

For *in vivo* experiments, patient-derived xenograft (PDX) cells were used, which closely reflect the patient situation as they have been generated from primary AML patient specimens. As primary cells are difficult to cultivate long-term *in vitro*, NSG mice are used to expand those PDX samples via serial *in vivo* transplantation. In order to facilitate the monitoring *in vivo*, the PDX cells have been stably transduced with vectors expressing luciferase to enable bioluminescence imaging (BLI) (132). Those experiments were planned in collaboration with Dr. Binje Vick and carried out by Annette Frank and Sandro Aidone (all AG Jeremias, Helmholtz Zentrum München). For the therapy experiment, NSG mice were transplanted with PDX samples from two different patients in the BM – AML-388 or AML-579 (see Table 17, Material and Methods for characteristics). AML-579 PDX cells were selected due to previous results with 20D9-MMAF (139, 143), AML-388 PDX cells were selected due to their particularly high *in vitro* sensitivity to both 20D9h3-ADCs (see also Figure 26A). Both PDX samples express FLT3 as previously shown (139, 143). After stable engraftment the mice were injected two (AML-388) or three times (AML-579) once per week i.v. with 3 mg/kg of either 20D9h3-DUBA or 20D9h3-MMAF (Figure 24A).

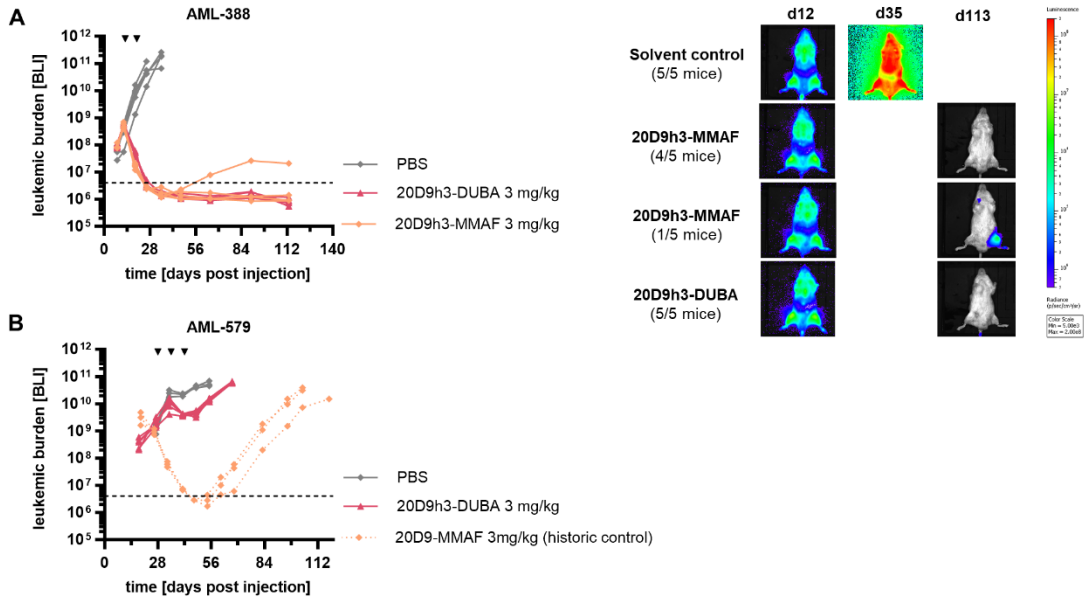

Figure 24: *In vivo* evaluation of FLT3-ADCs. 1x10^6 luciferase-expressing AML-388 (A) and AML-579 (B) PDX cells were transplanted in NSG mice. Mice were treated i.v. with 3 mg/kg of either ADC or PBS once per week for two (AML-388) or three (AML-579) weeks, as indicated by the black triangles. Tumor burden was monitored by BLI measurements in regular intervals. Representative BLI pictures for AML-388 xenografts are depicted on the right side. AML-388: n = 5 mice per group; AML-579: n = 6 mice per group (20D9h3-DUBA) and n = 3 mice per group (20D9-MMAF). Dashed black line = detection limit. Results for 20D9-MMAF treatment in AML-579 xenograft models (dashed orange lines) were obtained from Dr. Maike Roas (AG Spiekermann, LMU) with permission from *Blood* and Dr. Maike Roas (139, 143). Animal experiments were planned in collaboration with Dr. Binje Vick and carried out by Annette Frank and Sandro Aidone (all AG Jeremias, Helmholtz Zentrum München).

For AML-388, remarkably, either ADC drastically reduced tumor burden despite the poor PK of 20D9h3-DUBA. 4 weeks after treatment stop, one of five mice from the MMAF-group relapsed indicating the survival of leukemia-initiating cells (LICs). 20D9h3-DUBA, on the contrary, led to a tumor burden below detection limit in all treated mice for up to 112 d. The good response of the AML-388 PDX sample *in vivo* correlated with its very high sensitivity towards 20D9h3-DUBA *in vitro*. The AML-579 PDX sample showed a much lower *in vitro* sensitivity (IC_{50} of 775.2 ng/ml versus 4.6 ng/ml for AML-388 in 4 d cytotoxicity assay, data not shown). Also *in vivo*, 20D9h3-DUBA only reduced tumor burden to a small extent and was inferior to the MMAF-ADC when comparing to previously published results from Dr. Maike Roas (AG Spiekermann, LMU, Figure 24B) (139, 143). More specifically the mean BLI values after three doses were $4.28x10^{10}$, $4.39x10^{9}$ and $2.87x10^{6}$ photons/s for PBS, 20D9h3-DUBA and 20D9h3-MMAF, respectively. These data indicate that the poor PK of 20D9h3-DUBA in the NSG mouse model system probably underestimates its effectivity particularly towards samples with a generally lower sensitivity e.g. due to genetic factors or low target expression of FLT3. This considerably impedes adequate preclinical evaluation of the ADC. However, as the overarching goal of the project was to evaluate the anti-LSC activity of the FLT3-ADCs, the focus of the next part was placed on stem cell assays with *ex vivo*/*in vitro* ADC treatment rather than direct *in vivo* therapy.

3.6 Analysis of FLT3-ADCs in stem cell assays with *KMT2A*r AML PDX cells

Next, both FLT3-ADCs were evaluated for their potential to eradicate leukemic stem and progenitor cells within AML PDX samples using three different gold standard stem cell assays. 20D9h3-MMAF served as control for those experiments under the hypothesis that it has a limited anti-LSC activity due to the mechanism of action of MMAF.

3.6.1 Selection of *KMT2A*r PDX samples for stem cell assays

KMT2A gene fusions reprogram and transform differentiated cells and are sufficient for leukemia-initiation (169). For some forms of *KMT2A*-rearranged (*KMT2Ar*)-leukemia, e.g. *KMT2A*::*MLLT3*, a particularly high frequency of self-renewing cells has been reported (170). Those stem cell characteristics of *KMT2Ar*-leukemia are probably conferred by an altered *HOX* gene expression (171). This is advantageous for *in vitro* experiments, where those samples are better to cultivate compared to other PDX samples which usually do not survive for more than one week even at optimal culture conditions. Due to these properties, *KMT2Ar*-leukemia has been described as an excellent tool to explore self-renewing cells (169). Therefore, three *KMT2Ar* AML PDX samples were selected for stem cell assays (Table 17, Material and Methods): AML-388 with *KMT2A*::*AFDN* rearrangement, AML-393 with *KMT2A*::*MLLT10* rearrangement and AML-669 with *KMT2A*::*MLLT3* rearrangement. As a first step, the expression of FLT3 and FcγRI was analyzed in PDX cells with and without *KMT2Ar* (Figure 25, data was provided by Dr. Tobias Herold, LMU Klinikum (172)).

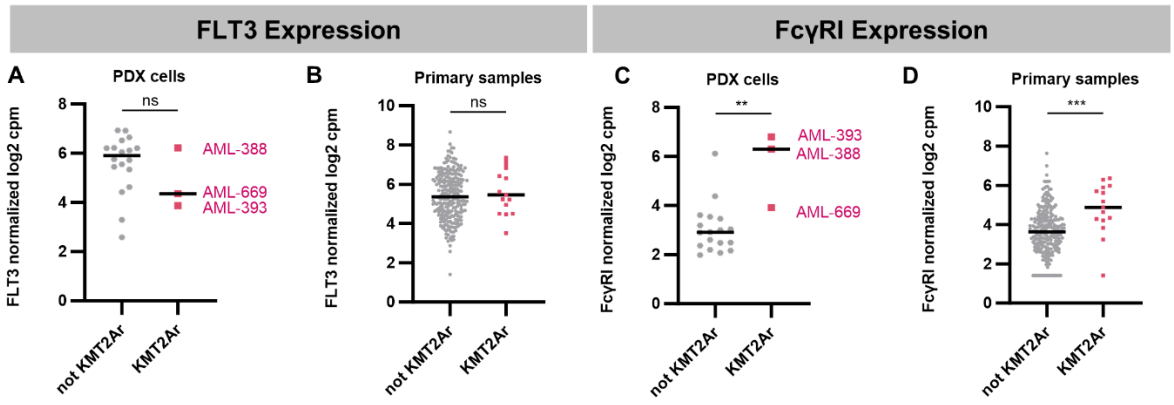

Figure 25: FLT3 and FcγRI expression in PDX and primary patient samples with and without *KMT2A*-rearrangement. FLT3 and FcγRI RNA expression in AML PDX (n = 21) and primary AML patient samples (n = 261) measured by SCBR sequencing (173) (normalized log2 counts per million (cpm)). (A-B) Comparison of FLT3 expression between AML PDX (A) and primary samples (B) with and without *KMT2Ar*. (C-D) Comparison of FcγRI expression between AML PDX (C) and primary samples (D) with and without *KMT2Ar*. PDX: Mann-Whitney test; Primary samples: Unpaired t test. **P<.01; ***P<.001; ns, not significant. Data was provided by Dr. Tobias Herold (LMU Klinikum) (172).

Interestingly, it was observed that while FLT3 levels were similar in PDX samples with and without *KMT2Ar* (Figure 25A and C), FcγRI levels were significantly elevated in *KMT2Ar* samples. These findings could be confirmed in primary patient samples (Figure 25B and D)

3.6.2 *In vitro* cytotoxicity of FLT3-ADCs on *KMT2Ar* AML PDX samples

To see how sensitive the three selected PDX samples are towards 20D9h3-DUBA and 20D9h3-MMAF, they were – in analogy to the cell line experiments – treated *in vitro* with a dilution row of either ADC for 4 d. Viable cells were subsequently measured with flow cytometry using DAPI staining and normalized to untreated control (Figure 26).

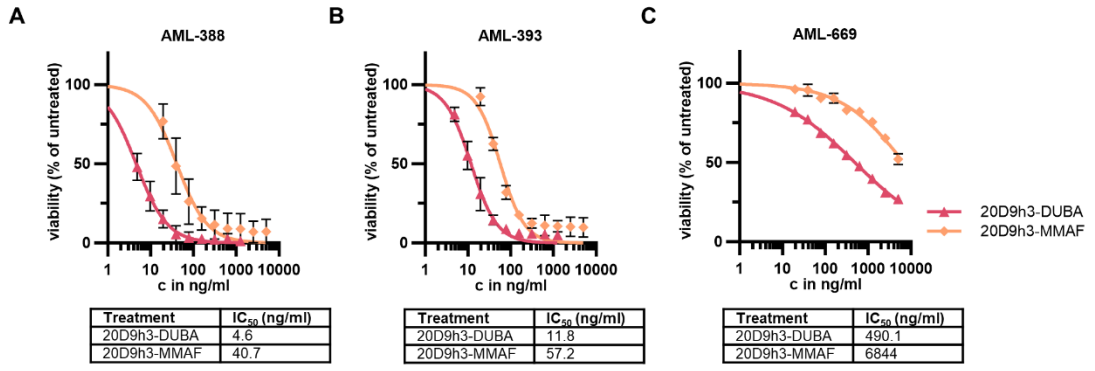

Treatment	IC_{50} (ng/ml)
20D9h3-DUBA	4.6
20D9h3-MMAF	40.7

Treatment	IC_{50} (ng/ml)
20D9h3-DUBA	11.8
20D9h3-MMAF	57.2

Treatment	IC_{50} (ng/ml)
20D9h3-DUBA	490.1
20D9h3-MMAF	6844

Figure 26: Cytotoxicity evaluation of FLT3-ADCs *in vitro* in *KMT2Ar* AML PDX cells. *KMT2Ar* AML PDX samples were treated with a dilution row of 20D9h3-DUBA or 20D9h3-MMAF for 96 h. Viable cells were then assessed by flow cytometry using DAPI as dead cell stain and normalized to untreated control. IC_{50} values were calculated using nonlinear fit – variable slope analysis in GraphPad Prism 10.1.2. mean ± s.d.; n = 3 biological replicates. PDX samples were provided by the group of Prof. Jeremias (Helmholtz Zentrum München).

All three PDX samples were highly sensitive to 20D9h3-DUBA with IC_{50} values of 4.6 ng/ml, 11.8 ng/ml and 490.1 ng/ml for AML-388, AML-393 and AML-669, respectively. The IC_{50} values were comparable to those observed in leukemia cell lines. 20D9h3-MMAF was less effective in all three samples with IC_{50} values of 40.7 ng/ml for AML-388 cells, 57.2 ng/ml for AML-393 cells and 6844 ng/ml for AML-669 cells. Both ADCs had a particularly strong effect on AML-388 PDX cells.

3.6.3 Activity of FLT3-ADCs towards short-term leukemic progenitors

Next, the potential of the FLT3-ADCs to eradicate leukemic progenitors was evaluated in colony-forming unit (CFU) assays. For those experiments, AML PDX or primary AML cells were cultivated with either ADC for 96 h and subsequently plated in methylcellulose for 14 d. On day 14, clusters (20-50 cells) and colonies (> 50 cells) were counted under the microscope (Figure 27).

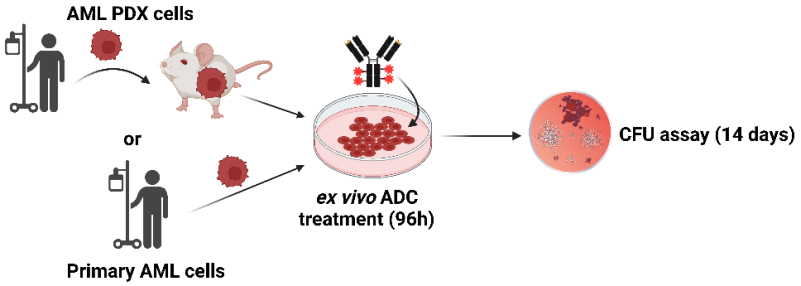

Figure 27: Schematic illustration of colony-forming unit assays. AML patient-derived xenograft (PDX) or primary cells were incubated for 96 h with FLT3-ADCs. Cells were then washed three times and plated in methylcellulose. On day 14, colonies (>50 cells) and clusters (20-50 cells) were counted by microscopy and normalized to untreated control.

3.6.3.1 Evaluation of FLT3-ADCs in CFU assay with AML PDX samples

First, the efficacy of 20D9h3-DUBA and 20D9h3-MMAF to eradicate colony-forming cells (CFCs) was tested on the selected *KMT2Ar* AML PDX samples (Figure 28).

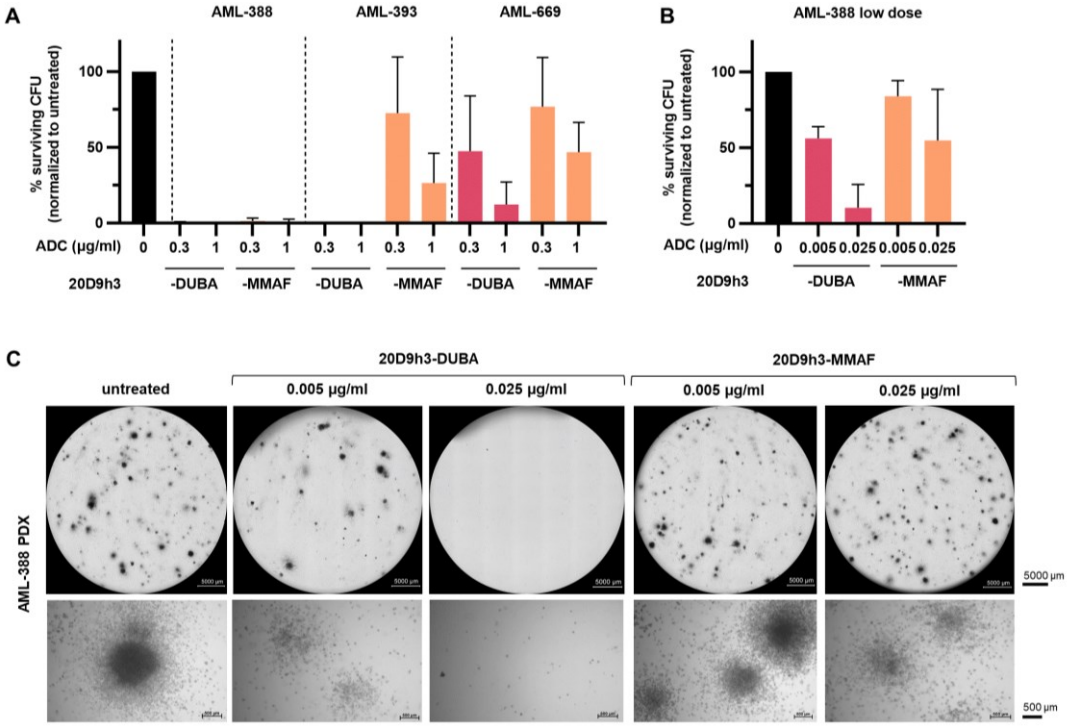

Figure 28: Effect of FLT3-ADCs on colony formation of *KMT2Ar* AML PDX samples in CFU assay. (A-B) The *KMT2Ar* AML PDX samples AML-388, -393 and -669 were treated with 20Dh3-ADCs in the indicated doses. After 4 d, remaining cells were transferred to methylcellulose. On day 14, clusters (20-50 cells) and colonies (> 50 cells) were counted and normalized to untreated control. (A) Treatment with ADC doses of 0.3 µg/ml and 1 µg/ml. mean ± s.d.; n = 3 biological replicates with two technical replicates each. (B) Treatment of AML-388 with doses of 0.005 µg/ml and 0.025 µg/ml. mean ± s.d.; n = 3 biological replicates with two technical replicates each. (C) Microscopy images of AML-388 PDX colonies after treatment with doses of 0.005-0.025 µg/ml. Upper panel: whole-well image acquired with Keyence BZ-X810 microscope by PlanApo 2x 0.10/8.50 mm objective; scale bar = 5000 µm. Lower panel: exemplary zoom-in pictures acquired with ZEISS Primovert and Axiocam 208 color by Primo Plan-ACHROMAT 4x/0.10 Ph0 objective; scale bar = 500 µm. AML PDX samples were kindly provided by the group of Prof. Jeremias (Helmholtz Zentrum München).

For the first experiment, ADC doses of 0.3 µg/ml and 1 µg/ml were selected, greater or equal to the IC_{50} values of both ADCs in all three PDX samples (Figure 28A, colony counts in supplemental Table 4, images of colonies in Supplementary Figure 5). At both concentrations, 20D9h3-DUBA was able to eliminate all AML-388 and AML-393 CFCs. AML-669 CFCs were reduced to 12.3% at the higher dose and 47.5% at the lower dose. For 20D9h3-MMAF on the contrary, the lower dose of 0.3 µg/ml decreased CFCs to only 72.7% and 76.9% for AML-393 and AML-669, respectively. The higher dose led to a reduction of AML-393 CFCs to 26.5% and AML-669 CFCs to 46.9%. Surprisingly, 20D9h3-MMAF quite potently reduced AML-388 CFCs (to 0.5% and 0.2% of untreated control at 0.3 µg/ml and 1 µg/ml, respectively). As AML-388 cells were quite sensitive to both ADCs, the concentrations were reduced in a follow-up experiment in order to find the lowest effective dose (Figure 28B-C). At doses as low as 0.005 µg/ml, 20D9h3-DUBA turned out to be highly efficient on AML-388 PDX cells, as it reduced CFCs to 14.1% and 52.9% of untreated control at doses of 0.025 µg/ml and 0.005 µg/ml, respectively. 20D9h3-MMAF, on the other hand, was not able to kill CFCs at these lower doses. In summary, these results demonstrate that FLT3-ADCs with both payloads are capable of eradicating CFCs from all tested *KMT2Ar* AML PDX samples, however 20D9h3-DUBA is more efficient at lower doses.

3.6.3.2 Validation of PDX CFU results in a primary patient sample

PDX cells have been described as a model system that closely reflects the patient situation (132). To validate this in the context of CFU assays, original primary patient cells that had been the source of the AML-393 PDX sample were used and assayed in the same experimental set-up (Figure 29A-B, colony counts in supplemental Table 4).

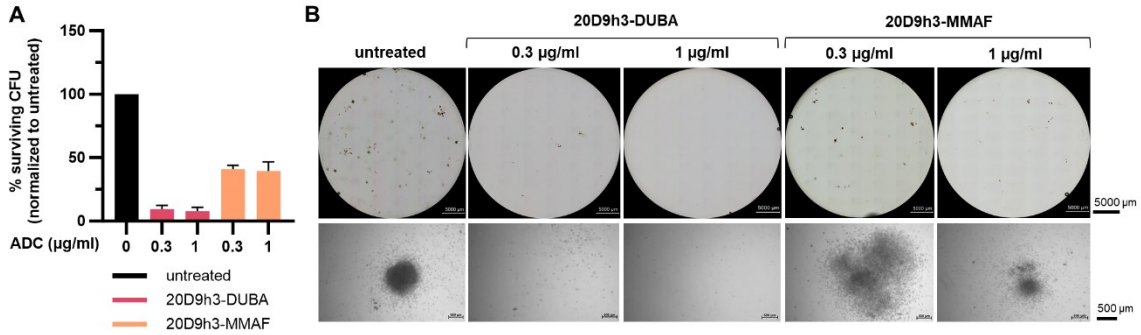

Figure 29: Validation of AML-393 PDX CFU results in the corresponding primary patient sample. Primary patient cells that had been source of the AML-393 PDX sample were treated with 0.3 µg/ml and 1 µg/ml of FLT3-ADCs for 4 d and subjected to CFU assay. On day 14, colonies were counted as described. Red colonies were excluded from counting as those are most probably CFU-E colonies from remaining healthy erythroid progenitors rather than blast colonies. (A) Colony counts normalized to control without treatment. mean ± s.d.; n = 2 technical replicates. (B) Microscopy images. Upper panel: whole-well image acquired with Keyence BZ-X810 microscope by PlanApo 2x 0.10/8.50 mm objective; scale bar = 5000 µm. Lower panel: exemplary zoom-in pictures of AML-393 blast colonies acquired with ZEISS Primovert and Axiocam 208 color using Primo Plan-ACHROMAT 4x/0.10 Ph0 objective; scale bar = 500 µm.

Once again, 20D9h3-DUBA greatly reduced CFCs to 9.4% and 7.9% of untreated control at doses of 0.3 µg/ml and 1 µg/ml, respectively, similar to the results with the AML-393 PDX sample. Likewise, 20D9h3-MMAF was less effective with a decrease of CFCs to 41% at 0.3 µg/ml and 39.6% at 1 µg/ml, validating that the CFU results gained with PDX samples can indeed be applied to primary patient cells.

3.6.3.3 FLT3- and FcγRI-mediated effects in CFU assay

As described before (chapter 3.3.4), the 20D9h3-ADCs exert an FLT3-mediated and an FcγRI-mediated effect via their variable and constant mAb parts, respectively. The goal of this experiment was to evaluate the individual contribution of both effects to the total efficacy of the ADC in CFU assay using the DUBA-conjugate. AML-393 primary patient cells were therefore treated with either 20D9h3-DUBA (targeting FLT3+FcγRI), 20D9h3-LALA-DUBA (targeting solely FLT3) or IgG1-DUBA (targeting solely FcγRI) for 4 d, transferred to methylcellulose and counted on day 14 (Figure 30). Single-targeting of the receptors decreased CFCs to 53.2% and 65.5% for FLT3 and FcγRI, respectively. However, co-targeting of FLT3 and FcγRI reduced CFCs to 9.4% indicating superiority of addressing both receptors in the elimination of short-term AML-393 progenitors.

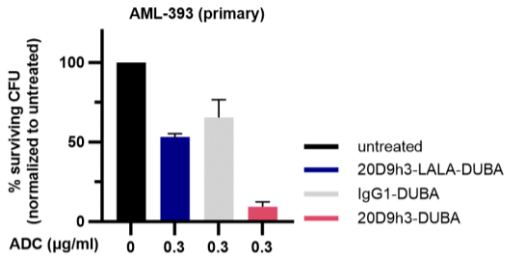

Figure 30: Investigation of the role of FLT3 and FcγRI for the effectiveness of FLT3-ADCs in CFU assay. Primary patient cells that had been the source of the AML-393 PDX cells were treated with 0.3 µg/ml of either 20D9h3-DUBA, 20D9h3-LALA-DUBA or IgG1-DUBA for 4 d and subjected to CFU assay as described. On day 14, colonies were counted and are depicted normalized to control without treatment. mean ± s.d.; n = 2 technical replicates.

3.6.4 Activity of FLT3-ADCs towards long-term leukemic progenitors

Long-term leukemic progenitors – that are functional equivalents to the *in vivo* LICs known from experiments in NSG mice – are better reflected *in vitro* using long-term culture initiating cell (LTC-IC) assay rather than CFU assay (149, 174). In this 7-week experiment, PDX cells are cultured for 5 weeks on layers of irradiated murine fibroblast. Afterwards, they are plated in methylcellulose and colony-formation is evaluated after 14 d in analogy to CFU assay (Figure 31). These experiments were carried out in close collaboration with the group of Prof. Michaela Feuring (University hospital Ulm).

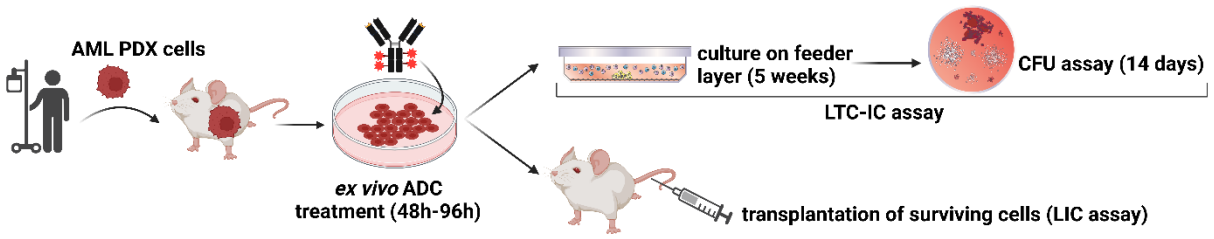

Figure 31: Schematic illustration of long-term culture initiating cell and leukemia-initiating cell assay. AML patient-derived xenograft (PDX) cells were incubated with FLT3-ADCs for 48 h (for long-term culture initiating cell (LTC-IC) assay) or 96 h (for leukemia-initiating cell (LIC) assay). Subsequently, cells were washed and subjected to the different assays. For LTC-IC assay, cells were cultured on feeder layers of irradiated murine fibroblasts for 5 weeks. They were then harvested, put in methylcellulose for 14 d and evaluated as described for CFU assay. For LIC assay, pre-treated PDX cells were transplanted into NSG mice by tail vein injection. Engraftment of the luciferase-expressing cells was then monitored using bioluminescence imaging (BLI). Image was generated with Biorender.com. Images of CFU assay plate and feeder cell co-culture were generated with Adobe Illustrator by Sonja Künzl (adapted from StemCell Technologies).

During the 5 weeks of co-culture, the more advanced leukemic progenitors differentiate and die. Only the very primitive progenitors remain and are analyzed as endpoint. These assays were planned in close collaboration with Prof. Feuring (University hospital Ulm) and carried out by me together with Dr. Xiang Gao (group of Prof. Feuring). Finally, the gold standard approach to study leukemic stem and progenitor cells is the LIC assay, which studies the potential of cells to engraft in NSG mice and to initiate leukemia (Figure 31). Both, LTC-IC and LIC assay, were carried out with AML PDX cells that have been pre-treated with either 20D9h3-DUBA or 20D9h3-MMAF or left untreated. All AML PDX samples for stem cell experiments were kindly provided by the group of Prof. Jeremias (Helmholtz Zentrum München) and LIC assays were carried out by Dr. Binje Vick together with Annette Frank and Sandro Aidone (all AG Jeremias).

3.6.4.1 Evaluation of FLT3-ADCs in LTC-IC assay with AML PDX samples

First, the efficacy of 20D9h3-DUBA and 20D9h3-MMAF to eradicate long-term CFCs in LTC-IC assay was tested on two of the three *KMT2Ar* AML PDX samples. For the assay, ADC concentrations were selected at which 20D9h3-DUBA had a higher efficacy than 20D9h3-MMAF in the CFU assay (Figure 32, colony counts in supplemental table 4). At a dose of 0.3 µg/ml 20D9h3-DUBA eliminated all AML-388 LTC-IC-CFCs while 20D9h3-MMAF reduced them to only 51.5% of untreated control. At a lower dose of 0.025 µg/ml, 20D9h3-DUBA still slightly decreased LTC-IC-CFCs to 86.1% of untreated control whereas 20D9h3-MMAF was completely inefficient and even led a small increase in LTC-IC-CFCs (to 128.7%). Both ADCs completely eliminated AML-393 LTC-IC-CFCs at 0.3 µg/ml. Collectively, 20D9h3-DUBA eradicated LTC-IC-CFCs of both tested PDX samples. While 20D9h3-DUBA had a better activity towards AML-388 PDX cells, both ADCs were highly efficacious towards AML-393 PDX cells.

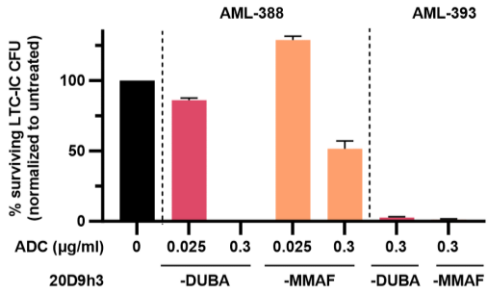

Figure 32: Effect of FLT3-ADCs on colony formation of *KMT2Ar* AML PDX samples in LTC-IC assay. AML-388 and AML-393 PDX cells were treated with 20D9h3-DUBA or 20D9h3-MMAF for 48 h and then subjected to LTC-IC assay as described in Figure 31. On the day of evaluation after 7 weeks, colonies were counted and are depicted normalized to control without treatment. mean ± s.d.; n = 2 technical replicates. Assays were carried out together with Dr. Xiang Gao (AG Feuring, University hospital Ulm).

3.6.4.2 Evaluation of FLT3-ADCs in LIC assays with AML PDX samples

Finally, I analyzed whether *ex vivo* ADC pre-treatment can prevent AML PDX engraftment in NSG mice. These experiments were planned in close collaboration with Dr. Binje Vick and carried out by Annette Frank and Sandro Aidone (all AG Jeremias, Helmholtz Zentrum München). To this end, luciferase-expressing *KMT2Ar* PDX samples AML-388 and AML-393 were incubated with 20D9h3-DUBA, 20D9h3-MMAF or PBS for 4 d and then transplanted into five NSG mice per group using tail vein injection. Engraftment and leukemia development were closely monitored with BLI. AML-388 PDX cells that have been treated with PBS engrafted within two weeks after injection and showed a very rapid and aggressive disease course where mice had to be sacrificed after 4-5 weeks (Figure 33A-B). Pre-treatment of AML-388 PDX cells with a high dose of 1 µg/ml of either ADC (20D9h3-DUBA or 20D9h3-MMAF), however, was highly potent in eradicating LICs. In both treatment groups all mice remained leukemia-free for more than 129 d after injection (Figure 33A). Additionally, a lower dose of 0.025 µg/ml – at which 20D9h3-DUBA outperformed 20D9h3-MMAF in colony assays – was tested on AML-388 PDX cells (Figure 33B). In accordance with the results from the CFU and LTC-IC assays where this dose of 20D9h3-MMAF had no effect on leukemic progenitors, AML-388 PDX cells treated with this ADC rapidly engrafted in NSG mice. For 20D9h3-DUBA, a dose of 0.025 µg/ml effectively prevented colony growth in CFU assay but had only limited efficacy in the LTC-IC assay. Also, in the LIC assay 1/5 mice receiving AML-388 PDX cells after 20D9h3-DUBA treatment engrafted indicating that not all LICs have been eliminated. Further, a second AML PDX sample was tested: AML-393. A dose of 0.3 µg/ml was selected, where 20D9h3-DUBA had a higher efficacy than 20D9h3-MMAF in CFU assay. While the BLI signal of all mice from the 20D9h3-DUBA group stayed below detection limit for up to 119 d, one of the five mice from the 20D9h3-MMAF group had a late outgrowth indicating that a portion of LICs survived treatment with the MMAF-ADC (Figure 33C). Similar as for AML-388, the PBS pre-treated AML-393 PDX sample engrafted within 14 d and mice had to be sacrificed after 50-60 d. To summarize, 20D9h3-DUBA pre-treatment of AML-388 and AML-393 PDX samples, was more

effective than 20D9h3-MMAF pre-treatment in the prevention of engraftment and onset of leukemia. Still 20D9h3-MMAF also effectively prevented outgrowth when used at higher doses.

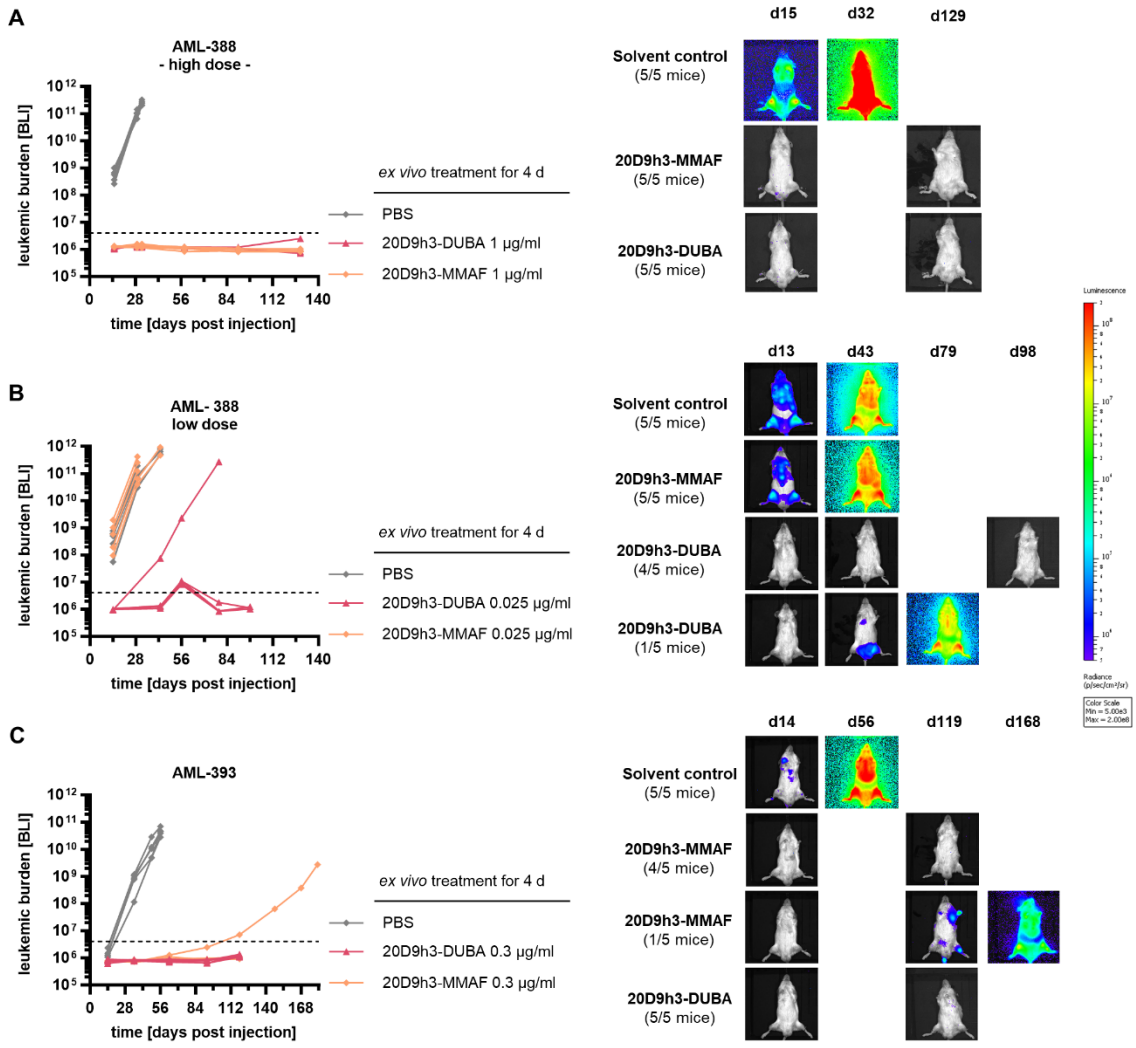

Figure 33: Effect of FLT3-ADCs on engraftment of *KMT2Ar* AML PDX samples in NSG mice. AML-388 (1x10^5 cells per condition and mouse, A-B) and AML-393 (5x10^4 cells per condition and mouse, C) PDX samples were treated *ex vivo* with 20D9h3-DUBA, 20D9h3-MMAF or PBS for 4 d in the indicated doses. On day 4, remaining cells were transplanted into five NSG mice per treatment group using tail vein injection. Engraftment of luciferase-expressing PDX cells and leukemic burden was monitored using bioluminescence imaging (BLI) in regular intervals for up to 168 d. On the right side representative BLI images are shown for each treatment group for AML-388 (top, middle) and AML-393 (bottom). Dashed line = detection limit. mean ± s.d.; n = 5 mice per group. Mouse experiments were planned together with Dr. Binje Vick and ADC pre-treatment and animal work were carried out by Annette Frank and Sandro Aidone (all AG Jeremias, Helmholtz Zentrum München).

3.7 Analysis of FLT3-ADCs in stem cell assays with healthy CD34-positive bone marrow samples

There is no AML target that is exclusively expressed on leukemic but not healthy stem and progenitor cells (47). However, ideally toxicities are limited to concentrations higher than the effective doses. To test this, CD34-positive bone marrow (BM) cells from healthy donors were treated with 20D9h3-DUBA or 20D9h3-MMAF and similarly as described in chapter 3.6 for leukemic cells, CFU and LTC-IC assays were performed.

3.7.1 Evaluation of the toxicity of FLT3-ADCs towards healthy short-term progenitors in CFU assay

First, healthy short-term progenitors were investigated using CFU assays. Those assays were planned in close collaboration with Prof. Katharina Götze and carried out by Dr. Marit Leilich (both TUM). BM cells were isolated from hip bones of patients that underwent replacement surgery for a total of five healthy donors (Table 16, Material and Methods). The isolated BM cells were enriched for CD34-positivity using magnetic activated cell sorting. The targets of 20D9h3-mAb, FLT3 and FcγRI, were expressed on 48% and 8.1% of healthy CD34-positive cells, respectively (Figure 34A). As described in the chapters 3.6.3-3.6.4, both ADCs were tested on leukemic cells at concentrations up to 1 µg/ml, but especially 20D9h3-DUBA was effective already far below that dose. This highest dose of 1 µg/ml was now selected to investigate toxicities of the ADCs towards healthy CD34-positive BM cells in CFU assay. As a control IgG1-DUBA was included. In comparison to the untreated control, none of the ADCs had a significant effect on total colony numbers (Figure 34B) or on any specific type of progenitor (Figure 34C).

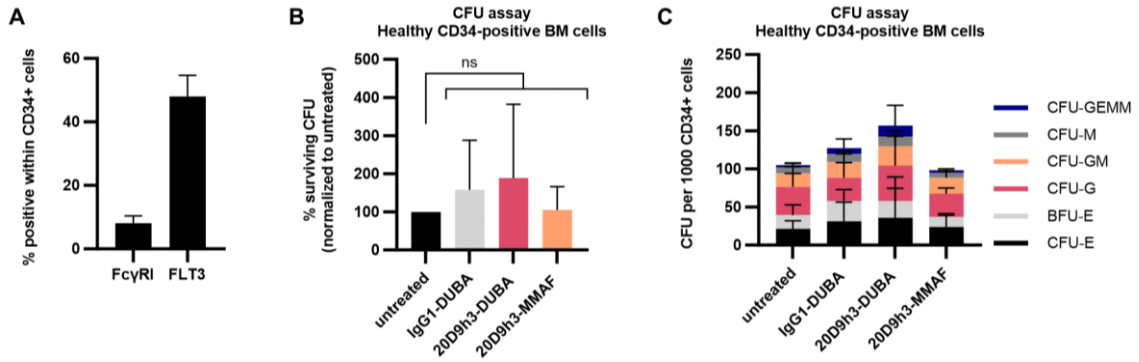

Figure 34: Evaluation of the hematotoxicity of FLT3-ADCs towards healthy short-term progenitors in CFU assay. The hematotoxicity of 20D9h3-DUBA, 20D9h3-MMAF and IgG1-DUBA control ADC were analyzed in CD34-positive bone marrow (BM) cells from healthy donors. mean ± s.d.; n = 5 donors (except 20D9h3-MMAF group: n = 4 donors). (A) Surface expression of FLT3 and FcγRI evaluated in CD34-positive BM cells by flow cytometry. (B) Total colony numbers were assessed by CFU assay and are depicted normalized to control without treatment. ns, not significant by Kruskal-Wallis test. (C) Colony counts per progenitor type. CFU: colony-forming unit; GEMM: granulocyte, erythrocyte, macrophage, megakaryocyte; M: macrophage; GM: granulocyte, macrophage; G: granulocyte; BFU-E: burst-forming unit erythrocyte; E: erythrocyte. These assays were performed by Dr. Marit Leilich (TUM, AG Götze).

3.7.2 Evaluation of the toxicity of FLT3-ADC towards healthy long-term progenitors in LTC-IC assay

In analogy to the analyses with leukemic cells, I now evaluated the more primitive healthy progenitors using LTC-IC assay. Healthy CD34-positive BM cells for those assays were purchased from StemCell technologies for a total of three donors (Table 16, Material and Methods). The assays were planned in close collaboration with Prof. Feuring (University hospital Ulm) and carried out by me together with Dr. Xiang Gao (group of Prof. Feuring). As described for leukemic cells (chapter 3.6.4), colonies were counted for all conditions as endpoint of the assay after 7 weeks (Figure 35).

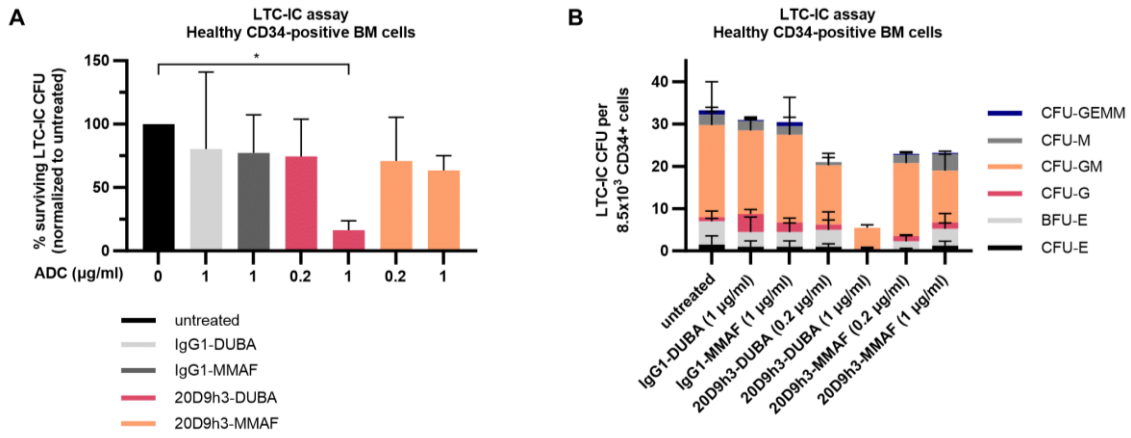

Figure 35: Evaluation of the hematotoxicity of FLT3-ADCs towards healthy long-term progenitors in LTC-IC assay. Healthy CD34-positive bone marrow (BM) cells were treated with 0.2-1 µg/ml 20D9h3-DUBA, 20D9h3-MMAF, IgG1-DUBA or IgG1-MMAF for 48 h and then subjected to LTC-IC assay as described in Figure 31. (A) Total colonies were counted as end-point of the assay after 7 weeks and normalized to control without treatment. mean ± s.d.; n = 3 donors. *P<.05 by One-way-ANOVA. (B) Total counts per colony type at the end-point of the assay after 7 weeks. mean ± s.d.; n = 2 donors (third donor was excluded as colony numbers were too low to reliably differentiate the colony types). CFU: colony-forming unit; GEMM: granulocyte, erythrocyte, macrophage, megakaryocyte; M: macrophage; GM: granulocyte, macrophage; G: granulocyte; BFU-E: burst-forming unit erythrocyte; E: erythrocyte. Assays were carried out by me together with Prof. Michaela Feuring and Dr. Xiang Gao (both University hospital Ulm).

Total colony numbers were normalized to untreated control (Figure 35A). At a dose of 1 µg/ml, 20D9h3-DUBA caused a significant reduction of healthy LTC-IC-CFCs to 16.4%. However, in colony assays with leukemic progenitors 20D9h3-DUBA has already been quite effective at doses between 0.005-0.3 µg/ml. Here, the toxic effect towards healthy LTC-IC-CFCs was limited: 20D9h3-DUBA caused a reduction of LTC-IC-CFCs to 74.5% of untreated control at a dose of 0.2 µg/ml. 20D9h3-MMAF has been less effective towards leukemic progenitors. Similarly, it was also less toxic towards healthy progenitors. It reduced LTC-IC-CFCs to 70.8% and 63.4% of untreated control for 0.2 µg/ml and 1 µg/ml of ADC, respectively. The isotype control ADCs IgG1-DUBA and IgG1-MMAF led to a reduction of LTC-IC-CFCs to 80.5% and 77.2% at a dose of 1 µg/ml,

respectively. Regarding the different colony types, 20D9h3-DUBA mainly affected the abundance of CFU-GM and CFU-M (Figure 35B). Likewise, 20D9h3-MMAF had a slight negative effect on CFU-GM numbers. Taken together, 20D9h3-DUBA toxicity towards healthy CD34-positive BM cells in CFU and LTC-IC assay was restricted to concentrations exceeding the dose range that was effective in leukemic cells. In those lower concentrations of 0.2 µg/ml and below it only had minor adverse effects. For 20D9h3-MMAF, toxicities were even lower, however its efficacy against leukemic cells has also been lower.

3.8 20D9h3-DUBA combination therapies

Cancer therapy rarely uses one single agent but rather a combination of different drugs to increase efficacy, lower toxicities, and overcome and prevent drug resistance (175). Drug combinations can be antagonistic, additive or synergistic. The latter means that the effect of a combination of drugs is greater than would be expected when adding up the effects of the single agents. (175, 176) There are different molecular mechanisms behind the synergy of two drugs: 1) Anti-counteractive actions where drug 2 antagonizes the cellular response to drug 1. 2) Complementary actions where two drugs act on multiple targets of one pathway or on multiple sites of one target. 3) Facilitating actions where drug 1 increases availability or activity of drug 2. (177)

As described above, out of the two ADCs 20D9h3-DUBA showed especially promising activity against leukemic stem and progenitor cells and I was therefore interested to evaluate combinations that could even potentiate the ADC's effect. 20D9h3-DUBA acts via DNA-damage triggering DNA-damage response and eventually apoptosis (see chapter 3.3.6). Considering this, it is not surprising that combinations of DNA-alkylating drugs – such as DUBA or IGN – with DNA-damage response inhibitors (166) or apoptosis-inducing agents (178, 179) have both been reported as promising. In the following, I therefore wanted to evaluate the combination of inhibitors of the DNA damage response protein ATR (ATRi) or the anti-apoptotic protein BCL-2 (BCL-2i) with the 20D9h3-DUBA FLT3-ADC that has been generated in this project.

3.8.1 Combination of 20D9h3-DUBA with ATR inhibitors

3.8.1.1 Cytotoxicity of 20D9h3-DUBA in cells with p53 deficiency

In his thesis, Dr. Marcel Rieker described the combination of HER2- and epidermal growth factor receptor (EGFR)-targeting DUBA-ADCs with the ATRi ceralasertib/AZD6738. Interestingly, he observed that cell lines carrying loss-of-function mutations in the *TP53* gene or with defects in this pathway were especially sensitive to the combination therapy with those agents. (166) p53 is downstream of ATR (165) and thus likely plays a crucial role in the response of cells to 20D9h3-DUBA. Firstly, I therefore wanted to investigate how the loss of p53 in a cell influences the general sensitivity towards 20D9h3-DUBA. To test this, MOLM-13, MV4-11 and OCI-AML3 cells with p53 knockdown (kd) were used (a kind gift from Dr. Andreef, MD Anderson Cancer Center (139, 144)). Successful kd of p53 in those cells was first confirmed using Western blotting (Figure 36A). Additionally, FLT3 and FcγRI expression was analyzed by flow cytometry to rule out that there are major differences between p53 wt and kd cells (Figure 36B-C). It was found that FLT3 was slightly (**P < .01) lower expressed in OCI-AML3 cells with p53 kd, but for the cell lines MOLM-13 and MV4-11 there were no significant differences. FcγRI, on the contrary, was significantly

(**P < .01) higher expressed in MOLM-13 cells with p53 kd. In MV4-11 and OCI-AML3 cells, however, there was no difference in FcγRI expression between p53 wt or kd cells.

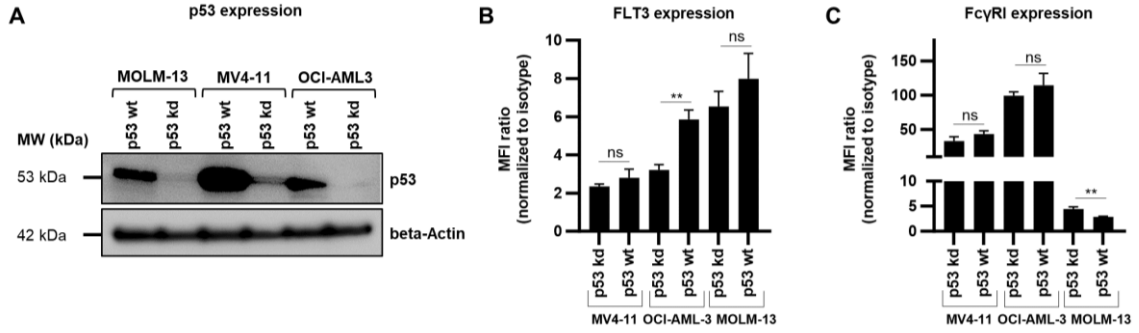

Figure 36: p53, FLT3 and FcγRI expression in MV4-11, OCI-AML3 and MOLM-13 cells with p53 wt or kd. (A) Expression of p53 was analyzed by Western blotting in cells with p53 wildtype (wt) or knockdown (kd). Beta-Actin was used as loading control. MW = molecular weight. (B-C) Expression of FLT3 (B) and FcγRI (C) was analyzed by flow cytometry. Mean fluorescence intensity (MFI) was normalized to isotype control. mean ± s.d.;, n = 3 biological replicates. **P < .01; ns, not significant by Unpaired t-test. Figure was adapted from Roas et al (139) with permission.

Next, p53 kd and wt cell lines were incubated with 20D9h3-DUBA ADC for 96 h and viable cells were assessed using a resazurin read-out (Figure 37). Not unexpectedly, it was observed that cells with p53 kd were significantly less sensitive towards 20D9h3-DUBA. The difference in the IC_{50} values between p53 wt and kd cells were 3.9x, 2.5x and 5.1x for MV4-11, OCI-AML3 and MOLM-13 cells, respectively.

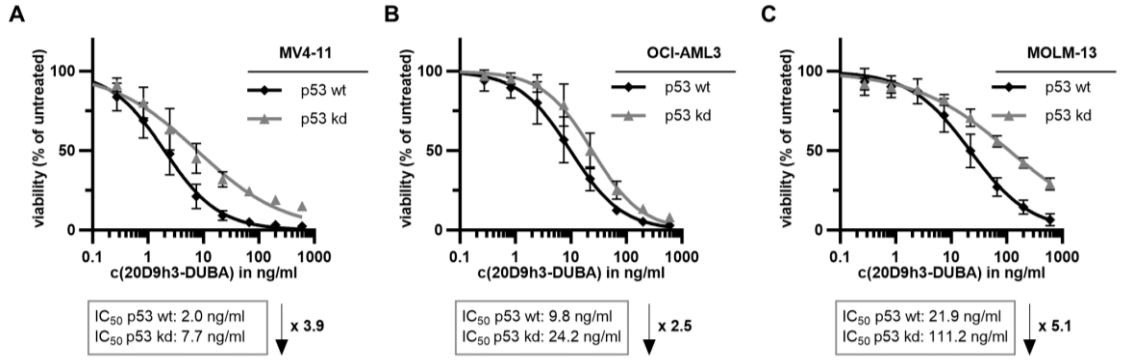

Figure 37: Evaluation of the effect of p53 kd on 20D9h3-DUBA ADC activity. (A-C) MV4-11 (A), OCI-AML3 (B) and MOLM-13 (C) cells with p53 wildtype (wt) or knockdown (kd) were treated with a dilution row of 20D9h3-DUBA ADC for 4 d. Viability was assessed by resazurin readout and is depicted normalized to untreated control. Curves were plotted and IC_{50} values calculated with GraphPad Prism 10.1.2 using non-linear fit, variable slope analysis. mean ± s.d.; n = 3 biological replicates.

At least in two of the cell lines, the lower response of p53 kd cells towards 20D9h3-DUBA cannot be attributed to reduced expression of FLT3 or FcγRI: In MV4-11 cells there was no expression difference and in MOLM-13 cells the expression of FcγRI was even higher in kd cells. It can be concluded that a dysfunctional p53 pathway decreases the effectivity of 20D9h3-DUBA.

3.8.1.2 Evaluation of synergy in cytotoxicity assay

In his PhD thesis, Dr. Marcel Rieker described that cells with defects in the p53 pathway are sensitive towards a combination of DUBA-ADCs and ATRi (166) and I therefore wanted to test if an inhibitor of ATR can restore the sensitivity to 20D9h3-DUBA. Further, it was investigated if p53 kd cells are particularly vulnerable to the combination in comparison to p53 wt cells. The ATRi ceralasertib/AZD6738 was used for those experiments, which is a selective inhibitor of ATR that is currently in phase II clinical trials for various indications (180, 181). Firstly, synergism between the drugs was evaluated using cytotoxicity assays in MOLM-13 (Figure 38) and MV4-11 cells (supplemental Figure 6) with p53 wt or kd.

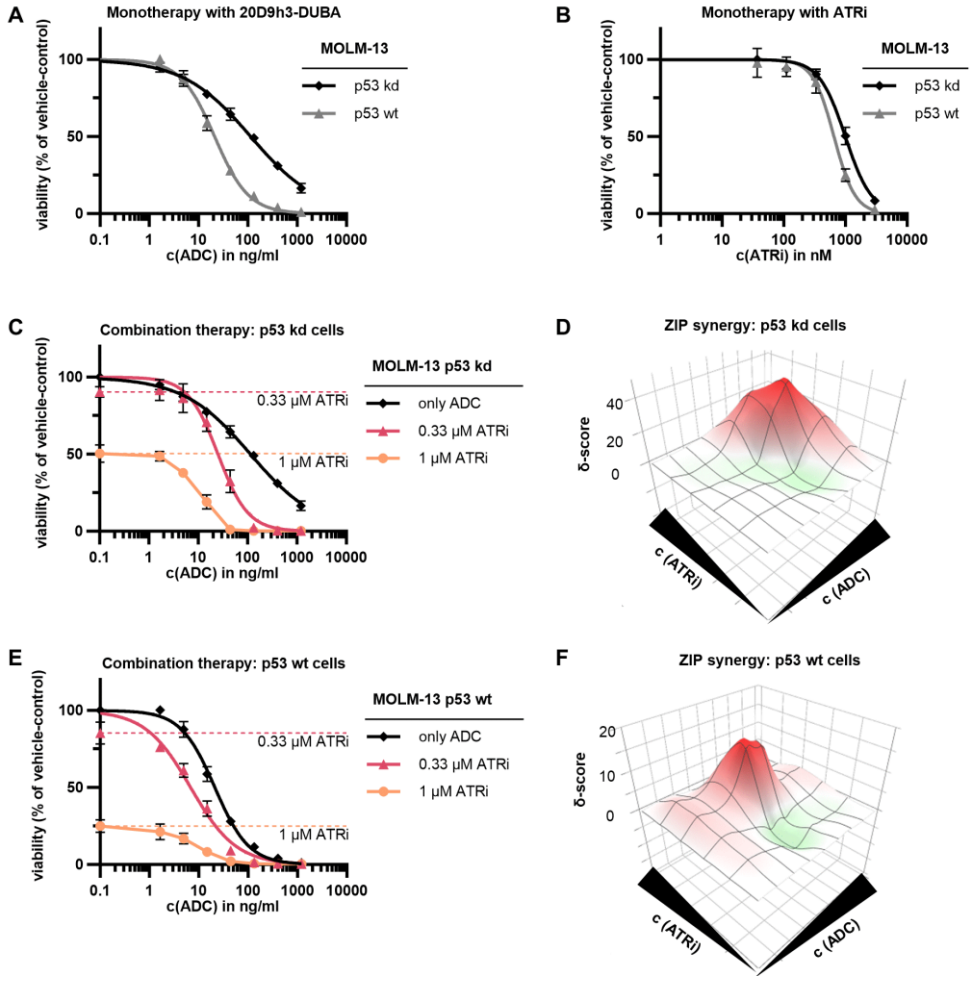

Figure 38: Cytotoxicity assay of 20D9h3-DUBA in combination with the ATRi ceralasertib in MOLM-13 cells with p53 wt or kd. MOLM-13 cell with p53 wt or kd were treated with either a monotherapy of 20D9h3-DUBA (A), a monotherapy of the ATRi ceralasertib (B), or a combination of both drugs (C-F) for 96 h. Viable cells were assessed by resazurin readout-out and normalized to vehicle-control (DMSO for ceralasertib; PBS for 20D9h3-DUBA). They were plotted using non-linear fit, variable slope analysis, in GraphPad Prism 10.1.2. Dashed lines in (C) and (E) mark effectivity of ATRi monotherapy. mean ± s.d.; n = 3 biological replicates. For the analysis of synergistic effects of the combination, dose-response curves were uploaded to SynergyFinder 3.0 and the zero interaction potency (ZIP) model without baseline correction was used for synergy calculations, which compares observed and expected effects for the drugs (145, 146). Synergy scores δ of > +10, < -10 or between both values indicate synergism, antagonism or additive effects, respectively.

Like observed before, MOLM-13 cells with p53 kd were less sensitive towards 20D9h3-DUBA monotherapy (Figure 38A). Similarly, they were also slightly less sensitive towards ATRi monotherapy (Figure 38B). Combination therapy, however, was strikingly very effective in p53 kd cells (Figure 38C-D). For example, at doses of 0.33 µM ATRi and 133 µg/ml 20D9h3-DUBA the monotherapies reduced cells to 90.5% (indicated by dashed horizontal pink line) and 49% (solid black line) of vehicle-control, respectively. The combination of both agents however reduced cells to 0.2% of control (solid pink line). Accordingly, when the drug combinations were evaluated with the online-tool SynergyFinder 3.0 using the zero-interaction potency (ZIP) calculation method (145, 146), it indicated a synergistic interaction of the two drugs for a wide range of dose combinations with ZIP scores of up to +40 (according to the tool's guidelines a δ-score > +10 for two drugs is likely synergistic). This effect was less pronounced for p53 wt cells where the δ-score was mostly around or below +10 suggesting that in those cells the drug combination is rather additive than synergistic (Figure 38E-F). The results in MV4-11 cells were quite similar with strong synergistic effects in the kd cells (supplemental Figure 6). Next, the drug combination was evaluated in the acute monocytic leukemia cell line MM-6 (Figure 39), which naturally has a loss-of-function of p53 due to a R273H point mutation in the DNA-binding domain (182).

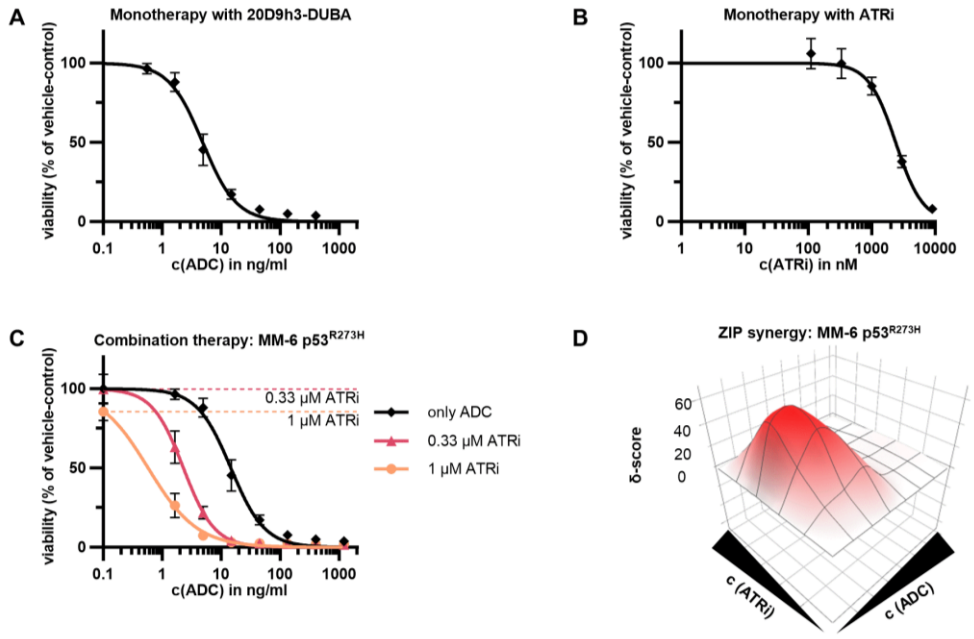

Figure 39: Cytotoxicity assay of 20D9h3-DUBA in combination with the ATRi ceralasertib in MM-6 p53^{R273H} cells. (A-C) MM-6 cells were treated with a dilution row of either 20D9h3-DUBA alone (A), ATRi (ceralasertib) alone (B) or a combination of both agents (C) for 96 h. Viable cells were assessed by resazurin read-out and are depicted normalized to vehicle-control (DMSO for ceralasertib; PBS for 20D9h3-DUBA). Curves were fitted using GraphPad Prism 10.1.2 non-linear fit, variable slope analysis. Dashed line in (C) marks effectivity of ATRi monotherapy. mean ± s.d.; n = 4 biological replicates. (D) Dose-response curves were subjected to zero interaction potency (ZIP) calculation without baseline correction to analyze synergism using the online-tool SynergyFinder 3.0 (145, 146). After a comparison of observed with expected values, δ-scores are calculated indicating synergism (δ > +10), antagonism (δ < -10) or additive effects (-10 < δ < +10).

Similarly, the combination of ATRi and 20D9h3-DUBA was highly synergistic here with the maximum ZIP score being > +60 for the combination of 1 µM ATRi and 1.6 ng/ml 20D9h3-DUBA. At those doses, the monotherapies with ATRi and ADC diminished viable cells to 85.6% and 96.5% of untreated control, respectively. The combination of both substances, however, reduced cells to 26.4% of the control. Figure 40 summarizes the most synergistic area scores for all tested cell lines. It highlights again that the combination of ATRi and 20D9h3-DUBA is significantly more synergistic in p53 kd compared to p53 wt cells, where the effect is only additive to slightly synergistic.

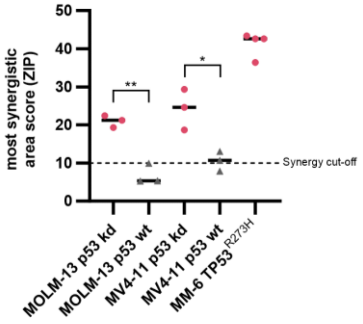

Figure 40: Most synergistic area scores for the combination of 20D9h3-DUBA with the ATRi ceralasertib. Most synergistic area ZIP scores were calculated with the online tool SynergyFinder 3.0 based on the results from Figure 38-39 and supplemental Figure 6. Synergy is defined as δ > +10 (indicated by the dashed line). n = 3 biological replicates (except MM-6: n = 4). *P < .05; **P < .01 by Unpaired t-test.

3.8.1.3 Synergy evaluation in apoptosis assay

As a next step, it was evaluated if the synergism of ATRi and 20D9h3-DUBA is due to increased apoptosis induction by the combination therapy. To test this, MOLM-13 cells with p53 wt or kd were incubated with doses of 0.33 µM ATRi and/or 44 ng/ml 20D9h3-DUBA, a combination which has been highly synergistic in the cytotoxicity assay (Figure 41).

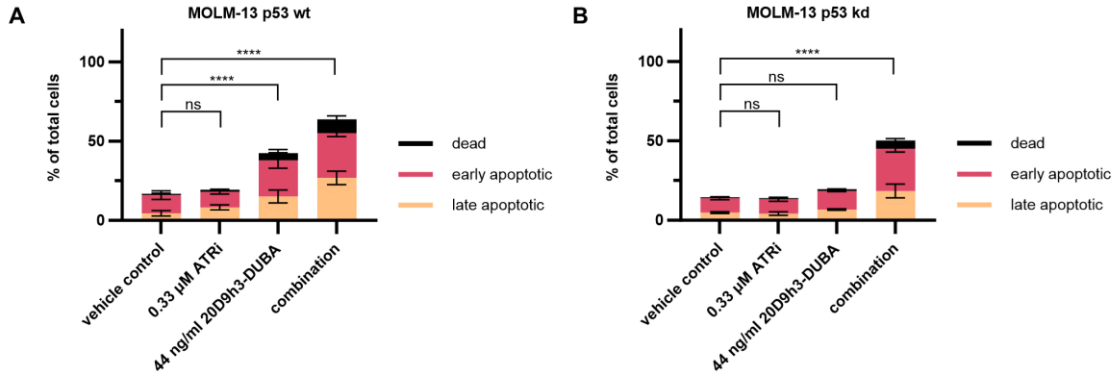

Figure 41: Apoptosis assay of 20D9h3-DUBA in combination with the ATRi ceralasertib in MOLM-13 cells with p53 wt or kd. (A-B) MOLM-13 cells with p53 wt (A) or kd (B) were incubated with either DMSO control, 0.33 µM ATRi (ceralasertib), 44 ng/ml 20D9h3-DUBA or 0.33 µM ATRi + 44 ng/ml 20D9h3-DUBA. After 96 h, cells were harvested, washed and stained with APC-Annexin V and DAPI for analysis of apoptotic and dead cells using BD FACS Canto II. mean ± s.d.; n = 3 biological replicates. ****P < .0001; ns, not significant by Ordinary two-way ANOVA and Dunnett's multiple comparison test.

For p53 wt cells, monotherapy with 0.33 µM ATRi did not significantly increase dead plus apoptotic cells compared to control (19.4% versus 16.9%). Treatment with 44 ng/ml 20D9h3-DUBA alone or the combination of ATRi and 20D9h3-DUBA, however, significantly increased the proportion of dead plus apoptotic cells to 42.4% (****P < .0001) and 63.8% (****P < .0001), respectively. In p53 kd cells both monotherapies had no significant effects in comparison to vehicle-control (13.9% and 18.5% dead plus apoptotic cells for ATRi and 20D9h3-DUBA monotherapies, respectively, versus 13.9% for vehicle-control). In contrast to that, the combination of both drugs was highly efficient leading to 50.3% (****P < .0001) dead plus apoptotic cells. These experiments confirm that the synergistic effect is also evident at the level of apoptosis induction. Similarly, as observed for the cytotoxicity assays, the effect was more pronounced in p53 kd compared to p53 wt cells. This suggests that the combination of 20D9h3-DUBA and the ATRi ceralasertib is very promising especially in the context of a dysfunctional p53 pathway.

3.8.2 Combination of 20D9h3-DUBA with BCL-2 inhibitors

As described, 20D9h3-DUBA acts via apoptosis induction suggesting that a combination of the ADC with compounds lowering the apoptotic threshold might be another possibility to potentiate its effect. This has e.g. been reported for a combination of the FDA-approved BCL-2i venetoclax and the CD123-targeting ADC IMGN632 that contains the DNA-alkylating drug IGN (178, 179). This provided the rationale to test this combination with the 20D9h3-DUBA ADC using a cytotoxicity assay. To this end, the AML cell line MOLM-13 was incubated with either 20D9h3-DUBA, the BCL-2i venetoclax or a combination of both agents for 96 h (Figure 42). The resulting dose-response curves were analyzed with the ZIP method using the SynergyFinder 3.0 online-tool to evaluate if the drug combination acts synergistically (145, 146). The highest ZIP δ-score of ~ +18.5 was observed for the combination of 6.2 nM venetoclax with 1.7 ng/ml 20D9h3-DUBA. At those doses, BCL-2i and ADC diminished viable cells to 87.9% and 95.4% of vehicle-control, respectively, while the combination of both agents reduced them to 63%, clearly exceeding a pure additive effect. The drug combination was further tested in a second cell line – the acute monocytic leukemia cells MV4-11 (supplemental Figure 7). 6.2 nM venetoclax, 1.7 ng/ml 20D9h3-DUBA and the combination of both led to reductions of viable cells to 64.9%, 66.5% and 37.2% of vehicle-control, respectively. In these cells the combination thus had a more additive rather than synergistic effect. This is reflected by a maximum ZIP δ-score of +7.1. Hence it can be concluded that the combination of 20D9h3-DUBA with a BCL-2i is additive to synergistic dependent on the cell line model.

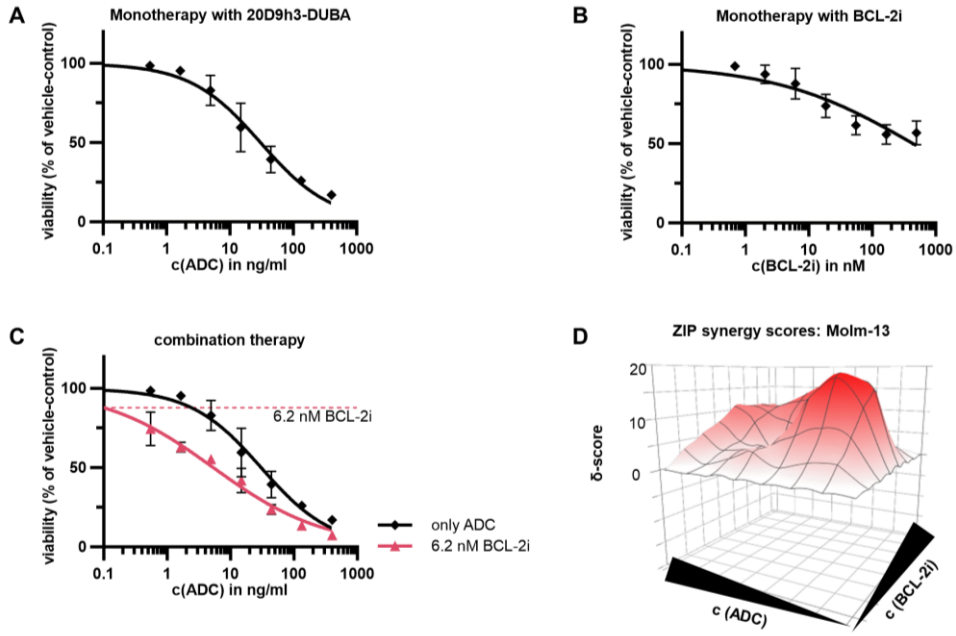

Figure 42: Cytotoxicity assay of 20D9h3-DUBA in combination with the BCL-2i venetoclax in MOLM-13 cells. (A-C) MOLM-13 cells were treated with a dilution row of either 20D9h3-DUBA alone (A), the BCL-2i venetoclax alone (B) or a combination of both drugs (C). Viable cells were assessed by resazurin assay and normalized to vehicle-control (DMSO for venetoclax; PBS for 20D9h3-DUBA) and fitted using GraphPad Prism 10.1.2 non-linear fit, variable slope analysis. Dashed line in (C) marks effectivity of BCL-2i monotherapy. mean ± s.d.; n = 3 biological replicates. (D) Dose-response curves were analyzed with zero interaction potency (ZIP) method by SynergyFinder 3.0 (no baseline correction) (145, 146). δ-score > +10 indicates synergy; δ-score < -10 indicates antagonism; -10 < δ-score > +10 indicates an additive effect.

4 Discussion

4.1 The antibody

4.1.1 Humanization and binding affinity

The FLT3-mAb 20D9, which was generated as part of a previous project (139, 143), is a chimeric antibody which means that it possesses human constant regions but variable domains from the host (in this case rat). For further development, it was decided to subject the antibody to a full humanization using CDR grafting and a 3D structure-based approach. The degree of humanization is here expressed by the germinality index (GI), which quantifies the similarity of the antibodies' variable region with the most similar human germline sequence (183). Compared to the original chimeric 20D9 with a mean GI_{VH+VL} of 84.7%, the humanized mAbs had a mean GI_{VH+VL} in a range of 90.2% – 100%. The selected lead candidate 20D9h3-mAb had a GI_{VH+VL} of 94.7%. A partial or full humanization of therapeutic antibodies is currently quite common with only a small number of rodent mAbs in clinical use. This has changed over time. As most antibodies are produced in mice, historically murine antibodies were the first ones to be applied as therapeutic antibodies in humans. However, it was soon noticed, that the application of murine antibodies in humans comes with certain challenges. One is the development of human anti-mouse antibodies which can lead to severe symptoms similar to an allergic reaction. Additionally, it increases mAb clearance and decreases therapeutic efficacy. (184) A further safety concern associated with murine mAbs is cytokine release syndrome (CRS) which is a serious and sometimes even fatal complication (185). This is the reason why there has been ongoing effort to increase the human proportion in therapeutic mAbs by either chimerization (those mAbs possess only murine variable regions), humanization (those mAbs possess only murine CDRs) or to produce fully human mAbs e.g. by using phage display libraries or transgenic mice (184). It was indeed shown that humanization reduces immunogenicity and anti-antibody responses (AAR). Hwang et al. analyzed immunogenicity in clinical studies with 44 murine, 15 chimeric and 22 humanized mAbs (151). Marked AAR, which was classified as AAR in > 15% of patients, occurred for 84%, 40% and 9% of murine, chimeric and humanized mAbs, respectively, and clinical development was usually stopped for these mAbs. This illustrates the advantage of humanization, however, even for those mAbs AAR can still occur. There are also arguments against humanization. First of all, it takes time and might prolong clinical development. (185) Additionally, AAR and CRS might play a role for the efficacy of some therapeutic mAbs. This is illustrated by Lym-1 therapy in B cell malignancies, where patients with high human anti-mouse antibody titers had a survival benefit (186) and catumaxomab therapy where the development of CRS seems to play a vital role for efficacy (187). The precise mechanisms of these observations remain to be elucidated. In ADCs not only the antibody moiety but also the payload bears a risk for toxicities, which might make a humanization

even more relevant to achieve an acceptable toxicity profile. This might be also the reason why all of the 15 worldwide approved ADCs are either chimeric or humanized (105). Humanization can be done by CDR grafting, whereby rodent CDRs are transferred to a human framework (188). Some framework amino acids might be crucial for antigen binding and they can be identified using cryo-electron microscopy or *in silico* homology modelling to optimize the humanization procedure (189).

Nevertheless, it is important to analyze if the target binding affinity is retained after the humanization, which was done in my project using flow cytometry and ELISA. In ELISA, EC_{50} values of the 12 humanized mAbs were between 11.0 ng/ml and 111.6 ng/ml (73.3 pM – 744 pM) versus 10.9 ng/ml (= 72.7 pM) for the original chimeric 20D9. Interestingly, EC_{50} values increased with increasing GI of the V_L domain, with the best binding observed for V_L1-mAbs (20D9h1-20D9h4) followed by V_L2-mAbs (20D9h5-20D9h8) and V_L3-mAbs (20D9h9-20D9h12). Conversely, the GI of the V_H domain did not seem to play a role for the binding affinity. Flow cytometry analysis in Ba/F3 cells expressing human surface FLT3 confirmed those results. Importantly, the binding of 20D9h1-20D9h4 mAbs was comparable to that of chimeric 20D9-mAb in both assays. 20D9h3-mAb was selected as a lead candidate out of the V_L1-mAbs due to its good producibility (144 mg/l cell culture) and superior GI (94.7%). As illustrated by a study with HER2-binding mAbs/ADCs in HER2-expressing cell lines a high binding affinity is related to improved internalization and superior cytotoxicity especially in cells with a low target expression (190), which is generally seen as advantageous as it expands the therapeutic benefit to this target-low patient group (191). But it might also be a disadvantage toxicity-wise if the therapeutic window of expression between tumor and healthy tissues is small, as argued by others (190). The EC_{50} value of 20D9h3-mAb was 11.3 ng/ml, which corresponds to approximately 75.3 pM. For two other approved ADCs, HER2-directed trastuzumab emtansine (T-DM1)/Kadcyla and CD33-directed GO/Mylotarg, EC_{50} values of 0.4-0.9 µg/ml (around 2.7-6 nM) (191) and 11.6 nM (52) were reported, respectively. Compared to that, 20D9h3-mAb binding is superior although it has to be noted that those studies used different assays to assess the EC_{50} value, the payload conjugation might reduce the binding affinity, and both ADCs – T-DM1 and GO – are directed against highly expressed targets. Better suited might be the comparison with the FLT3-mAb IMC-EB10 and the FLT3-ADC AGS62P1/ASP1235. For those, EC_{50} values of 158 pM (99) and 100-500 pM (192) were reported, respectively. Here, 20D9h3-mAb is in a similar range. All three FLT3-mAbs – including 20D9h3 – have rather high binding affinities compared to T-DM1 and GO. Both, IMC-EB10 (NCT00887926, (193)) and AGS62P1/ASP1235 (NCT02864290, (102, 194)) proceeded to phase I clinical studies, but in both cases those studies were terminated due to lack of efficacy without giving further information.

4.1.2 Internalization

Unlike therapeutic antibodies, ADCs must be internalized into the target cell to exert their main effect, which is mediated by their payload. Successful internalization of 20D9h3-mAb was confirmed by flow cytometry and microscopy in FLT3-expressing Ba/F3 cells using a secondary antibody coupled to a pH-sensitive dye that is only fluorescent in late endosomes or lysosomes where the pH is low. As soon as after 1 h, 20D9h3-mAb could be detected via flow cytometry indicating that it was already present in late stages of the endocytic process. The signal approximately doubled after 5 h with only a slight further increase after 24 h. The signal intensity was dependent on FLT3 surface expression levels. In microscopy, pHrodo signal did not co-localize with YFP signal. As YFP should be only expressed in the cytoplasm but not in endosomes/lysosomes, this further confirms that 20D9h3-mAb internalizes in the desired compartment. Similar kinetics were observed by other groups that developed therapeutic antibodies. Zheng et al. also describe a microscopy experiment in CLL1-positive HL-60 cells where they show that their CLL1-mAb co-localized with LysoTracker after 2 h, indicating that it was present in the lysosome, and the signal became abundant after 18 h (195). For gemtuzumab – the antibody part of GO – a study shows that depending on the cell line 15-50% of the antibody are internalized after 1 h and the amount inside the cells approximately doubles after around 4 h (196). In summary, 20D9h3-mAb has comparable internalization kinetics to other therapeutic antibodies that are in development or approved.

4.1.3 Specificity and cross-reactivity

Antibody specificity and cross-reactivity were also evaluated in detail. In flow cytometry binding analyses, 20D9h3-mAb bound to human and cynomolgus monkey FLT3, but not rat or murine FLT3. This is relevant for later toxicological studies. For therapeutic mAbs it is crucial that toxicological studies are carried out in species that have mAb cross-reactivity to produce meaningful results, as most associated toxicities are target-mediated. For ADCs not only the antibody but also the payload moiety could cause side effects. Therefore, studies in non-cross-reactive species can be meaningful to some extent. It is not uncommon for therapeutic mAbs and ADCs that toxicity studies in rodent species are not possible due to missing cross-reactivity. (156, 197) Iwasaki et al. tested a panel of therapeutic mAbs for their cross-reactivity with different animal species: 0% (0 out of 30) displayed cross-reactivity in rats and only 7% (2 out of 31) in mice. However, 82% (32 out of 39) bound to receptor orthologues from cynomolgus monkey. The non-rodent cross-reactivity of 20D9h3-mAb is therefore not surprising. Cynomolgus monkey is also typically the animal of choice for toxicity evaluations and ADME studies with therapeutic mAbs and ADCs producing the most relevant results. (198)

Further, 20D9h3-mAb cross-reactivity to the FLT3 receptor paralogues c-KIT, VEGFR-2, PDGFRα and CSF1R was tested, which are structurally most similar to FLT3. 20D9h3-mAb did not bind to any of the receptors and accordingly no cytotoxic effect was mediated via those targets in viability assays with 20D9h3-DUBA or -MMAF ADCs. None of the tested FLT3 receptor paralogues is a frequently mentioned AML LSC marker (35, 36, 41). Binding to receptor paralogues would thus likely not confer additional benefits concerning efficacy of an anti-LSC ADC, but rather increase toxicities. For first-generation TKIs, which often lack specificity and target multiple kinases, various toxicities have been reported related to the targeting of FLT3 receptor paralogues. Off-target effects on c-KIT expressing cells have been related to myelosuppression as illustrated by quizartinib (199, 200). VEGFR inhibition – e.g. by sorafenib, sunitinib or pazopanib – has been related to arterial dissections and aneurysms (201). Likewise PDGFR inhibition by sunitinib (202) or dasatinib (203) is associated with cardiotoxicity, as PDGFR plays a vital role in the proliferation of cardiomyocytes and heart regeneration (204). CSF1R inhibitors have been described to deplete macrophages. This also includes Kupffer cells, which could explain why CSF1R inhibition is associated with hepatotoxicity. (205) For ADCs, toxicities via off-target effects might be even more severe due to the high potency of the payload. All-in-all, the specificity of the 20D9h3-mAb for FLT3 is a desirable feature of the antibody preserving the favorable therapeutic window provided by FLT3 expression.

Lastly, cross-reactivity towards mutant FLT3 was assessed using chimeric 20D9-mAb, which has identical binding properties compared to humanized 20D9h3-mAb. Binding studies with flow cytometry using the Ba/F3 model confirmed that 20D9-mAb binds to all mutant versions of FLT3. Binding to mutant FLT3 seemed to be reduced compared to wildtype FLT3, however this was probably an artefact caused by different expression efficiency of the constructs in Ba/F3 cells. Cytotoxicity assays with 20D9-MMAF ADC further confirmed that Ba/F3 cells expressing mutant FLT3 are sensitive towards the ADC. Here, IC_{50} values were increased in Ba/F3 cells expressing mutant FLT3 compared to those expressing wildtype FLT3 in analogy to the binding studies. It was expected that the tested *FLT3* mutations do not affect binding and cytotoxicity of FLT3-mAb and FLT3-ADC, respectively, as all of them are intracellular and distant from the binding epitope of 20D9/20D9h3. In fact, most reported *FLT3* mutations occur in the intracellular domains. Ge et al. analyzed *FLT3* mutation type and location in a cohort of 869 *FLT3*-mutated patients with different forms of acute leukemia and myelodysplastic syndrome (206). Here, canonical intracellular *FLT3*-ITD and -TKD mutation accounted for 55.8% and 23% of detected *FLT3* mutations, respectively. The remaining mutations occurred in all FLT3 domains, but predominantly also intracellularly in TKD1 and 2. Of the mutations occurring in the extracellular Ig-like domain, most were located in domains 3-5, which would not be expected to affect 20D9/20D9h3 binding as it has been shown previously that the antibody epitope is located in domain 1 (50-KSSSYPM-55, (139, 143)). Therefore, a broad group of patients with and without

FLT3 mutations at the start of treatment could potentially benefit from 20D9h3-ADC therapy. Nevertheless, the emergence of secondary mutations in the FLT3 binding epitope in response to treatment is conceivable and has been reported to be a factor responsible for the resistance to other antibody therapeutics such as the EGFR-directed antibody cetuximab (207). However, the relevance of this finding for FLT3 remains to be investigated. Further, a downregulation of the target antigen on the cell surface either initially or in response to therapy could pose challenges to effective treatment. For FLT3, it has been reported that certain mutations such as ITD or D835Y shift the preferential localization of the receptor from the cell surface to the ER (136). This could also explain the lower surface expression of the FLT3 mutant receptors in comparison to FLT3 wildtype observed in the Ba/F3 model. It was shown by our group that TKIs such as midostaurin or quizartinib can be used to shift FLT3 receptor expression back to the cell surface (136, 139). This probably provides the basis for a synergistic effect between TKIs and 20D9-ADC that has been demonstrated previously by our group in Roas et al (139). In summary, it can be concluded that 20D9h3-ADCs are effective in the context of FLT3 mutations and that cell surface downregulation of FLT3 may be overcome with TKIs, so that eventually a broad group of patients can benefit from this treatment irrespective of their mutational status.

4.2 Efficacy of ADC payloads and 20D9h3-ADCs in cell line models

Besides the selection of an antibody with good binding, internalization and specificity properties, an ideal payload for the desired application needs to be chosen. Currently, DNA-damaging agents, topoisomerase I inhibitors and microtubule inhibitors are the most frequently used payloads in ADCs (105). Representative agents of each category were tested on a panel of four leukemia cell lines and Ba/F3 cells, which served as a model system. Overall, the DNA-damaging agent DUBA was most efficient in all cell lines with IC_{50} values of 0.6-21.3 nM after a 24 h incubation. This was followed by the topoisomerase I inhibitor exatecan (2.4-790.9 nM) and the microtubule inhibitors MMAE (1.6-2834 nM) and MMAF (> 1000 nM). The latter compound is difficult to compare in this experiment as it has a low membrane permeability and is only potent when delivered inside the cell in the form of an ADC. One of the cell lines – K-562 – showed a higher resistance towards all of the compounds. Generally, the IC_{50} values were in line with reported values for DNA-damaging agents (*seco*-DUBA: 0.08-0.4 nM (191); PBD: 0.15-1 nM; calicheamicin: 0.01-0.06 nM (208)), topoisomerase inhibitors (1.7-700 nM (208)) and microtubule-inhibitors (MMAE: 0.07-3.1 nM; MMAF: 100-200 nM (208)) albeit a direct comparison is very difficult as different cell types and mostly longer time spans were used for those assays. Due to the results of the cytotoxicity assay together with considerations about the anti-LSC potential of the selected agents, which is discussed in detail in chapter 4.4, DUBA was selected as ADC payload to be conjugated to 20D9h3-

mAb (20D9h3-DUBA). Further MMAF was chosen as a second agent to generate 20D9h3-MMAF. The potency and specificity of the ADCs was evaluated in the FLT3-positive leukemia cell lines MOLM-13, MV4-11 and OCI-AML3 and the FLT3-negative leukemia cell lines HL-60 and K-562. FLT3-positive cell lines had 96 h IC_{50} values between 8.2-16.0 ng/ml for 20D9h3-DUBA and 25.7-35.5 ng/ml for 20D9h3-MMAF. Both ADCs had no effect on the target-negative cell lines. The similar or even higher efficacy of 20D9h3-DUBA compared to 20D9h3-MMAF despite the lower DAR of 4.8 versus 8.0 further illustrates the high potency of the DUBA payload. These findings are in line with a study comparing the DUBA-ADC SYD985 (DAR 2.8) and the maytansinoid-conjugate T-DM1/Kadcyla (DAR 3.7) on HER2-positive cell lines. Here, SYD985 was also superior to T-DM1 despite a lower DAR (IC_{50} values of 6.9 ng/ml to 67.4 ng/ml versus 15.7 ng/ml to > 1000 ng/ml), especially in cells with a low target expression. This translated into a better *in vivo* activity of SYD985 compared to T-DM1. (191) The IC_{50} values of both 20D9h3-DUBA and 20D9h3-MMAF in AML cell lines were in a similar range compared to the IC_{50} values of the HER2-conjugates. This is remarkable considering that for HER2-positive cell lines an expression of 7900 to over 100 000 antigens per cell has been reported (109, 209) compared to 350-4700 antigens per cell for FLT3-positive AML cells (64). Compared to the FLT3-directed ADC AGS62P1/ASP1235, which has a 72 h IC_{50} value of around 3 µg/ml in MV4-11 cells, both 20D9h3-ADCs are also far superior (194). It is encouraging that 20D9h3-ADCs would fall in the range of the more effective ADCs, although a direct comparison to approved ADCs is difficult as they target a variety of different antigens and disease entities and their reported *in vitro* IC_{50} values vary accordingly with reported concentrations between 0.45 ng/ml and 4350 ng/ml (208). I further analyzed the correlation of FLT3 surface expression and efficacy using Ba/F3 cells that express FLT3 at three different surface levels. In cytotoxicity assays, it was observed that IC_{50} values decreased with increasing FLT3 surface expression. Due to the limited number of data points, a correlation analysis was not performed. However, when looking at the data it seemed that there was no clear linear correlation between FLT3 levels and efficacy, but rather a saturation effect. This could have to do with the kinetics of internalization and processing of the ADC which are both processes that have limited capacities or with the high potency of the drug that only requires a certain level inside the cell to be efficacious. *In vivo* other factors also come into play making target response relationship a complex issue and currently it is not clearly established if a higher target expression necessarily translates into a higher ADC efficacy in patients (210). Collectively, the *in vitro* efficacy of both 20D9h3-conjugates is promising in comparison to other pre-clinical and clinical ADC candidates.

4.3 The ADCs stability and pharmacokinetic properties

Besides antibody and payload, the linkage of both components is a very important step in ADC development. Whether a certain linker technology can be applied is highly dependent on the

chemical structure of the payload. For 20D9h3-DUBA the commercial linker-payload vc-*seco*-DUBA was used, which is connected to the antibody through maleimide-cysteine conjugation (162). 20D9h3-MMAF is conjugated by P5-technology, which uses electrophilic phosphonamidates to functionalize cysteines (150, 163, 164). For the linker-payload of 20D9h3-DUBA, several drawbacks have been described including I) tendency to aggregate (211), II) loss of payload to blood proteins due to maleimide-exchange reaction *in vivo* (116) and III) loss of linker-payload through CES1c-mediated cleavage in the circulation of rodents but not humans (162, 168, 212, 213). P5-technology, on the contrary, was invented to tackle exactly these drawbacks (164, 214). Indeed, SEC-based analyses after ADC conjugation showed that 20D9h3-DUBA but not 20D9h3-MMAF has a tendency to aggregate. Further, maleimide-exchange reaction but not CES1c cleavage could be confirmed by MS after ADC incubation with fresh mouse serum for 20D9h3-DUBA, while 20D9h3-MMAF was stable in this experiment. However, cultivation of target-negative cells with CES1c-pretreated ADCs clearly showed unspecific killing of those cells when the cleavage-susceptible 20D9h3-DUBA was applied indicating that free payload was liberated. This was not observed for the P5-conjugated 20D9h3-MMAF. The discrepancy between MS and the cell line experiment may be explained by the poor stability of carboxylesterases *in vitro* making CES1c cleavage difficult to assess. In order to understand the full impact of the ADC's stability, NSG mice were administered once with either 20D9h3-DUBA or 20D9h3-MMAF and blood samples were drawn in regular intervals to assess *in vivo* PK. While 20D9h3-MMAF was highly stable in this experiment, 20D9h3-DUBA rapidly lost payload attributable to the mentioned drawbacks of the linker. There are several other ADCs that use the vc-*seco*-DUBA linker-payload e.g., directed against HER2 (SYD981-SYD985; SYD985 in phase III, but current status unclear) or B7-H3 (MGC018, phase II). As can be expected from the poor PK, all of them require relatively high doses for a reasonable *in vivo* efficacy in cell line xenografts despite a very high target expression of 7900 to over 100 000 antigens per cell for HER2 (109, 209) and 4750 to 93 544 antigens per cell for B7-H3 (215). For example, the HER2-ADCs SYD981-SYD984 required a dose of 3x5 mg/kg for a complete stop of tumor growth of BT-474 cell line xenografts (> 50 000 HER2 antigens per cell (209)) in Balb/c nu/nu mice, while the effect was only moderate at 3x1 mg/kg (162). Also, MGC018 – a B7-H3 DUBA-ADC – was dosed once at 6-10 mg/kg to achieve a full response in different breast, lung and ovarian cancer cell line xenografts in CD-1 nude mice (213). For 20D9h3-DUBA it was observed that after *in vivo* treatment of xenograft mouse models with 2x (AML-388) or 3x (AML-579) 3 mg/kg, a response is achieved only for very sensitive AML PDX samples like AML-388. As the poor PK of 20D9h3-DUBA is partly caused by CES1c-cleavage – a rodent-specific problem – those animal models could highly underestimate the efficacy of this ADC especially in samples that have a generally lower sensitive (like e.g. AML-579) or a low target expression. In contrast, 20D9h3-MMAF was highly effective in reducing leukemic cells in both AML PDX models although in both cases some mice relapsed indicating the survival of LICs. The

main goal of the project was the evaluation of the ADC's anti-LSC efficacy. It was thus decided to focus mainly on stem cell assays with *in vitro*/*ex vivo* treatment. The toxicity aspects of instable ADCs and future considerations are further discussed in chapter 4.5.2 and in the outlook section, respectively.

4.4 The ADCs anti-LSC activity

4.4.1 Role of payload choice

The primary goal of this project was the development of an ADC with a payload that is active against LSCs. Due to its potency and mode of action DUBA was regarded as a very promising choice. First, the mode of action of 20D9h3-DUBA was validated in AML cell lines using 20D9h3-MMAF as control. Treatment of MOLM-13 cells with 20D9h3-DUBA led to a phosphorylation of ATR at Thr1989 and CHK1 at Ser345 indicating an activation of the ATR-CHK1 DNA damage repair pathway. In contrast, this was not observed for 20D9h3-MMAF. Furthermore, both ADCs led to cell cycle arrests, however in different phases. While 20D9h3-DUBA halted MV4-11 cells in the S phase, 20D9h3-MMAF led to a G2/M-arrest. Both ADCs induced apoptosis in MV4-11 and MOLM-13 cells with very similar kinetics and intensity. Comparable results have been described in a paper analyzing two HER2-directed ADCs, one coupled to MMAF and one to the DNA-crosslinker PNU-159682. Here, the PNU-159682-ADC led to a phosphorylation of CHK1 at Ser345 and subsequent intra-S arrest of HER2-positive KPL-4 cells indicating DNA-damage, while the MMAF-ADC did not lead to CHK1 phosphorylation and caused a G2/M-arrest (216). My results further align with the mechanisms of action of the two payloads that have been described in the literature. For DUBA this has been summarized in the PhD thesis of Dr. Marcel Rieker (166): In brief, DUBA leads to a DNA alkylation, which provides an obstacle for the DNA polymerase during replication in the S phase of the cell cycle. This leads to the formation of ssDNA, which in turn activates the DNA damage repair master regulator ATR. ATR slows down cell cycle progression – via the effector proteins p53, CHK1 and WEE1 – and prevents a collapse of the replication fork. If the DNA damage is too severe, the replication fork collapses and double strand breaks occur – the so-called replication catastrophe (217) – inevitably causing apoptosis. MMAF, in contrast, belongs to the microtubule-targeting agents and has been described to block tubulin polymerization which halts cell division and ultimately also causes apoptosis (218). Due to those differences in their mode of action, it is a common belief that microtubule-targeting agents affect mainly dividing cells, while DNA-damaging agents can act on both dividing and resting cells and are thus the better choice to target cancer stem cells (104, 124, 125, 216). My first results supported this hypothesis: Different ADC payloads were tested in two cell lines that have been arrested in G1 using aphidicolin. While the efficacy of all tested agents was reduced in the proliferation-inhibited cells,

this reduction was smallest for DUBA followed by exatecan (both DNA-damaging agents) and lastly MMAE (microtubule-targeting) – the membrane-permeable surrogate of MMAF. Similarly, it was reported in the literature that prior treatment with aphidicolin did not reduce the efficacy of adozelesin (219) – which belongs to the class of DNA-damaging DCMs – but clearly protects cells from the microtubule-targeting agent paclitaxel (220). Other methods of proliferation-inhibition also led to comparable results: Junttila et al. inhibited cell division of adherent SK-BR-3 cells by growing them confluent. Subsequently, they tested the efficacy of different agents on those non-dividing versus dividing cells. They found that the IC_{50} values of the anthracyclines doxorubicin and PNU159682 were only reduced by factors of 7.8x and 5.8x in non-dividing compared to dividing cells, respectively, while the IC_{50} values of the microtubule-targeting agents vincristine and MMAE were diminished by factors of > 53x (vincristine) and > 450x (MMAE) (221). However, proliferation-inhibited cell lines are no adequate model of LSCs. Thus, in the following three gold-standard stem cell assays were carried out using AML PDX and primary cells to better reflect the real patient situation and to further investigate the question which payload is most suitable for an anti-LSC ADC.

PDX and primary cells were treated with 20D9h3-DUBA or 20D9h3-MMAF *in vitro* and the colony formation potential of early (CFU assay) and very early (LTC-IC assay) progenitors and the engraftment capability were analyzed (LIC assay). In CFU assays, 20D9h3-DUBA had a higher efficacy at lower doses compared to 20D9h3-MMAF in AML-388, AML-393 and AML-669 PDX cells as well as the primary sample that had been used to generate AML-393. In LTC-IC assays, 20D9h3-DUBA also had a higher efficacy compared to 20D9h3-MMAF in eliminating very early progenitors of the AML-388 PDX sample, but both ADCs were similarly efficient towards AML-393 PDX cells. Both ADCs were capable of preventing engraftment of AML-388 PDX cells at a dose of 1 µg/ml. At a dose of 25 ng/ml, 20D9h3-DUBA still prevented engraftment in 4 of 5 mice indicating that at least part of the LICs have been eliminated, while 20D9h3-MMAF had no effect at that dose. AML-393 PDX cells pre-treated with 0.3 µg/ml of ADC engrafted in 1 of 5 mice in the 20D9h3-MMAF group, while all mice stayed healthy in the 20D9h3-DUBA group. In conclusion, there was a trend towards a better activity of 20D9h3-DUBA against leukemic stem and progenitor cells, however 20D9h3-MMAF was surprisingly also quite efficient albeit higher doses were needed to achieve the same effect. When looking at the literature, studies that compare the effect of different payloads towards cancer stem cells are scarce. A study using 5T4-targeting ADCs with either the DNA-crosslinker PBD (MEDI0641) or the microtubule-toxin tubulysin as a payload reported that the PBD-ADC showed a superior activity towards cancer stem cells *in vivo* likely explaining its overall better and more durable antitumor activity in comparison to the tubulysin-conjugate (222). But there are also several studies supporting the finding that microtubule-targeting agents can also be active towards cancer stem cells. In a LIC assay it has been shown that a 5T4-MMAF ADC eliminates tumor-initiating cells in a non-small cell lung cancer PDX model (223).

Comparable results were reported for a PTK7-ADC that employs the auristatin payload Aur0101 using a similar set-up (224). Furthermore, impressive and most importantly durable antitumor responses have been described for several MMAF-conjugates using PDX xenograft models including the recently published work from our group (139, 225). As a persistent treatment effect is only achieved if no tumor re-initiating cells remain, these studies also support the finding that ADCs with tubulin-inhibitor payloads also have the potential to eliminate LSCs. There are several possible explanations for that: It has been proposed that breast cancer stem cells cycle between a resting and a proliferative state (226) and Damelin et al. speculated that this might eventually make them vulnerable to microtubule-toxins (224). This functional plasticity of stem cells has been similarly described for AML LSCs in *in vivo* experiments (130). Furthermore, microtubules do not only play a role in cell division but also in the intracellular trafficking of proteins, which is also important in resting cells (227, 228). And finally, the type of genetic abnormality of leukemic cells from individual patients influences the responsiveness towards certain agents. For example, it has been reported that the chromosomal rearrangement *KMT2A::AFDN* deranges the cell's cytoskeleton (229) and those cells might be especially vulnerable towards agents that further interfere with those structures. This might explain why 20D9h3-MMAF is especially potent against the *KMT2A::AFDN* rearranged AML-388 PDX sample. Interestingly, a recent phosphoproteomic analysis found that *KMT2A::AFDN* cases (such as AML-388) and *KMT2A:MLLT10* cases (such as AML-393) cluster separate from other *KMT2Ar* and non-*KMT2Ar* cases and show increased phosphorylation of proteins with functions in DNA damage repair, replication and splicing. In a subsequent drug screen, those samples further showed a particularly high sensitivity towards mitotic and genotoxic compounds (230).

In conclusion, the experimental results point towards a better anti-LSC activity of the DNA alkylator DUBA compared to microtubule-toxins. However, microtubule-toxins can still be efficacious against LSCs especially in patients with certain genetic abnormalities that sensitize them to these agents. Eventually, in the pharmaceutical development process the choice of the right payload does not only depend on efficacy towards LSCs, as other factors such as producibility, overall antitumor efficacy, PK, and toxicity need to be considered.

4.4.2 Role of target choice

In this work, I have shown that 20D9h3-ADCs are active towards leukemic stem and progenitor cells in various assays. This experimentally validates that FLT3 is indeed an attractive LSC target as has been proposed by various groups because of its favorable expression pattern (63, 66). FLT3 surface abundance is rather low compared to other AML targets, as discussed above (see chapter 4.2). Nevertheless, the success of the FLT3-mAb FLYSYN/4G8-SDIEM in phase I studies (NCT02789254, (231)) shows that it can be efficaciously targeted with an antibody alone and the

coupling of a toxin to such an antibody would bring additional efficacy benefits. Furthermore, the therapeutic window between expression on leukemic and healthy cells is more important than expression level alone and here FLT3 is superior to other AML targets such as CD33, CD123 or CLL1 (66). In the literature it has been described that FLT3 is highly expressed in AML samples that are classified M5a or M5b according to FAB classification, which also includes a large part of *KMT2Ar* samples that have been used for the stem cell assays (232, 233). However, looking at available RNA expression data from the LMU Klinikum, there was no significant difference in FLT3 expression between *KMT2Ar* and non-*KMT2Ar* PDX or patient samples, although the number of *KMT2Ar* patient samples in the used data set was relatively small (n=15) and a larger data set may be required to see significant differences.

Antibodies or ADCs with an IgG1-backbone also bind to FcγRs and as shown in the Ba/F3 model especially FcγRI also contributes to 20D9h3-DUBA efficacy *in vitro*. FcγRI-mediated effects also seemed to play a role for the efficacy of 20D9h3-DUBA towards leukemic progenitors in CFU assay. Interestingly, it was observed that FcγRI was significantly higher expressed in *KMT2Ar* PDX cells and also in patient samples compared to non-*KMT2Ar* samples. This is in line with data from the literature, where it has been described that FcγRI is overexpressed specifically in M5-classified AML and AML with *KMT2Ar* (234, 235). Furthermore, a very recent work described that *KMT2Ar* LSCs have a specific monocytic gene expression signature enriched for pathways involved in OXPHOS, cell cycle, DNA repair and replication. Remarkably, those m-LSCs were also FcγRI-positive (236). This could explain the surprisingly high efficacy of the isotype control IgG1-ADC – which solely targets FcγRI via the Fc part but not FLT3 – towards leukemic progenitors in CFU assays.

Finally, I want to discuss the question whether the antibodies' FcγR binding should be abrogated or whether it is beneficial. My results indicated that targeting both FLT3 and FcγRI is superior to targeting either of the receptors alone in the Ba/F3 model and in CFU assays. Also, in previous work from our group the efficacy of double-targeting was analyzed using deglycosylation instead of LALA-mutation to abrogate FcγR-binding (139, 143). Here, it seemed that the efficacy benefit of targeting FcγRI only existed *in vitro* but could not be re-produced *in vivo*. However, as the overall efficacy of 20D9-MMAF was quite high in those experiments, a small difference might have been missed. Considering the higher FcγRI expression on *KMT2Ar* versus non-*KMT2Ar* bulk cells and probably also LSCs, the efficacy benefit of double-targeting might be especially high in this patient subset. Additionally, ADCC, ADCP and CDC can further increase the activity of mAbs or ADCs and they require an intact Fc part. However, these effects cannot be studied in the immunocompromised NSG mouse model. To address whether an intact Fc part is beneficial or not one has to consider not only efficacy but also toxicity aspects. These are discussed in the following.

4.5 Hematopoietic and non-hematopoietic toxicities

The concept of ADCs as a "magic bullet" (103) essentially includes the idea of a specific targeting of cancer but not healthy cells to expand the therapeutic window of conventional chemotherapy. Many molecules still face toxicity challenges leading to failures in clinical trials. Toxicities can be "on-target", e.g. due to target expression on healthy cells, or "off-target", e.g. due to FcγR-mediated internalization, bystander toxicity towards healthy cells, payload-loss or non-specific uptake. (237) In this project only toxicities towards the hematopoietic system were experimentally evaluated. Non-hematopoietic toxicities will only be discussed with the help of literature. They are not as easy to assess as they would require additional model systems such as humanized immunocompetent mice, cynomolgus monkeys or *in vitro* models of certain tissues, which were beyond the scope of this thesis. Each component of an ADC can contribute to toxicities and will be discussed separately.

4.5.1 Role of target choice for toxicity

Toxicity towards early and very early healthy hematopoietic progenitors was evaluated in analogy to the leukemic progenitors using CFU and LTC-IC assays. Pre-treatment of CD34-positive healthy BM cells with a dose of 1 µg/ml of either 20D9h3-DUBA or 20D9h3-MMAF did not affect colony formation in CFU assays. When looking at the very early progenitors in LTC-IC assays, 20D9h3-DUBA reduced colonies to 74.5% and 16.4% of untreated control at 0.2 µg/ml and 1 µg/ml, respectively, and affected mainly CFU-GM and CFU-M colonies. 20D9h3-MMAF led to a reduction of LTC-IC-CFCs to 70.8% (0.2 µg/ml) and 63.4% (1 µg/ml) of untreated control. The isotype control ADCs diminished LTC-IC-CFCs to 80.5% (IgG1-DUBA) and 77.2% (IgG1-MMAF) of untreated controls, respectively. In summary, early progenitors were not harmed by both ADCs in CFU assays and only the high dose of 1 µg/ml 20D9h3-DUBA but not 20D9h3-MMAF substantially affected colony formation of very early progenitors in LTC-IC assays. As 1 µg/ml of IgG1-DUBA had a lower impact in LTC-IC assay compared to 20D9h3-DUBA, the toxicities of 20D9h3-DUBA towards CFU-GM and CFU-M at 1 µg/ml are probably more FLT3- than FcγR-mediated. This fits with the expression profile of FLT3, which is present on part of the GMPs but not on erythroid progenitors (59-63). However, the effective dose of 20D9h3-DUBA in the assays with leukemic progenitors was far below 1 µg/ml and in this range of 0.025-0.3 µg/ml the negative impact on healthy hematopoietic progenitors was only minor. In the literature, several FLT3-directed therapies have been described with an encouraging safety profile. The FLT3-mAb FLYSYN/4G8-SDIEM was tested in a phase I clinical trial (NCT02789254). It caused mainly mild to moderate mostly hematology associated adverse events such as decreased neutrophil (in 22.6% of patients) or white blood cell (in 19.4% of patients) count and anemia (in 19.4% of patients). The most

frequent grade 3 adverse events were neutropenia (in 6.5% of patients) and back pain (in 3.2% of patients) (231). Further, two studies were carried out with FLT3-BiTEs, which analyzed safety in cynomolgus monkeys (63, 66). Both reported a transient decrease of some hematological cell subsets mostly dendritic cells, B cells, monocytes and FLT3-positive HSPCs, with no toxicities in brain, testes or pancreas. This is in line with reports that FLT3 is barely expressed in non-hematopoietic tissues and in the tissues where it has been detected – such as brain and pancreas – it occurs only intracellular (63). Brauchle et al. further reported that within each HSPC subpopulation only a portion of the cells was FLT3-positive suggesting that the FLT3-negative portion might be able to re-initiate normal hematopoiesis after treatment (63). For AGS62P1/ASP1235, the only FLT3-ADC that reached clinical studies so far, there are currently unfortunately no published trial results available. A phase I study of this molecule has been terminated, however the reason stated on clinicaltrials.gov is "lack of efficacy" with no statement on tolerability or safety (NCT02864290, (102, 194)). The only approved FLT3-directed therapy so far are TKIs and – as discussed in 4.1.3 – most side effects that occur in TKI therapies are thought to be off-target toxicities on structurally related RTKs rather than FLT3-mediated effects (238).

For FcγRs, and especially FcγRI where 20D9h3-mAb mostly binds to, my results with isotype control ADCs indicated that only minor toxicities of wildtype-Fc-ADCs (such as the 20D9h3-ADCs) on hematopoietic progenitor cells have to be expected via those receptors. This is in line with published results, where FcγRI-targeting CAR-T cells had no significant effects on any colony type in CFU assays with CD34-positive cord blood cells. Interestingly, this therapy was quite effective on AML cell lines, primary samples and in the U937 cell line xenograft model. (239) One reason for the low toxicity of the isotype control ADCs observed in CFU assays is probably that FcγRI – the Fc receptor that showed most binding to wildtype-Fc-mAbs – was only expressed on 8.1% of healthy CD34-positive BM cells. Generally, FcγRI expression in the hematopoietic system was reported on a subset of granulocyte-monocyte progenitors and common myeloid progenitors but not on multipotent progenitors, megakaryocyte-erythroid progenitors or HSCs. On more differentiated cells FcγRI occurs on monocytes, granulocytes and partially dendritic cells, but not on T cells, B cells, NK cells, erythrocytes or platelets. (239, 240) Further, a low expression in some healthy tissues was reported including neuronal and endothelial cells (241, 242). The reported expression on monocytes and megakaryocyte-erythroid progenitors might explain some of the toxicities that have been described for approved ADCs. For example, interstitial lung disease, which is a life-threatening adverse event associated with HER2-targeting therapies such as T-DM1/Kadcyla, is thought to be caused by FcγR-mediated drug internalization in alveolar macrophages (237, 243). Also, thrombocytopenia, which frequently occurs after treatment with T-DM1, might be due to endocytosis of the ADC in megakaryocytes, however in this case the uptake has been discussed to occur via FcγRIIa or micropinocytosis rather than FcγRI (244, 245).

ADC toxicities via FcγRs can be reduced by ablating Fc binding e.g., with the use of LALA-mutations. If only the toxicities towards the hematopoietic system are considered, one might conclude that they are outweighed by the efficacy benefits caused by FcγRI-mediated killing of leukemic cells especially of *KMT2Ar* samples as they overexpress FcγRI. However, ideally toxicity should be also studied *in vivo* e.g., in humanized immunocompetent mice or cynomolgus monkeys to draw a final conclusion on the advantages or disadvantages of FcγR binding.

4.5.2 Role of linker and physicochemical ADC properties for toxicity

Besides the antibody, the linkage of antibody and payload and the physicochemical properties of the resulting ADC are critical components that need to be optimized to reduce toxicities. The most obvious linker-related toxicity is a loss of payload due to insufficient ADC stability in the blood stream. This payload loss has been observed for 20D9h3-DUBA using maleimide-linkage but not for 20D9h3-MMAF using P5-technology as already discussed in detail in chapter 4.3. While linker instability does not change the total payload exposure, it has been speculated that the main problem is rather that it decreases on-target and increases off-target cytotoxicity and hereby reduces efficacy in relation to toxicity. Also potentially causing problems is the linkage of a high number of drugs per antibody – a high DAR – as this usually also comes with an increase in hydrophobicity of the ADC. Both a high hydrophobicity and a high positive charge of an ADC can enhance its non-specific uptake in healthy cells. (237) And finally a high hydrophobicity causes another problem: increased aggregation. Also, this was observed for 20D9h3-DUBA already after conjugation. It has been reported that ADC aggregates can activate FcγRs and enhance the internalization of those aggregates in FcγR-expressing cells potentially elevating toxicity in healthy tissues (246, 247). The P5-conjugation technology as employed for 20D9h3-MMAF would allow the easy integration of hydrophilic PEG chains to decrease hydrophobicity and to solve this problem (164). Another possibility to tackle these issues could be a DAR reduction, which can for example be achieved by mutating some of the cysteine residues that are used to attach the linker on the antibody.

4.5.3 Role of payload for toxicity

The target determines the site of action of an ADC and is typically carefully selected to avoid on-target off-tumor toxicities as discussed. However, available evidence suggests that the biggest part of ADC-mediated toxicities in humans is payload-mediated as very often ADCs with the same payload have similar toxicity profiles independent of their target antigen (237).

To evaluate toxicities towards the hematopoietic system, CFU and LTC-IC assays were carried out using CD34-positive BM cells from healthy donors. No toxicities were observed in the CFU assay, but in the LTC-IC assay 20D9h3-DUBA was more toxic to very early progenitors at the same dose compared to 20D9h3-MMAF. DUBA was chosen as a payload specifically to target resting leukemia cells and it could be shown that it indeed had a better activity than MMAF in proliferation-arrested AML cell lines and leukemic stem and progenitor cells. Thus, it is not surprising that it is also more toxic than MMAF towards target-expressing healthy progenitors, which are also quiescent.

Dose-limiting payload toxicities towards other tissues have not been addressed in this work and can only be discussed according to the available literature of ADCs that employ the same payload. Here, DUBA is not as established as an ADC payload as MMAF, but there is safety data available from several DUBA-ADCs that reached clinical trials. The currently most-advanced DUBA-ADC is the HER2-targeting SYD985, which advanced to phase III clinical trials (NCT03262935, (126)). For SYD985 the most common severe adverse events (grade 3 or higher) were neutropenia, conjunctivitis and fatigue. Other adverse events were keratitis, decreased appetite, dry eye, dry skin, skin hyperpigmentation, nausea, alopecia and stomatitis. (248). The current status of SYD985 development is unclear as the FDA requested further information. Byondis did however not reveal what kind of information is required (249). Additionally, two other DUBA-ADCs reached clinical trials: MGC018 (a B7-H3-targeting ADC (250)) and BMS-936561/MDX-1203 (a CD70-targeting ADC (251)). When looking at all three clinical trials most or all of them reported neutropenia, skin hyperpigmentation, fatigue, and nausea among the common adverse events. For all of them the safety profile was generally manageable.

As MMAF has been a well-established ADC payload for many years, there is a lot of data available concerning its toxicity profile. A well-described dose-limiting toxicity for tubulin-inhibiting cytotoxins are ocular events. Eaton et al. reviewed 22 clinical trials that reported ocular events and found that despite many differences in indication and target antigen all but one study used ADCs with either MMAF (but not MMAE), DM1 or DM4, which all belong to the tubulin-inhibitors (252). The reported ocular events included blurred vision, conjunctivitis, keratitis, dry eye and corneal deposits or inclusions. Possible explanations for those toxic effects specifically in the eye are the occurrence of rapidly dividing cells in the eye, the expression of a variety of different surface receptors, the eye's strong blood supply, linker instabilities of the ADCs and unspecific uptake via macropinocytosis (252, 253). Recent results with FDA-approved belantamab mafodotin / Blenrep, however, suggest that despite those toxicities patients can still significantly benefit from therapy with MMAF-ADCs and side-effects are controllable by dose delays and reductions (254, 255). Other common non-ocular adverse events that have been described for this ADC are thrombocytopenia, anemia, cough, nausea, pyrexia, and elevated aspartate amino-transferase. The most frequent severe adverse events (grade 3 or higher) with this therapy were thrombocytopenia, anemia, infusion-related reactions and pneumonia (256, 257).

Another important characteristic of payloads that influences their toxicity profile is their membrane-permeability. Membrane-permeable payloads can diffuse out of the target cell and kill neighboring tumor cells, a phenomenon known as bystander effect. This was e.g., shown for DUBA-ADCs such as SYD985 (191). MMAF-ADCs do not show bystander effects as MMAF – in contrast to its structural analogue MMAE – is not able to penetrate through the cell membrane (258), which is also the reason why it was not very effective in cytotoxicity assays when tested as a payload alone (see 3.2.1). Generally, the bystander effect is regarded as an efficacy advantage as neighboring cancer cells can be eliminated and most approved ADCs employ membrane-permeable payloads (237). The ability of payloads to diffuse out of certain cells could also prevent accumulation in and toxic effects towards certain tissues e.g., the eye as described for MMAF (252). It could however also increase off-target toxicities in healthy cells and it is currently unclear whether the advantages outweigh the disadvantages especially in hematological diseases.
Collectively, both DUBA and MMAF lead to a unique payload-specific toxicity profile that has to be kept in mind during further development. Besides a stable linker system, a carefully adapted DAR is necessary to find the optimal balance between efficacy and toxicity. For MMAF-ADCs ophthalmic examinations e.g., using *in vitro* assays with corneal epithelial cells (253), could be included in preclinical studies to help with those adaptions.

4.6 Combination therapy with 20D9h3-DUBA

Usually, AML therapy does not consist of a single treatment, but rather a combination of several drugs. I wanted to test different agents that could potentially increase the efficacy of 20D9h3-DUBA.

4.6.1 Combination of 20D9h3-DUBA and an inhibitor of ATR

The rationale behind the combination of 20D9h3-DUBA with an inhibitor of ATR was based on two reasons: 1) the finding of Dr. Marcel Rieker that breast, lung and ovarian carcinoma cell lines with a defective p53 pathway have an increased vulnerability to a combination of DUBA/DUBA-ADCs and ATRi (166) and 2) my observation that cell lines with a knockdown of p53 were less sensitive to 20D9h3-DUBA. To prove Rieker's hypothesis that p53 defect/loss makes cells more sensitive to the combined treatment, I tested the combination on p53 kd cell lines and corresponding isogenic p53 wt controls. Indeed, p53 kd cell lines were extremely sensitive to simultaneous treatment with both 20D9h3-DUBA and the ATRi ceralasertib/AZD6738 with very high synergy scores. In the isogenic p53 wt cell lines the effect was additive rather than synergistic confirming the importance of p53 loss for the specific vulnerability to this combination. To further validate this, the combination was tested in the cell line MM-6, which has a defect in the p53 pathway due to the point mutation R273H in the p53 DNA-binding domain (182). Here, 20D9h3-

DUBA plus ceralasertib showed an impressive efficacy compared to each single treatment with synergy scores of up to +60 (> +10 is synergistic). Those results are in line with literature where it was described that ATR inhibitors synergize with several DNA-damaging and topoisomerase-inhibiting drugs e.g., cisplatin, etoposide, gemcitabine or irinotecan especially in cells with deficiencies in either p53 or ataxia telangiectasia mutated (ATM) (259-262). It has been speculated that p53 loss might increase ATR dependence and limit the cell's remaining possibilities of DNA damage repair (260, 262). As shown by me and others, DUBA-ADCs such as 20D9h3-DUBA lead to an activation of ATR-CHK1 DNA damage repair pathway. Under ATR inhibitor treatment this activation is blocked preventing repair and leading to fork collapse, double strand breaks and eventually "replication catastrophe" (166, 217). My results indicate that especially patients with defects in p53 – and maybe other proteins involved in DNA damage repair – would benefit from a combination of 20D9h3-DUBA and ceralasertib. P53 mutations are not very frequent in AML patients (~9% of patients, (16)), however they are associated with an especially poor prognosis and thus finding new treatment options for this group is highly relevant (12, 16). Further, mutation-independent inactivation of wildtype p53, e.g. through the inhibition of protein acetylation, and other p53 abnormalities are found in specific patient subsets e.g. *FLT3*-ITD patients and those mechanisms could also contribute to LSC survival and relapse (263). To further validate this combination, synergism should be analyzed in *in vivo* xenograft models using PDX cells with p53 defects. Further, it would be very interesting to test the combined effect of both agents towards p53 mutated LSCs using CFU and LIC assays.

4.6.2 Combination of 20D9h3-DUBA and an inhibitor of BCL-2

The rationale behind the combination of 20D9h3-DUBA and a BCL-2 inhibitor was my finding that 20D9h3-DUBA acts via apoptosis induction and the targeting of BCL-2 – a crucial anti-apoptotic protein – could thus be promising. Further, the BCL-2 inhibitor venetoclax is already an approved agent in AML therapy and new standard-of-care for patients that are not tolerating intensive chemotherapy (22).

Indeed, it was observed that the combination of 20D9h3-DUBA with the BCL-2i venetoclax was synergistic in MOLM-13 cells and additive to synergistic in MV4-11 cells. Generally, the synergistic effect was lower than what has been observed for the ATRi combinations. In the literature, similar results have been described for the combination of the CD123-targeting DUBA-ADC IMGN632 with venetoclax. These two agents also acted additive to synergistic *in vitro* depending on the used cell line models and the combined treatment was superior to each single drug in cell line and PDX xenograft models. (178, 179) Interestingly, it has been reported that venetoclax can selectively eliminate LSCs by targeting OXPHOS, which is an LSC-specific vulnerability (48). As 20D9h3-DUBA

alone also showed impressive efficacy against LSCs, both agents together might be a very promising anti-LSC combination. In order to predict venetoclax responses in AML patients, BH3 profiling is an increasingly popular technique (264) and in further experiments this might be a useful tool to foresee which patient subsets benefit most from the 20D9h3-DUBA plus venetoclax combination.

4.7 Summary and Outlook

In this project, two IgG1-based FLT3-targeting ADCs were developed employing the DNA-damaging agent DUBA or the microtubule-targeting drug MMAF, respectively. It was shown that both ADCs have the potential to eliminate leukemic while sparing healthy stem and progenitor cells validating FLT3 as an LSC target. In these assays 20D9h3-DUBA had a higher potency on leukemic cells compared to 20D9h3-MMAF (Figure 43).

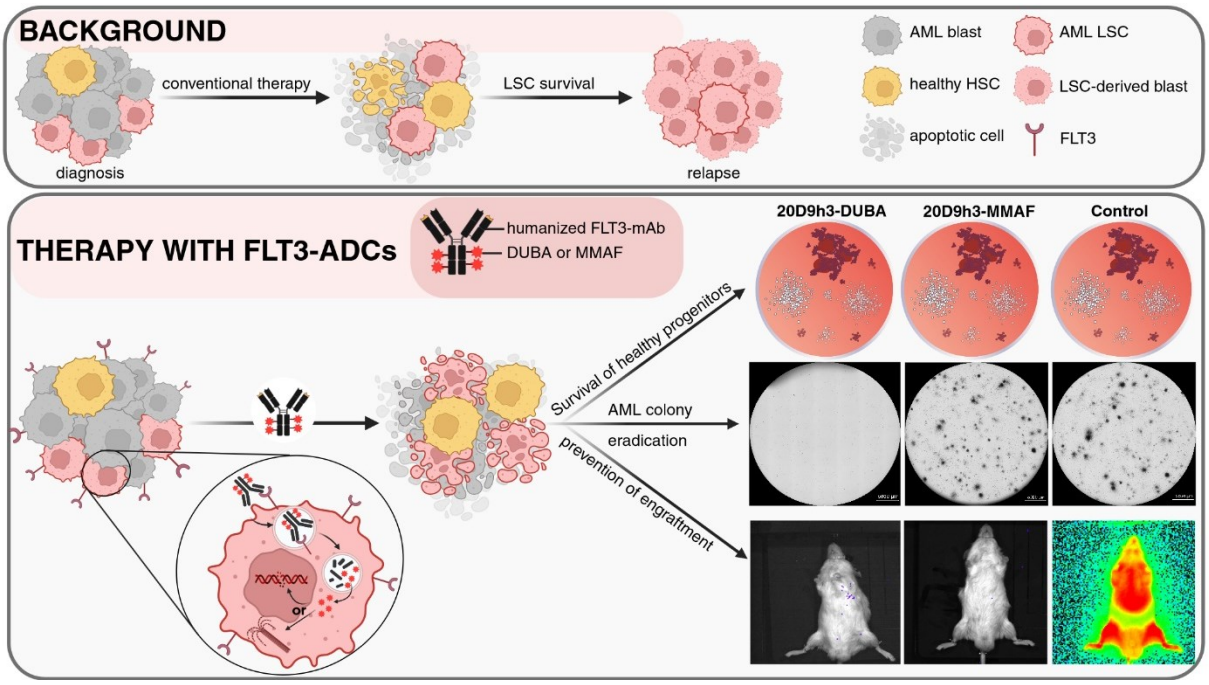

Figure 43: Graphical summary of the project. Rationale for the design of FLT3-targeting anti-LSC ADCs that employ either the DNA-damaging agent DUBA or the microtubule-targeting agent MMAF and summary of the main results of both ADCs in three gold-standard leukemic stem cell assays.

Generally, 20D9h3-ADC was active on cells with mutant and wildtype FLT3 which would make it an attractive therapy for a wide range of AML patients. Especially the 20D9h3-ADC with the DUBA payload could complement existing therapies by its ability to eliminate LSCs which will eventually prevent a relapse. My results further indicated that particularly some patient subsets might benefit from 20D9h3-ADC mono- or combination-therapies: 1) As shown by me and others, ADCs

with an IgG1 backbone do not only bind to the target with their variable part, but also have the potential to bind to FcγRs. As especially FcγRI is highly expressed in *KMT2Ar*-leukemia, those patients might be especially vulnerable to ADCs with an intact Fc part. 2) Due to its mechanism of action, the 20D9h3-DUBA ADC has a lower efficacy in cell lines with p53 loss, however this may be overcome and even exploited by a combination of the ADC with ATR inhibitors such as ceralasertib, making this a promising approach for p53 mutated patients. 3) Another interesting combination for 20D9h3-DUBA could be with the BCL-2 inhibitor venetoclax, an agent which is currently especially valuable for chemotherapy ineligible patients.

A clinical study with the Fc-optimized FLT3-mAb FLYSYN/4G8-SDIEM and pre-clinical tests with FLT3-BiTEs in cynomolgus monkeys have shown that the toxicities of FLT3-targeted therapies are generally manageable (63, 66, 231). For ADCs, the payload brings additional toxicity risks and here both 20D9h3-DUBA and 20D9h3-MMAF should be further optimized to maximize efficacy and minimize toxicity. For 20D9h3-DUBA it was shown that the used linker system is not ideal and leads to aggregation, thiol-exchange reaction and the rodent-specific problem of CES1c-mediated payload loss. Still this linker technology is quite common (105). For a better *in vivo* evaluation one could consider the development of CES1c-KO mouse models, as described by Ubink et al. (168), with an NSG background. However, another more stable and hydrophilic linkage should ideally be developed for DUBA in the future to also avoid aggregation and thiol-exchange reaction, but this will require in depth chemical developments including linker structure-activity relationship studies. As 20D9h3-MMAF was surprisingly also quite efficient against LSCs with low hematotoxicity and superior stability, a further development of this ADC could be considered as well. Here, the main concern is the payload-associated ocular toxicity that is well described (252). As MMAF is not membrane-permeable (159), the ADC could accumulate in the eye and a lower DAR might thus be beneficial to decrease the drug exposure. Currently the DAR of 20D9h3-MMAF is 8.0, which is high compared to other approved ADCs (105). Additional toxicity evaluations in *in vitro* ocular model systems could be useful for DAR and hydrophobicity optimizations. Further, recent results with Belantamab mafodotin / Blenrep show that ocular toxicities are to some extent also controllable by dose modifications (254, 255). Eventually, for both ADCs studies in humanized immunocompetent mouse models or cynomolgus monkeys will be necessary to study the advantages and disadvantages of FcγR-mediated ADC effects and Fc effector functions as well as the full extent of on-target off-tumor and non-specific toxicities.

5 References

1. Bray F, Laversanne M, Sung H, Ferlay J, Siegel RL, Soerjomataram I, et al. Global cancer statistics 2022: GLOBOCAN estimates of incidence and mortality worldwide for 36 cancers in 185 countries. CA Cancer J Clin. 2024.

2. Chennamadhavuni A, Lyengar V, Mukkamalla S, Shimanovsky A. 'Leukemia' in *StatPearls*. Treasure Island (FL): StatPearls Publishing. 2024. Available at: https://www.ncbi.nlm.nih.gov/books/NBK560490/ (accessed: 28 May 2024).

3. Siegel RL, Giaquinto AN, Jemal A. Cancer statistics, 2024. CA: A Cancer Journal for Clinicians. 2024;74(1):12-49.

4. Krebs in Deutschland für 2019/2020. 14. Ausgabe. Robert Koch-Institut (Hrsg) und die Gesellschaft der epidemiologischen Krebsregister in Deutschland e.V. (Hrsg). Berlin, 2023.

5. SEER Cancer Stat Facts: Acute Myeloid Leukemia. National Cancer Institute. Bethesda, MD. Available at: https://seer.cancer.gov/statfacts/html/amyl.html (accessed: 13 August 2024) [

6. Kantarjian H, Kadia T, DiNardo C, Daver N, Borthakur G, Jabbour E, et al. Acute myeloid leukemia: current progress and future directions. Blood Cancer Journal. 2021;11(2):41.

7. Short NJ, Rytting ME, Cortes JE. Acute myeloid leukaemia. The Lancet. 2018;392(10147):593-606.

8. DiNardo CD, Erba HP, Freeman SD, Wei AH. Acute myeloid leukaemia. The Lancet. 2023;401(10393):2073-86.

9. Ganzel C, Manola J, Douer D, Rowe JM, Fernandez HF, Paietta EM, et al. Extramedullary Disease in Adult Acute Myeloid Leukemia Is Common but Lacks Independent Significance: Analysis of Patients in ECOG-ACRIN Cancer Research Group Trials, 1980-2008. J Clin Oncol. 2016;34(29):3544-53.

10. Khoury JD, Solary E, Abla O, Akkari Y, Alaggio R, Apperley JF, et al. The 5th edition of the World Health Organization Classification of Haematolymphoid Tumours: Myeloid and Histiocytic/Dendritic Neoplasms. Leukemia. 2022;36(7):1703-19.

11. Short NJ, Konopleva M, Kadia TM, Borthakur G, Ravandi F, DiNardo CD, et al. Advances in the Treatment of Acute Myeloid Leukemia: New Drugs and New Challenges. Cancer Discovery. 2020;10(4):506-25.

12. Döhner H, Wei AH, Appelbaum FR, Craddock C, DiNardo CD, Dombret H, et al. Diagnosis and management of AML in adults: 2022 recommendations from an international expert panel on behalf of the ELN. Blood. 2022;140(12):1345-77.

13. Martelli MP, Sportoletti P, Tiacci E, Martelli MF, Falini B. Mutational landscape of AML with normal cytogenetics: Biological and clinical implications. Blood Reviews. 2013;27(1):13-22.

14. Ley TJ, Miller C, Ding L, Raphael BJ, Mungall AJ, Robertson A, et al. Genomic and epigenomic landscapes of adult de novo acute myeloid leukemia. N Engl J Med. 2013;368(22):2059-74.

15. Papaemmanuil E, Gerstung M, Bullinger L, Gaidzik VI, Paschka P, Roberts ND, et al. Genomic Classification and Prognosis in Acute Myeloid Leukemia. N Engl J Med. 2016;374(23):2209-21.

16. Metzeler KH, Herold T, Rothenberg-Thurley M, Amler S, Sauerland MC, Görlich D, et al. Spectrum and prognostic relevance of driver gene mutations in acute myeloid leukemia. Blood. 2016;128(5):686-98.

17. Arber DA, Orazi A, Hasserjian RP, Borowitz MJ, Calvo KR, Kvasnicka H-M, et al. International Consensus Classification of Myeloid Neoplasms and Acute Leukemias: integrating morphologic, clinical, and genomic data. Blood. 2022;140(11):1200-28.

18. Döhner H, Estey E, Grimwade D, Amadori S, Appelbaum FR, Büchner T, et al. Diagnosis and management of AML in adults: 2017 ELN recommendations from an international expert panel. Blood. 2017;129(4):424-47.

19. Lancet JE, Uy GL, Cortes JE, Newell LF, Lin TL, Ritchie EK, et al. Final results of a phase III randomized trial of CPX-351 versus 7+3 in older patients with newly diagnosed high risk (secondary) AML. Journal of Clinical Oncology. 2016;34(15_suppl):7000-00.

20. Dombret H, Seymour JF, Butrym A, Wierzbowska A, Selleslag D, Jang JH, et al. International phase 3 study of azacitidine vs conventional care regimens in older patients with newly diagnosed AML with >30% blasts. Blood. 2015;126(3):291-9.

21. Kantarjian HM, Thomas XG, Dmoszynska A, Wierzbowska A, Mazur G, Mayer J, et al. Multicenter, randomized, open-label, phase III trial of decitabine versus patient choice, with physician advice, of either supportive care or low-dose cytarabine for the treatment of older patients with newly diagnosed acute myeloid leukemia. J Clin Oncol. 2012;30(21):2670-7.

22. DiNardo CD, Jonas BA, Pullarkat V, Thirman MJ, Garcia JS, Wei AH, et al. Azacitidine and Venetoclax in Previously Untreated Acute Myeloid Leukemia. N Engl J Med. 2020;383(7):617-29.

23. Senapati J, Kadia TM, Ravandi F. Maintenance therapy in acute myeloid leukemia: advances and controversies. Haematologica. 2023;108(9):2289-304.

24. Shireen I, Komal S, Ansari AM, Meraj L. Frequency of complete remission after standard 3+7 induction therapy in patients with acute myeloid leukemia. Pak J Med Sci. 2022;38(5):1138-42.

25. Yanada M, Garcia-Manero G, Borthakur G, Ravandi F, Kantarjian H, Estey E. Potential cure of acute myeloid leukemia. Cancer. 2007;110(12):2756-60.

26. Jongen-Lavrencic M, Grob T, Hanekamp D, Kavelaars FG, Al Hinai A, Zeilemaker A, et al. Molecular Minimal Residual Disease in Acute Myeloid Leukemia. N Engl J Med. 2018;378(13):1189-99.

27. Estey E, Keating MJ, Pierce S, Stass S. Change in karyotype between diagnosis and first relapse in acute myelogenous leukemia. Leukemia. 1995;9(6):972-6.

28. Nakano Y, Kiyoi H, Miyawaki S, Asou N, Ohno R, Saito H, et al. Molecular evolution of acute myeloid leukaemia in relapse: unstable N-ras and FLT3 genes compared with p53 gene. Br J Haematol. 1999;104(4):659-64.

29. Krönke J, Bullinger L, Teleanu V, Tschürtz F, Gaidzik VI, Kühn MW, et al. Clonal evolution in relapsed NPM1-mutated acute myeloid leukemia. Blood. 2013;122(1):100-8.

30. Breems DA, Van Putten WL, Huijgens PC, Ossenkoppele GJ, Verhoef GE, Verdonck LF, et al. Prognostic index for adult patients with acute myeloid leukemia in first relapse. J Clin Oncol. 2005;23(9):1969-78.

31. Pemmaraju N, Kantarjian H, Garcia-Manero G, Pierce S, Cardenas-Turanzas M, Cortes J, et al. Improving outcomes for patients with acute myeloid leukemia in first relapse: a single center experience. Am J Hematol. 2015;90(1):27-30.

32. Shlush LI, Mitchell A, Heisler L, Abelson S, Ng SWK, Trotman-Grant A, et al. Tracing the origins of relapse in acute myeloid leukaemia to stem cells. Nature. 2017;547(7661):104-08.

33. Ng SW, Mitchell A, Kennedy JA, Chen WC, McLeod J, Ibrahimova N, et al. A 17-gene stemness score for rapid determination of risk in acute leukaemia. Nature. 2016;540(7633):433-37.

34. Eppert K, Takenaka K, Lechman ER, Waldron L, Nilsson B, van Galen P, et al. Stem cell gene expression programs influence clinical outcome in human leukemia. Nature Medicine. 2011;17(9):1086-93.

35. van Gils N, Denkers F, Smit L. Escape From Treatment; the Different Faces of Leukemic Stem Cells and Therapy Resistance in Acute Myeloid Leukemia. Frontiers in Oncology. 2021;11:659253.

36. Stelmach P, Trumpp A. Leukemic stem cells and therapy resistance in acute myeloid leukemia. Haematologica. 2023;108(2):353-66.

37. Goardon N, Marchi E, Atzberger A, Quek L, Schuh A, Soneji S, et al. Coexistence of LMPP-like and GMP-like leukemia stem cells in acute myeloid leukemia. Cancer Cell. 2011;19(1):138-52.

38. Kreso A, Dick JE. Evolution of the cancer stem cell model. Cell Stem Cell. 2014;14(3):275-91.

39. Lapidot T, Sirard C, Vormoor J, Murdoch B, Hoang T, Caceres-Cortes J, et al. A cell initiating human acute myeloid leukaemia after transplantation into SCID mice. Nature. 1994;367(6464):645-48.

40. Bonnet D, Dick JE. Human acute myeloid leukemia is organized as a hierarchy that originates from a primitive hematopoietic cell. Nat Med. 1997;3(7):730-37.

41. Niu J, Peng D, Liu L. Drug Resistance Mechanisms of Acute Myeloid Leukemia Stem Cells. Frontiers in Oncology. 2022;12:896426.

42. Ishikawa F, Yoshida S, Saito Y, Hijikata A, Kitamura H, Tanaka S, et al. Chemotherapy-resistant human AML stem cells home to and engraft within the bone-marrow endosteal region. Nature Biotechnology. 2007;25(11):1315-21.

43. Popp HD, Naumann N, Brendel S, Henzler T, Weiss C, Hofmann WK, et al. Increase of DNA damage and alteration of the DNA damage response in myelodysplastic syndromes and acute myeloid leukemias. Leuk Res. 2017;57:112-18.

44. de Grouw EPLM, Raaijmakers MHGP, Boezeman JB, van der Reijden BA, van de Locht LTF, de Witte TJM, et al. Preferential expression of a high number of ATP binding cassette transporters in both normal and leukemic CD34+CD38− cells. Leukemia. 2006;20(4):750-54.

45. Nabinger SC, Chen S, Gao R, Yao C, Kobayashi M, Vemula S, et al. Mutant p53 enhances leukemia-initiating cell self-renewal to promote leukemia development. Leukemia. 2019;33(6):1535-39.

46. Valent P, Sadovnik I, Eisenwort G, Bauer K, Herrmann H, Gleixner KV, et al. Immunotherapy-Based Targeting and Elimination of Leukemic Stem Cells in AML and CML. Int J Mol Sci. 2019;20(17).

47. Haubner S, Perna F, Köhnke T, Schmidt C, Berman S, Augsberger C, et al. Coexpression profile of leukemic stem cell markers for combinatorial targeted therapy in AML. Leukemia. 2019;33(1):64-74.

48. Lagadinou ED, Sach A, Callahan K, Rossi RM, Neering SJ, Minhajuddin M, et al. BCL-2 inhibition targets oxidative phosphorylation and selectively eradicates quiescent human leukemia stem cells. Cell Stem Cell. 2013;12(3):329-41.

49. Pollyea DA, Stevens BM, Jones CL, Winters A, Pei S, Minhajuddin M, et al. Venetoclax with azacitidine disrupts energy metabolism and targets leukemia stem cells in patients with acute myeloid leukemia. Nat Med. 2018;24(12):1859-66.

50. Hills RK, Castaigne S, Appelbaum FR, Delaunay J, Petersdorf S, Othus M, et al. Addition of gemtuzumab ozogamicin to induction chemotherapy in adult patients with acute myeloid leukaemia: a meta-analysis of individual patient data from randomised controlled trials. Lancet Oncol. 2014;15(9):986-96.

51. Zhang CC, Yan Z, Pascual B, Jackson-Fisher A, Huang DS, Zong Q, et al. Gemtuzumab Ozogamicin (GO) Inclusion to Induction Chemotherapy Eliminates Leukemic Initiating Cells and Significantly Improves Survival in Mouse Models of Acute Myeloid Leukemia. Neoplasia. 2018;20(1):1-11.

52. Ali S, Dunmore HM, Karres D, Hay JL, Salmonsson T, Gisselbrecht C, et al. The EMA Review of Mylotarg (Gemtuzumab Ozogamicin) for the Treatment of Acute Myeloid Leukemia. Oncologist. 2019;24(5):e171-e79.

53. Taussig DC, Pearce DJ, Simpson C, Rohatiner AZ, Lister TA, Kelly G, et al. Hematopoietic stem cells express multiple myeloid markers: implications for the origin and targeted therapy of acute myeloid leukemia. Blood. 2005;106(13):4086-92.

54. Matthews W, Jordan CT, Wiegand GW, Pardoll D, Lemischka IR. A receptor tyrosine kinase specific to hematopoietic stem and progenitor cell-enriched populations. Cell. 1991;65(7):1143-52.

55. Rosnet O, Marchetto S, deLapeyriere O, Birnbaum D. Murine Flt3, a gene encoding a novel tyrosine kinase receptor of the PDGFR/CSF1R family. Oncogene. 1991;6(9):1641-50.

56. Rosnet O, Schiff C, Pébusque MJ, Marchetto S, Tonnelle C, Toiron Y, et al. Human FLT3/FLK2 gene: cDNA cloning and expression in hematopoietic cells. Blood. 1993;82(4):1110-9.

57. Small D, Levenstein M, Kim E, Carow C, Amin S, Rockwell P, et al. STK-1, the human homolog of Flk-2/Flt-3, is selectively expressed in CD34+ human bone marrow cells and is involved in the proliferation of early progenitor/stem cells. Proc Natl Acad Sci U S A. 1994;91(2):459-63.

58. Lyman SD. Biology of flt3 ligand and receptor. Int J Hematol. 1995;62(2):63-73.

59. Ratajczak MZ, Ratajczak J, Ford J, Kregenow R, Marlicz W, Gewirtz AM. FLT3/FLK-2 (STK-1) Ligand Does Not Stimulate Human Megakaryopoiesis In Vitro. STEM CELLS. 1996;14(1):146-50.

60. Hjertson M, Sundström C, Lyman SD, Nilsson K, Nilsson G. Stem cell factor, but not flt3 ligand, induces differentiation and activation of human mast cells. Exp Hematol. 1996;24(6):748-54.

61. Rosnet O, Bühring HJ, Marchetto S, Rappold I, Lavagna C, Sainty D, et al. Human FLT3/FLK2 receptor tyrosine kinase is expressed at the surface of normal and malignant hematopoietic cells. Leukemia. 1996;10(2):238-48.

62. Gabbianelli M, Pelosi E, Montesoro E, Valtieri M, Luchetti L, Samoggia P, et al. Multi-Level Effects of flt3 Ligand on Human Hematopoiesis: Expansion of Putative Stem Cells and Proliferation of Granulomonocytic Progenitors/Monocytic Precursors. Blood. 1995;86(5):1661-70.

63. Brauchle B, Goldstein RL, Karbowski CM, Henn A, Li C-M, Bücklein VL, et al. Characterization of a Novel FLT3 BiTE Molecule for the Treatment of Acute Myeloid Leukemia. Molecular Cancer Therapeutics. 2020;19(9):1875-88.

64. Hofmann M, Große-Hovest L, Nübling T, Pyż E, Bamberg ML, Aulwurm S, et al. Generation, selection and preclinical characterization of an Fc-optimized FLT3 antibody for the treatment of myeloid leukemia. Leukemia. 2012;26(6):1228-37.

65. Karsunky H, Merad M, Cozzio A, Weissman IL, Manz MG. Flt3 ligand regulates dendritic cell development from Flt3+ lymphoid and myeloid-committed progenitors to Flt3+ dendritic cells in vivo. J Exp Med. 2003;198(2):305-13.

66. Yeung YA, Krishnamoorthy V, Dettling D, Sommer C, Poulsen K, Ni I, et al. An Optimized Full-Length FLT3/CD3 Bispecific Antibody Demonstrates Potent Anti-leukemia Activity and Reversible Hematological Toxicity. Mol Ther. 2020;28(3):889-900.

67. Schmidt-Arras DE, Böhmer A, Markova B, Choudhary C, Serve H, Böhmer FD. Tyrosine phosphorylation regulates maturation of receptor tyrosine kinases. Mol Cell Biol. 2005;25(9):3690-703.

68. Mackarehtschian K, Hardin JD, Moore KA, Boast S, Goff SP, Lemischka IR. Targeted disruption of the flk2/flt3 gene leads to deficiencies in primitive hematopoietic progenitors. Immunity. 1995;3(1):147-61.

69. Stirewalt DL, Radich JP. The role of FLT3 in haematopoietic malignancies. Nat Rev Cancer. 2003;3(9):650-65.

70. Brasel K, Escobar S, Anderberg R, de Vries P, Gruss HJ, Lyman SD. Expression of the flt3 receptor and its ligand on hematopoietic cells. Leukemia. 1995;9(7):1212-8.

71. Turner AM, Lin NL, Issarachai S, Lyman SD, Broudy VC. FLT3 Receptor Expression on the Surface of Normal and Malignant Human Hematopoietic Cells. Blood. 1996;88(9):3383-90.

72. Kiyoi H, Kawashima N, Ishikawa Y. FLT3 mutations in acute myeloid leukemia: Therapeutic paradigm beyond inhibitor development. Cancer Science. 2020;111(2):312-22.

73. Kiyoi H, Naoe T. Biology, Clinical Relevance, and Molecularly Targeted Therapy in Acute Leukemia with Flt3 Mutation. International Journal of Hematology. 2006;83(4):301-08.

74. Abu-Duhier FM, Goodeve AC, Wilson GA, Care RS, Peake IR, Reilly JT. Identification of novel FLT-3 Asp835 mutations in adult acute myeloid leukaemia. Br J Haematol. 2001;113(4):983-8.

75. Kihara R, Nagata Y, Kiyoi H, Kato T, Yamamoto E, Suzuki K, et al. Comprehensive analysis of genetic alterations and their prognostic impacts in adult acute myeloid leukemia patients. Leukemia. 2014;28(8):1586-95.

76. Nakao M, Yokota S, Iwai T, Kaneko H, Horiike S, Kashima K, et al. Internal tandem duplication of the flt3 gene found in acute myeloid leukemia. Leukemia. 1996;10(12):1911-8.

77. Yanada M, Matsuo K, Suzuki T, Kiyoi H, Naoe T. Prognostic significance of FLT3 internal tandem duplication and tyrosine kinase domain mutations for acute myeloid leukemia: a meta-analysis. Leukemia. 2005;19(8):1345-9.

78. Kelly LM, Liu Q, Kutok JL, Williams IR, Boulton CL, Gilliland DG. FLT3 internal tandem duplication mutations associated with human acute myeloid leukemias induce myeloproliferative disease in a murine bone marrow transplant model. Blood. 2002;99(1):310-8.

79. Meyer SE, Qin T, Muench DE, Masuda K, Venkatasubramanian M, Orr E, et al. DNMT3A Haploinsufficiency Transforms FLT3ITD Myeloproliferative Disease into a Rapid, Spontaneous, and Fully Penetrant Acute Myeloid Leukemia. Cancer Discov. 2016;6(5):501-15.

80. Spiekermann K, Bagrintseva K, Schoch C, Haferlach T, Hiddemann W, Schnittger S. A new and recurrent activating length mutation in exon 20 of the FLT3 gene in acute myeloid leukemia. Blood. 2002;100(9):3423-5.

81. Hayakawa F, Towatari M, Kiyoi H, Tanimoto M, Kitamura T, Saito H, et al. Tandem-duplicated Flt3 constitutively activates STAT5 and MAP kinase and introduces autonomous cell growth in IL-3-dependent cell lines. Oncogene. 2000;19(5):624-31.

82. Spiekermann K, Bagrintseva K, Schwab R, Schmieja K, Hiddemann W. Overexpression and Constitutive Activation of FLT3 Induces STAT5 Activation in Primary Acute Myeloid Leukemia Blast Cells1. Clinical Cancer Research. 2003;9(6):2140-50.

83. Choudhary C, Olsen JV, Brandts C, Cox J, Reddy PNG, Böhmer FD, et al. Mislocalized Activation of Oncogenic RTKs Switches Downstream Signaling Outcomes. Molecular Cell. 2009;36(2):326-39.

84. Stone RM, Mandrekar SJ, Sanford BL, Laumann K, Geyer S, Bloomfield CD, et al. Midostaurin plus Chemotherapy for Acute Myeloid Leukemia with a FLT3 Mutation. N Engl J Med. 2017;377(5):454-64.

85. Pulte ED, Norsworthy KJ, Wang Y, Xu Q, Qosa H, Gudi R, et al. FDA Approval Summary: Gilteritinib for Relapsed or Refractory Acute Myeloid Leukemia with a FLT3 Mutation. Clin Cancer Res. 2021;27(13):3515-21.

86. Perl AE, Martinelli G, Cortes JE, Neubauer A, Berman E, Paolini S, et al. Gilteritinib or Chemotherapy for Relapsed or Refractory FLT3-Mutated AML. N Engl J Med. 2019;381(18):1728-40.

87. Erba HP, Montesinos P, Kim HJ, Patkowska E, Vrhovac R, Žák P, et al. Quizartinib plus chemotherapy in newly diagnosed patients with FLT3-internal-tandem-duplication-positive

acute myeloid leukaemia (QuANTUM-First): a randomised, double-blind, placebo-controlled, phase 3 trial. Lancet. 2023;401(10388):1571-83.

88. Smith CC, Wang Q, Chin C-S, Salerno S, Damon LE, Levis MJ, et al. Validation of ITD mutations in FLT3 as a therapeutic target in human acute myeloid leukaemia. Nature. 2012;485(7397):260-63.

89. McMahon CM, Ferng T, Canaani J, Wang ES, Morrissette JJD, Eastburn DJ, et al. Clonal Selection with RAS Pathway Activation Mediates Secondary Clinical Resistance to Selective FLT3 Inhibition in Acute Myeloid Leukemia. Cancer Discov. 2019;9(8):1050-63.

90. Zhang H, Savage S, Schultz AR, Bottomly D, White L, Segerdell E, et al. Clinical resistance to crenolanib in acute myeloid leukemia due to diverse molecular mechanisms. Nature Communications. 2019;10(1):244.

91. Piloto O, Wright M, Brown P, Kim KT, Levis M, Small D. Prolonged exposure to FLT3 inhibitors leads to resistance via activation of parallel signaling pathways. Blood. 2007;109(4):1643-52.

92. Chang YT, Hernandez D, Alonso S, Gao M, Su M, Ghiaur G, et al. Role of CYP3A4 in bone marrow microenvironment-mediated protection of FLT3/ITD AML from tyrosine kinase inhibitors. Blood Adv. 2019;3(6):908-16.

93. Almatani MF, Ali A, Onyemaechi S, Zhao Y, Gutierrez L, Vaikari VP, et al. Strategies targeting FLT3 beyond the kinase inhibitors. Pharmacol Ther. 2021;225:107844.

94. Mitra A, Barua A, Huang L, Ganguly S, Feng Q, He B. From bench to bedside: the history and progress of CAR T cell therapy. Frontiers in Immunology. 2023;14.

95. Garrison B, Deng H, Yucel G, Frankel NW, Gordley R, Hung M, et al. Senti-202, a Selective, Off-the-Shelf, Preclinical CAR-NK Cell Therapy with CD33 and/or FLT3 Activating CAR, Healthy Cell Protection from Endomucin (EMCN) Inhibitory CAR and Calibrated Release IL-15 for Hematologic Malignancies Including AML. Blood. 2022;140(Supplement 1):4531-32.

96. Eisfelder BJ, Saygin C, Wynne J, Colton MW, Fischietti M, Beauchamp EM, et al. OTS167 blocks FLT3 translation and synergizes with FLT3 inhibitors in FLT3 mutant acute myeloid leukemia. Blood Cancer J. 2021;11(3):48.

97. Wallace JA, Kagele DA, Eiring AM, Kim CN, Hu R, Runtsch MC, et al. miR-155 promotes FLT3-ITD-induced myeloproliferative disease through inhibition of the interferon response. Blood. 2017;129(23):3074-86.

98. Piloto O, Levis M, Huso D, Li Y, Li H, Wang MN, et al. Inhibitory anti-FLT3 antibodies are capable of mediating antibody-dependent cell-mediated cytotoxicity and reducing engraftment of acute myelogenous leukemia blasts in nonobese diabetic/severe combined immunodeficient mice. Cancer Res. 2005;65(4):1514-22.

99. Li Y, Li H, Wang MN, Lu D, Bassi R, Wu Y, et al. Suppression of leukemia expressing wild-type or ITD-mutant FLT3 receptor by a fully human anti-FLT3 neutralizing antibody. Blood. 2004;104(4):1137-44.

100. Saunders KO. Conceptual Approaches to Modulating Antibody Effector Functions and Circulation Half-Life. Frontiers in Immunology. 2019;10.

101. Heitmann JS, Schlenk RF, Dörfel D, Kayser S, Döhner K, Heuser M, et al. Phase I study evaluating the Fc-optimized FLT3 antibody FLYSYN in AML patients with measurable residual disease. Journal of Hematology & Oncology. 2023;16(1):96.

102. Snyder JT, Malinao M-C, Dugal-Tessier J, Atkinson JE, Anand BS, Okada A, et al. Metabolism of an Oxime-Linked Antibody Drug Conjugate, AGS62P1, and Characterization of Its Identified Metabolite. Molecular Pharmaceutics. 2018;15(6):2384-90.

103. Schwartz RS. Paul Ehrlich's magic bullets. N Engl J Med. 2004;350(11):1079-80.

104. Fu Z, Li S, Han S, Shi C, Zhang Y. Antibody drug conjugate: the "biological missile" for targeted cancer therapy. Signal Transduction and Targeted Therapy. 2022;7(1):93.

105. Sasso JM, Tenchov R, Bird R, Iyer KA, Ralhan K, Rodriguez Y, et al. The Evolving Landscape of Antibody-Drug Conjugates: In Depth Analysis of Recent Research Progress. Bioconjug Chem. 2023;34(11):1951-2000.

106. Metrangolo V, Engelholm LH. Antibody–Drug Conjugates: The Dynamic Evolution from Conventional to Next-Generation Constructs. Cancers [Internet]. 2024; 16(2).

107. Dan N, Setua S, Kashyap VK, Khan S, Jaggi M, Yallapu MM, et al. Antibody-Drug Conjugates for Cancer Therapy: Chemistry to Clinical Implications. Pharmaceuticals (Basel). 2018;11(2).

108. Slamon DJ, Leyland-Jones B, Shak S, Fuchs H, Paton V, Bajamonde A, et al. Use of chemotherapy plus a monoclonal antibody against HER2 for metastatic breast cancer that overexpresses HER2. N Engl J Med. 2001;344(11):783-92.

109. Sharma S, Li Z, Bussing D, Shah DK. Evaluation of Quantitative Relationship Between Target Expression and Antibody-Drug Conjugate Exposure Inside Cancer Cells. Drug Metab Dispos. 2020;48(5):368-77.

110. Modi S, Jacot W, Yamashita T, Sohn J, Vidal M, Tokunaga E, et al. Trastuzumab Deruxtecan in Previously Treated HER2-Low Advanced Breast Cancer. New England Journal of Medicine. 2022;387(1):9-20.

111. Padlan EA. Anatomy of the antibody molecule. Mol Immunol. 1994;31(3):169-217.

112. Huber R, Deisenhofer J, Colman PM, Matsushima M, Palm W. Crystallographic structure studies of an IgG molecule and an Fc fragment. Nature. 1976;264(5585):415-20.

113. Silverton EW, Navia MA, Davies DR. Three-dimensional structure of an intact human immunoglobulin. Proc Natl Acad Sci U S A. 1977;74(11):5140-4.

114. Nimmerjahn F, Ravetch JV. Fcgamma receptors as regulators of immune responses. Nat Rev Immunol. 2008;8(1):34-47.

115. Schumacher D, Hackenberger CP, Leonhardt H, Helma J. Current Status: Site-Specific Antibody Drug Conjugates. J Clin Immunol. 2016;36 Suppl 1:100-07.

116. Shen BQ, Xu K, Liu L, Raab H, Bhakta S, Kenrick M, et al. Conjugation site modulates the in vivo stability and therapeutic activity of antibody-drug conjugates. Nat Biotechnol. 2012;30(2):184-89.

117. Junutula JR, Raab H, Clark S, Bhakta S, Leipold DD, Weir S, et al. Site-specific conjugation of a cytotoxic drug to an antibody improves the therapeutic index. Nature Biotechnology. 2008;26(8):925-32.

118. Liu W, Brock A, Chen S, Chen S, Schultz PG. Genetic incorporation of unnatural amino acids into proteins in mammalian cells. Nat Methods. 2007;4(3):239-44.

119. Jeger S, Zimmermann K, Blanc A, Grünberg J, Honer M, Hunziker P, et al. Site-Specific and Stoichiometric Modification of Antibodies by Bacterial Transglutaminase. Angewandte Chemie International Edition. 2010;49(51):9995-97.

120. Beerli RR, Hell T, Merkel AS, Grawunder U. Sortase Enzyme-Mediated Generation of Site-Specifically Conjugated Antibody Drug Conjugates with High In Vitro and In Vivo Potency. PLoS One. 2015;10(7):e0131177.

121. Zhou Q, Stefano JE, Manning C, Kyazike J, Chen B, Gianolio DA, et al. Site-specific antibody-drug conjugation through glycoengineering. Bioconjug Chem. 2014;25(3):510-20.

122. Collins DM, Bossenmaier B, Kollmorgen G, Niederfellner G. Acquired Resistance to Antibody-Drug Conjugates. Cancers (Basel). 2019;11(3).

123. Yao H-P, Zhao H, Hudson R, Tong X-M, Wang M-H. Duocarmycin-based antibody–drug conjugates as an emerging biotherapeutic entity for targeted cancer therapy: Pharmaceutical strategy and clinical progress. Drug Discovery Today. 2021;26(8):1857-74.

124. Marcucci F, Caserta CA, Romeo E, Rumio C. Antibody-Drug Conjugates (ADC) Against Cancer Stem-Like Cells (CSC)-Is There Still Room for Optimism? Front Oncol. 2019;9:167.

125. Jiang YP, Liu BY, Zheng Q, Panuganti S, Chen R, Zhu J, et al. CLT030, a leukemic stem cell-targeting CLL1 antibody-drug conjugate for treatment of acute myeloid leukemia. Blood Adv. 2018;2(14):1738-49.

126. Manich CS, O'Shaughnessy J, Aftimos PG, van den Tweel E, Oesterholt M, Escriva-de-Romani SI, et al. Primary outcome of the phase III SYD985.002/TULIP trial comparing vic-trastuzumab duocarmazine to physician's choice treatment in patients with pre-treated HER2-positive locally advanced or metastatic breast cancer. Annals of Oncology. 2021;32(suppl_5):1283-346.

127. U.S. Food and Drug Administration Issues Complete Response Letter for Byondis' [Vic-]Trastuzumab Duocarmazine. [press release]. 15 May 2023 2023.

128. Metzeler KH, Herold T, Rothenberg-Thurley M, Amler S, Sauerland MC, Görlich D, et al. Spectrum and prognostic relevance of driver gene mutations in acute myeloid leukemia. Blood. 2016;128(5):686-98.

129. Heckl BC, Carlet M, Vick B, Roolf C, Alsadeq A, Grunert M, et al. Frequent and reliable engraftment of certain adult primary acute lymphoblastic leukemias in mice. Leuk Lymphoma. 2019;60(3):848-51.

130. Ebinger S, Zeller C, Carlet M, Senft D, Bagnoli JW, Liu WH, et al. Plasticity in growth behavior of patients' acute myeloid leukemia stem cells growing in mice. Haematologica. 2020;105(12):2855-60.

131. Jensen P, Carlet M, Schlenk RF, Weber A, Kress J, Brunner I, et al. Requirement for LIM kinases in acute myeloid leukemia. Leukemia. 2020;34(12):3173-85.

132. Vick B, Rothenberg M, Sandhöfer N, Carlet M, Finkenzeller C, Krupka C, et al. An advanced preclinical mouse model for acute myeloid leukemia using patients' cells of various genetic subgroups and in vivo bioluminescence imaging. PLoS One. 2015;10(3):e0120925.

133. Sandhöfer N, Metzeler KH, Rothenberg M, Herold T, Tiedt S, Groiß V, et al. Dual PI3K/mTOR inhibition shows antileukemic activity in MLL-rearranged acute myeloid leukemia. Leukemia. 2015;29(4):828-38.

134. Tzelepis K, De Braekeleer E, Aspris D, Barbieri I, Vijayabaskar MS, Liu WH, et al. SRPK1 maintains acute myeloid leukemia through effects on isoform usage of epigenetic regulators including BRD4. Nat Commun. 2018;9(1):5378.

135. Stief SM, Hanneforth AL, Weser S, Mattes R, Carlet M, Liu WH, et al. Loss of KDM6A confers drug resistance in acute myeloid leukemia. Leukemia. 2020;34(1):50-62.

136. Reiter K, Polzer H, Krupka C, Maiser A, Vick B, Rothenberg-Thurley M, et al. Tyrosine kinase inhibition increases the cell surface localization of FLT3-ITD and enhances FLT3-directed immunotherapy of acute myeloid leukemia. Leukemia. 2018;32(2):313-22.

137. Baroni ML, Sanchez Martinez D, Gutierrez Aguera F, Roca Ho H, Castella M, Zanetti SR, et al. 41BB-based and CD28-based CD123-redirected T-cells ablate human normal hematopoiesis in vivo. J Immunother Cancer. 2020;8(1).

138. Wenk C, Garz AK, Grath S, Huberle C, Witham D, Weickert M, et al. Direct modulation of the bone marrow mesenchymal stromal cell compartment by azacitidine enhances healthy hematopoiesis. Blood Adv. 2018;2(23):3447-61.

139. Roas M, Vick B, Kasper MA, Able M, Polzer H, Gerlach M, et al. Targeting FLT3 with a new-generation antibody-drug conjugate in combination with kinase inhibitors for treatment of AML. Blood. 2023;141(9):1023-35.

140. Bonnet D. In Vivo Evaluation of Leukemic Stem Cells through the Xenotransplantation Model. Current Protocols in Stem Cell Biology. 2008;7(1):3.2.1-3.2.11.

141. Robin T, Capes-Davis A, Bairoch A. CLASTR: The Cellosaurus STR similarity search tool - A precious help for cell line authentication. International Journal of Cancer. 2020;146(5):1299-306.

142. Polzer H. Aktivierung des FLT3-Signalweges als molekulare Zielstruktur in der akuten myeloischen Leukämie [dissertation]. Munich (Germany): Ludwig-Maximilians-Universität; 2013.

143. Roas M. FLT3 specific antibody-drug-conjugate for the treatment of acute myeloid leukemia [dissertation]. Munich (Germany): Ludwig-Maximilians-Universität München; 2021.

144. Pan R, Ruvolo V, Mu H, Leverson JD, Nichols G, Reed JC, et al. Synthetic Lethality of Combined Bcl-2 Inhibition and p53 Activation in AML: Mechanisms and Superior Antileukemic Efficacy. Cancer Cell. 2017;32(6):748-60.e6.

145. Ianevski A, Giri AK, Aittokallio T. SynergyFinder 3.0: an interactive analysis and consensus interpretation of multi-drug synergies across multiple samples. Nucleic Acids Res. 2022;50(W1):W739-w43.

146. Yadav B, Wennerberg K, Aittokallio T, Tang J. Searching for Drug Synergy in Complex Dose-Response Landscapes Using an Interaction Potency Model. Comput Struct Biotechnol J. 2015;13:504-13.

147. Zeller C, Richter D, Jurinovic V, Valtierra-Gutiérrez IA, Jayavelu AK, Mann M, et al. Adverse stem cell clones within a single patient's tumor predict clinical outcome in AML patients. J Hematol Oncol. 2022;15(1):25.

148. Feuring-Buske M, Frankel A, Gerhard B, Hogge D. Variable cytotoxicity of diphtheria toxin 388–granulocyte-macrophage colony-stimulating factor fusion protein for acute myelogenous leukemia stem cells. Experimental Hematology. 2000;28(12):1390-400.

149. Ailles LE, Gerhard B, Hogge DE. Detection and Characterization of Primitive Malignant and Normal Progenitors in Patients With Acute Myelogenous Leukemia Using Long-Term Coculture With Supportive Feeder Layers and Cytokines. Blood. 1997;90(7):2555-64.

150. Kasper MA, Stengl A, Ochtrop P, Gerlach M, Stoschek T, Schumacher D, et al. Ethynylphosphonamidates for the Rapid and Cysteine-Selective Generation of Efficacious Antibody-Drug Conjugates. Angew Chem Int Ed Engl. 2019;58(34):11631-36.

151. Hwang WY, Foote J. Immunogenicity of engineered antibodies. Methods. 2005;36(1):3-10.

152. Dean AQ, Luo S, Twomey JD, Zhang B. Targeting cancer with antibody-drug conjugates: Promises and challenges. MAbs. 2021;13(1):1951427.

153. Harrison PW, Amode MR, Austine-Orimoloye O, Azov Andrey G, Barba M, Barnes I, et al. Ensembl 2024. Nucleic Acids Research. 2024;52(D1):D891-D99.

154. Madej T, Marchler-Bauer A, Lanczycki C, Zhang D, Bryant SH. Biological Assembly Comparison with VAST. Methods Mol Biol. 2020;2112:175-86.

155. Scholl S, Fleischmann M, Schnetzke U, Heidel FH. Molecular Mechanisms of Resistance to FLT3 Inhibitors in Acute Myeloid Leukemia: Ongoing Challenges and Future Treatments. Cells. 2020;9(11).

156. Hinrichs MJ, Dixit R. Antibody Drug Conjugates: Nonclinical Safety Considerations. Aaps j. 2015;17(5):1055-64.

157. Hezareh M, Hessell Ann J, Jensen Richard C, van de Winkel Jan GJ, Parren Paul WHI. Effector Function Activities of a Panel of Mutants of a Broadly Neutralizing Antibody against Human Immunodeficiency Virus Type 1. Journal of Virology. 2001;75(24):12161-68.

158. Fenton C, Scott LJ, Plosker GL. Palivizumab: a review of its use as prophylaxis for serious respiratory syncytial virus infection. Paediatr Drugs. 2004;6(3):177-97.

159. Kratschmer C, Levy M. Targeted Delivery of Auristatin-Modified Toxins to Pancreatic Cancer Using Aptamers. Mol Ther Nucleic Acids. 2018;10:227-36.

160. Ikegami S, Taguchi T, Ohashi M, Oguro M, Nagano H, Mano Y. Aphidicolin prevents mitotic cell division by interfering with the activity of DNA polymerase-alpha. Nature. 1978;275(5679):458-60.

161. Matherly LH, Schuetz JD, Westin E, Goldman ID. A method for the synchronization of cultured cells with aphidicolin: application to the large-scale synchronization of L1210 cells and the study of the cell cycle regulation of thymidylate synthase and dihydrofolate reductase. Anal Biochem. 1989;182(2):338-45.

162. Elgersma RC, Coumans RGE, Huijbregts T, Menge WMPB, Joosten JAF, Spijker HJ, et al. Design, Synthesis, and Evaluation of Linker-Duocarmycin Payloads: Toward Selection of HER2-Targeting Antibody–Drug Conjugate SYD985. Molecular Pharmaceutics. 2015;12(6):1813-35.

163. Kasper MA, Glanz M, Stengl A, Penkert M, Klenk S, Sauer T, et al. Cysteine-Selective Phosphonamidate Electrophiles for Modular Protein Bioconjugations. Angew Chem Int Ed Engl. 2019;58(34):11625-30.

164. Ochtrop P, Jahzerah J, Machui P, Mai I, Schumacher D, Helma J, et al. Compact hydrophilic electrophiles enable highly efficacious high DAR ADCs with excellent in vivo PK profile. Chemical Science. 2023;14(9):2259-66.

165. O'Connor MJ. Targeting the DNA Damage Response in Cancer. Mol Cell. 2015;60(4):547-60.

166. Rieker M. Targeted Combination Therapy: Discovery and Evaluation of Synergistic Anticancer Effects of Anti-HER2-Duocarmycin Antibody-Drug Conjugates Combined with ATR Inhibitors [dissertation]. Darmstadt (Germany): Technische Universität Darmstadt; 2018.

167. Chen H, Lin Z, Arnst KE, Miller DD, Li W. Tubulin Inhibitor-Based Antibody-Drug Conjugates for Cancer Therapy. Molecules. 2017;22(8).

168. Ubink R, Dirksen E, Rouwette M, Bos E, Janssen I, Egging D, et al. Unraveling the Interaction between Carboxylesterase 1c and the Antibody-Drug Conjugate SYD985: Improved Translational PK/PD by Using Ces1c Knockout Mice. Molecular Cancer Therapeutics. 2018;17:2389-98.

169. Krivtsov AV, Armstrong SA. MLL translocations, histone modifications and leukaemia stem-cell development. Nature Reviews Cancer. 2007;7(11):823-33.

170. Somervaille TCP, Cleary ML. Identification and characterization of leukemia stem cells in murine MLL-AF9 acute myeloid leukemia. Cancer Cell. 2006;10(4):257-68.

171. Yu BD, Hess JL, Horning SE, Brown GAJ, Korsmeyer SJ. Altered Hox expression and segmental identity in Mll-mutant mice. Nature. 1995;378(6556):505-08.

172. Herold T, Jurinovic V, Batcha AMN, Bamopoulos SA, Rothenberg-Thurley M, Ksienzyk B, et al. A 29-gene and cytogenetic score for the prediction of resistance to induction treatment in acute myeloid leukemia. Haematologica. 2018;103(3):456-65.

173. Bagnoli JW, Ziegenhain C, Janjic A, Wange LE, Vieth B, Parekh S, et al. Sensitive and powerful single-cell RNA sequencing using mcSCRB-seq. Nature Communications. 2018;9(1):2937.

174. Conneally E, Cashman J, Petzer A, Eaves C. Expansion in vitro of transplantable human cord blood stem cells demonstrated using a quantitative assay of their lympho-myeloid repopulating activity in nonobese diabetic-scid/scid mice. Proc Natl Acad Sci U S A. 1997;94(18):9836-41.

175. Roell KR, Reif DM, Motsinger-Reif AA. An Introduction to Terminology and Methodology of Chemical Synergy-Perspectives from Across Disciplines. Front Pharmacol. 2017;8:158.

176. Greco WR, Faessel H, Levasseur L. The search for cytotoxic synergy between anticancer agents: a case of Dorothy and the ruby slippers? J Natl Cancer Inst. 1996;88(11):699-700.

177. Jia J, Zhu F, Ma X, Cao ZW, Li YX, Chen YZ. Mechanisms of drug combinations: interaction and network perspectives. Nature Reviews Drug Discovery. 2009;8(2):111-28.

178. Adams S, Zhang Q, McCarthy R, Flaherty L, Kuruvilla V, Watkins K, et al. The Combination of IMGN632, a CD123-Targeting ADC, with Venetoclax Enhances Anti-Leukemic Activity In vitro

and Prolongs Survival In vivo in Pre-Clinical Models of Human AML. Poster session presented at: 24th Congress of the European Hematology Association, June 13-16, 2019.2019.

179. Kuruvilla V, McCarthy R, Zhang Q, Watkins K, Adams S, Sloss C, et al. AML-367: IMGN632, a CD123-Targeting ADC Bearing a DNA-Alkylating IGN Payload, Combines Effectively as a Triplet Regimen with Azacitidine and Venetoclax In Vivo, Prolonging Survival in Preclinical Models of Human Acute Myeloid Leukemia (AML). Clinical Lymphoma Myeloma and Leukemia. 2020;20:S208-S09.

180. Kwon M, Kim G, Kim R, Kim K-T, Kim ST, Smith S, et al. Phase II study of ceralasertib (AZD6738) in combination with durvalumab in patients with advanced gastric cancer. Journal for ImmunoTherapy of Cancer. 2022;10(7):e005041.

181. Mei L, Zhang J, He K, Zhang J. Ataxia telangiectasia and Rad3-related inhibitors and cancer therapy: where we stand. J Hematol Oncol. 2019;12(1):43.

182. Gerritsen M, Hilgendorf S, Yi G, Wierenga ATJ, Schuringa J-J, Martens JHA, et al. Presence of mutant p53 increases stem cell frequency and is associated with reduced binding to classic TP53 binding sites in cell lines and primary AMLs. Experimental Hematology. 2022;110:39-46.

183. Pelat T, Bedouelle H, Rees AR, Crennell SJ, Lefranc M-P, Thullier P. Germline Humanization of a Non-human Primate Antibody that Neutralizes the Anthrax Toxin, by in Vitro and in Silico Engineering. Journal of Molecular Biology. 2008;384(5):1400-07.

184. Lu R-M, Hwang Y-C, Liu IJ, Lee C-C, Tsai H-Z, Li H-J, et al. Development of therapeutic antibodies for the treatment of diseases. Journal of Biomedical Science. 2020;27(1):1.

185. Getts DR, Getts MT, McCarthy DP, Chastain EM, Miller SD. Have we overestimated the benefit of human(ized) antibodies? MAbs. 2010;2(6):682-94.

186. Azinovic I, DeNardo GL, Lamborn KR, Mirick G, Goldstein D, Bradt BM, et al. Survival benefit associated with human anti-mouse antibody (HAMA) in patients with B-cell malignancies. Cancer Immunol Immunother. 2006;55(12):1451-8.

187. Bokemeyer C, Heiss M, Gamperl H, Linke R, Schulze E, Friccius-Quecke H, et al. Safety of catumaxomab: Cytokine-release-related symptoms as a possible predictive factor for efficacy in a pivotal phase II/III trial in malignant ascites. Journal of Clinical Oncology. 2009;27:3036-36.

188. Riechmann L, Clark M, Waldmann H, Winter G. Reshaping human antibodies for therapy. Nature. 1988;332:323-7.

189. Choi Y, Hua C, Sentman CL, Ackerman ME, Bailey-Kellogg C. Antibody humanization by structure-based computational protein design. MAbs. 2015;7(6):1045-57.

190. Zwaagstra JC, Sulea T, Baardsnes J, Radinovic S, Cepero-Donates Y, Robert A, et al. Binding and functional profiling of antibody mutants guides selection of optimal candidates as antibody drug conjugates. PLoS One. 2019;14(12):e0226593.

191. van der Lee MM, Groothuis PG, Ubink R, van der Vleuten MA, van Achterberg TA, Loosveld EM, et al. The Preclinical Profile of the Duocarmycin-Based HER2-Targeting ADC SYD985 Predicts for Clinical Benefit in Low HER2-Expressing Breast Cancers. Mol Cancer Ther. 2015;14(3):692-703.

192. Rudra-Ganguly N, Lowe C, Virata C, Leavitt M, Jin L, Mendelsohn B, et al. AGS62P1, a Novel Anti-FLT3 Antibody Drug Conjugate, Employing Site Specific Conjugation, Demonstrates

Preclinical Anti-Tumor Efficacy in AML Tumor and Patient Derived Xenografts. Blood. 2015;126:3806-06.

193. Piloto O, Nguyen B, Huso D, Kim KT, Li Y, Witte L, et al. IMC-EB10, an anti-FLT3 monoclonal antibody, prolongs survival and reduces nonobese diabetic/severe combined immunodeficient engraftment of some acute lymphoblastic leukemia cell lines and primary leukemic samples. Cancer Res. 2006;66(9):4843-51.

194. Tsuzuki H, Kawase T, Nakazawa T, Mori M, Yoshida T. Anti-tumor effect of antibody drug conjugate ASP1235 targeting Fms-like tyrosine kinase 3 with venetoclax plus azacitidine in an acute myeloid leukemia xenograft mouse model. Oncotarget; Vol 13 (2022). 2022.

195. Zheng B, Yu SF, Del Rosario G, Leong SR, Lee GY, Vij R, et al. An Anti-CLL-1 Antibody-Drug Conjugate for the Treatment of Acute Myeloid Leukemia. Clin Cancer Res. 2019;25(4):1358-68.

196. Walter RB, Raden BW, Kamikura DM, Cooper JA, Bernstein ID. Influence of CD33 expression levels and ITIM-dependent internalization on gemtuzumab ozogamicin–induced cytotoxicity. Blood. 2005;105(3):1295-302.

197. Saber H, Leighton JK. An FDA oncology analysis of antibody-drug conjugates. Regulatory Toxicology and Pharmacology. 2015;71(3):444-52.

198. Iwasaki K, Uno Y, Utoh M, Yamazaki H. Importance of cynomolgus monkeys in development of monoclonal antibody drugs. Drug Metabolism and Pharmacokinetics. 2019;34(1):55-63.

199. Galanis A, Levis M. Inhibition of c-Kit by tyrosine kinase inhibitors. Haematologica. 2015;100(3):e77-9.

200. Cortes JE, Perl AE, Dombret H, Kayser S, Steffen B, Rousselot P, et al. Final Results of a Phase 2 Open-Label, Monotherapy Efficacy and Safety Study of Quizartinib (AC220) in Patients ≥ 60 Years of Age with FLT3 ITD Positive or Negative Relapsed/Refractory Acute Myeloid Leukemia. Blood. 2012;120(21):48.

201. Wu C-W, Huang H-Y, Lin S-Y, Wang C-C, Huang C-F, Wu IH. Vascular Endothelial Growth Factor Inhibitors and the Risk of Aortic Aneurysm and Aortic Dissection. JAMA Network Open. 2024;7(3):e240940-e40.

202. Chu TF, Rupnick MA, Kerkela R, Dallabrida SM, Zurakowski D, Nguyen L, et al. Cardiotoxicity associated with tyrosine kinase inhibitor sunitinib. Lancet. 2007;370(9604):2011-9.

203. Motokawa T, Ikeda S, Ueno Y, Eguchi M, Minami T, Kawano H, et al. Comparison of Dasatinib- and Imatinib-Related Cardiotoxic Adverse Events in Japanese Patients With Chronic Myeloid Leukemia and Gastrointestinal Stromal Tumor. Circ Rep. 2022;4(1):1-8.

204. Yue Z, Chen J, Lian H, Pei J, Li Y, Chen X, et al. PDGFR-β Signaling Regulates Cardiomyocyte Proliferation and Myocardial Regeneration. Cell Rep. 2019;28(4):966-78.e4.

205. Lewis JH, Gelderblom H, van de Sande M, Stacchiotti S, Healey JH, Tap WD, et al. Pexidartinib Long-Term Hepatic Safety Profile in Patients with Tenosynovial Giant Cell Tumors. The Oncologist. 2021;26(5):e863-e73.

206. Ge SS, Qiu QC, Dai HP, Shen XD, Wu TM, Du JH, et al. Mutation spectrum of FLT3 and significance of non-canonical FLT3 mutations in haematological malignancy. Br J Haematol. 2023;202(3):539-49.

207. Arena S, Bellosillo B, Siravegna G, Martínez A, Cañadas I, Lazzari L, et al. Emergence of Multiple EGFR Extracellular Mutations during Cetuximab Treatment in Colorectal Cancer. Clin Cancer Res. 2015;21(9):2157-66.

208. López de Sá A, Díaz-Tejeiro C, Poyatos-Racionero E, Nieto-Jiménez C, Paniagua-Herranz L, Sanvicente A, et al. Considerations for the design of antibody drug conjugates (ADCs) for clinical development: lessons learned. Journal of Hematology & Oncology. 2023;16(1):118.

209. Lo E, Campton D, Costandy L, Itamoto H, Huston R, Gardner B, et al. Abstract 5368: A multiparameter assay for HER2 protein detection on circulating tumor cells in non-small cell lung cancer2020. 5368-68 p.

210. Williams M, Spreafico A, Vashisht K, Hinrichs MJ. Patient Selection Strategies to Maximize Therapeutic Index of Antibody–Drug Conjugates: Prior Approaches and Future Directions. Molecular Cancer Therapeutics. 2020;19(9):1770-83.

211. Guo J, Kumar S, Prashad A, Starkey J, Singh SK. Assessment of Physical Stability of an Antibody Drug Conjugate by Higher Order Structure Analysis: Impact of Thiol- Maleimide Chemistry. Pharmaceutical Research. 2014;31(7):1710-23.

212. Dokter W, Ubink R, van der Lee M, van der Vleuten M, van Achterberg T, Jacobs D, et al. Preclinical Profile of the HER2-Targeting ADC SYD983/SYD985: Introduction of a New Duocarmycin-Based Linker-Drug Platform. Molecular Cancer Therapeutics. 2014;13(11):2618-29.

213. Scribner JA, Brown JG, Son T, Chiechi M, Li P, Sharma S, et al. Preclinical Development of MGC018, a Duocarmycin-based Antibody–drug Conjugate Targeting B7-H3 for Solid Cancer. Molecular Cancer Therapeutics. 2020;19(11):2235-44.

214. Schmitt S, Machui P, Mai I, Herterich S, Wunder S, Cyprys P, et al. Design and Evaluation of Phosphonamidate-Linked Exatecan Constructs for Highly Loaded, Stable, and Efficacious Antibody-Drug Conjugates. Mol Cancer Ther. 2024;23(2):199-211.

215. Majzner RG, Theruvath JL, Nellan A, Heitzeneder S, Cui Y, Mount CW, et al. CAR T Cells Targeting B7-H3, a Pan-Cancer Antigen, Demonstrate Potent Preclinical Activity Against Pediatric Solid Tumors and Brain Tumors. Clin Cancer Res. 2019;25(8):2560-74.

216. Nilchan N, Li X, Pedzisa L, Nanna AR, Roush WR, Rader C. Dual-mechanistic antibody-drug conjugate via site-specific selenocysteine/cysteine conjugation. Antib Ther. 2019;2(4):71-78.

217. Toledo LI, Altmeyer M, Rask MB, Lukas C, Larsen DH, Povlsen LK, et al. ATR prohibits replication catastrophe by preventing global exhaustion of RPA. Cell. 2013;155(5):1088-103.

218. Čermák V, Dostál V, Jelínek M, Libusová L, Kovář J, Rösel D, et al. Microtubule-targeting agents and their impact on cancer treatment. European Journal of Cell Biology. 2020;99(4):151075.

219. Smith KS, Folz BA, Adams EG, Bhuyan BK. Synergistic and additive combinations of several antitumor drugs and other agents with the potent alkylating agent adozelesin. Cancer Chemotherapy and Pharmacology. 1995;35(6):471-82.

220. Shi J, Orth JD, Mitchison T. Cell Type Variation in Responses to Antimitotic Drugs that Target Microtubules and Kinesin-5. Cancer Research. 2008;68(9):3269-76.

221. Junttila MR, Mao W, Wang X, Wang B-E, Pham T, Flygare J, et al. Targeting LGR5+ cells with an antibody-drug conjugate for the treatment of colon cancer. Science Translational Medicine. 2015;7(314):314ra186-314ra186.

222. Harper J, Lloyd C, Dimasi N, Toader D, Marwood R, Lewis L, et al. Preclinical Evaluation of MEDI0641, a Pyrrolobenzodiazepine-Conjugated Antibody-Drug Conjugate Targeting 5T4. Mol Cancer Ther. 2017;16(8):1576-87.

223. Sapra P, Damelin M, Dijoseph J, Marquette K, Geles KG, Golas J, et al. Long-term tumor regression induced by an antibody-drug conjugate that targets 5T4, an oncofetal antigen expressed on tumor-initiating cells. Mol Cancer Ther. 2013;12(1):38-47.

224. Damelin M, Bankovich A, Bernstein J, Lucas J, Chen L, Williams S, et al. A PTK7-targeted antibody-drug conjugate reduces tumor-initiating cells and induces sustained tumor regressions. Sci Transl Med. 2017;9(372):eaag2611.

225. Satomaa T, Pynnönen H, Aitio O, Hiltunen JO, Pitkänen V, Lähteenmäki T, et al. Targeting CD33+ acute myeloid leukemia with GLK-33, a lintuzumab-auristatin conjugate with a wide therapeutic window. Molecular Cancer Therapeutics. 2024.

226. Liu S, Cong Y, Wang D, Sun Y, Deng L, Liu Y, et al. Breast cancer stem cells transition between epithelial and mesenchymal states reflective of their normal counterparts. Stem Cell Reports. 2014;2(1):78-91.

227. Poruchynsky MS, Komlodi-Pasztor E, Trostel S, Wilkerson J, Regairaz M, Pommier Y, et al. Microtubule-targeting agents augment the toxicity of DNA-damaging agents by disrupting intracellular trafficking of DNA repair proteins. Proc Natl Acad Sci U S A. 2015;112(5):1571-76.

228. Komlodi-Pasztor E, Sackett D, Wilkerson J, Fojo T. Mitosis is not a key target of microtubule agents in patient tumors. Nat Rev Clin Oncol. 2011;8(4):244-50.

229. Tregnago C, Da Ros A, Porcù E, Benetton M, Simonato M, Simula L, et al. Thioridazine requires calcium influx to induce MLL-AF6-rearranged AML cell death. Blood Adv. 2020;4(18):4417-29.

230. Casado P, Rio-Machin A, Miettinen JJ, Bewicke-Copley F, Rouault-Pierre K, Krizsan S, et al. Integrative phosphoproteomics defines two biologically distinct groups of KMT2A rearranged acute myeloid leukaemia with different drug response phenotypes. Signal Transduct Target Ther. 2023;8(1):80.

231. Heitmann J, Schlenk R, Dörfel D, Kayser S, Döhner K, Heuser M, et al. Phase I study evaluating the Fc-optimized FLT3 antibody FLYSYN in AML patients with measurable residual disease. Journal of hematology & oncology. 2023;16:96.

232. Kuchenbauer F, Kern W, Schoch C, Kohlmann A, Hiddemann W, Haferlach T, et al. Detailed analysis of FLT3 expression levels in acute myeloid leukemia. Haematologica. 2005;90(12):1617-25.

233. Schoch C, Schnittger S, Klaus M, Kern W, Hiddemann W, Haferlach T. AML with 11q23/MLL abnormalities as defined by the WHO classification: incidence, partner chromosomes, FAB subtype, age distribution, and prognostic impact in an unselected series of 1897 cytogenetically analyzed AML cases. Blood. 2003;102(7):2395-402.

234. Coustan-Smith E, Song G, Shurtleff S, Yeoh AE, Chng WJ, Chen SP, et al. Universal monitoring of minimal residual disease in acute myeloid leukemia. JCI Insight. 2018;3(9).

235. Dunphy CH, Tang W. The Value of CD64 Expression in Distinguishing Acute Myeloid Leukemia With Monocytic Differentiation From Other Subtypes of Acute Myeloid Leukemia: A Flow Cytometric Analysis of 64 Cases. Archives of Pathology & Laboratory Medicine. 2007;131(5):748-54.

236. Pei S, Shelton IT, Gillen AE, Stevens BM, Gasparetto M, Wang Y, et al. A Novel Type of Monocytic Leukemia Stem Cell Revealed by the Clinical Use of Venetoclax-Based Therapy. Cancer Discov. 2023;13(9):2032-49.

237. Nguyen TD, Bordeau BM, Balthasar JP. Mechanisms of ADC Toxicity and Strategies to Increase ADC Tolerability. Cancers (Basel). 2023;15(3).

238. Cerchione C, Peleteiro Raíndo A, Mosquera Orgueira A, Mosquera Torre A, Bao Pérez L, Marconi G, et al. Safety of FLT3 inhibitors in patients with acute myeloid leukemia. Expert Review of Hematology. 2021;14(9):851-65.

239. Sun X, Wang G, Zuo S, Niu Q, Chen X, Feng X. Preclinical Evaluation of CD64 As a Potential Target For CAR-T-cell Therapy For Acute Myeloid Leukemia. J Immunother. 2022;45(2):67-77.

240. Izumi Y, Kanayama M, Shen Z, Kai M, Kawamura S, Akiyama M, et al. An Antibody-Drug Conjugate That Selectively Targets Human Monocyte Progenitors for Anti-Cancer Therapy. Front Immunol. 2021;12:618081.

241. Pan LF, Kreisle RA, Shi YD. Detection of Fcgamma receptors on human endothelial cells stimulated with cytokines tumour necrosis factor-alpha (TNF-alpha) and interferon-gamma (IFN-gamma). Clin Exp Immunol. 1998;112(3):533-8.

242. Loughlin AJ, Woodroofe MN, Cuzner ML. Modulation of interferon-gamma-induced major histocompatibility complex class II and Fc receptor expression on isolated microglia by transforming growth factor-beta 1, interleukin-4, noradrenaline and glucocorticoids. Immunology. 1993;79(1):125-30.

243. Hackshaw MD, Danysh HE, Singh J, Ritchey ME, Ladner A, Taitt C, et al. Incidence of pneumonitis/interstitial lung disease induced by HER2-targeting therapy for HER2-positive metastatic breast cancer. Breast Cancer Res Treat. 2020;183(1):23-39.

244. Uppal H, Doudement E, Mahapatra K, Darbonne WC, Bumbaca D, Shen BQ, et al. Potential mechanisms for thrombocytopenia development with trastuzumab emtansine (T-DM1). Clin Cancer Res. 2015;21(1):123-33.

245. Zhao H, Gulesserian S, Ganesan SK, Ou J, Morrison K, Zeng Z, et al. Inhibition of Megakaryocyte Differentiation by Antibody-Drug Conjugates (ADCs) is Mediated by Macropinocytosis: Implications for ADC-induced Thrombocytopenia. Mol Cancer Ther. 2017;16(9):1877-86.

246. Tada M, Aoyama M, Ishii-Watabe A. Fcγ Receptor Activation by Human Monoclonal Antibody Aggregates. J Pharm Sci. 2020;109(1):576-83.

247. Ahmadi M, Bryson CJ, Cloake EA, Welch K, Filipe V, Romeijn S, et al. Small amounts of sub-visible aggregates enhance the immunogenic potential of monoclonal antibody therapeutics. Pharm Res. 2015;32(4):1383-94.

248. Banerji U, van Herpen CML, Saura C, Thistlethwaite F, Lord S, Moreno V, et al. Trastuzumab duocarmazine in locally advanced and metastatic solid tumours and HER2-

expressing breast cancer: a phase 1 dose-escalation and dose-expansion study. Lancet Oncol. 2019;20(8):1124-35.

249. U.S. Food and Drug Administration Issues Complete Response Letter for Byondis' [Vic-]Trastuzumab Duocarmazine. [updated 15 May 2023; cited 03 July 2024] [press release]. 2023.

250. Powderly Ii J, Jang S, Lohr J, Spira A, Bohac G, Sharma M. Preliminary dose escalation results from a phase I/II, first-in-human study of MGC018 (anti-B7-H3 antibody-drug conjugate) in patients with advanced solid tumors. Journal of Clinical Oncology. 2020;38:3071-71.

251. Owonikoko TK, Hussain A, Stadler WM, Smith DC, Kluger H, Molina AM, et al. First-in-human multicenter phase I study of BMS-936561 (MDX-1203), an antibody-drug conjugate targeting CD70. Cancer Chemotherapy and Pharmacology. 2016;77(1):155-62.

252. Eaton JS, Miller PE, Mannis MJ, Murphy CJ. Ocular Adverse Events Associated with Antibody-Drug Conjugates in Human Clinical Trials. J Ocul Pharmacol Ther. 2015;31(10):589-604.

253. Zhao H, Atkinson J, Gulesserian S, Zeng Z, Nater J, Ou J, et al. Modulation of Macropinocytosis-Mediated Internalization Decreases Ocular Toxicity of Antibody-Drug Conjugates. Cancer Res. 2018;78(8):2115-26.

254. Hungria V, Robak P, Hus M, Zherebtsova V, Ward C, Ho PJ, et al. Belantamab Mafodotin, Bortezomib, and Dexamethasone for Multiple Myeloma. N Engl J Med. 2024;391(5):393-407.

255. Dimopoulos Meletios A, Beksac M, Pour L, Delimpasi S, Vorobyev V, Quach H, et al. Belantamab Mafodotin, Pomalidomide, and Dexamethasone in Multiple Myeloma. New England Journal of Medicine. 2024;391(5):408-21.

256. Lonial S, Lee HC, Badros A, Trudel S, Nooka AK, Chari A, et al. Belantamab mafodotin for relapsed or refractory multiple myeloma (DREAMM-2): a two-arm, randomised, open-label, phase 2 study. Lancet Oncol. 2020;21(2):207-21.

257. Trudel S, Lendvai N, Popat R, Voorhees PM, Reeves B, Libby EN, et al. Targeting B-cell maturation antigen with GSK2857916 antibody-drug conjugate in relapsed or refractory multiple myeloma (BMA117159): a dose escalation and expansion phase 1 trial. Lancet Oncol. 2018;19(12):1641-53.

258. Hingorani DV, Doan MK, Camargo MF, Aguilera J, Song SM, Pizzo D, et al. Precision Chemoradiotherapy for HER2 Tumors Using Antibody Conjugates of an Auristatin Derivative with Reduced Cell Permeability. Molecular Cancer Therapeutics. 2020;19(1):157-67.

259. Reaper PM, Griffiths MR, Long JM, Charrier J-D, MacCormick S, Charlton PA, et al. Selective killing of ATM- or p53-deficient cancer cells through inhibition of ATR. Nature Chemical Biology. 2011;7(7):428-30.

260. Hall AB, Newsome D, Wang Y, Boucher DM, Eustace B, Gu Y, et al. Potentiation of tumor responses to DNA damaging therapy by the selective ATR inhibitor VX-970. Oncotarget. 2014;5(14).

261. Kwok M, Davies N, Agathanggelou A, Smith E, Oldreive C, Petermann E, et al. ATR inhibition induces synthetic lethality and overcomes chemoresistance in TP53- or ATM-defective chronic lymphocytic leukemia cells. Blood. 2016;127(5):582-95.

262. Sangster-Guity N, Conrad BH, Papadopoulos N, Bunz F. ATR mediates cisplatin resistance in a p53 genotype-specific manner. Oncogene. 2011;30(22):2526-33.

263. Kuo Y-H, Qi J, Cook GJ. Regain control of p53: Targeting leukemia stem cells by isoform-specific HDAC inhibition. Experimental Hematology. 2016;44(5):315-21.

264. Vo TT, Ryan J, Carrasco R, Neuberg D, Rossi DJ, Stone RM, et al. Relative mitochondrial priming of myeloblasts and normal HSCs determines chemotherapeutic success in AML. Cell. 2012;151(2):344-55.

6 Annex

Supplementary Tables

Supplementary Table 1: IC_{50} values of ADC payloads in aphidicolin-arrested and proliferating cells. IC_{50} = 50% inhibitory concentration as calculated with GraphPad Prism Software 10.1.2, non-linear fit variable slope analysis.

toxin	IC_{50} in nM no aphidicolin	IC_{50} in nM 3.3 µM aphidicolin	ratio (no aphidicolin/3.3 µM aphidicolin)
	MOLM-13		
DUBA	2.8	27.5	9.8
MMAE	1.3	166	127.7
Exatecan	1.8	99.8	55.4
	MV4-11		
DUBA	6.4	15.1	2.4
MMAE	19.8	87.7	4.4
Exatecan	21.7	64.2	3

Supplementary Table 2: IC_{50} values of 20D9h3- and IgG1- ADCs with and without LALA mutation in cytotoxicity assays with Ba/F3 cells with FLT3 and/or FcγRI expression. IC_{50} = 50% inhibitory concentration as calculated with GraphPad Prism Software 10.1.2, non-linear fit variable slope analysis. ev = empty vector; FLT3 = fms-related tyrosine kinase 3; FcγRI = Fc gamma receptor 1; LALA = Leu234/235Ala; pMIY = MSCV-IRES-YFP vector; na = not assessed

Ba/F3 pMIY	IC_{50} 20D9h3-DUBA (in ng/ml)	IC_{50} 20D9h3-LALA-DUBA (in ng/ml)	IC_{50} IgG1-DUBA (in ng/ml)	IC_{50} IgG1-LALA-DUBA (in ng/ml)
ev	-	-	-	670.4
hFLT3low	2814	na	na	na
hFLT3medium	177.4	na	na	na
hFLT3high	69.3	142.9	-	-
hFcγRI	86.5	-	125.3	1344
hFLT3+hFcγRI	30.1	107.6	552.2	1433

Supplementary Table 3: IC_{50} values of 20D9h3- and IgG1-ADCs in cytotoxicity assays with leukemia cell lines. IC_{50} = 50% inhibitory concentration as calculated with GraphPad Prism Software 10.1.2, non-linear fit variable slope analysis. FLT3 = fms-related tyrosine kinase 3; mAb = monoclonal antibody

Name	IC_{50} 20D9h3-DUBA (in ng/ml)	IC_{50} 20D9h3-MMAF (in ng/ml)	IC_{50} IgG1-DUBA (in ng/ml)	IC_{50} IgG1-MMAF (in ng/ml)	IC_{50} 20D9h3-mAb (in ng/ml)
		FLT3-positive			
MOLM-13	15.9	28.4	360.5	153.8	-
MV4-11	8.7	25.7	143.6	247.4	-
OCI-AML3	8.2	35.5	159.3	43.4	
		FLT3-negative			
HL-60	-	-	> 2000	-	-
K-562	> 2000	-	-	-	-

Supplementary Table 4: CFU and LTC-IC assay colony counts. CFC = colony-forming cells; CFU = colony-forming unit; LTC-IC = long-term culture initiating cells; s.d. = standard deviation; na = not assessed.

sample	treatment	dose (µg/ml)	AML-CFC in CFU assay per 10^5 cells (technical mean±SD) - replicate 1 -	AML-CFC in CFU assay per 10^5 cells (technical mean±SD) - replicate 2 -	AML-CFC in CFU assay per 10^5 cells (technical mean±SD) - replicate 3 -	LTC-IC-CFC in LTC-IC assay per $2.5x10^6$ cells (technical mean ± SD)
AML-388 (high dose)*	control	-	296 ± 39.6	472.5 ± 6.4	2152 ± 113.1	50.5 ± 9.2
	20D9h3-DUBA	0.3	1.5 ± 0.7	0 ± 0	18 ± 8.5	0 ± 0
		1	0.5 ± 0.7	0 ± 0	12 ± 5.7	na
	20D9h3-MMAF	0.3	2.5 ± 0.7	0.5 ± 0.7	78 ± 8.5	26 ± 2.8
		1	1 ± 1.4	0 ± 0	60 ± 5.7	na
AML-388 (low dose)*	control	-	704 ± 107.5	1824 ± 118.8	2152 ± 113.1	na
	20D9h3-DUBA	0.005	334 ± 19.8	1064 ± 5.7	1348 ± 141.4	na
		0.025	0 ± 0	514 ± 48.1	64 ± 11.3	43.5 ± 0.7
	20D9h3-MMAF	0.005	594 ± 19.8	1340 ± 271.5	2024 ± 135.8	na
		0.025	592 ± 107.5	1142 ± 19.8	388 ± 22.6	65 ± 1.4
AML-393**	control	-	471.5 ± 180	109.5 ± 0.7	21.5 ± 6.4	124.5 ± 13.4
	20D9h3-DUBA	0.3	0 ± 0	0 ± 0	0 ± 0	3.5 ± 0.7
		1	0.5 ± 0.7	0 ± 0	0 ± 0	na
	20D9h3-MMAF	0.3	523.5 ± 16.3	76.5 ± 4.9	8 ± 1.4	1.5 ± 0.7
		1	200 ± 36.8	5 ± 1.4	7 ± 2.8	na
AML-393 Primary	control	-	69.5 ± 14.8			
	20D9h3-DUBA	0.3	6.5 ± 2.1			
		1	5.5 ± 2.1			
	20D9h3-MMAF	0.3	28.5 ± 2.1	na	na	na
		1	27.5 ± 4.9			
	IgG1-DUBA	0.3	45.5 ± 7.8			
	20D9h3-LALA-DUBA	0.3	37 ± 1.4			
AML-669***	control	-	86.0 ± 25.5	1572 ± 265.9	2920 ± 192.3	
	20D9h3-DUBA	0.3	6.5 ± 0.7	1240 ± 90.5	1640 ± 373.4	
		1	3.5 ± 0.7	464 ± 45.3	94 ± 8.5	na
	20D9h3-MMAF	0.3	34 ± 1.4	1464 ± 11.3	2864 ± 248.9	
		1	24.5 ± 4.9	1064 ± 215.0	1296 ± 90.5	

**for CFU assay replicate 1 (high + low dose) and for LTC-IC assay PDX cells were thawed; for CFU assay replicate 2 and 3 PDX cells were freshly isolated from NSG mice*
***all assays were done with thawed PDX cells*
****for CFU assay replicate 1 thawed PDX cells were used; for CFU assay replicate 2+3 PDX cells were freshly isolated from NSG mice*

Supplementary Figures

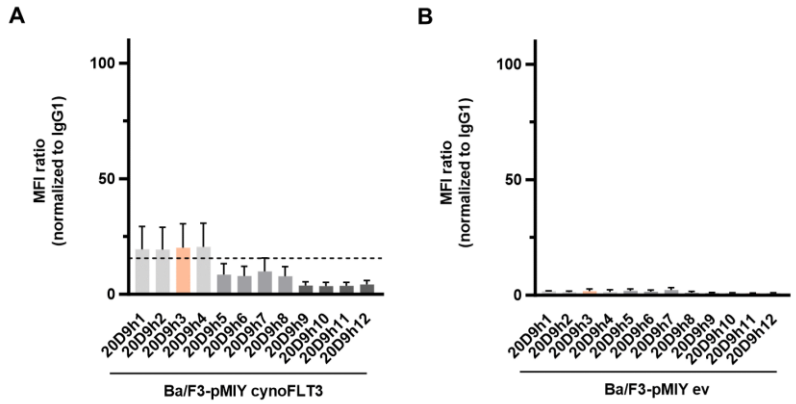

Supplementary Figure 1: Binding analysis of humanized FLT3-mAbs in Ba/F3 cells expressing empty vector or cynomolgus monkey FLT3. (A-B) Binding of humanized mAbs to Ba/F3 cells expressing MSCV-IRES-YFP vector (pMIY) and cynomolgus monkey FLT3 (cynoFLT3, A) or empty vector (ev, B). Binding was assessed with flow cytometry and is expressed as mean fluorescence intensity (MFI) normalized to IgG1 isotype control. Dashed line marks MFI of chimeric 20D9-mAb. mean ± s.d.; n = 3 biological replicates.

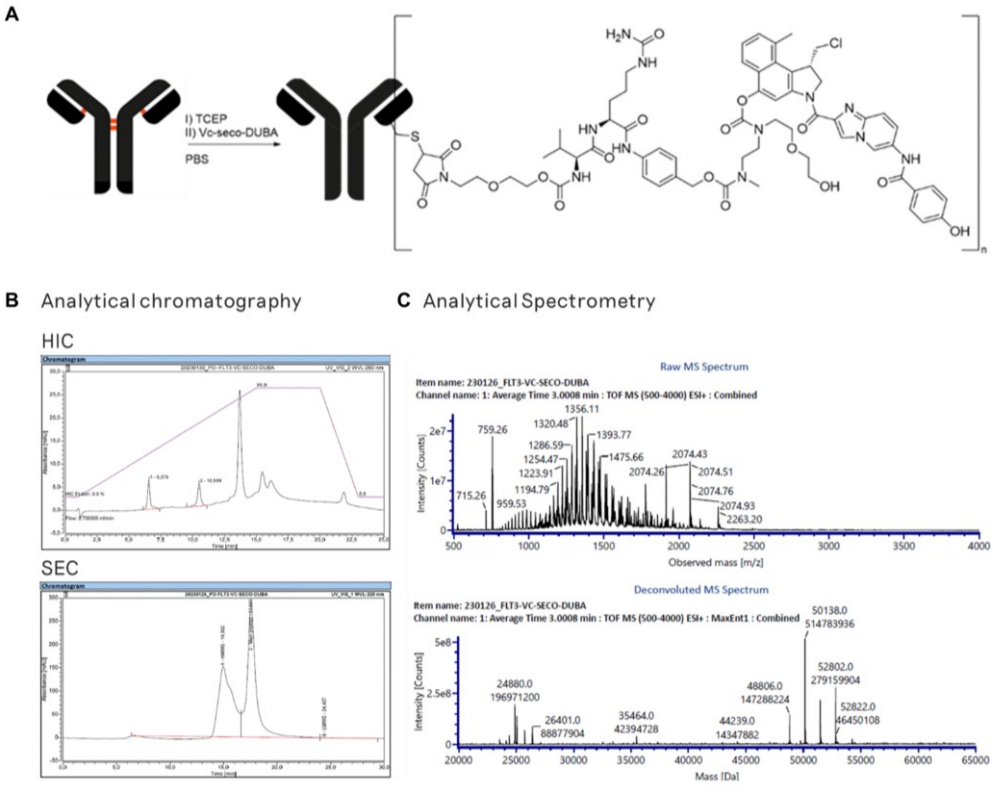

Supplementary Figure 2: Quality control of 20D9h3-DUBA ADC. (A) Schematic image of 20D9h3-DUBA ADC. (B-C) Analytics of 20D9h3-vc-*seco*-DUBA (20D9h3-DUBA) using hydrophobic interaction chromatography (HIC, B top), size-exclusion chromatography (SEC, B bottom) and mass spectrometry (MS, C). For MS, crude and deconvoluted spectrums are shown in the top and bottom images, respectively. A drug-to-antibody ratio (DAR) of 4.8 was calculated from the deconvoluted MS spectrum using heavy and light chain species intensities. ADC conjugation and analytics were carried by Dr. Marc-André Kasper and Dr. Philipp Ochtrop (both Tubulis GmbH).

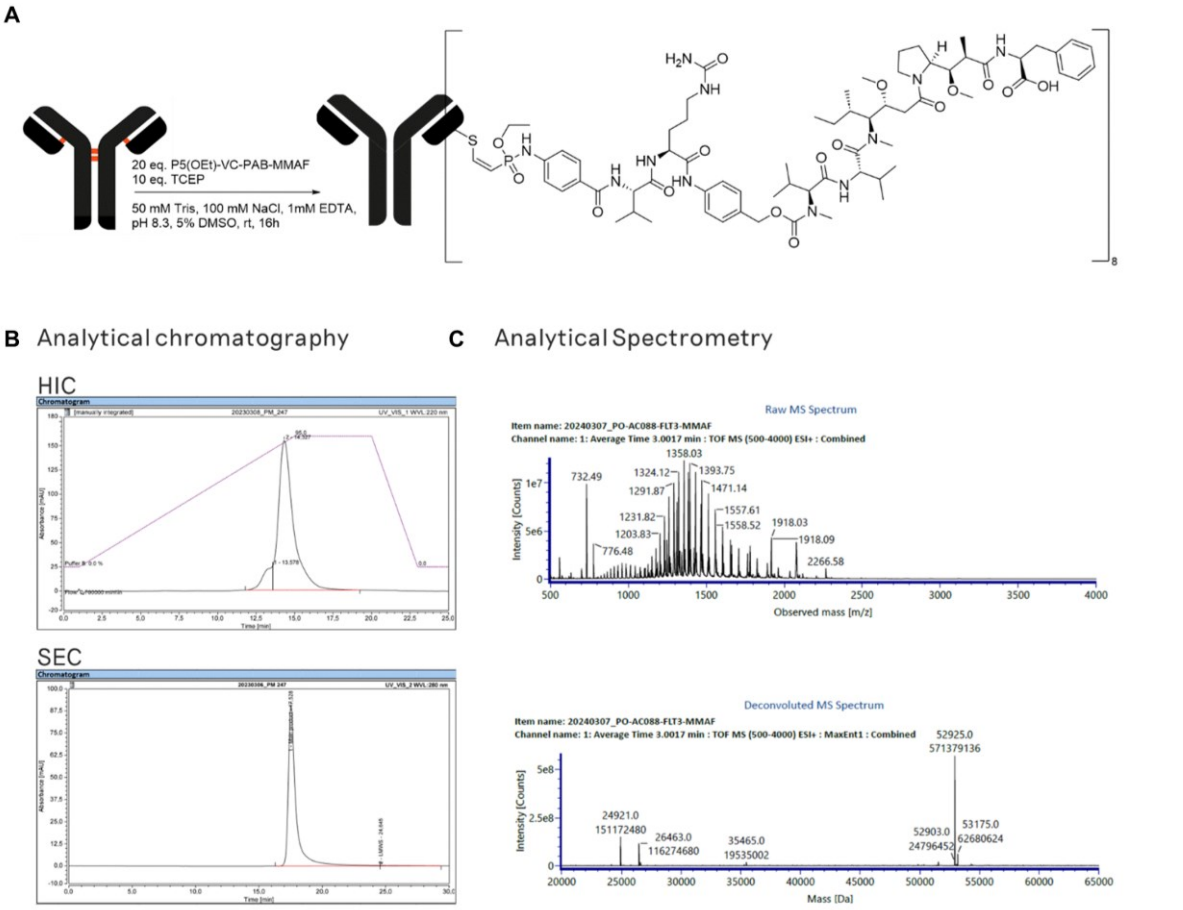

Supplementary Figure 3: Quality control of 20D9h3-MMAF ADC. (A) Schematic image of 20D9h3-MMAF ADC. (B-C) Analytics of 20D9h3-P5(OEt)-vc-PAB-MMAF (20D9h3-MMAF) using hydrophobic interaction chromatography (HIC, B top), size-exclusion chromatography (SEC, B bottom) and mass spectrometry (MS, C). For MS, crude and deconvoluted spectrums are shown in the top and bottom images, respectively. A drug-to-antibody ratio (DAR) of 4.8 was calculated from the deconvoluted MS spectrum using heavy and light chain species intensities. ADC conjugation and analytics were carried by Dr. Marc-André Kasper and Dr. Philipp Ochtrop (both Tubulis GmbH).

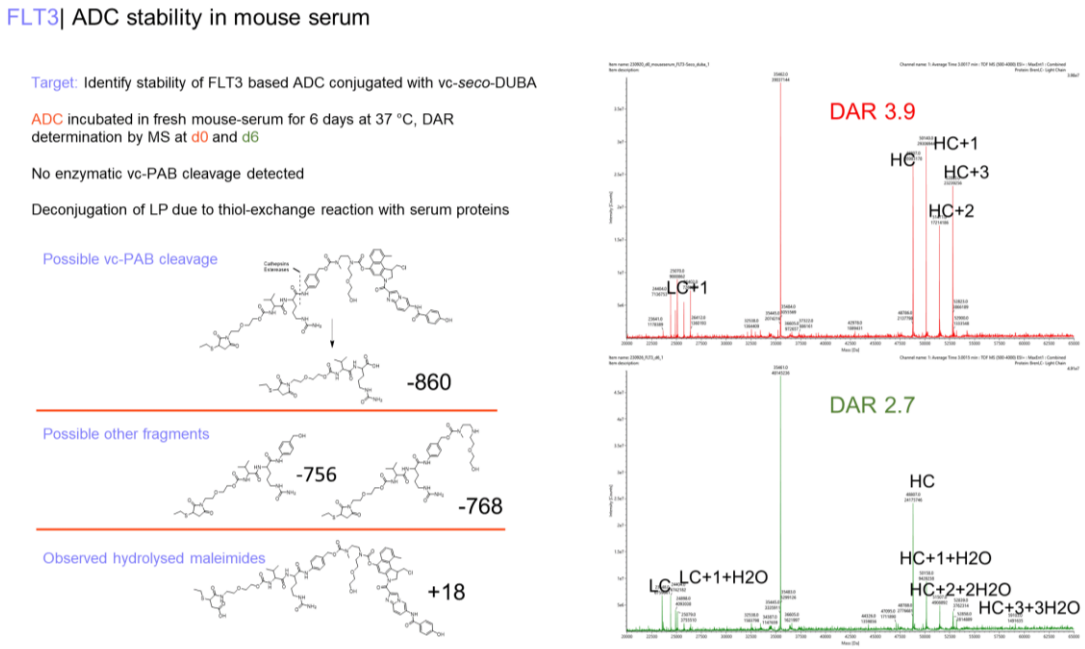

Supplementary Figure 4: MS analysis of FLT3-ADCs after incubation in mouse serum. After a 6 d incubation of 20D9h3-DUBA or 20D9h3-MMAF in fresh mouse-serum (37 °C), both ADCs were analyzed by mass spectrometry (MS). Left side: Possible linker-payload fragments (with their masses) that would be present upon CES1-cleavage, drug or maleimide hydrolysis. Right side: Top and bottom plot show MS spectra of day 0 and of day 6 of mouse serum incubation, respectively. Drug-to-antibody ratio (DAR) was reduced from 3.9 to 2.7. This was partly due to retro-Michael addition mediated linker-payload loss (-1331 Dalton) and partly due to maleimide hydrolysis (+18 Dalton) in accordance with previous results (150). Fragments from CES1c-mediated cleavage were not observed. Experiment was performed by Dr. Marc-André Kasper (Tubulis GmbH).

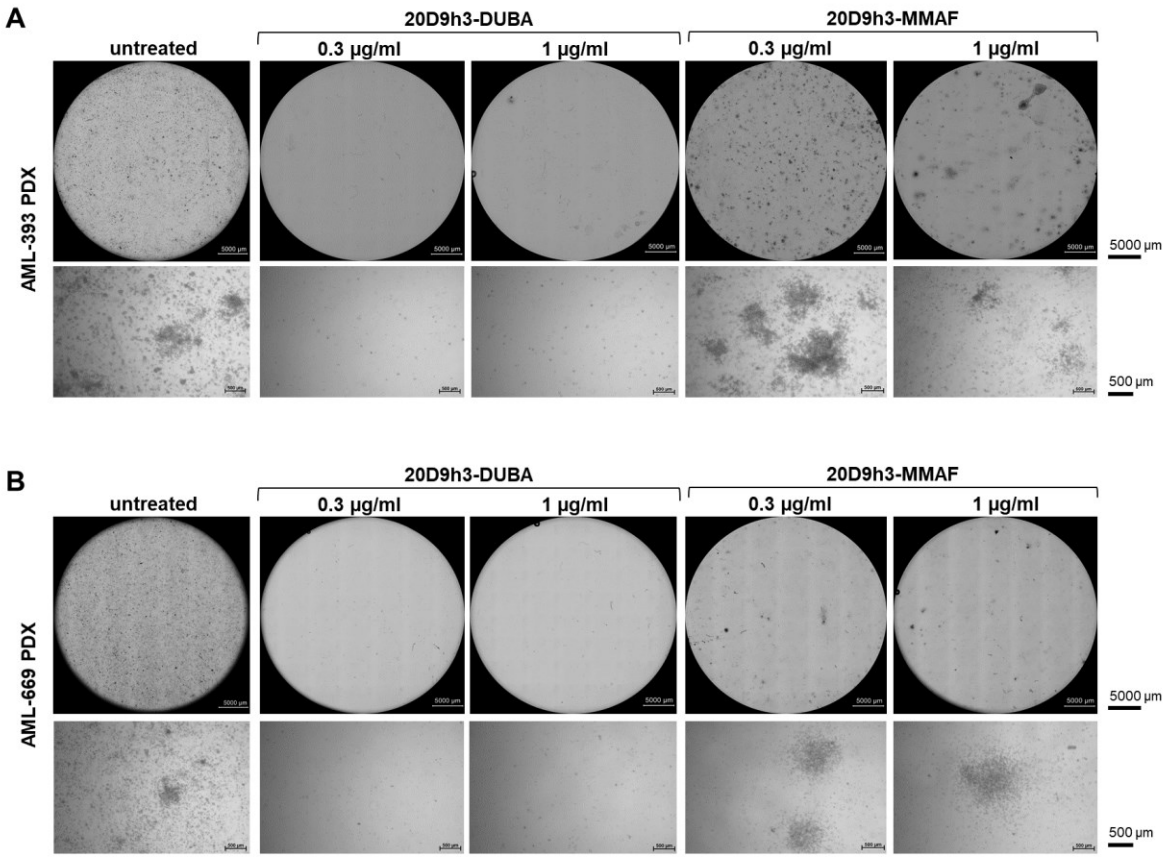

Supplementary Figure 5: Images of AML-393 and AML-669 PDX colonies in CFU assay. AML-393 and AML-669 PDX cells were treated for 4 d with 0.3 or 1 µg/ml of either 20D9h3-DUBA or 20D9h3-MMAF. Remaining cells were plated for 14 d in methylcellulose (CFU assay). On day 14, colonies were imaged. Upper panel: Images of the whole well acquired with Keyence BZ-X810 microscope and PlanApo 2x 0.10/8.50 mm objective; scale bar = 5000 µm. Lower panel: Representative images of single colonies acquired with ZEISS Primovert and Plan-ACHROMAT 4x/0.10 Ph0 objective; scale bar = 500 µm. (A) Images of AML-393 PDX colonies. (B) Images of AML-669 PDX colonies.

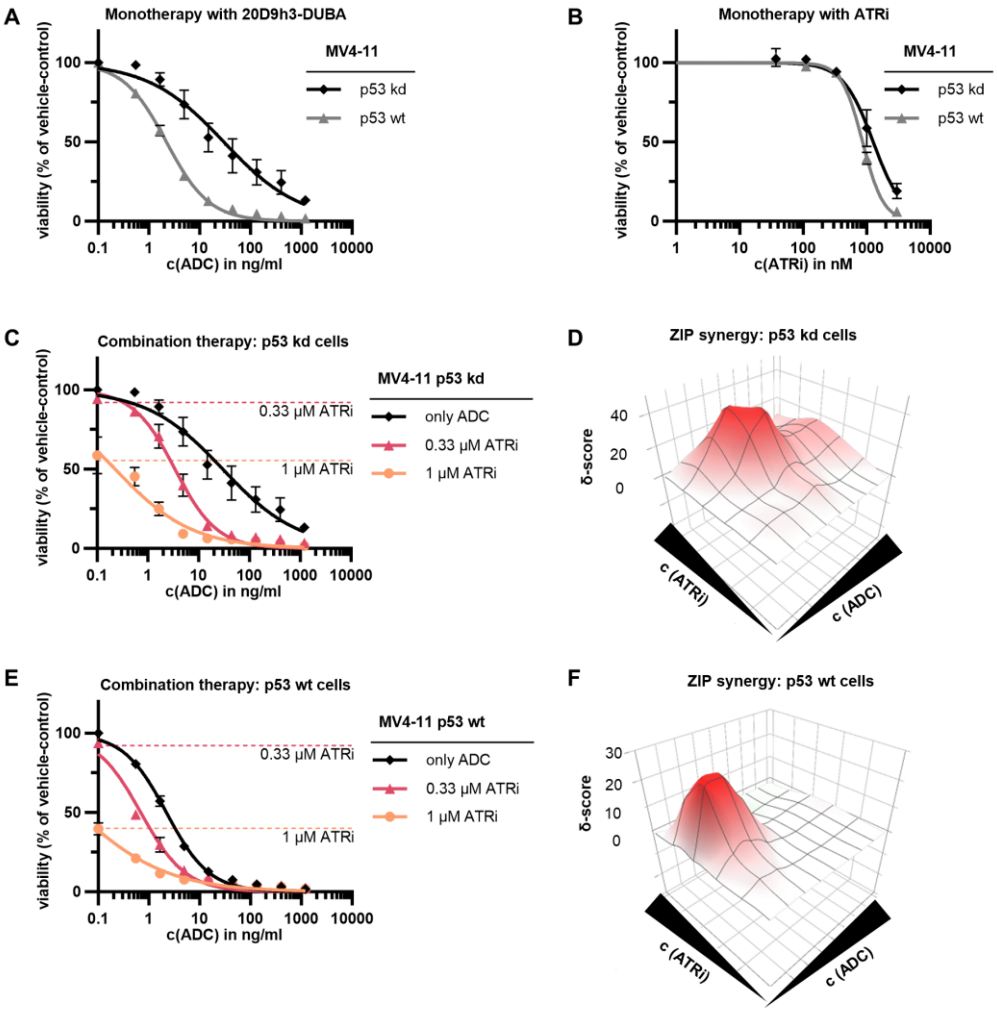

Supplementary Figure 6: Cytotoxicity assay of 20D9h3-DUBA in combination with the ATRi ceralasertib in MV4-11 cells with p53 wt or kd. p53 wt or kd MV4-11 cells were treated either with 20D9h3-DUBA monotherapy (A), ATRi (ceralasertib) monotherapy, (B) or the combination of both agents (C-F) for a total of 96 h. Then, viable cells were measured by resazurin assay and are depicted normalized to vehicle-control (DMSO for ceralasertib; PBS for 20D9h3-DUBA). They were plotted in GraphPad Prism 10.1.2 using non-linear fit, variable slope. mean ± s.d.; n = 3 biological replicates. To analyze synergistic effects for the combination of both drugs, dose-response curves were uploaded to SynergyFinder 3.0 and the zero interaction potency (ZIP) model without baseline correction was used for synergy calculations which compares the observed an expected effects (145). Synergy scores δ of >+10 or <-10 indicate synergism and antagonism, respectively.

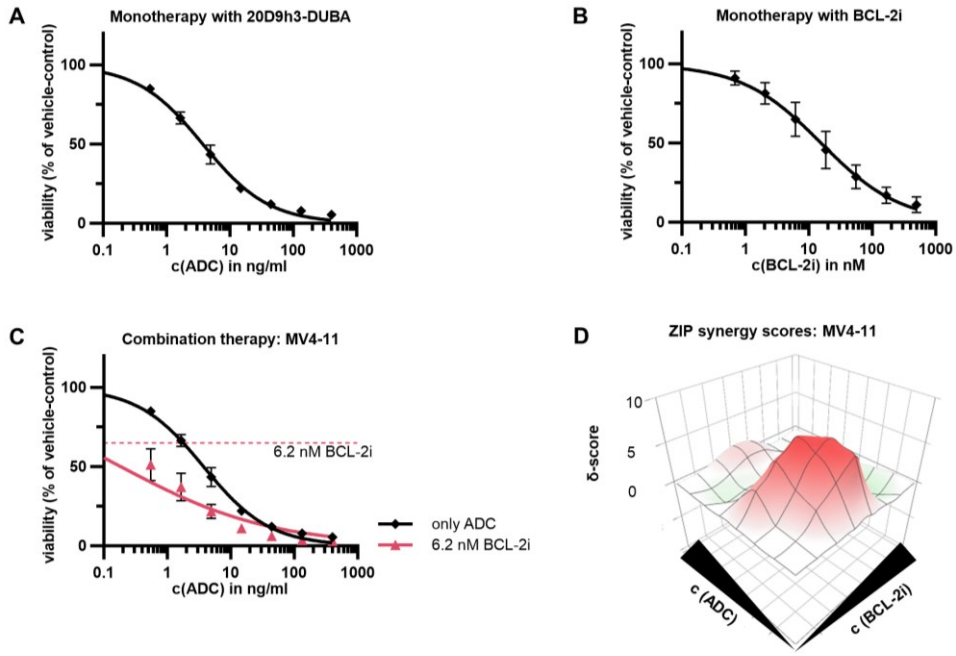

Supplementary Figure 7: Cytotoxicity assay of 20D9h3-DUBA in combination with the BCL-2i venetoclax in MV4-11 cells. (A-C) MV4-11 cells were treated with different doses of 20D9h3-DUBA (A), the BCL-2i venetoclax (B) or a combination of both agents (C) Curves were fitted with non-linear fit, variable slope in GraphPad Prism 10.1.2 and are depicted normalized to vehicle-control (DMSO for venetoclax; PBS for 20D9h3-DUBA). mean ± s.d.; n = 3 biological replicates. (D) Dose-response curves were uploaded to SynergyFinder 3.0 and analyzed with zero interaction potency (ZIP) without using baseline correction (145). δ-score > +10 indicates synergy; δ-score < -10 indicates antagonism; -10 < δ-score > +10 indicates an additive effect.

7 Acknowledgements

Allen voran möchte ich Karsten Spiekermann danken, der mir die Möglichkeit gegeben hat während meines Doktors ein Teil dieses tollen Kooperationsprojektes zu sein. Danke, dass ich jederzeit mit allen Fragen und Problemen vorbeikommen konnte, für den wertvollen Input, die Möglichkeit das Projekt frei zu gestalten und meine eigenen Ideen einzubringen und die großartige Unterstützung in den letzten 3 Jahren. Danke auch an die Mitglieder meines TAC Komitees Heinrich Leonhardt und Irmela Jeremias, die beide stets mit Begeisterung zum Erfolg dieses Projekts beigetragen haben innerhalb und außerhalb der TAC Meetings.

Ein ganz großes Dankeschön auch an Binje Vick, die mich nicht nur fachlich großartig unterstützt hat, sondern mich auch stets motiviert, inspiriert und aufgebaut hat. Danke auch für die Korrektur meiner Doktorarbeit. Ebenso möchte ich meinen tollen Kooperationspartnern danken: Marc-André Kasper, Saskia Schmitt und dem ganze Tubulis Team, Jonathan Schwach, Andreas Stengl, Mark de Geus, Christian Hackenberger, Michaela Feuring, Xiang Gao, Marit Leilich und Katharina Götze. Es hat großen Spaß gemacht mit euch allen zusammenzuarbeiten. Danke für das Einbringen eurer fachlichen Expertise und Begeisterung für dieses Projekt. Ohne euch wäre es nicht möglich gewesen das FLT3-ADC Paper zu veröffentlichen und das Projekt trotz aller Schwierigkeiten so gut abzuschließen!

Großer Dank geht auch an meine ehemaligen und derzeitigen Kollegen aus der Spiekermann Gruppe: Maike Roas, Alexander Ludwig, Kilian Lischeid, Ricarda Knabe, Amrei Fischer, Sarah Künzl, Anna Vetter und Belay Tizazu. Ich bin sehr froh, dass ich mit euch so liebe und hilfsbereite Kollegen hatte und habe, so dass wir darüber hinaus auch privat Freunde geworden sind.

Insgesamt schätze ich auch die Atmosphäre im ELLF mit den vielen Laborgruppen unter einem Dach wirklich sehr. Danke an alle ehemaligen und derzeitigen ELLF Kollegen: Johannes Hildebrand, William Keay, Lisa Wurdak, Alisa Maier, Carolin Strobl, Martina Antoniolli, Quentin Fichaux, Lukas Ulrich, Louisa Adolph, Sarah Häbe, Michael Heide, Korbinian Hasselmann, Anton Gaiderov, Lamija Alibegovic, Tabea Freyholdt, Sogand Ghasemi, Maximilian Köstler, Pranavkumar Rengasayee, Alessandra Caroleo, Paul Kerbs, Anja Swoboda, Vanessa Arfelli, Simona di Gaetano, Lisa Latzko, Paulina Uhl, Mariia Bashaeva, Antonia Pailhes, Anna Jäkel, Yana Dragieva. Danke für die vielen coolen Grillpartys, ELLFgivings und ELLFtoberfeste! Bitte in Zukunft nicht mehr gegen die Zentrifugen rennen…

Danke auch an meine Freunde außerhalb der Arbeit: Luisa Lange, Veronika Zeller, Kathrin Leitner, Johanna Pleintinger, Patrick Stahl, Lisa Gartner, Anja Kiermayer, Amelie Eschenbacher, Lena Zach und Lea Schneider. Hab euch alle sehr lieb! Ganz spezieller Dank noch an Lisa für die Englisch-Korrektur meiner Doktorarbeit. Danke auch an meine Boulderfreunde aus dem Element; dieses Hobby hat wirklich extrem zu meinem psychischen Wohlbefinden beigetragen und ich habe es während des Doktors wirklich lieben gelernt.

Zu guter Letzt: Das allergrößte Dankeschön geht natürlich an meine Eltern Sylvia Able und Helmut Able und meine Schwester Julia Able ohne die ich diese Zeit aus Höhen und Tiefen nicht durchgestanden hätte! Danke, dass ihr mich immer unterstützt und ermutigt egal was ich vorhabe, dass ihr immer ein offenes Ohr habt und dass ich immer heimkommen kann.

8 Affidavit

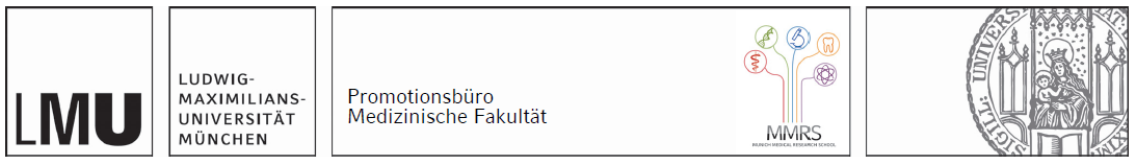

Affidavit

Able, Marina

Surname, first name

Street

Zip code, town, country

I hereby declare, that the submitted thesis entitled:

FLT3-Directed Antibody-Drug Conjugates to Target Leukemic Stem Cells in Acute Myeloid Leukemia

is my own work. I have only used the sources indicated and have not made unauthorised use of services of a third party. Where the work of others has been quoted or reproduced, the source is always given.

I further declare that the dissertation presented here has not been submitted in the same or similar form to any other institution for the purpose of obtaining an academic degree.

München, 02.10.2024 — Marina Able

place, date — Signature doctoral candidate

9 Confirmation of congruency

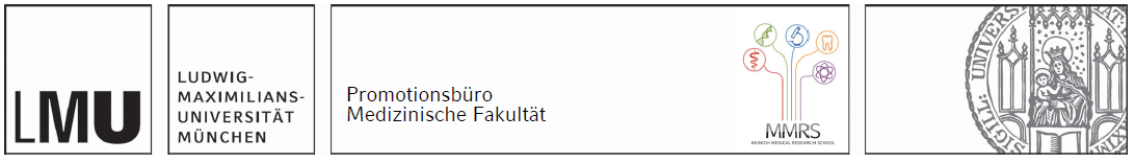

Confirmation of congruency between printed and electronic version of the doctoral thesis

Able, Marina

Surname, first name

Street

Zip code, town, country

I hereby declare, that the submitted thesis entitled:

FLT3-Directed Antibody-Drug Conjugates to Target Leukemic Stem Cells in Acute Myeloid Leukemia

is congruent with the printed version both in content and format.

München, 02.10.2024 — Marina Able

place, date — Signature doctoral candidate

10 List of publications

Most results presented in this thesis are part of the manuscript “Effective eradication of acute myeloid leukemia stem cells with FLT3-directed antibody-drug conjugates”, by Able et al., *Leukemia*, 2025.

- **Marina Able**, Marc-André Kasper, Binje Vick, Jonathan Schwach, Xiang Gao, Saskia Schmitt, Belay Tizazu, Amrei Fischer, Sarah Künzl, Marit Leilich, Isabelle Mai, Philipp Ochtrop, Andreas Stengl, Mark A.R. de Geus, Michael von Bergwelt-Baildon, Dominik Schumacher, Jonas Helma, Christian P. R. Hackenberger, Katharina S. Götze, Irmela Jeremias, Heinrich Leonhardt, Michaela Feuring and Karsten Spiekermann: Effective eradication of acute myeloid leukemia stem cells with FLT3-directed antibody-drug conjugates, *Leukemia*, 2025. DOI: 10.1038/s41375-024-02510-5

- Maike Roas, Binje Vick, Marc-André Kasper, **Marina Able**, Harald Polzer, Marcus Gerlach, Elisabeth Kremmer, Judith S. Hecker, Saskia Schmitt, Andreas Stengl, Verena Waller, Natascha Hohmann, Moreno Festini, Alexander Ludwig, Lisa Rohrbacher, Tobias Herold, Marion Subklewe, Katharina S. Götze, Christian P. R. Hackenberger, Dominik Schumacher, Jonas Helma-Smets, Irmela Jeremias, Heinrich Leonhardt and Karsten Spiekermann: Targeting FLT3 by new generation antibody-drug-conjugate in combination with kinase inhibitors for treatment of AML, *Blood*, 2023. DOI: 10.1182/blood.2021015246

- **Marina Able**, Marc-André Kasper, Binje Vick, Jonathan Schwach, Xiang Gao, Saskia Schmitt, Belay Tizazu, Amrei Fischer, Sarah Künzl, Marit Leilich, Isabelle Mai, Philipp Ochtrop, Andreas Stengl, Mark A.R. de Geus, Michael von Bergwelt-Baildon, Dominik-Schumacher, Jonas Helma, Christian P. R. Hackenberger, Katharina S. Götze, Irmela Jeremias, Heinrich Leonhardt, Michaela Feuring and Karsten Spiekermann: Effektive Eliminierung von leukämischen Stammzellen mit FLT3-gerichteten Antikörper-Wirkstoff-Konjugaten, *DGHO Abstract*, accepted as poster presentation on 18th of July 2024

- **Marina Able**, Marc-André Kasper, Binje Vick, Jonathan Schwach, Xiang Gao, Saskia Schmitt, Belay Tizazu, Amrei Fischer, Sarah Künzl, Marit Leilich, Isabelle Mai, Philipp Ochtrop, Andreas Stengl, Mark A.R. de Geus, Michael von Bergwelt-Baildon, Dominik-Schumacher, Jonas Helma, Katharina S. Götze, Irmela Jeremias, Michaela Feuring and Karsten Spiekermann: Potent Activity of Duocarmyin- and MMAF-Conjugated FLT3-Directed Antibody-Drug Conjugates towards Acute Myeloid Leukemia Stem Cells *in Vitro* and *in Vivo*, *ASH Abstract*, accepted as poster presentation on 1st of October 2024

- Part of the work is further included in a patent application.